Multiple strategies govern a layered zinc homeostasis in *Cupriavidus metallidurans*

Dissertation

Zur Erlangung des akademischen Grades
doctor rerum naturalium (Dr. rer. nat.)

vorgelegt der
Naturwissenschaftlichen Fakultät I - Biowissenschaften
der Martin-Luther-Universität Halle-Wittenberg

von Diana Galea

Assessors:
1. Prof. Dr. Dietrich H. Nies
2. Prof. Dr. Andrea Sinz
3. Prof. Dr. Kevin Waldron

Halle (Saale), 10th December 2025

Table of contents

Introduction

1. Life depends on metal ions

Living cells rely on various elements of the periodic table to survive. These elements are divided in three categories: i) non-metals, representing structural elements that build proteins, nucleic acids, carbohydrates, and lipids (C, O, H, N, P and S), and compose 96% of the dry mass of the cell, ii) macronutrients (K, Na, Mg, Ca), and iii) micronutrients or trace elements, represented by metal ions (Frieden, 1985). The macro- and micronutrients are mostly found as cations or anions, are immutable, and are critical for the cell function. The monovalent cations of potassium and sodium are used to regulate cellular osmotic pressure, to act as counter-ions for the negatively charged, non-metallic building blocks and metabolites of the cell, and are exchanged during transport processes (Halle and Denisov, 1998; Morbach and Krämer, 2002; Gouaux and MacKinnon, 2005).

The divalent magnesium cation, a highly abundant element in cells, is needed in general metabolic pathways and in nucleic acid biochemistry. The most representative example is the binding of Mg^{2+} to ATP to promote nucleophilic attack at the γ-phosphate during phosphoryl transfer reactions, rendering magnesium chelates of ATP as co-substrates for enzymes that catalyze phosphorylation of substrates (Cowan, 1991; Cowan, 2002). Relevant for the nucleic acid biochemistry are restriction endonucleases, exonuclease or polymerases, enzymes that bind the divalent cation of magnesium as cofactor, or Mg^{2+} - ATP (Cowan, 2002; Wilcox, 1996). The magnesium cation is centrally chelated by the porphyrin ring of chlorophyll, located in the inner membrane of the chloroplast, to absorb photons, which makes this cation vital in the process of photosynthesis (Mauzerall, 1976; Fiedor *et al*., 2008). The divalent calcium serves as an intracellular second messenger in eukaryotic cells to regulate cellular processes, whereas in bacteria the role of this cation as an intracellular messenger is more elusive, and is rather involved in the process of chemotaxis, stabilization of the cell wall, and accumulates in bacterial endospores (Campbell, 1990; Dominguez, 2004).

The micronutrients needed by biological systems are represented by metal cations of the first transition period of the periodic system of the elements, or the late 3*d* block metals. These are the cations of manganese, iron, cobalt, nickel, copper, and zinc. These elements can fill up their 3*d*-orbitals based on the configuration of their electron shells, from $3d^5$ for Mn^{2+} to $3d^{10}$ for Zn^{2+}. All these transitional metal cations fulfil, due to their

unique chemical properties, specific roles in biology. Several metal ions can be reduced or oxidized and are used in redox processes. The metal ions which possess redox-compatible chemistry are the cations of manganese, iron, copper and nickel, and can reach more oxidation states. The manganese ion is inserted into the active sites of the tetrameric Mn superoxide dismutases (Mn-SOD), which are metalloenzymes used by some bacteria, yeast and mitochondria to catalyse the disproportionation of superoxide into hydrogen peroxide and dioxygen in order to protect cells from damage caused by reactive oxygen species (Borgstahl *et al.,* 1992). In plant cells, four manganese ions are essential for the formation of the Mn-centre of the oxygen-evolving complex (OEC) of Photosystem II, which is responsible for the oxidation of the water molecule (Ferreira *et al*., 2004).

Living organisms have a substantial requirement for iron because of its role in fundamental metabolic and biological processes, such as photosynthesis, N_2 fixation, methanogenesis, respiration, oxygen transport, H_2 production, and the trichloroacetic acid (TCA) cycle (Andrews *et al*., 2003). For instance, iron can act as a cofactor in mono- or binuclear enzymes, or can be part of more complex forms, such as [Fe-S] clusters or heme groups. Iron-sulfur clusters act as cofactors for a considerate number of enzymes, where they are incorporated as inorganic prosthetic groups. From bacteria to plants, proteins found in the membrane-bound electron transport chains of respiration and photosynthesis are abundant in iron-sulfur clusters, such as [2Fe-2S], [3Fe-3S] or [4Fe-4S] (Beinert *et al*., 1997; Johnson *et al*., 2005).

In biological cells, copper cycles between the +1 and +2 oxidation state, with Cu^{2+} being the predominant form under oxic conditions. In prokaryotic cells, copper is used as a cofactor in haem-copper oxidases, such as cytochrome *c* oxidase, multicopper oxidases, superoxide dismutase, and blue copper proteins (Rensing and McDevitt, 2013). The copper-dependent oxidases exploit the ability of copper to be involved in O_2 metabolism, by facilitating the four-electron reduction of O_2 to water (Sousa *et al*., 2012). Copper is involved in the process of photosynthesis when inserted into blue copper proteins that act as electron transfer proteins (Gray *et al*., 2000). The role of copper in respiratory processes makes this cation important for Eukaryotes, as well, and this is reflected by its usage in the mitochondrial cytochrome *c* oxidase (COX) (Horn and Barrientos, 2008).

Nickel and cobalt ions are either incorporated into enzymes that catalyze hydrolytic and redox reactions, or in tetrapyrroles acting as organic metal cofactors. The most spread nickel-dependent enzymes are [Ni-Fe] hydrogenases and ureases, mainly found in bacteria and archaea (Zhang *et al*., 2009; Boer *et al*., 2014), while ureases can be found in plants and single-celled eukaryotes (Thauer *et al*., 1980; Dixon *et al*., 1975; Christians and Kaltwasser, 1986). Nickel is extremely important for methanogenic Archaea, which have high level requirements of nickel ions for their existence (Thauer, 1998). Methanogenic Archaea considerably incorporate this divalent cation into Factor 430 (F_{430}), which is the prosthetic group of methyl-coenzyme M reductase necessary for methane formation (Ellefson *et al*., 1982).

The usage of cobalt ions in biological systems is even more restricted than that of nickel ions. Cobalt ions are used by two *bona fide* cobalt-requiring enzymes, the cobalt-dependent (aceto)nitrile hydratase (NHases) and prolidases, both found in Bacteria (Ghosh *et al*., 1998; Kobayashi and Shimizu, 1999). Nevertheless, the main utilization of cobalt ions in biological systems results from the incorporation of the trivalent cobalt ion into the corrin ring of cobalamin or vitamin B_{12}. Consequently, the number of cobalamin-dependent enzymes exceeds the number of cobalt-dependent enzymes. Despite being required by the majority of bacteria, cobalamin can be synthesized *de novo* only by a subset of microbes in a complex biosynthetic pathway that involves ~30 enzymatic steps (Warren *et al*., 2002; Shelton *et al*., 2019). Many animals, including humans, and protists require vitamin B_{12}, whereas plants and fungi have evolved to neither synthesize nor use B_{12} in their metabolism (Roth *et al*., 1996). Cobalamin-dependent enzymes are involved in methyl transfer reactions and fatty acid catabolism, and some representatives are methionine synthetase and methylmalonyl CoA mutase (Roth *et al*., 1996).

Divalent zinc ions act as catalytic and structural cofactors in proteins. From the discovery of their essentiality for the enzymatic function of erythrocyte carbonic anhydrase in 1939, zinc ions are found in all classes of enzymes, *e.g.* oxidoreductases, transferases, hydrolases, lyases, isomerases, and ligases (Keilin and Mann, 1939; Vallee and Galdes, 1984). It has been estimated that approximately 3.000 human proteins bind zinc, which accounts for almost 10% of the human proteome, and zinc-fingers are the most abundant class of zinc-binding proteins (Andreini *et al*., 2006). Zinc fingers are small proteins involved in DNA transcription in eukaryotes, and are composed of repetitive sequences of cysteine (Cys) and histidine (His) residues that act as zinc structural sites, *e.g.* C_2H_2

(Capdevila *et al*., 2024). The transcription factor IIIA (TFIIIA) from *Xenopus laevis* was the first example of such a zinc finger-containing protein (Shang *et al*., 1988). The catalytic zinc-binding sites use as ligands glutamate (Glu) and aspartate (Asp), in addition to cysteine (Cys) and histidine (His), in representative zinc-proteins such as carboxypeptidases, carbonic anhydrases, alcohol dehydrogenases, and histone deacetylases (Andreini *et al*., 2006). Zinc ions are used as protein cofactors by microbes, and the zinc proteome in Bacteria and Archaea accounts for 6.0%, and 4.9% respectively (Andreini *et al*., 2006).

The use of transition metals in modern prokaryotes generally follows the hierarchy Fe >> Zn > Mn >> Mo, Co, Cu >> Ni, which correlates with changes in Earth's geochemistry once the redox state of the oceans and atmosphere influenced both the trace metal chemistry and their bioavailability (Zerkle *et al*., 2005; Anbar, 2008). The emergence of oxygenic photosynthesis and the subsequent oxygenation of the deep oceanic waters led to the oxidation of ferrous iron to ferric iron and to an increase of zinc and copper concentrations, while decreasing the concentrations of other transition metals, such as iron, nickel, manganese and cobalt. In the sulfide dominated oceans, iron was abundant in the form of ferrous iron, Fe^{2+}, and the availability of trace elements was: Fe > Mn, Ni, Co >> Zn, Cu, Cd (Saito *et al*., 2003). These changes in trace metal geochemistry and availability leave imprints within genomes and proteomes of modern life (Dupont *et al*., 2006). Thus, in modern organisms, copper and zinc ions are considerably incorporated into metal-requiring enzymes, while nickel-and cobalt-containing proteins are considered "remnants from early life" (da Silva and Williams, 1991).

2. Metalation and key concepts

A significant portion of the divalent transition metal cations are incorporated into proteins to sustain cellular biochemistry, highlighting their utility in metabolism, where metalloenzymes ultimately act as "cellular metal sinks". Consequently, it has been estimated that one-third of all structurally characterized proteins require metals (Finney and O'Halloran, 2003), and almost half of all enzymes are metalloenzymes (Andreini *et al*., 2008). Apo-proteins bind their cognate metal ion through a process termed *metalation*. A significant portion of the cellular proteome is represented by metalloproteins (Andreini *et al.,* 2004). Consequently, the term *metalloproteome* has been coined in order to define

the portion of the proteome that binds metal ions and needs to be metalated. In order for metalloproteins to exert their biological function, metalation with their cognate metal cofactor is vital. Metalloproteins can bind non-cognate metal ions, as well, but this process often leads to non-functional proteins and has been termed *mismetalation*. Thus, cells survive and proliferate when their metal-requiring proteins contain the correct metal ion to perform either a catalytic function, to retain the right structural conformation, or to operate as regulatory proteins involved in gene expression.

This chapter will address the challenges living cells face in order to ensure metalation. Firstly, biological systems accumulate intracellularly a variety of metal ions, at different metal concentrations. For instance, in *Escherichia coli* the total magnesium concentration is >10 mM, followed by calcium, iron and zinc at about 100 μM, copper and manganese at about 10 μM, and cobalt and nickel are found at a lower concentration (Finney and O'Halloran, 2003). The *metallome* of biological systems is thus, heterogenous and the concentrations of metal ions in the "intracellular milieu" differ by several orders of magnitude. The term *metallome* has been established initially in 2001 to define "the element distribution" in a cell (Williams, 2001). Secondly, both metal ions and proteins have preferences that influence the selection of metal ions to be incorporated into the metal-binding sites of apo-proteins. Some of these preferences are the valence state, ionic radius, coordination geometry, ligand number, second-shell ligands, or other ligand characteristics (Dudev and Lim, 2014). Structural properties of polypeptide chains can impose steric restrains on final coordination geometries. For instance, the cations of manganese and iron prefer octahedral coordination geometries, nickel can adopt a degenerated octahedral or square planar coordination, while zinc ions form predominantly stable tetrahedral coordination with their ligands.

The thermodynamic stability of metal complexes can be generalised by the principles of "hard-soft acid-base theory", where the metal ion represents the acid and the ligands are bases (Parr and Pearson, 1983; Pearson, 1963). For example, Cu^{+} is considered a "soft" metal that tends to form stable complexes with "soft" ligands, sulfur-containing thiols and thioethers, observed in its preference for cysteine and methionine residues when bound to proteins. Ferric iron is considered a "hard" metal ion, and has a tendency to form complexes with "hard" ligands, such as hydroxyl or carboxylate oxygens. Consequently, this metal ion has a preference for aspartate, glutamate and tyrosine residues. The divalent transition metal ions, except Mn^{2+}, are considered "borderline" and have more

flexibility in terms of their ligand preferences, towards nitrogen in histidine residues, or a mixture of sulfur- and oxygen-containing residues.

Nevertheless, crucial for *in vivo* metalation is the thermodynamic stability of metal complexes of the first row of the *d*-block metals, knows as the Irving-Williams series (Irving and Williams, 1948). If nascent proteins possess a negligible steric selection, binding of the metals will follow the Irving-Williams series: Mg(II) < Mn(II) < Fe(II) < Co(II) < Ni(II) < Cu(II) > Zn(II) (Irving and Williams, 1948; Robinson and Glasfeld, 2020).

Thus, *in vivo* metalation takes place in a highly crowded, competing, heterogenous cytosolic environment, needs to cross a multitude of selectivity filters, pertaining to the metal, the apo-protein and the cytosolic milieu, and is dependent on the intracellular metal availability. In this scenario, it is estimated that metalation of 30% of metalloenzymes is ensured by specific metal delivery systems, such as metallochaperones, and the remaining 70% of metalloenzymes compete for their cognate metal ions from buffered metal pools (Foster *et al*., 2014).

2.1 Metallochaperone-assisted metalation

The definition of metallochaperones has been refined to a group of specialized proteins that both shield metal ions from inadvertent reactions by intracellular sequestration to avoid binding to nontarget proteins and facilitate distribution of metal ions to the target apo-proteins (Kunkle and Skaar, 2023). The idea that metalloproteins are metalated by metallochaperones has its origins and inspiration in bacterial copper homeostasis. CopZ from *Enterococcus hirae* was the first described bacterial metallochaperone facilitating the transfer of Cu^{+}, as a result of a direct protein-protein interaction between CopZ itself and CopY, the repressor of the *cop* operon, which ensures copper homeostasis as a consequence of copper uptake and efflux (Cobine *et al*., 1999; Wimmer *et al*., 1999; Cobine *et al*., 2002). Other direct protein-protein interactions in case of copper homeostasis are known between the periplasmic copper chaperone CusF from *E.* coli and the inner membrane P_1-type ATPase CopA, as well as metalation of SodCII from *Salmonella enterica* sv. *Typhimurium* by the periplasmic copper chaperone CueP (Padilla-Benavides *et al*., 2014; Osman *et al*., 2013). Homologous copper chaperones to CopZ exist in yeast (Atx1), plants (CCH) and humans (HAH1) and helped to postulate early on the definition of metallochaperones as ‘diffusible cytosolic proteins for the membrane

transporters which protect and guide metal ions through the cytoplasm, and transfer the ions to specific proteins' (Lin and Culotta, 1995; Lin *et* al., 1997; Klomp *et al*., 1997; Himelblau and Amasino, 2001; Finney and O'Halloran, 2003).

Intracellular copper trafficking and metallochaperone-mediated transfer is also needed for the metalation of the superoxide dismutase 1 enzyme, SOD1, from *Saccharomyces cerevisiae*, accomplished by CCS (copper chaperone for SOD) (Culotta *et al*., 1997; Rae *et al*., 1999). Copper ions are transferred from a donor protein to an acceptor protein *via* an associative mechanism that involves molecular recognition between the two proteins, and is based on the affinity gradients between the two proteins, *e.g.* between the metal transporters and the metal-receiving protein, generally facilitated by a conserved cysteine-rich metal binding motif found in a large share of copper transport proteins (Robinson and Winge, 2010).

Metal delivery systems are known for the insertion of nickel ions into [Ni-Fe]-hydrogenases or ureases, such as HypA/HypB/SlyD or UreE/UreG, respectively (Kuchar and Hausinger, 2004; Leach and Zamble, 2007; Fong *et al*., 2013). In contrast to the copper metallochaperones, nickel metallochaperones facilitate metal insertion with consumption of nucleotide cofactors, such as GTP (Kaluarachchi *et al*., 2010; Higgins *et al*., 2013). HypB and UreG are SIMIBI P-loop GTPases from the G3E family of metallochaperones, which additionally includes MeaB and COG0523-proteins (Leipe *et al*., 2002; Haas *et al*., 2009). MeaB is an auxiliary protein which appears to fulfil the role of an adenosylcobalamin (Co^{2+})-insertase and facilitates the insertion of B_{12} into methylmalonyl-CoA mutase (Padovani *et al.,* 2006). All the aforementioned proteins are thus involved in cofactor insertion and metallocenter maturation by functioning as either metal insertases or having a dual function as a metallochaperone/insertase.

Furthermore, the COG0523-family is furthermore divided into three subfamilies: i) CobW subfamily involved in cobalamin biosynthesis,ii) the Nitrile hydratase activator subfamily and iii) Zur-regulated COG0523 proteins (Haas *et al*., 2009). As the name suggests, members of the CobW subfamily are related to cobalamin biosynthesis and represent only 12.5% of the COG0523 family (Haas *et al*., 2009). The *cobW* genes are located within B_{12} biosynthesis gene clusters and can be under the control of B_{12} riboswitch (Rodionov *et al*., 2003). In some instances, however, such as in *Rhodospirillaceae* family, the *cobW* genes belong to the cobalamin biosynthesis clusters, but are not preceded by

B_{12} riboswitches (Haas *et al*., 2009). The first identified member of the COG0523 family was the CobW protein from *Pseudomonas denitrificans*, where the disruption of the corresponding gene resulted in the inability to aerobically synthesize cobalamin (Crouzet *et al*., 1991). Since the initial observation that CobW is linked to cobalamin biosynthesis and the co-localization of the *cobW* gene is usually adjacent to *cobN* gene in aerobic cobalamin biosynthesis gene clusters (Haas *et al*., 2009), it has been proposed that CobW functions in Co^{2+} delivery by presenting the ion to CobN. The functional role of CobW in Co^{2+} supply has been elucidated and CobW was shown to acquire Co^{2+} *in vivo* (Young *et* al., 2021), but despite the cobaltchelatase CobNST being the anticipated target for CobW, no specific protein interaction has been demonstrated to date. The subfamily with the least representatives is the Nitrile hydratase (NHase) activator subfamily, which accounts for less than 0.7% of the COG0523 family (Haas *et al*., 2009). The NHase activators are clustered exclusively with the genes encoding the two subunits of the Fe-type NHase and are required for the *in vivo* activity of Fe-type NHase, by exerting an insertase role and incorporating iron into the active site of the hydratase (Nojiri *et al*., 1999; Lu *et al*., 2003). Co-expression of both the nitrile hydratase genes and the corresponding activator gene from *Rhodococcus equi* TG328-2 in *E. coli* led to the maximum enzyme activity reinforcing that Nha3 is implicated in the delivery of Fe ions to the NHases (Rzeznicka *et al*., 2009). The Fe-type Nha3 from *R. equi* TG328-2 was subsequently purified and its GTPase activity was confirmed, but the GTP-dependent Fe delivery has still to be established (Gumataotao *et al*., 2017).

2.2 *In vivo* metalation from cellular buffered metal pools

In absence of a metal delivery system, metalloenzymes acquire their cognate metal ion cofactors from cellular buffered metal pools in the cytosol, where they compete with other ligands for limited amounts of metal ions. A general rule of metalation *in vivo* is driven by thermodynamic gradients, in which high-affinity ligands are metalated first, followed by lower-affinity ligands as the metal pool becomes saturated (Young *et al*., 2021). Apo-proteins must acquire their cognate metal ion and retain it in their metal-binding site despite the presence of competing ligands and the intermetal competitions of the cytosol. In this way, a theoretical model based on metal pools can be envisioned (Barwinska-Sendra and Waldron, 2017). The notion of “free” ions in the cytosol is essential to this model, or rather, the lack of “*free*” ions in the cytosol. “Free” metal ions are found in hexa-aqua complexes, meaning six water molecules act as ligands, and the oxygen atom of

each coordinated water molecule acts as the donor of the electron pairs. To exemplify, it is important to consider copper homeostasis again. It is widely accepted that there are no "*free*" copper ions inside the cell, and the formed copper pool is tightly bound and buffered at extremely low values, whereas its intracellular movement is mediated by copper chaperones *via* direct protein-protein interactions (Finney and O'Halloran, 2003). The copper regulator CueR is responsible for maintaining cytosolic copper concentrations at low levels the cell due to its zeptomolar affinity for copper ions (Changela *et al*., 2003). Metalation of the majority of metalloenzymes in absence of dedicated metal delivery systems is thus conditioned by the metal availability within the cellular buffered pool (Foster *et al*., 2014). Bacterial cells accomplish this process flawlessly due to the finely tuned homeostatic control of metal ions they possess.

3. *Cupriavidus metallidurans* CH34 as model organism for metal homeostasis

Model organisms enable us to elucidate fundamental mechanisms through which metal homeostasis and metalation processes are enabled. *Cupriavidus metallidurans* CH34 serves as a model organism for the study of multiple metal homeostasis. It was first isolated in 1976 from a decantation tank at a zinc factory in Belgium and its distribution is associated with metal-rich environments such as zinc desserts or auriferous soils in Australia (Diels and Mergeay, 1990; Reith *et al*., 2006; Reith *et al*., 2007). It belongs to the phylum *Proteobacteria*, class *Betaproteobacteria*, order *Burkholderiales*, family *Burkholderiaceae*, whose name underwent several taxonomic changes (formerly known as *Alcaligenes eutrophus*, *Ralstonia* sp., *Ralstonia metallidurans*, *Wautersia metallidurans*) (Goris *et al*., 2001; Vaneechoutte *et al*., 2004; Vandamme and Coenye, 2004). It is a mesophilic bacterium able to grow both heterotrophically on a variety of organic compounds and chemolitoautotrophically as hydrogen-oxidizing bacterium under a gas mixture of H_2, O_2, and CO_2, preferably at 30°C, and is unable to produce toxins which makes it harmless (Mergeay *et al*., 1985). The wild type strain CH34 contains four replicons, one chromosome, a second chromosome or "chromid", and two megaplasmids, pMOL28 and pMOL30, which accommodate various metal resistance determinants (Gerstenberg *et* al., 1982; Mergeay *et al*., 1985; Janssen *et al*., 2010). Thus, several derivatives from the wild type strain CH34 were produced, depending on which replicon they possess. These are i) AE126 with the two chromosomes and pMOL28, ii)

AE128 with the two chromosomes and pMOL30, and iii) AE104 which only contains the two chromosomes and is devoid of the two plasmids (Mergeay *et al*., 1985).

3.1 Multiple metal resistance

C. metallidurans contains metal resistance determinants on all four replicons, and additionally on genomic islands. Some of these determinants were acquired during the evolution of this bacterium by horizontal gene transfer, and ensure its survival in the presence of high concentrations of transition metals (Janssen *et al*., 2010; Van Houdt *et al*., 2009; Van Houdt *et al*.,2012; Große *et al*., 2022). A plethora of proteins belonging to multiple protein families with different substrate specificities as well as mechanisms of transport, and covering almost the whole spectrum of the transition metals are employed by this bacterium (Nies, 2016).

C. metallidurans CH34 contains genes which encode for almost 40 outer membrane porins, yet only a few are grouped with porins representative to *E. coli*, while the rest are specific to this organism (Nies, 2016). For substrates which are either too large to pass through the outer membrane porins or are found in low concentrations, TonB-dependent proteins complement the high-rate, low-specificity transport with a substrate-specific import. These substrates can be the Fe^{3+} siderophore or cobalamin and the import is fuelled by the proton motive force (pmf*)* of the inner membrane, as well as a conformational change energized by the ExbB-ExbD-TonB protein complex to facilitate the passage of the substrate into the cytoplasm (Braun, 1995; Higgs *et* al., 1998; Noinaj *et* al., 2010). There are 18 such TonB-dependent outer membrane proteins in *C. metallidurans* CH34 which import staphyloferrin B, the Fe^{3+} siderophore, cobalamin or other unknown metal complexes (Schmidt *et al*., 2014; Nies, 2016).

Transition metal cations are exported from the periplasm by the RND-driven (Resistance Nodulation Cell division) efflux systems in a secondary active efflux mechanism driven by cation-proton antiport (Nies and Silver, 1995; Tseng *et al*.,1999). The structure of such an RND-efflux system is composed of the three components: i) a trimeric RND protein, located in the inner membrane, also the engine part of the entire system, ii) a tube-like trimeric outer membrane factor OMF, and iii) a hexameric membrane fusion protein MFP which connects the RND and OMF (Koronakis *et al*., 2000; Murakami *et al*., 2002; Seeger *et al*., 2006; Symmons *et al*., 2009; Su *et al*., 2011). In the genome of *C. metallidurans*

CH34, 12 putative gene clusters encoding for RND-driven systems are present, but only a few are expressed and mediate resistance to transition or toxic metals (Nies *et al*., 2006). These are CzcCBA, CnrCBA, ZniCBA, ZneCBA, CusCBA and SilCBA and mediate high-rate active efflux of Zn^{2+}, Co^{2+}, Cd^{2+}, Ni^{2+}, Cu^{+}, Ag^{+}, while the remaining gene regions are silent, interrupted or inactivated (Nies, 2016).

Regulation of synthesis of these systems and their substrate specificity differ. Regulation can occur either by two-component regulatory systems, which regulate periplasmic metal homeostasis, or by sigma factors from the extracytoplasmic function (ECF) family, and is highly specific, so that the metal specificity of each transport system is a consequence of the metal specificity of its respective regulator (Nies, 2016).

The cobalt-zinc-cadmium CzcCBA efflux system is encoded by the gene cluster *czcNICBADRSEJ* on plasmid pMOL30, and confers resistance to the divalent metal cations of zinc, cobalt, cadmium, with zinc being the prime substrate (Nies *et al*., 1987; Nies *et al*., 1989; Große *et al*., 2004; Monchy *et al*., 2007). Its synthesis is controlled by the two-component regulatory systems CzcRS, upon sensing elevated concentrations of zinc ions in the periplasm by the histidine kinase CzcS, and binding of the reponse regulator CzcR to the *czcPp* and the *czcNp* promoters to induce transcription of the *czc* genes (van der Lelie *et al*., 1997; Große *et al*., 1999; Scherer and Nies, 2009). The CnrCBA efflux system mediates resistance to nickel and cobalt, is located on plasmid pMOL28, and is organized in two gene clusters which contain the structural genes *cnrCBAT*, with *cnrT* encoding for a nickel exporter of the inner membrane, and the regulatory genes *cnrYXH* (Mergeay et al., 1985; Collard *et al*., 1993; Janssen *et al*., 2010). The nickel-specific transcriptional regulation of this RND-efflux system occurs through the products of the regulatory genes: i) CnrH, an extracytoplasmic function sigma (ECF) factor, necessary for transcription initiation from the *cnrYp* and *cnrCp*, and ii) the nickel-sensing, membrane-bound anti-sigma factor complex CnrYX, which is needed to repress the action of CnrH in absence of Ni(II), by sequestration of CnrH to CnrYX (Grass *et al*., 2000; Tibazarwa *et al*., 2000; Grass *et al*., 2005).

On the other hand, ZniCBA and ZneCBA are rather involved in a global response to environmental stress and are both regulated by two-component regulatory systems (Nies, 2016). CusCBA and SilCBA are RND-efflux systems involved in copper and silver resistance, are located on the chromid and pMOL30, respectively (Silver, 2003; Nies,

2016). Detoxification of periplasmic copper ions is achieved by the gene products of the *cusDCBAF* determinant, whose regulation, however, is not under the control of a CusRS two-component system, as in *E. coli*, but might be under the control of another two-component system, CopRS (Munson *et al*., 2000; Hirth *et al*., 2023). *In E. coli* detoxification of copper ions requires an interaction between CusF, a periplasmic copper chaperone, and the CusB protein of the RND-efflux system, whereas in *C. metallidurans* both CusD and CusF might act like periplasmic copper-chaperones (Ucisik *et al*., 2015; Bagai *et al*., 2008; Hirth *et al*., 2023).

Several candidate sulphate permeases and the phosphate importer PitA do not only provide sulphate and inorganic phosphate, respectively, but also structural analogues such as chromate or arsenate to the cytosol (Aguilar-Barajas *et al*., 2001). PitA belongs to the PiT protein family (TC 2.A.20) and is able to import transition metal cations, such as Zn^{2+}, as metal:complexes coupled with proton symport (Saier *et al*., 1999; Herzberg *et al*., 2016). The MIT protein family (TC 1.A.35) is represented by four members in this betaproteobacterium: $CorA_1$, $CorA_2$, CorA3 and ZntB, which exhibit broad substrate specificity for the divalent metal cations of magnesium, zinc, nickel and cobalt (Kirsten *et al*., 2011). HoxN from the nickel/cobalt NiCoT protein family (TC 2.A.52) is found within the hydrogenase cluster and is the responsible nickel uptake system for hydrogenase biosynthesis (Eitinger *et al*., 2005). Primary import of transition metal cations is also ensured by two P-type ATPases (TC 3.A.3), MgtA and MgtB, whose main specificity is for Mg^{2+} (Kirsten *et al*., 2011; Nies, 2016). Import across the inner membrane is thus achieved by a battery of redundant metal importers which supply an overall mixture of transition metal cations to the cytoplasm, at a high-rate, but with low substrate-specificity.

The wild type strain CH34 accomplishes a two-step detoxification of surplus transition metal cations by using, in addition to the RND-efflux systems, a repertoire of inner membrane efflux proteins. On the other hand, in the plasmid-free strain AE104, detoxification is achieved only by the inner membrane efflux transportome, and can be considered that its metal homeostasis is “more reflective of bacterial metal homeostasis in general” (Kwiatos and Waldron, 2024). These transport systems are responsible for the export of metal ions from the cytoplasm to the periplasm against their concentration gradient, either in a primary transport by coupling the energy provided by ATP hydrolysis or in a secondary transport process, coupling an antiport of protons and metal ions (Argüello *et al*., 2007; Chao and Fu, 2004; Guffanti *et al*., 2002). The inner membrane

efflux transportome contains several representatives from different protein families: P_{1B}-type ATPases as primary transport systems, Cation Diffusion Facilitator (CDF) proteins which are secondary efflux systems, and other protein families, such as the ATP-Binding Cassette (ABC) protein family (TC 3.A.1), DMT protein family (TC 2.A.7) or proteins from the CHR family (TC 2.A.51) (Paulsen and Saier, 1996; Schneider and Hunke, 1998; Jack *et al*., 2001; Argüello, 2003; Nies *et al*., 1998).

Detoxification of the divalent metal cations of zinc, cadmium and lead occurs through proteins from the P_{IB2}-type ATPases (TC 3.A.3), ZntA, CadA and PbrA (Borremans *et al.*, 2001; Legatzki *et al*., 2003; Scherer and Nies, 2009). The genes encoding for the respective proteins are located on the two chromosomes and their metal-dependent induction transcription and induction is under the control of metal-ion sensing MerR-type regulators, either acting as activators or co- repressors, ZntR, CadR and PbrR (Schulz *et al*., 2021; Borremans *et al.*, 2001). The P_{IB4}-type ATPase CzcP, whose associated gene is found in the *czc* cluster on pMOL30*,* mediates zinc resistances in combination with the other P-type ATPases (Scherer and Nies, 2009).

The CDF protein family has three representatives in *C. metallidurans*: i) CzcD, encoded on plasmid pMOL30, in the *czc* resistance molecular determinant with transport specificity for Co^{2+}, Zn^{2+}, Cd^{2+}; ii) DmeF, encoded on the chromosome which exports mainly Co^{2+} and Ni^{2+}, at low concentrations; and iii) FieF, an iron exporter (Anton *et al*., 1999; Munkelt *et al*., 2004; Grass *et al*., 2005; Scherer and Nies, 2009). AtmA, from the ABC-family of transporters (TC 3.A.1) and CnrT, from the DMT family (TC 2.A.7) mediate nickel resistance (Mikolay and Nies, 2009). Representatives of the P_{IB1}-type ATPases, CupA and CopF, mediate copper resistance by active export of the copper ions in the periplasm (Wiesemann *et al*., 2013; Hirth *et al*., 2023).

Apart from being able to handle excess amounts of essential metal ions by active export, *C. metallidurans* is able to withstand metals with no biological function, such as the hexavalent chromate, divalent mercury and pentavalent arsenate. The gene clusters which handle the toxicity of these compounds encode for proteins with a very specific function, either to import or bind, to metabolize, generally by reduction, and then to export these compounds. Four *mer* clusters confer resistance to mercury, which involves periplasmic sequestration by MerP and direct transfer of Hg^{2+} to membrane proteins MerT, with subsequent cytosolic reduction by the NADPH-dependent mercuric reductase

MerA, generating metallic mercury which diffuses out of the cell (Silver and Hobman, 2007; von Rozycki and Nies, 2009). Chromate resistance is mediated by gene products of the two *chr* gene clusters located on pMOL28 and the chromid. Chromate detoxification involves unspecific uptake through the sulphate importers, and specific secondary efflux through two inner membrane proteins, ChrA1 and ChrA2 (Nies *et al*., 1989; Nies *et al*., 1990; Nies *et al*., 1998; Cervantes and Campos-García, 2007). Resistance to arsenate is mediated by the chromosomally-encoded *ars* cluster, and involves unspecific uptake of arsenate through the PitA importer, reduction to As^{3+} by arsenate reductases $ArsC_{1/2}$ and efflux by an ArsP transmembrane proteins, from the MFS protein family (TC 2.A.1) (Bhattacharjee and Rosen, 2007).

3.2 Zinc homeostasis in *C. metallidurans*

In many bacteria, the Zur regulon is central to the zinc starvation response. Zur (Zinc Uptake Regulator) is a metalloregulatory protein from the Fur family of transcriptional regulators, with representatives regulating transcription of genes involved in iron, manganese or nickel homeostasis, or response to peroxide stress (Fillat, 2014). Zur is ubiquitous to many bacterial species, Gram-negative bacteria such as *E. coli*, or Gram-positive such as *Bacillus subtilis*, and its central function is to regulate the transcription of the set of genes which encode for proteins involved in Zn homeostasis, referred to as the Zur regulon (Patzer and Hantke, 1998; Hantke, 2005; Gaballa and Helmann, 1998).

In most cases, Zur acts as a transcriptional repressor for genes associated with the physiological response to zinc depletion. Cases in which it acts as transcriptional activator for genes that encode for transporters mediating zinc efflux or intracellular chelators, such as metallothioneins for zinc sequestration, have also been described (Huang *et al*., 2008; Choi *et al*., 2017). As a transcriptional repressor it requires both i) binding of the zinc ion as a co-repressor at the regulatory sites of each protomer and ii) binding to specific palindromic Zur boxes in the operator region in the promoter sites, which generates the $Zur_{2\text{-}4}$::Zn_2 homodimer and the subsequent zinc-dependent transcriptional repression of the regulated genes (Patzer and Hantke, 2000; Panina *et al*., 2003; Shin *et al*., 2011; Kim *et al*., 2024). In this way, Zur can regulate genes encoding for transporters involved in high-affinity zinc uptake, paralogs of zinc-dependent proteins, zinc-independent ribosomal proteins or periplasmic zinc binding chaperones, depending on the specific

requirement of each organism and the intracellular zinc status (Makarova *et al*., 2001; Panina *et al*., 2003; Graham *et al*., 2009; Ueta *et al.,* 2020).

Known high-affinity zinc uptake systems are the ZnuABC transporters, which are composed of a soluble periplasmic binding protein ZnuA, an ATPase ZnuC, and an integral membrane protein ZnuB in *E. coli, Acinetobacter baumannii* or *B. subtilis*, formerly known as YcdHI-YceA (Patzer and Hantke, 1998; Gaballa and Helmann, 1998; Hood *et al*., 2012). In contrast to the abovementioned bacterial strains and many other which possess a member of the ABC-family of transporters (TC 3.A.1) responsible for zinc uptake in low zinc availability, in *C. metallidurans* the high-affinity zinc uptake system is represented by ZupT, from the ZIP family (ZRT/IRT-like Protein) (Eide, 1998; Kirsten *et al*., 2011). Zinc homeostasis in this bacterium is additionally characterized by the formation of two intracellular zinc pools (Herzberg *et al*., 2014). Different zinc pools or speciation have been described in both bacterial or eukaryotic cells, as well as a surplus of unbound ligands which increase the zinc-buffering capacity and thus control the availability of zinc (Krezel and Maret, 2006).

4. Goal of this thesis

Zinc is an important micronutrient that is essential for the survival of living cells. It is incorporated into proteins that harness its catalytic or structural properties to sustain cellular biochemistry. Nevertheless, concentrations that are too low or too high can have detrimental effects on cell viability. Thus, maintaining enough zinc availability is an essential task of any living cell. This doctoral thesis focuses on bacterial zinc homeostasis. To that end, *C. metallidurans* was used as a model organism due to its intricate metal homeostasis pathways. Additionally, this bacterium contains three metallochaperones from the SIMIBI P-loop GTPases of the COG0523 family. The main goal of this thesis was to determine the contribution of the metallochaperones to the homeostasis of zinc.

Chapter 1 – A new model for zinc ions movement in bacterial cells

I) A flow equilibrium of zinc in cells of *Cupriavidus metallidurans*

Summary of the publication

This publication demonstrates that at the core of zinc homeostasis in *Cupriavidus metallidurans* is a kinetical flow equilibrium of simultaneously occurring import and export reactions of zinc ions. Additionally, the existence of the two zinc pools was demonstrated and experimentally measured in this bacterium.

The experimental strategy combined pulse-chase experiments with radioactive ^{65}Zn and ICP-MS measurements using the isotope-enriched stable ^{67}Zn. The plasmid-free derivative AE104 and knock-out mutants of known import and export systems, as well as cytoplasmic metal-binding components, were investigated, on one hand to measure zinc uptake and efflux using the radioactive-enriched ^{65}Zn, and on the other hand, to determine changes of zinc pools using the stable zinc isotope ^{67}Zn. Moreover, the flow equilibrium of zinc ions and the zinc pools were investigated in three conditions by cultivating cells in Tris minimal medium with different zinc availability: TMM with 200 nM $ZnCl_2$ which led to zinc-replete cells, TMM with 35 nM $ZnCl_2$ which led to zinc-starved cells and TMM with 35 nM $ZnCl_2$ and 100 µM $MgCl_2$ which led to metal-starved cells.

Mid-exponential AE104 cells were incubated with ^{67}Zn. Subsequently, two zinc contents were measured: i) a zinc pool 1 (ZP1) represented by residing zinc ions already found in the cell at the time of incubation with ^{67}Zn, and ii) a technical zinc pool 2 (ZP2) that contains the stable isotope ^{67}Zn ions after the pulse. Zinc-replete cells contained 100.000 resident zinc ions in ZP1. Incubation with 1µM of ^{67}Zn-isotope enriched solution led to the formation of ZP2 with a zinc content of 27.000 ^{67}Zn, while 76.000 zinc ions were found in ZP1. Chase with non-enriched zinc indicated export of ^{67}Zn ions.

The zinc importer ZupT had an important role in zinc homeostasis, but it was not essential for zinc import. Pulse-chase experiments done with a Δ*zupT* mutant revealed that this zinc importer is responsible for 40% of the zinc uptake rate in zinc-replete cells and 70% in zinc-starved cells. The Δ*zupT* mutant was also not able to accumulate the same zinc content as its parent strain in zinc-replete cells. Despite sufficient zinc availability in the Tris minimal medium to reach the level of its parent strain, Δ*zupT* accumulated only 42.800 zinc ions while the parent strain AE104 was able to accumulate 100.000 zinc ions.

AMERICAN SOCIETY FOR MICROBIOLOGY | Journal of Bacteriology

Check for updates

| Genetics and Molecular Biology | Full-Length Text

A flow equilibrium of zinc in cells of *Cupriavidus metallidurans*

Dietrich H. Nies,[1] Grit Schleuder,[1] Diana Galea,[1] Martin Herzberg[1,2]

AUTHOR AFFILIATIONS See affiliation list on p. 24.

ABSTRACT The hypothesis was tested that a kinetical flow equilibrium of uptake and efflux reactions is responsible for balancing the cellular zinc content. The experiments were done with the metal-resistant bacterium *Cupriavidus metallidurans*. In pulse-chase experiments, the cells were loaded with radioactive ^{65}Zn and chased with the 100-fold concentration of non-radioactive zinc chloride. In parallel, the cells were loaded with isotope-enriched stable ^{67}Zn and chased with non-enriched zinc to differentiate between zinc pools in the cell. The experiments demonstrated the existence of a kinetical flow equilibrium, resulting in a constant turnover of cell-bound zinc ions. The absence of the metal-binding cytoplasmic components, polyphosphate and glutathione, metal uptake, and metal efflux systems influenced the flow equilibrium. The experiments also revealed that not all zinc uptake and efflux systems are known in *C. metallidurans*. Cultivation of the cells under zinc-replete, zinc-, and zinc-magnesium-starvation conditions influenced zinc import and export rates. Here, magnesium starvation had a stronger influence compared to zinc starvation. Other metal cations, especially cobalt, affected the cellular zinc pools and zinc export during the chase reaction. In summary, the experiments with ^{65}Zn and ^{67}Zn demonstrated a constant turnover of cell-bound zinc. This indicated that simultaneously occurring import and export reactions in combination with cytoplasmic metal-binding components resulted in a kinetical flow equilibrium that was responsible for the adjustment of the cellular zinc content.

IMPORTANCE Understanding the biochemical action of a single enzyme or transport protein is the pre-requisite to obtain insight into its cellular function but this is only one half of the coin. The other side concerns the question of how central metabolic functions of a cell emerge from the interplay of different proteins and other macromolecules. This paper demonstrates that a flow equilibrium of zinc uptake and efflux reactions is at the core of cellular zinc homeostasis and identifies the most important contributors to this flow equilibrium: the uptake and efflux systems and metal-binding components of the cytoplasm.

KEYWORDS *Cupriavidus metallidurans*, zinc, zinc transport

No organisms are known that can survive without zinc ions, which are essential cofactors in many enzymes (1), for example, RNA polymerase (2–4). Nevertheless, zinc ions are toxic at higher concentrations. Zinc homeostasis requires a walk on a fine line between zinc starvation on the one hand and zinc toxicity on the other hand (5).

Cupriavidus metallidurans strain CH34 is a beta-proteobacterium adapted to high concentrations of zinc and other transition metal cations (6) but is surprisingly also able to manage zinc starvation conditions (7–9). It survives in environments such as zinc deserts and auriferous soils (10–13). Its genome is composed of a chromosome, a chromid, and two large plasmids, which all contain metal resistance determinants that were acquired during the evolution of this bacterium by horizontal gene transfer (6, 14–16). The high level of zinc resistance is mediated by the *czc* (cobalt-zinc-cadmium) resistance determinant on plasmid pMOL30, which encodes two inner membrane efflux

Editor Conrad W. Mullineaux, Queen Mary University of London, London, United Kingdom

Address correspondence to Dietrich H. Nies, d.nies@mikrobiologie.uni-halle.de.

The authors declare no conflict of interest.

See the funding table on p. 25.

This paper is dedicated to Simon Silver, who introduced me to the world of uptake using radioactive metal isotopes.

Received 28 February 2024
Accepted 3 April 2024
Published 25 April 2024

systems and the transenvelope efflux complex CzcCBA [Fig. 1 (5, 17)]. Without plasmid pMOL30 or *czc* on this plasmid, zinc resistance of *C. metallidurans* is on a similar level as that of *Escherichia coli* as has been determined, for instance, in the plasmid-free strain *C. metallidurans* AE104 (18, 19).

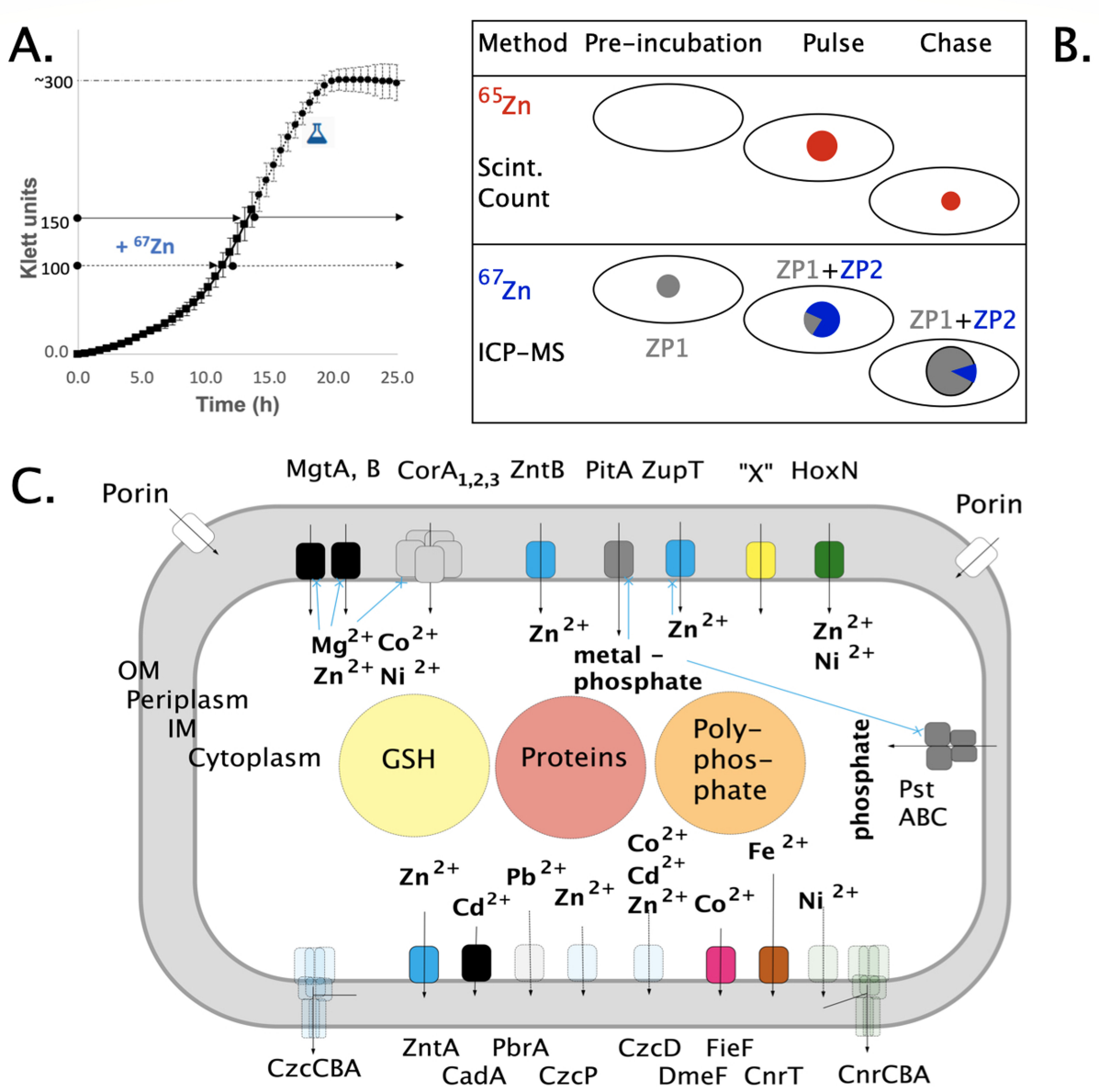

FIG 1 Schematic diagram of the methods used and the transport systems involved. Panel A. Growth curve of *C. metallidurans*. For the establishment of the method using stable ^{67}Zn, the metal was added at 100 Klett units, the cells were harvested and analyzed by inductively coupled plasma mass spectrometry (ICP-MS) at 150 Klett units. Panel B. Cells harvested at 150 Klett units were used for pulse-chase studies with radioactive ^{65}Zn (red) and in parallel with isotope-enriched ^{67}Zn (blue). The ellipsoids are the cells, the circles inside the zinc pools. Radioactive ^{65}Zn is the only zinc that can be measured with the scintillation counter. With stable isotope-enriched zinc and ICP-MS, a pool ZP1 (gray) with the natural isotope composition could be discriminated from a pool with a higher percentage of ^{67}Zn ZP2 (blue). Panel C. Transition metal cations and Mg(II) cross the outer membrane (OM) into the periplasm (gray) and further into the cytoplasm by uptake systems (on top). They can be bound inside the cells by glutathione, proteins, and polyphosphate (big circles). They may be exported from the cytoplasm to the periplasm by efflux systems (bottom row) and further on the outside by RND-driven transenvelope efflux systems (corners). Plasmid-encoded systems dashed, regulatory events concerning uptake systems (5) in blue.

Strain AE104 contains on its chromosome and chromid two inner membrane efflux pumps ZntA and CadA that belong to the P_{IB2}-type ATPases, and the two CDF proteins DmeF and FieF of the cation diffusion family of exporters [Fig. 1, (5)]. These proteins mediate in strain AE104 an IC_{50} of zinc of about 1 mM compared to 3.4 mM in pMOL30-containing strains (19). Deletion of the genes for the two P_{IB2}-type ATPases results in a decrease of the IC_{50} to 7.7 µM and this value declined only slightly further when *dmeF* and *fieF* were additionally eliminated (19) so that ZntA and CadA were responsible for zinc efflux in strain AE104. While *zntA* was similarly up-regulated by Zn(II) in the presence or absence of CadA, *cadA* was only up-regulated by Zn(II) in the absence of ZntA (20). ZntA is the main inner membrane efflux system for Zn(II) in strain AE104 and CadA with respect to zinc and especially cadmium a backup system. Expression of both genes for these P_{IB2}-type ATPases was regulated by a MerR-type regulator, ZntR and CadR, respectively (7) so that ZntR and ZntA maintain zinc homeostasis in strain AE104 at higher zinc concentrations.

Zinc ions were imported into TMM-grown AE104 cells with a K_m of 137 ± 87 µM and a v_{max} of 3.7 ± 2.1 µmol min^{-1} g^{-1} dry weight. Uptake was competitively inhibited by Mg(II) and the import rate increased sevenfold when the cells were cultivated in TMM (Tris-buffered mineral salts medium) with 100 µM Mg(II) instead of 1 mM magnesium in the standard TMM (21). Assuming a dry mass of 615 fg per cell as calculated from the cellular dimensions of *C. metallidurans* (22), the v_{max} of 3.7 ± 2.1 µmol min^{-1} g^{-1} dry weight would mean an import of 22,800 ± 13,000 Zn(II) s^{-1} $cell^{-1}$. Following Michaelis-Menten kinetics, this would mean an initial import rate at 1 µM Zn(II) of 166 ± 94 Zn(II) s^{-1} $cell^{-1}$.

Responsible for zinc import into *C. metallidurans* cells are at least nine import systems (Fig. 1). The ZIP protein [TC 2.A.5; Transporter Classification Database; (23, 24)] ZupT is up-regulated under conditions of zinc starvation (25). Expression of *zupT* is controlled by the zinc uptake regulator Zur, as in many bacteria (8, 9, 26–29). Four MIT (TC 1.A.35) proteins, $CorA_1$, $CorA_2$, $CorA_3$, and ZntB, are not regulated by zinc but $CorA_1$ is by magnesium (25) and the metal-phosphate importer PitA of the PiT family (protein inorganic transport family, TC 2.A.20) by phosphate. The HoxN NiCoT (Nickel-cobalt transporter family, TC 2.A.52) protein should be mainly a Ni(II) importer and the two P-type ATPases (TC 3.A.3) MgtA and MgtB Mg(II)/Ca(II) importers (25, 30). *C. metallidurans* does not contain an ABC-type (TC 3.A.1) zinc importer such as ZnuABC from *E. coli* (25, 27, 31, 32) so ZupT is an important zinc importer in this bacterium.

Deletion of *zupT* leads to a pleiotropic phenotype, for instance lacking incorporation of zinc into the beta-prime subunit RpoC of the RNA polymerase, although the cells were very well able to import zinc ions (33). Deletion of all seven known secondary zinc importers ZupT, $CorA_1$, $CorA_2$, $CorA_2$, ZntB, PitA, and HoxN (Fig. 1) in mutant strain Δ7 did not abolish zinc import but reduced fitness and metal resistance of the cells (34). Not even the additional deletion of *mgtA* and *mgtB* in the mutant strain Δ9 prevented zinc uptake but decreased the fitness of the cell even more (30, 34) so that at least one additional zinc import pathway exists in *C. metallidurans* (Fig. 1C, upper row, yellow "X").

The uptake and efflux systems of *C. metallidurans* strain AE104 may be responsible for the cellular zinc content as the result of a kinetical flow equilibrium with the activity of the individual transport systems regulated by gene expression, flux control, and other processes (5, 35, 36). Such a flow equilibrium would be a futile cycle that is required to constantly adjust the composition of the cellular metal pool and the concentration of each metal, all in cooperation with the metal-binding capacity of the cytoplasm. This process would be at the core of the multiple metal homeostasis of the cell; however, its very existence has not been demonstrated.

If such a kinetical flow equilibrium exists, metal ions should be continuously imported and exported into and out of the cell. Cells incubated with radioactive ^{65}Zn should import the metal cation. Subsequent incubation with a higher concentration of non-radioactive Zn(II) (pulse-chase experiment) should not only decrease the uptake rate by dilution of the radioactive substrate but should result in a decrease of the

^{65}Zn content of the cells (Fig. 1B). The flow equilibrium should be altered in the absence of uptake and efflux systems. Metal starvation conditions, leading to up- or down-regulation of transport systems, are supposed to change the flow equilibrium too. Moreover, different media should influence the supply of zinc ions and other metals to metal-requiring enzymes. To analyze the zinc pools in *C. metallidurans*, additionally, the stable zinc isotope ^{67}Zn was used. This allows to accompany the ^{65}Zn with parallel ^{67}Zn pulse-chase experiments to discriminate between zinc that was originally present in the cells with a natural isotope composition, isotope-enriched zinc that is accumulated by the cells during the pulse phase, and the change of both zinc pools during the chase (Fig. 1B). In this publication, we show that a flow equilibrium of zinc import and export indeed exists and that this flow equilibrium impacts with the zinc pools of the *C. metallidurans* cell.

RESULTS

Experimental approach and outline

To investigate the kinetical flow equilibrium of zinc in the plasmid-free strain *C. metallidurans* AE104 and the influence of this flow equilibrium on the zinc pools in the cell, radioactive ^{65}Zn was used to measure the zinc uptake and efflux reactions (Fig. 1). This work was mainly carried out with the plasmid-free *C. metallidurans* strain AE104 and its mutants (Table S1) because deletion of *zupT* for this important zinc importer is only possible in the absence of the plasmids (18, 33). For the pulse-chase experiments, the cells were loaded for 20 min with 1 µM ^{65}Zn and subsequently chased with 100 µM non-radioactive zinc (Fig. 1 and 2). Controls were not chased. Experiments with other metals or 1 mM zinc were also performed.

In parallel, stable enriched ^{67}Zn was employed to determine changes in the cellular zinc pool. Here, the cells were loaded with 1 µM ^{67}Zn and chased with 100 µM zinc ions that were not enriched in ^{67}Zn. After harvest, the cellular zinc content was determined using inductively coupled plasma-mass spectrometry (ICP-MS). The natural isotope composition of stable zinc is 48.6% ^{64}Zn, 27.9% ^{66}Zn, 4.1% ^{67}Zn, and 0.6% ^{70}Zn (37). The ICP-MS procedure measures the abundance of every isotope and calculates from each of these results the amount of total zinc by dividing it by the percentage of the respective isotope in the natural isotope composition. Using a solution with 94% ^{67}Zn leads to an over-calculation of the total amount of zinc in the ^{67}Zn compared to the ^{64}Zn channel. From the ^{64}Zn- and over-calculated ^{67}Zn-values, the amount of zinc in the zinc pool ZP1 with the natural isotope composition can be calculated, and that of ZP2, which represents the additional zinc pool stemming from the ^{67}Zn-isotope-enriched solution. That way, two zinc pools can be measured with ^{67}Zn. By contrast, the method using radioactive ^{65}Zn determines only this isotope (Fig. 1).

After the kinetical flow equilibrium had been analyzed in *C. metallidurans* AE104, other transition metal cations were also used for the chase period. The influence of metal uptake, efflux, and metal-binding cellular components on the zinc pools and the flow equilibrium was characterized using mutants of *C. metallidurans* AE104 (Table S1). Finally, *C. metallidurans* CH34 wild type was included, which possessed all the plasmid-encoded metal transport systems (Fig. 1).

Proof of concept for the methodology used

All bacteria were cultivated in three derivatives of the Tris-buffered mineral salts medium TMM (18) with gluconate as the carbon source to the exponential phase of growth (Fig. 1). In moderate zinc medium mZn, the zinc content was adjusted to 200 nM. The second medium was a low zinc medium lZn that was TMM without the trace element solution SL6 (38) and contained 35.2 ± 30.4 nM zinc. It was used to investigate the influence of zinc starvation on the flow equilibrium of zinc. The third medium did not contain SL6 and also a lowered magnesium concentration of 0.1 mM instead of 1 mM so that magnesium starvation was added on top of the zinc starvation condition.

To obtain a proof of concept for the usage of ^{67}Zn to measure different zinc pools in the cell, the cells were cultivated in these three media with Zn(II) present in the natural isotope composition to the mid-exponential phase of growth at 150 Klett units (Fig. 1) and harvested. The zinc content was determined by ICP-MS (Table S2). The cellular zinc content was at the expected and published level of 100,000 Zn per cell in the presence of 200 nM Zn(II) in mZn-TMM medium and lower zinc contents under zinc starvation conditions. The total zinc content of the cells as determined by the ICP-MS method was a half-exponential function of the zinc content of the growth medium (Fig. S1A). No zinc appeared in the zinc pool ZP2, which was an indicator of imported zinc from the ^{67}Zn-isotope-enriched solution. All zinc resided in the ZP1, which represented zinc in the natural isotope composition.

In the next step, 1, 10, or 100 µM of ^{67}Zn-isotope-enriched or not -enriched solution was added at a turbidity of 100 Klett units and the cells were harvested at 150 Klett units, which was still in the mid-exponential phase of growth (Fig. 1A). With increasing zinc concentration, the total zinc content ZP1 + ZP2 increased to very similar levels in cells cultivated in the three different media, in the absence or presence of ^{67}Zn-isotope-enriched solution (Table S2). But zinc appeared in ZP2 only when ^{67}Zn-isotope-enriched solution was used. Moreover, the zinc content in ZP2 increased at the cost of a decreasing zinc content in ZP1. When 1 to 100 µM zinc was added to the cells, zinc that was already residing in the cells in ZP1 with the natural isotope composition was exchanged against incoming isotope-enriched ^{67}Zn that went into ZP2 (Table S2). There was no influence of the usage of ^{67}Zn-isotope-enriched zinc solution on the content of other metals in *C. metallidurans* (Table S3).

A ^{67}Zn-isotope-enriched zinc solution could be used to discriminate between incoming zinc (ZP2, isotope-enriched) and already residing zinc (ZP1, natural isotope composition). This method strictly depended on the usage of the ^{67}Zn-isotope-enriched zinc solution and did not influence the cellular content of other metals. Moreover, first evidence was obtained that cell-bound zinc was exchanged for incoming zinc.

Compared to the zinc content determined by the ICP-MS method, the content of radioactive ^{65}Zn increased with a double-logarithmical function (Fig. S1B). This was due to different procedures used to harvest the cells, rapid filtration and quick washing with ^{65}Zn, centrifugation, and washing for the determination by ICP-MS. At 1 µM and incubation times of 2 h and below, the ^{65}Zn data were in the same range as ZP2 determined with ^{67}Zn so both methods gave compatible results when the cells were loaded for 20 min with 1 µM Zn(II), between 70,000 and 100,000 zinc per cell.

In summary, at zinc concentrations up to 1 µM, determination of the cellular zinc content using radioactive zinc and by ICP-MS gave similar results. At higher zinc concentrations, labeling with radioactive zinc yielded a higher cellular zinc content than centrifugation followed by ICP-MS measurement, indicating that the ^{65}Zn method revealed a more loosely bound zinc pool than the ICP-MS method.

C. metallidurans strain AE104 as a reference point

Pulse-chase experiments with the plasmid-free *C. metallidurans* strain AE104 were performed in moderate zinc medium mZn-TMM adjusted to 200 nM Zn(II), in low zinc lZn and low zinc, low magnesium lZn_lMg medium, yielding zinc-replete, zinc-starved, and metal-starved cells, respectively. After loading with 1 µM of radioactive ^{65}Zn, the cells were chased with 1 mM or 100 µM non-radioactive zinc (Fig. 2), 100 µM of other metal cations, or the metal chelator EDTA (ethylenediaminetetraacetate) (Fig. 2; Fig. S2). From these data, the initial uptake $v_{up}(0)$, initial efflux rate $v_{eff}(0)$ at the beginning of the chase, zinc contents after 20 min C_{20}, extrapolated zinc equilibrium content after the uptake phase C_{max}, calculated zinc content at the beginning of the chase C_0, and zinc content after 40 min C_{40} were determined, ZP1 and ZP2 in parallel experiments with isotope-enriched zinc (Tables 1 to 4)

The mean initial uptake velocity $v_{up}(0)$ of all these experiments was 162 ± 25 ^{65}Zn cell^{-1} s^{-1} in mZn-TMM and 1,147 ± 351 ^{65}Zn cell^{-1} s^{-1} under zinc and magnesium

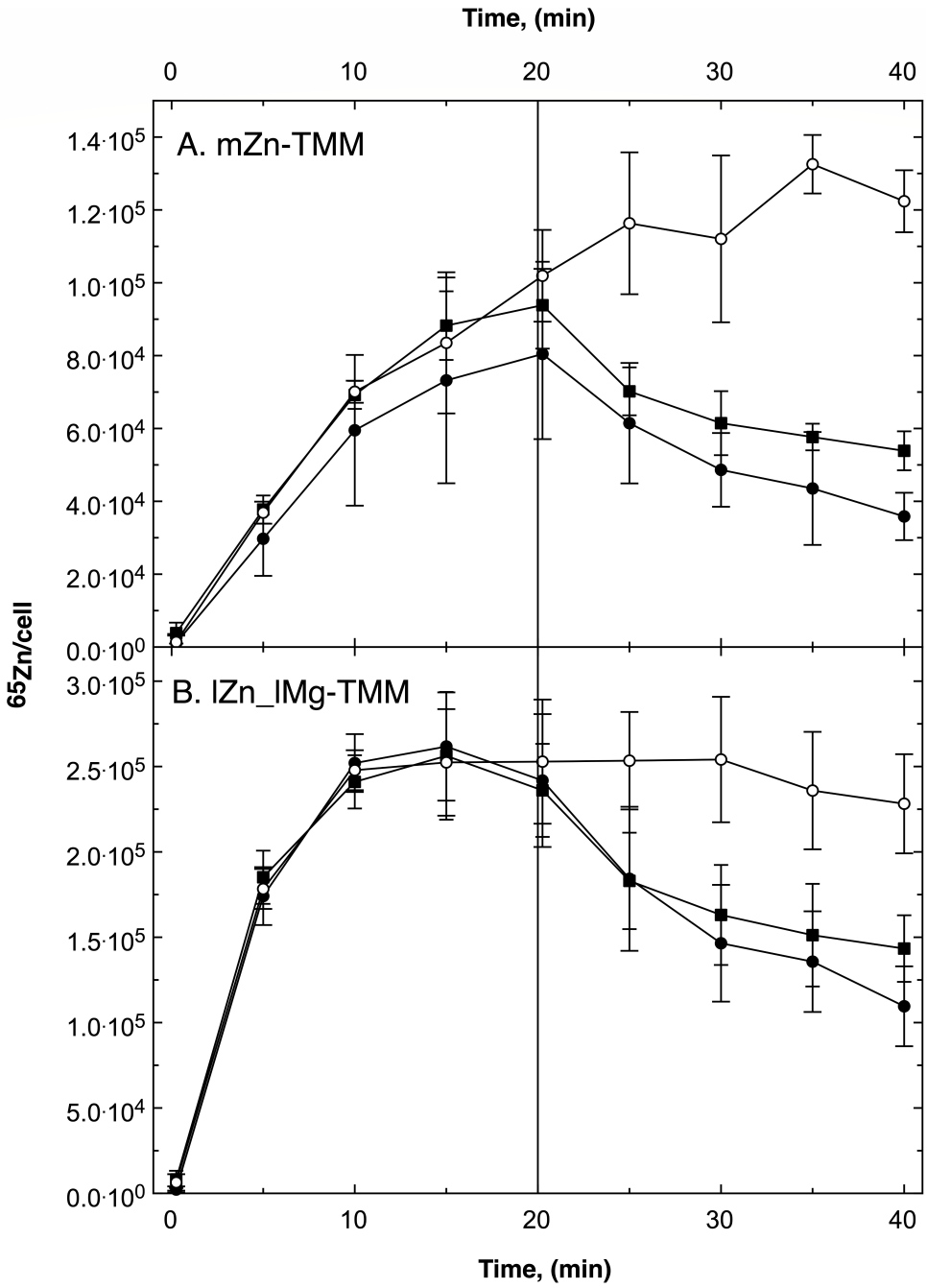

FIG 2 Pulse-chase experiment with *C. metallidurans* strain AE104 and zinc. The cells were cultivated in TMM containing 200 nM Zn(II) (mZn-TMM, Panel A) or in a low metal medium without added zinc and 100 µM Mg(II) instead of 1 mM (lZn_lMg-TMM, Panel B). A preculture of the same medium was used. At turbidity of 150 Klett units, the cells were harvested by centrifugation, suspended in an equal volume of 10 mM TrisHCl (pH 7.0), and stored on ice until needed but no longer than a few hours. To 6 mL of this cell suspension, 2 g/L Na gluconate was added before the experiment. The uptake reaction (pulse) was started by the addition of 12 µL ^{65}Zn (500 µM, 12 µCi, 1 µM final concentration). The cells were incubated with shaking at 30°C. Samples of 500 µL were collected by filtration (0.2 µm pore size), washed twice with 5 mL ice-cold wash solution (50 mM Tris-HCl pH 7.0, 50 mM EDTA), and radioactivity was measured in a scintillation counter. After 20 min (bar), non-radioactive Zn(II) was added (chase) to a final concentration of 100 µM (closed circles), 1 mM (closed squares) or not (open circles) and sampling was continued. Three biological repeats and deviation bars are given.

TABLE 1 Pulse-chase with *C. metallidurans* strain AE104[a]

Chase		None	Zn(II)	Zn(II)	EDTA	Ni(II)	Co(II)	Cd(II)	Mn(II)	Mg(II)
Concentration		**0**	**1 mM**	**100 µM**						
mZn-TMM										
C_{max}-uptake	1,000 /cell	263 ± 61	229 ± 48	250 ± 98	260 ± 36	204 ± 5	152 ± 7	160 ± 10	215 ± 14	174 ± 18
$v_{up}(0)$	1 /s	145 ± 34	153 ± 32	115 ± 45	150 ± 21	165 ± 4	195 ± 9	187 ± 11	161 ± 11	184 ± 19
Coefficient		99.6%	99.5%	99.2%	99.8%	100.0%	99.9%	99.9%	99.9%	99.7%
C_o-efflux	1,000 /cell	*86 ± 1*	146 ± 2	170 ± 2	255 ± 4	156 ± 1	165 ± 1	*90 ± 0*	141 ± 0	120 ± 1
$v_{eff}(0)$	1 /s	−14 ± 0	64 ± 1	112 ± 1	214 ± 3	57 ± 0	79 ± 1	*−5 ± 0*	42 ± 0	20 ± 0
Coefficient		*79.7%*	93.9%	98.9%	98.2%	99.2%	98.5%	*−69.0%*	99.2%	93.7%
Low metal lZn_lMg										
C_{max}-uptake	1,000 /cell	315 ± 27	289 ± 27	319 ± 43	418 ± 59	486 ± 60	421 ± 64	456 ± 42	525 ± 102	327 ± 34
$v_{up}(0)$	1 /s	1,430 ± 123	1,812 ± 167	1,355 ± 184	943 ± 134	836 ± 103	954 ± 144	894 ± 82	764 ± 149	1,336 ± 138
Coefficient		96.3%	92.5%	92.5%	97.5%	98.9%	97.2%	99.2%	98.0%	95.8%
C_o-efflux	1,000 /cell	290 ± 1	354 ± 4	495 ± 5	512 ± 5	529 ± 6	483 ± 6	323 ± 1	535 ± 4	372 ± 4
$v_{eff}(0)$	1 /s	27 ± 0	141 ± 2	314 ± 3	285 ± 3	271 ± 3	251 ± 3	18 ± 0	273 ± 2	142 ± 2
Coefficient		88.2%	94.6%	98.4%	97.5%	96.6%	96.1%	80.2%	98.2%	93.5%

[a]*C. metallidurans* strain AE104 was cultivated in moderate zinc (mZn) or low zinc-low magnesium (lZn_lMg) medium to a turbidity of 150 Klett units, harvested by centrifugation and resuspended in uptake buffer. The cells were kept in ice until needed. Na gluconate was added to a final concentration of 2 g/L, the experiment started by adding 1 µM ^{65}Zn (60 nCi/mL), and the cells were incubated with shaking at 30°C. Samples (500 µL) were removed after 0.25, 5, 10, and 15 min. At 20 min, non-radioactive Zn(II), other metal cation, or EDTA was added and samples were removed at 20.25, 25, 30, 35, and 40 min. The samples were filtrated through membrane filters with a pore diameter of 0.2 µm and immediately washed twice with 5 mL ice-cold washing buffer (50 mM Tris-HCl, pH 7.0; 50 mM EDTA). Radioactivity was measured using a scintillation counter. The number of ^{65}Zn atoms per cell was determined from the cpm values, the number of cells per mL, and the total radioactivity in 100 µL cell suspension. At least three biologically independent experiments were done. The number of ^{65}Zn per cell before the chase was adapted in a Lineweaver-Burke-like plot to the function "1 /C = 1/C_{max} + $t_{0.5}$/C_{max}*t." v_{up} is the first deviation of time at t = 0 of this function, v_{up} = C_{max}/$t_{0.5}$. After the chase, the number of ^{65}Zn per cell was adapted to an exponential decay-curve "C = C_o * e^(τ*t)" with $t_{0.5}$ =ln(2)/τ. v_{eff} is the first deviation of time at t = 0 of this function, v_{eff} = −τ*C_0. The regression coefficients of these curve fittings are given. Numbers in italics indicate a coefficient <80%.

TABLE 2 Summary of the ^{65}Zn pulse-chase experiments[a]

Medium	Uptake (pulse)			Chase		Pulse continued (control)	
Strains	v_{up} (s^{-1}), % AE104	C_{20}, 1000 Zn/cell	C_{max}/C_{20}	v_{eff} (s^{-1}), % AE104	C_{40}/C_{20}	v_{eff} (s^{-1}), % AE104	C_{40}/C_{20}
Moderate Zn							
AE104	162 ± 25; 100% ± 15%	96 ± 7; 100% ± 7%	2.20	112.3 ± 1.0; 100.0% ± 0.9%	37.2% ± 6.7%	−14.4 ± −0.2; −12.8% ± −0.2%	127.0% ± 8.8%
Chase with 1 mM				63.9 ± 0.9; 58.9% ± 0.8%	57.4% ± 5.7%		
AE104, ^{63}Ni	934 ± 551	93 ± 12 (10^3 Ni/cell)	1.05	8.7 ± 0.0; 100.0% ± 0.1%	86.0% ± 6.3%	−13.2 ± 0.0; −152.0% ± −0.2%	107.6% ± 19.8%
Δ*zupT*	94 ± 7; 58% ± 4%	64 ± 4; 66% ± 4%	2.67	38.8 ± 0.3; 34.5% ± 0.2%	46.4% ± 12.7%	2.1 ± 0.0; 1.9% ± 0.0%	102.5% ± 2.5%
Δ7	211 ± 117; 131% ± 73%	37 ± 6; 39% ± 6%	1.37	11.4 ± 0.1; 10.2% ± 0.1%	71.8% ± 11.2%	5.8 ± 0.0; 5.2% ± 0.0%	67.6% ± 8.7%
Δ9	356 ± 57; 220% ± 36%	88 ± 2; 91% ± 2%	1.46	15.0 ± 0.1; 13.3% ± 0.1%	77.5% ± 2.2%	12.3 ± 0.0; 10.9% ± 0.0%	83.9% ± 25.4%
Δe2	84 ± 4; 52% ± 2%	73 ± 2; 76% ± 2%	5.54	29.0 ± 0.1; 25.8% ± 0.1%	64.5% ± 7.3%	−18.3 ± 0.0; −16.3% ± 0.0%	133.0% ± 6.4%
Δe4	68 ± 8; 42% ± 5%	62 ± 1; 64% ± 1%	8.34	18.5 ± 0.0; 16.5% ± 0.0%	70.2% ± 5.2%	−9.7 ± 0.0; −8.7% ± 0.0%	117.5% ± 6.9%
Δ*ppk*	71 ± 30; 44% ± 19%	45 ± 8; 47% ± 8%	4.72	13.2 ± 0.0; 11.7% ± 0.0%	85.6% ± 29.6%	−22.5 ± −0.2; −20.0% ± −0.2%	159.6% ± 52.3%
Δ*gshA*	63 ± 10; 39% ± 6%	42 ± 0; 44% ± 0%	2.67	26.9 ± 0.3; 23.9% ± 0.3%	37.9% ± 8.5%	−5.1 ± 0.0; −4.5% ± 0.0%	111.6% ± 60.5%
CH34	146 ± 17; 90% ± 11%	30 ± 1; 31% ± 1%	1.05	4.7 ± 0.0; 4.2% ± 0.0%	83.4% ± 29.7%	−10.3 ± 0.0; −9.2% ± 0.0%	148.9% ± 49.9%
Chase with 1 mM				11.0 ± 0.1; 9.8% ± 0.0%	63.6% ± 6.5%		
CH34 induced	69 ± 11; 43% ± 7%	27 ± 5; 28% ± 6%	1.75	0.5 ± 0.0; 0.5% ± 0.0%	122.3% ± 62.6%	−12.8 ± −0.1; −11.4% ± −0.1%	169.0% ± 74.9%
Chase with 1 mM				16.0 ± 0.2; 14.2% ± 0.2%	53.2% ± 35.5%		
Low zinc							
AE104	227 ± 17; 100% ± 8%	92 ± 3; 100% ± 3%	1.62	125.4 ± 1.3; 100.0% ± 1.0%	45.2% ± 16.6%	−11.2 ± −0.1; −8.9% ± −0.1%	128.1% ± 10.4%
Δ*zupT*	67 ± 1; 30% ± 0%	63 ± 4; 68% ± 4%	7.44	15.4 ± 0.1; 12.2% ± 0.0%	67.7% ± 2.1%	−6.7 ± 0.0; −5.3% ± 0.0%	118.8% ± 12.9%
Low Zn and Mg							
AE104	1147 ± 351; 100% ± 31%	272 ± 28; 100% ± 10%	1.45	314.4 ± 3.0; 100.0% ± 0.9%	40.2% ± 8.6%	27.1 ± 0.1; 8.6% ± 0.0%	83.8% ± 10.7%
AE104, Ni	1,911 ± 218	387 ± 22	1.26	63.5 ± 0.1; 100.0% ± 0.1%	77.6% ± 6.2%	−12.7 ± 0.0; −19.9% ± 0.0%	100.6% ± 12.5%
Δ*zupT*	509 ± 10; 44% ± 1%	115 ± 4; 42% ± 1%	1.38	53.3 ± 0.2; 16.9% ± 0.1%	52.5% ± 12.3%	−2.1 ± 0.0; −0.7% ± 0.0%	101.4% ± 11.4%
Δ7	212 ± 39; 18% ± 3%	45 ± 6; 17% ± 2%	1.46	9.5 ± 0.0; 3.0% ± 0.0%	65.8% ± 12.7%	4.6 ± 0.0; 1.5% ± 0.0%	96.5% ± 5.9%
Δ9	281 ± 189; 24% ± 16%	50 ± 12; 18% ± 4%	1.40	6.6 ± 0.0; 2.1% ± 0.0%	69.0% ± 2.3%	2.9 ± 0.0; 0.9% ± 0.0%	100.9% ± 16.6%
Δe2	812 ± 66; 71% ± 6%	244 ± 4; 90% ± 2%	1.42	85.0 ± 0.1; 27.0% ± 0.0%	67.3% ± 10.0%	34.6 ± 0.1; 11.0% ± 0.0%	88.6% ± 5.5%
Δe4	479 ± 1; 42% ± 0%	197 ± 27; 73% ± 10%	1.59	28.5 ± 0.0; 9.1% ± 0.0%	74.3% ± 4.3%	14.9 ± 0.0; 4.7% ± 0.0%	104.7% ± 7.9%
Δ*ppk*	378 ± 60; 33% ± 5%	177 ± 8; 65% ± 3%	2.04	81.3 ± 0.3; 25.9% ± 0.1%	55.1% ± 17.5%	−6.3 ± 0.0; −2.0% ± 0.0%	110.8% ± 6.7%
Δ*gshA*	797 ± 407; 69% ± 36%	99 ± 15; 36% ± 6%	1.23	50.6 ± 0.4; 16.1% ± 0.1%	40.6% ± 9.6%	−0.1 ± 0.0; 0.0% ± 0.0%	106.2% ± 13.9%

[a]As in Table 1 but additionally low zinc medium lZn was used for strain AE104 and its Δ*zupT* mutant.

TABLE 3 Pulse with ^{67}Zn, chase with other metals in strain AE104[a]

Medium	10^3 Zn			Metal of chase[b]	All except chase[c]	
Chase	ZP1	ZP2	ZP1 + 2			
mZn-TMM						
Initial cells	76.3 ± 4.7	< 0 ± .2	76.2 ± 4.9			
^{67}Zn-pulse	59.5 ± 0.7	22.4 ± 1.4	81.9 ± 2.1			
Chase Ni	54.9 ± 1.4	28.2 ± 0.4	83.2 ± 1.8	86.2 ± 2.9	3.3 ± 0.1	10^3 Ni
Chase Co	50.4 ± 1.8	17.5 ± 1.1	67.8 ± 2.9	197 ± 8	9 ± 1	10^3 Co
Chase Cd	47.8 ± 1.3	13.4 ± 0.3	61.2 ± 1.6	103 ± 3	0 ± 0	10^3 Cd
Chase Mn	54.7 ± 0.7	33.2 ± 0.9	87.8 ± 1.6	44.1 ± 4.3	0.2 ± 0.1	10^3 Mn
Chase Mg	52.4 ± 1.2	30.9 ± 1.0	83.3 ± 2.3	9.62 ± 0.17	9.64 ± 0.31	10^6 Mg
Chase EDTA	50.1 ± 3.9	13.9 ± 1.1	64.0 ± 5.0			
lZn_lMg-TMM						
Initial cells	3.5 ± 1.1	0.0 ±< 0	3.5 ± 1.1			
^{67}Zn-pulse	4.7 ± 0.3	70.6 ± 5.5	75.3 ± 5.8			
Chase Ni	7.3 ± 0.8	46.8 ± 1.0	54.2 ± 1.8	278 ± 6.3	5.0 ± 0.3	10^3 Ni
Chase Co	5.7 ± 2.4	35.2 ± 1.8	40.9 ± 4.2	564 ± 15	0.3 ± 0.3	10^3 Co
Chase Cd	5.1 ± 1.3	44.1 ± 0.3	49.2 ± 1.5	89.1 ± 7.0	0.3 ± 0.4	10^3 Cd
Chase Mn	5.9 ± 1.1	71.2 ± 2.7	77.1 ± 3.8	43.6 ± 2.3	0.4 ± 0.3	10^3 Mn
Chase Mg	5.4 ± 0.5	72.3 ± 1.9	77.8 ± 2.4	10.1 ± 0.4	10.1 ± 0.5	10^6 Mg
Chase EDTA	4.5 ± 0.7	48.3 ± 2.8	52.8 ± 3.5			

[a]The cells were cultivated in moderate zinc (mZn) or low zinc, low magnesium medium (lZn-lMg) and loaded with 1 µM ^{67}Zn for 20 min at 30°C with shaking, followed by 100 µM of other metal cations or EDTA. Samples for the metal determination by ICP_MS were taken before and after the uptake period as well as after the chase.
[b]This lists only the content of a metal cation used for the chase after the chase period with this metal.
[c]This lists the mean values for all the other experiments. At least three experiments and deviation are indicated. Please note that the magnesium content is millions of atoms per cell, that of the other metal thousand atoms per cell.

starvation conditions (Table 1), respectively, which was a sevenfold increase as previously published (21). Moreover, since the expected $v_{up}(0)$ at 1 µM Zn was 166 ± 94 Zn(II) s^{-1} $cell^{-1}$, the measured $v_{up}(0)$ was in agreement with previously published experiments (21). Metal-starved cells displayed a higher initial zinc import rate than cells that had been cultivated under zinc-replete conditions.

Zinc-replete AE104 accumulated C_{20} = 96,000 ^{65}Zn atoms within 20 min (Table 2). The ratio C_{max}/C_{20} indicated that an equilibrium had not been reached within this time period. Consequently, the non-chased cells continued to accumulate ^{65}Zn to a level of about 130,000 ^{65}Zn per cell (Fig. 2). When chased with 100 µM non-radioactive zinc, the cellular ^{65}Zn content decreased with an initial net efflux rate of 112 ± 1 ^{65}Zn $cell^{-1}$ s^{-1} to a level of 37% of the C_{20} level (C_{40}/C_{20}) at the end of the experiment. As measured with stable, isotope-enriched ^{67}Zn, zinc-replete AE104 contained 103,000 zinc atoms per cell at the beginning of the uptake period (Table 4). After the uptake period, the total number of zinc ions remained the same; however, the initial zinc in ZP1 decreased to 76,600 Zn per cell and 26.4% of the zinc was now present in ZP2. After the chase with non-isotope-enriched zinc, the zinc content of the cells increased to 260,000 Zn per cell but only 2.5% resided in ZP2.

In zinc-replete AE104 cells, about 25% of the zinc ions were exchanged against incoming zinc ions at the uptake period. These zinc ions in ZP2 were subsequently exported again during the chase period. These data were in full agreement with a flow equilibrium governing the cellular zinc content. Zinc ions were constantly imported into and exported from the cells (Fig. 2).

Metal-starved AE104 cells that accumulated zinc with a sevenfold higher $v_{up}(0)$ compared to zinc-replete cells already reached an equilibrium of the cellular zinc content after 15 min at 272,000 ^{65}Zn per cell (Fig. 2B; Table 2). After 20 min, even the non-chased control cells exported zinc with $v_{eff}(0)$ = 27 ^{65}Zn $cell^{-1}$ s^{-1}, the cells chased with 100 µM non-radioactive zinc with 314 ± 3 ^{65}Zn $cell^{-1}$ s^{-1} (Tables 1 and 2). As determined with ^{67}Zn, the initial zinc content at the onset of the experiment was about 30,000 Zn per cell,

TABLE 4 Summary of the experiments with stable ^{67}Zn that accompanied the pulse-chase experiments with radioactive ^{65}Zn[a]

Strains	Initial 10^3 Zn			10^3 Zn after pulse			10^3 Zn after chase (0.1 mM)		
Medium	**ZP1**	**ZP2; %ZPt**	**ZP1 +ZP2**	**ZP1**	**ZP2; %ZPt**	**ZP1 +ZP2**	**ZP1**	**ZP2; %ZPt**	**ZP1 +ZP2**
Moderate Zn									
AE104	103 ± 9	0.0 ± 0.2; 0.0%	103 ± 9	76.6 ± 1.8	27.4 ± 2.2; 26.4%	104 ± 4	240 ± 20	6.1 ± 0.8; 2.5%	246 ± 21
Chase 1 mM							2,401 ± 420	6.3 ± 0.1; 0.3%	2,407 ± 420
Δ*zupT*	42.8 ± 1.8	<0	42.6 ± 1.7	37.8 ± 2.1	20.5 ± 1.2; 35%	58.3 ± 3.3	226 ± 15	4.1 ± –0.1; 2%	230 ± 14
Δ7	44.0 ± 2.3	<0	43.9 ± 2.2	36.5 ± 2.2	17.3 ± 0.6; 32%	53.8 ± 2.8	272 ± 22	4.5 ± 0.3; 2%	276 ± 22
Δ9	40.3 ± 2.3	<0	40.2 ± 2.4	32.8 ± 2.0	13.2 ± 0.9; 29%	46.0 ± 2.9	204 ± 8	4.1 ± 0.0; 2%	209 ± 8
Δe2	91.5 ± 3.8	<0	91.2 ± 3.8	76.2 ± 3.9	27.5 ± 3.2; 27%	104 ± 7	535 ± 49	7.4 ± –0.9; 1%	542 ± 48
Δe4	84.4 ± 3.1	<0	84.2 ± 3.1	78.5 ± 4.8	23.2 ± 0.3; 23%	102 ± 5	502 ± 49	7.2 ± –0.3; 1%	509 ± 49
Δ*ppk*	88.7 ± 4.1	<0	88.3 ± 4.1	67.4 ± 3.2	22.9 ± 3.3; 25%	90.4 ± 6.4	201 ± 19	4.1 ± 0.3; 2%	206 ± 19
Δ*gshA*	75.2 ± 1.6	<0	75.0 ± 1.6	60.8 ± 1.1	15.4 ± 0.2; 20%	76.2 ± 1.3	179 ± 6	3.5 ± 0.2; 2%	183 ± 6
CH34	77.0 ± 1.8	<0	76.6 ± 1.8	65.9 ± 0.7	11.5 ± 0.7; 15%	77.4 ± 1.4	150 ± 3	3.2 ± 0.0; 2%	153 ± 3
Chase 1 mM							864 ± 32	<0	863 ± 32
CH34 induced	235 ± 11	<0	234 ± 10	192 ± 6	0.20 ± 0.04; 0%	192 ± 6	215 ± 4	<0	214 ± 4
Chase 1 mM							429 ± 31	<0	428 ± 31
Low Zn									
AE104	11.0 ± 1.9	0.0 ± 0.0; 0.1%	11.1 ± 1.9	6.7 ± 0.7	79.4 ± 5.3; 92.3%	86.1 ± 6.0	181 ± 17	24.6 ± 1.4; 12.0%	206 ± 19
Chase 1 mM							6,171 ± 118	24.1 ± –0.1; 0.4%	6,195 ± 118
Δ*zupT*	43.2 ± 1.4	<0	43.0 ± 1.4	37.0 ± 0.8	30.8 ± 2.5; 45%	67.8 ± 3.3	190 ± 8	6.9 ± 0.2; 4%	197 ± 8
Low Zn and Mg									
AE104	29.5 ± 10.2	0.5 ± 0.0; 1.6%	30.0 ± 10.1	6.3 ± 1.3	85.0 ± 3.9; 93.1%	91.3 ± 5.3	201 ± 33	25.4 ± 2.0; 11.2%	226 ± 35
Chase 1 mM							5,261 ± 552	27.0 ± –1.1; 0.5%	5,288 ± 551
Δ*zupT*	8.3 ± 0.8	<0	8.3 ± 0.8	8.0 ± 0.3	57.4 ± 3.0; 88%	65.4 ± 3.3	169 ± 22	13.9 ± 0.3; 8%	183 ± 22
Δ7	10.4 ± 0.8	<0	10.3 ± 0.8	9.00 ± 1.4	67.4 ± 4.4; 88%	76.4 ± 5.8	248 ± 24	20.2 ± 1.1; 8%	268 ± 25
Δ9	8.5 ± 1.4	0.0 ± 0.0; 0%	8.5 ± 1.4	8.00 ± 1.2	75.8 ± 10.8; 90%	83.8 ± 12.0	404 ± 67	19.2 ± 1.6; 5%	423 ± 68
Δe2	8.6 ± 0.6	0.0 ± 0.0; 0%	8.6 ± 0.6	8.8 ± 0.8	97.1 ± 3.7; 92%	106 ± 5	560 ± 18	38.2 ± 3.0; 6%	599 ± 21
Δe4	7.6 ± 0.8	0.0 ± 0.0; 0%	7.6 ± 0.8	8.1 ± 0.3	91.6 ± 5.1; 92%	99.7 ± 5.5	767 ± 100	37.1 ± –0.4; 5%	805 ± 99
Δ*ppk*	7.7 ± 1.0	0.0 ± 0.0; 0%	7.7 ± 1.0	8.9 ± 0.6	75.7 ± 3.7; 89%	84.6 ± 4.3	161 ± 11	20.2 ± –0.1; 11%	181 ± 11
Δ*gshA*	7.6 ± 0.2	<0	7.6 ± 0.2	10.4 ± 3.0	50.2 ± 2.9; 83%	60.5 ± 5.8	165 ± 21	16.5 ± 0.1; 9%	182 ± 21

[a]The cells of the indicated *C. metallidurans* mutants were incubated in Tris-buffered mineral salts medium adjusted to 200 nM Zn(II) (moderate zinc), the same medium without trace element solution SL6 and 0.1 mM Mg(II) instead of 1 mM Mg(II) (low Zinc and Mg) or TMM medium without SL6 but 1 mM Mg(II) (low Zn). Zinc coming from SL6 or contaminations was in the natural isotope composition. These cells were incubated with 1 µM enriched stable ^{67}Zn for 20 min (pulse) and subsequently chased with 100 µM Zn(II) (or 1 mM when indicated) with the natural isotope composition again. The zinc pools ZP1 and ZP2 were calculated from the ICP-MS measurements and ZPt = ZP1+ZP2 was determined.

increased to about 90,000 Zn per cell after the uptake period with 1 µM ^{67}Zn with most of this zinc residing in ZP2. Comparable to zinc-replete cells, about ¾ of the zinc in ZP2 was removed again in the subsequent chase period (Table 4).

To analyze, whether this increased uptake rate was caused by zinc or the magnesium starvation conditions in metal-starved cells, zinc-replete and -starved cells (mZn- and lZn-medium, respectively) were compared. There was no difference between these cells in pulse-chase experiments (Fig. S3) and the cells reached similar C_{20} values, although the initial zinc uptake rate was increased by 40% (D = 1.55) from 162 ± 25 to 227 ± 17 ^{65}Zn cell^{-1} s^{-1} (Table 2). The initial zinc content of zinc-starved cells was only 11,000 Zn per cell, much lower than that of zinc-replete AE104 cells. Nevertheless, the influence of the decreased zinc content of the medium on the import and export rate of zinc in the pulse-chase experiment was much smaller than that of the lower magnesium content, although the lower magnesium content in the respective medium did not result in a lower magnesium content in the cells (Table S4).

Compared to zinc-replete cells and magnesium-replete but zinc-starved cells, zinc-magnesium-starved AE104 cells imported zinc with a sevenfold higher initial rate, reached equilibrium after 15 min at a threefold higher ^{65}Zn level, exported zinc with a threefold higher rate in the subsequent chase period, thereby removing 60% (^{65}Zn) or 70% (ZP2) of the previously imported zinc again (Tables 2 and 4). This was again evidence in favor of a flow equilibrium being in charge of the cellular zinc homeostasis and that the magnesium content of the medium was crucial for the up-regulation of the import rates.

Other metals and EDTA

Metal ions that interfere with zinc uptake or complex the metal ion in the growth medium should influence the flow equilibrium because they should decrease the influx rates of zinc of residual ^{65}Zn during the chase period. In addition to zinc, strain AE104 was also chased with 100 µM of other metal cations or EDTA after being loaded with 1 µM ^{65}Zn or ^{67}Zn (Tables 1 and 3; Fig. S2). In zinc-replete cells, the ^{65}Zn content decreased when cells were chased with Mg(II) <Mn(II) <Ni(II) <Co(II) <EDTA (Fig. S2A), which was paralleled by an increase in the $v_{eff}(0)$ from Mg(II)- to EDTA-chased cells (Table 1). The efflux rate caused by a chase with 100 µM EDTA was 214 ^{65}Zn cell^{-1} s^{-1} and twofold higher than the 112 ^{65}Zn cell^{-1} s^{-1} after a chase with 100 µM non-radioactive zinc in zinc-replete cells. This indicated that the complexation of the remaining ^{65}Zn in the medium by EDTA may have decreased the residual net import of ^{65}Zn. This was no longer the case in zinc-starved cells. Cells chased with 100 µM Cd(II) did not decrease their zinc content during the chase period but the increase in this value was smaller than that of the control cells (Fig. S2A; Table 1).

Zinc-replete cells contained about 80,000 Zn ions in ZP1 at the onset of the experiment and remained at this total zinc level after the uptake period (Table 3, ^{67}Zn-pulse), albeit with about 22,000 Zn ions now residing in ZP2 so that 25% of the zinc in ZP1 had been exchanged against incoming zinc. The chase resulted in a strong accumulation of the metals used for the chase, namely nickel, cobalt, cadmium, and manganese, but the magnesium content did not change (Table 3). The chase was also accompanied by a decreased total zinc content in ZP1 + ZP2 in the case of cobalt, cadmium, and EDTA but not after a chase with Mn, Mg, or Ni. The zinc level in ZP2 was decreased by EDTA and Cd, to a smaller level by Co, but increased when the cells were chased with Ni, Mg, or Mn (Table 3). All substances also decreased the zinc level in ZP1 between −20% (Cd) and −8% (Ni). In comparison, a chase with 100 µM Zn-depleted ZP2 down to 6,000 Zn per cell (Table 4). Compounds that interfered with zinc uptake most strongly (EDTA >Co) decreased the zinc content in ZP2 and those that interfered to a smaller degree (Ni, Mn, and Mg) increased this level, while all compounds decreased the zinc content in ZP1. There was a constant turnover of zinc in zinc-replete cells. Even when chased with other metal cations, zinc was still imported into the cells but uptake was affected by complexation (EDTA) or competition for uptake systems (Co).

In metal-starved cells of strain AE104, the other metal cations, and EDTA also interfered with ^{65}Zn uptake (Tables 1 and 3; Fig. S2B). The net efflux rates caused by chase with Ni, Co, Mn, Mg, or EDTA were not much different from that of Zn, whereas cells chased by 100 µM Cd(II) were again comparable to the negative control, un-chased cells. The initial zinc content of these cells was below 7,300 Zn per cell in ZP1 (Table 3) and increased during the uptake phase to 71,000 Zn per cell, predominantly residing in ZP2. While a chase with other metal cations or EDTA did not change the low zinc content in ZP1, that in ZP2 decreased after a chase with Co > Cd > Ni >EDTA but not with Mn or Mg. Except for Mg, again, the chasing metals were accumulated by the cells, Co even to a very high level of 564,000 ± 15,000 Co per cell (Table 3).

Zinc-replete and metal-starved AE104 cells were also incubated in the presence of 1 µM ^{63}Ni and chased with 100 µM non-radioactive nickel. The cellular nickel content decreased compared to the non-chased control (Fig. S4; Table S5). A chase with 100 µM non-radioactive zinc also decreased the cellular nickel level but to a smaller degree than a chase with nickel. This demonstrated the existence of a kinetical flow equilibrium also for nickel ions. An accompanying experiment using the ICP-MS determination of the cellular metal content verified that strain AE104 was able to accumulate Mn, Co, Ni, and Cd under both physiological conditions (Table S5); however, accumulation of Mn and Ni in zinc-replete cells was only to a small extend.

The data coming from chase experiments with other metal cations or substances, which interfered with zinc uptake, again presented evidence for the flow equilibrium. A net efflux of zinc could also be observed under these conditions (Fig. S2). Ni, Mn, and Mg did not remove zinc from ZP1 or ZP2 (Table 3). This was also true for Mn and Mg under metal-starvation conditions but no longer for Ni, which accumulated to levels of 278,000 Ni per cell and removed 1/3 of the zinc from ZP2. A chase with cobalt ions decreased the zinc content in ZP1 and ZP2 in zinc-replete cells and ZP2 in metal-starved cells (Table 3) but much less than zinc itself (Table 4). Cd was a special case, with only minor interference with zinc uptake but a strong depletion of zinc from the zinc pools. This was probably based on the up-regulation of the cadmium-exporter CadA by CadR since CadA and ZntA are both exporting zinc from *C. metallidurans* cells (7, 19). In total, Co and to a lesser degree Ni seemed to interfere not only with zinc uptake but may also mobilize Zn from its binding sites for subsequent export.

Role of uptake systems

Removal of zinc uptake systems should affect the cellular zinc turnover. ZupT of the ZIP protein family is the only zinc-regulated uptake system in *C. metallidurans* and is under the control of the zinc uptake regulator Zur [Fig. 1, (7–9, 25, 26, 33)]. Pulse-chase experiments were performed with zinc-replete, zinc-starved, and metal-starved cells of the Δ*zupT* strain of *C. metallidurans* AE104. Zinc-starved and -replete Δ*zupT* cells imported ^{65}Zn with half of the uptake rate and 2/3 of the C_{20} value of the parent cells. As with the parent, the difference between the two differently cultivated Δ*zupT* cells was small. Although the pulse-chase curves are not much different from each other (Fig. S3) but resulted in slightly different parameters (Table 2). While the $v_{up}(0)$ increased from zinc-replete to -starved parent cells, the $v_{up}(0)$ in Δ*zupT* cells decreased from 94 ^{65}Zn cell^{-1} s^{-1} to 67 ^{65}Zn cell^{-1} s^{-1}. The subsequent efflux rates in the chase period were similar to parent cells but decreased in Δ*zupT* cells from 38.8 ^{65}Zn cell^{-1} (moderate Zn) to 15.4 ^{65}Zn cell^{-1} (low Zn, Table 2). As has also been observed with the parent cells, the influence of zinc starvation on the flow equilibrium was much smaller than that of magnesium-zinc starvation. Consequently, only cells cultivated in moderate zinc medium mZn and low zinc-low magnesium medium lZn_lMg were subsequently compared with each other.

In the accompanying ^{67}Zn experiments (Table 4), zinc-replete *ΔzupT* cells contained half of the zinc content of the parent at the beginning of the experiment, lost only a smaller number of zinc atoms from ZP1 during the uptake phase but gained 20,000 ^{65}Zn cell^{-1} in this period, resulting in a net increase in the cellular zinc content. Nevertheless, zinc-replete Δ*zupT* cells contained only half as much zinc compared to the parent after

the uptake phase (Table 4). These experiments revealed an important role of ZupT in zinc homeostasis, although ZupT was not essential for zinc import into *C. metallidurans*. It was responsible for 42% of the uptake rate in zinc-replete and 70% in zinc-starved cells. As indicated by the C_{max}/C_{20} values, none of these cells reached equilibrium after the uptake period. Especially zinc-starved Δ*zupT* cells were far from equilibrium (C_{max}/C_{20} = 7.44, Table 2). Consequently and due to the lower import rate, the Δ*zupT* cells reached only 2/3 of the ^{65}Zn content of the parent cells and exported at a lower rate during the chase period. Despite a similar C_{20}- and also a similar ZP1 + ZP2- level of zinc-replete and -starved Δ*zupT* cells, the efflux rate of the starved cells was only 40% of that of the replete cells. This indicated that regulatory processes of the cellular zinc homeostasis might originate from ZupT or ZupT-dependent zinc import.

Zn-Mg-starved Δ*zupT* cells also accumulated ^{65}Zn to a smaller extent than the parent cells (Fig. S5; Fig. 3; Table 2). ZupT was responsible for 56% of the initial import rate. As indicated by the pulse-chase curves and the C_{max}/C_{20} values, metal-starved Δ*zupT* and parent cells were closer to an import-export equilibrium than cells cultivated under replete conditions.

When the genes for further uptake systems were deleted leading to the Δ7 (*ΔzupT ΔcorA1 ΔcorA2 ΔcorA3 ΔzntB ΔpitA ΔhoxN*) and Δ9 (Δ7 *ΔmgtA ΔmgtB::kan*) mutants, ^{65}Zn import into metal-starved (lZn_lMg) cells decreased even more compared to the Δ*zupT* mutant (Fig. 3B; Table 2) and was on a similar level. The initial import rate decreased from 509 ^{65}Zn cell^{-1} s^{-1} in the Δ*zupT* mutant to about 250 ^{65}Zn cell^{-1} s^{-1} in Δ7 and Δ9, reaching an equilibrium after 20 min of uptake of C_{20} = 45,000 to 50,000 ^{65}Zn cell^{-1} in Δ7 and Δ9 cells. The chased and control cells subsequently exported ^{65}Zn again with net efflux rates of 9.5 ^{65}Zn cell^{-1} s^{-1} (chased Δ7), 6.6 ^{65}Zn cell^{-1} s^{-1} (chased Δ9), 4.6 ^{65}Zn cell^{-1} s^{-1} (Δ7 control), and 2.9 ^{65}Zn cell^{-1} s^{-1} (Δ9 control). The number of ^{65}Zn atoms per cell in both mutants was much lower than that of the Δ*zupT* cells (C_{20} = 115,000 ± 4,000 ^{65} Zn cell^{-1}), which corresponded to 65,400 ± 5,800 Zn cell^{-1} in ZP1 +ZP2 after 20 min (Table 4). In comparison, this ZP1 + ZP2-level after 20 min was higher in Δ7 and Δ9 cells, about 80,000 Zn cell^{-1}. These zinc ions were mostly residing in ZP2 and had been imported during the uptake period (Table 4). Metal-starved Δ7 and Δ9 cells were still able to accumulate sufficient levels of zinc when the metal was provided at a concentration of 1 µM.

In zinc-replete Δ7 cells, zinc import was also lower than that in Δ*zupT* and parent cells. Despite a duplication of the $v_{up}(0)$ value from Δ*zupT* to Δ7, only half of the C_{20} value was reached (Table 2). The decrease in ZP1 and the total ^{67}Zn content during the uptake phase was similar in both cells but the ZP2 level of the Δ7 cells was only 84% of that of the Δ*zupT* cells (Table 4). Since the initial efflux rate of 11.4 ^{65}Zn cell^{-1} s^{-1} in Δ7 cells was much lower than that of Δ*zupT* cells, rapid down-regulation of zinc import during the uptake phase rather than up-regulation of efflux was responsible for the decreased zinc import in zinc-replete Δ7 cells.

Surprisingly, initial zinc import into zinc-replete Δ9 cells was much higher than that of parent, Δ*zupT* and Δ7 cells (Fig. 3; Fig. S5A, triangle compared to circles) with the highest measured ^{65}Zn import rate of 356 ^{65}Zn cell^{-1} s^{-1} in all zinc-replete cells (Table 2). The cells rapidly reached an equilibrium after 15 min. The subsequent initial efflux rate was not much enhanced compared to Δ7 cells (Table 2). After the uptake period, the Δ9 cells had not accumulated more ^{67}Zn than before this time and contained only 60% of the ZP2 level of Δ*zupT* cells. This indicated an unexpected feature of the unknown zinc importer "X" (Fig. 1), which was activated under zinc-replete but not metal-starved conditions in Δ9 cells only and rapidly switched off when zinc became available.

These data demonstrated again that all nine systems and "X" (Fig. 1) were involved in zinc uptake in *C. metallidurans* (25, 30, 33, 34). "X" might be a third magnesium import system besides MgtA and MgtB with a broad substrate specificity.

Role of efflux systems

The four known efflux systems ZntA, CadA, DmeF, and FieF (Fig. 1) may export zinc from cells of *C. metallidurans* AE104. ZntA and CadA are the main contributors because the

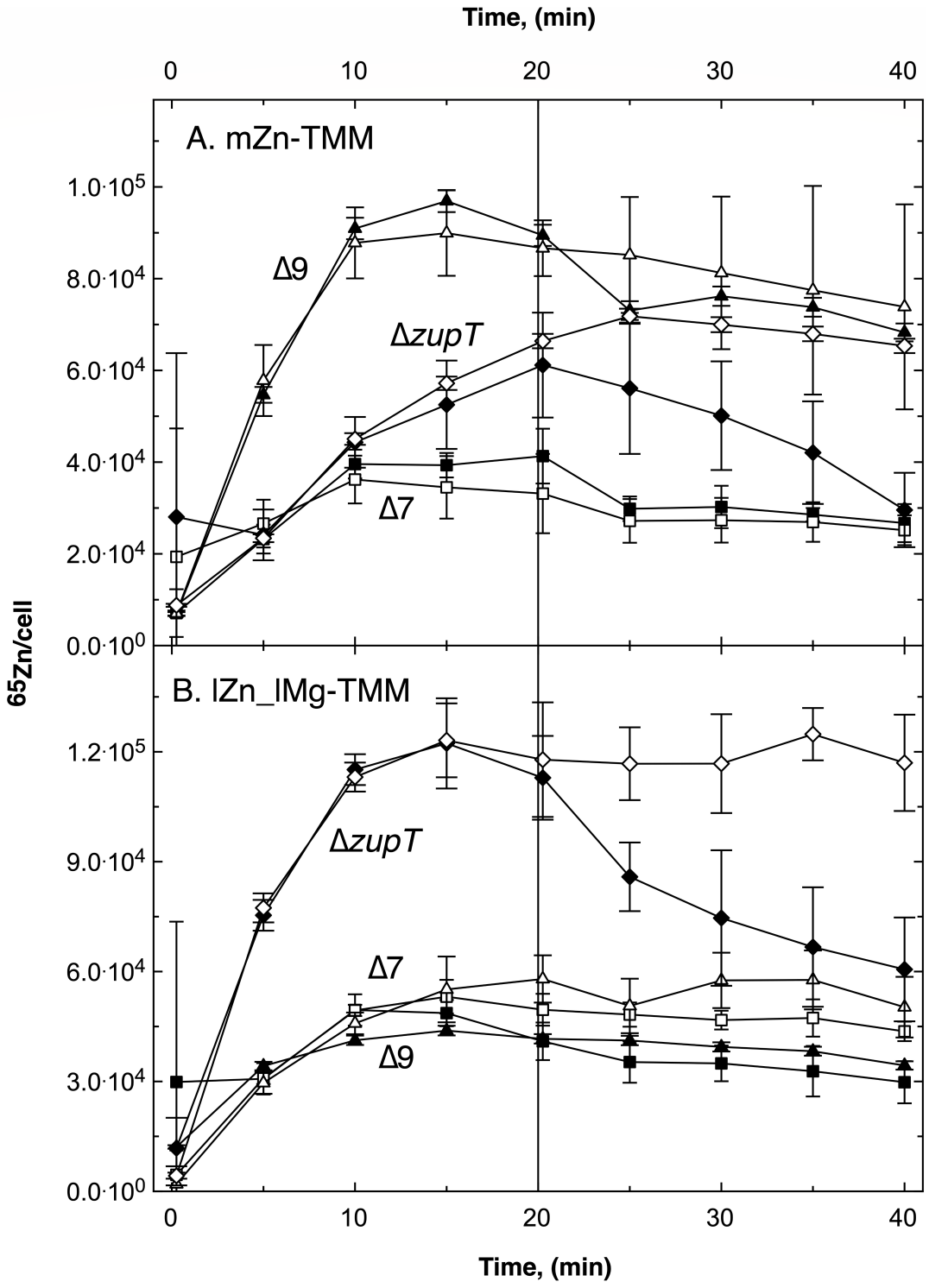

FIG 3 Pulse-chase experiment with *C. metallidurans* AE104 uptake mutants Δ*zupT*, Δ7 and Δ9. Cells of strain Δ*zupT* (diamonds), Δ7 (Δ*zupT* Δ*corA1* Δ*corA2* Δ*corA3* Δ*zntB* Δ*pitA* Δ*hoxN,* squares), and Δ9 (Δ7 Δ*mgtA* Δ*mgtB*::*kan,* triangles) were cultivated in TMM containing 200 nM zn(II) (mZn-TMM, Panel A) or no added Zn(II) and 0.1 mM Mg(II) (lZn_lMg, Panel B) as described in Fig. 2. Pulse at t = 0 with 1 µM ^{65}Zn(II), chase at t = 20 min with 100 µM non-radioactive Zn(II) (black symbols), or not chased (open symbols). Figure S5 provides an additional comparison with and without parent strain AE104.

zinc resistance of the double mutant Δe2 (Δ*zntA ΔcadA*) is 7.7 ± 0.6 µM zinc only slightly higher than that of the quadruple mutant Δe4 (Δ*zntA ΔcadA ΔdmeF ΔfieF*) with 7.1 ± 0.7 µM; the IC_{50} value of the parent is 1,056 ± 28 µM (19). Zinc-replete cells of the Δe2 mutant imported ^{65}Zn with half of the initial uptake rate of the parent and Δe4 mutants with 42%, reaching C_{20} of 76% and 64% of the parent values, respectively (Table 2). Both mutants displayed a clear chase reaction (Fig. 4) with initial net efflux rates of 26% and 16% of the parent (Table 2; Fig. S6). The initial zinc content, accumulation of zinc in ZP2 during the uptake period, and removal of zinc from ZP2 during the chase period were not much different from the parent; however, the mutants accumulated large amounts of zinc during the chase period, more than 500,000 Zn per cell (Table 4). The absence of the two major or all known four zinc efflux systems increased zinc availability at the onset of the experiment, leading to decreased initial import rates, but even the Δe4 mutant displayed a residual efflux reaction during the chase period.

In metal-starved cells, accumulation of zinc during the uptake phase was decreased in the efflux mutants compared to the parent (Fig. S6), in the Δe4 mutant more than in the Δe2 mutant (Fig. 4B). The Δe2 mutant imported zinc with 71% of the import rate of the parent, reaching 90% of its C_{20} value, and exported the metal during the chase period with 27% of the net efflux rate (Table 2). Import into the Δe4 mutant was much slower with 42% of the initial import rate of the parent but reached a C_{20} value of 73%. The Δe4 mutant still exported zinc during the chase period with 9% of the net efflux rate of the parent. The initial zinc content of metal-starved mutant cells and the accumulated amount of zinc in ZP2 during the uptake period were comparable to the parent but more zinc was left in ZP2 after the chase period, which again resulted in a high amount of zinc bound by the mutant cells, nearly 600,000 in strain Δe2 and 805,000 in strain Δe4 (Table 4).

The four efflux systems ZntA, CadA, but unexpectedly also DmeF and FieF, clearly contributed to the efflux of zinc from cells of *C. metallidurans*, the P-type ATPases ZntA and CadA with 74% of the initial net efflux rate in zinc-replete cells and DmeF and FieF with about 10%. At least one additional efflux activity seems to exist in strain AE104. The contribution of efflux systems was in agreement with a flow equilibrium of zinc in *C. metallidurans*.

Impact of metal-binding substance in the cytoplasm

Metal-binding sites in proteins including ribosomal ones, the cellular thiol glutathione GSH, and polyphosphate may sequester cytoplasmic zinc ions and interfere with its homeostasis (Fig. 1). In the case of GSH and polyphosphate, this influence was studied using the well-characterized Δ*gshA* (39) and Δ*ppk* (40) mutants of *C. metallidurans* strain AE104. In zinc-replete cells, the uptake phase of both mutants was not different from each other but different from the parent strain (Fig. 5). The initial uptake rates of both strains were similar and half of that of the parent strain AE104, leading to C_{20} values of 42,000 to 45,000 ^{65}Zn per cell (Table 2). As indicated by the C_{max}/C_{20} values, neither strain had reached an equilibrium after 20 min. Consequently, both strains continued a net import of ^{65}Zn in the non-chased control (Table 2; Fig. 5). Both strains displayed net ^{65}Zn efflux during the chase period. The Δ*gshA* strain with 27 ^{65}Zn cell^{-1} s^{-1} and removing 62% of the ^{65}Zn during the chase, the Δ*ppk* strain with 13 ^{65}Zn cell^{-1} s^{-1} and removing 14%.

Zinc-replete Δ*gshA* and Δ*ppk* cells initially contained about 80,000 zinc atoms in ZP1 (Table 4). This content remained the same during the uptake period but with about 20,000 Zn per cell now in ZP2. During the chase period, zinc was depleted from ZP2 and the cells reached values after 40 min of about 200,000 zinc per cell, respectively. All these values were smaller compared to the respective AE104 data, the Δ*gshA* 56% and Δ*ppk* 84% of the value in parent cells.

In metal-starved cells, the Δ*ppk* mutant accumulated much more ^{65}Zn than the Δ*gshA* cells (Fig. 5) but still on a lower level compared to the parent. The initial uptake rates of the Δ*ppk* mutant were 1/3 but they accumulated 2/3 of the C_{20} value of the parent AE104 (Table 2). The initial uptake rate of the *ΔgshA* mutant was 69% but the C_{20} value

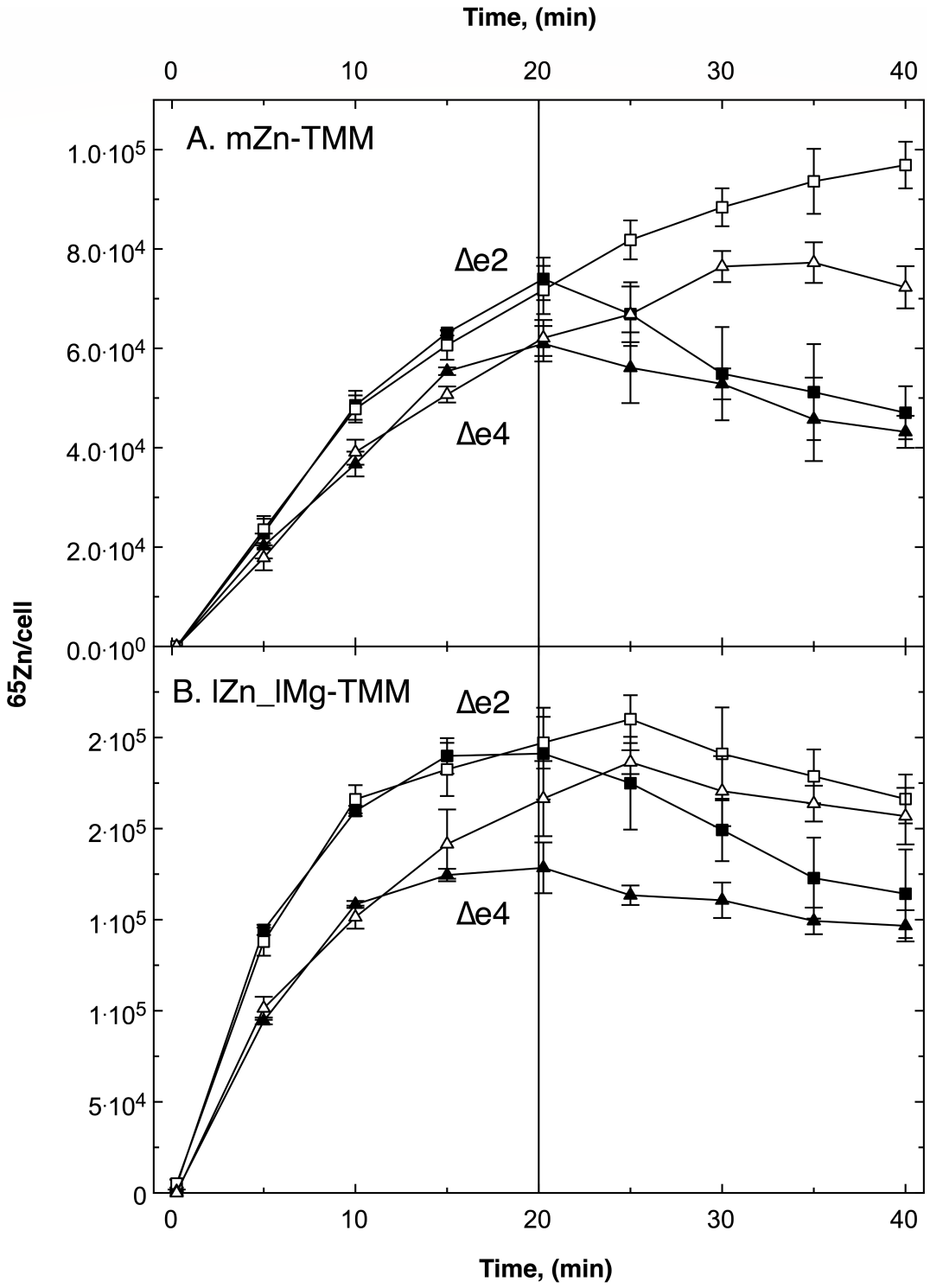

FIG 4 Pulse-chase experiment with *C. metallidurans* AE104 efflux mutants Δe2 and Δe4. Cells of strain Δe2 (*ΔzntA ΔcadA,* squares) and Δe4 (Δe2 *ΔdmeF ΔfieF,* triangles) were cultivated in TMM containing 200 nM Zn(II) (mZn-TMM, Panel A) or no added Zn(II) and 0.1 mM Mg(II) (lZn_lMg, Panel B) as described in Fig. 2. Pulse at t = 0 with 1 µM ^{65}Zn(II), chase at t = 20 min with 100 µM non-radioactive Zn(II) (black symbols), or not chased (open symbols). Figure S6 provides an additional comparison with parent strain AE104.

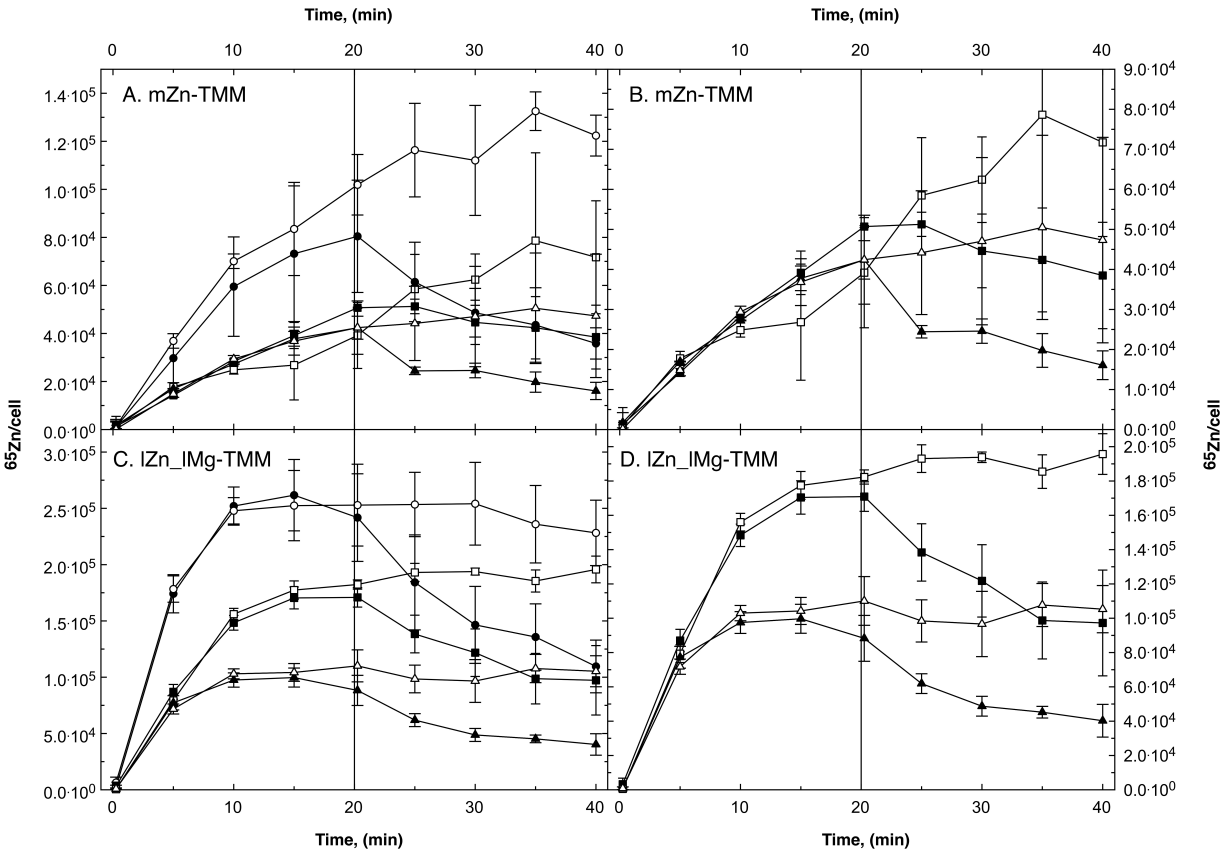

FIG 5 Pulse-chase experiment with *C. metallidurans* AE104 pool mutants Δ*ppk*::*kan* and Δ*gshA*::*kan*. Cells of strain AE104 (circles), Δ*ppk*::*kan* (squares), and Δ*gshA*::*kan* (triangles) were cultivated in TMM containing 200 nM zn(II) (mZn-TMM, Panels A and B) or no added Zn(II) and 0.1 mM Mg(II) (lZn_lMg, Panels C and D) as described in Fig. 2. Pulse at t = 0 with 1 µM ^{65}Zn(II), chase at t = 20 min with 100 µM non-radioactive Zn(II) (black symbols), or not chased (open symbols). Panels B and D contain the same data as Panels A and C except the AE104 values.

was only 36% of that of the parent. The C_{max}/C_{20} ratio for both strains indicated that an equilibrium had not been reached after 20 min. Consequently, both strains continued to import zinc in the negative control, while the parent exported ^{65}Zn before the end of the uptake period. The net efflux velocities were 26% (Δ*ppk*) and 16% (Δ*gshA*) of that of the parent.

Metal-starved cells of both mutant strains possessed a zinc level below 8,000 Zn per cell at the onset of the experiment (Table 4), imported zinc during the uptake phase exclusively into ZP2, and removed about 2/3 of the zinc from ZP2 during the chase period. With respect to other metals (Table S4), Δ*gshA* cells contained a lower iron, cobalt, and nickel content in both media, and the Δ*ppk* cells had a higher nickel content in metal-starved cells.

Polyphosphate and glutathione were involved in zinc homeostasis. The lower initial uptake rates and C_{20} levels reached in the mutant cells compared to the parent suggested that zinc was more available for efflux during the turnover of the metal, which would be in agreement with a sequestration of zinc by both compounds in the cytoplasm. The metal-binding capacity of the cytoplasm interacted with the flow equilibrium to adjust the cytoplasmic zinc content.

C. metallidurans CH34 wild type

Compared to strain AE104, the CH34 wild type contains a variety of plasmid-encoded metal transport systems (Fig. 1), which should affect the flow equilibrium of zinc. When the plasmid-free strain AE104 was chased with 1 mM non-radioactive zinc instead of 0.1 mM, efflux of ^{65}Zn decreased at the higher zinc concentration used for the chase (Fig. 2, closed squares compared to circles), although the difference was very small and not significant in case of the metal-starved cells (Fig. 2B). The initial efflux velocity decreased from 112 ± 1 ^{65}Zn cell^{-1} s^{-1} to 64 ^{65}Zn cell^{-1} s^{-1} in zinc-replete and from 314 ^{65}Zn cell^{-1} s^{-1} to 141 ^{65}Zn cell^{-1} s^{-1} in metal-starved cells (Table 1). Because 1 mM should compete more efficiently than 100 µM non-radioactive zinc with uptake of the 1 µM ^{65}Zn during the chase period and should mediate in a better mobilization of cytoplasmic ^{65}Zn for efflux, this result was not expected. It may indicate an inhibition of the chased cells by 1 mM Zn(II). Indeed, the metal content of the AE104 cells after chase with 1 mM Zn(II) was 2.4 million (zinc-replete) or even 5.2 million (metal-starved) zinc per cell (Table 4).

C. metallidurans CH34 wild type should be capable of handling this problem. It contains in comparison to strain AE104 the plasmid-encoded efflux systems such as the CzcCBA transenvelope efflux system (Fig. 1). The CzcCBA system is also present under non-challenging conditions, growth in TMM without the addition of zinc (41). In pulse-chase experiments, zinc-replete CH34 wild type accumulated only 30,000 ^{65}Zn during the uptake phase, and the C_{max}/C_{20} ratio of 1.05 indicated that an equilibrium had been reached at 20 min (Table 2; Fig. S7). The $v_{up}(0)$ of CH34 was 146 ± 17 ^{65}Zn cell^{-1} s^{-1} and not different from the AE104 values over all experiments of 162 ± 25 ^{65}Zn cell^{-1} s^{-1} (Table 2). The CzcCBA system did not prevent zinc uptake into the cytoplasm at low zinc concentrations but strain CH34 was able to adjust rapidly to changing zinc availability. In contrast to strain AE104, the initial net efflux velocity more than doubled in strain CH34 from 4.7 ^{65}Zn cell^{-1} s^{-1} to 11.0 ^{65}Zn cell^{-1} s^{-1} when these cells were chased with 1 mM instead of 100 µM Zn(II) (Table 2). These values were only 9.8% and 4.2%, respectively, of the efflux velocity of AE104 cells chased with 100 µM zinc. Concerning the pulse-chase curves, these differences were not significant in non-induced CH34 cells (Fig. S7A) but the calculated v_{eff} values clearly were significant (Table 2).

When *C. metallidurans* was additionally cultivated in the presence of 0.1 mM Zn(II) used for an up-regulation of its efflux systems (Fig. S7; Tables 2 and 4; "CH34 induced"), again about 30,000 ^{65}Zn were accumulated during the uptake period. There was no longer a significant ^{65}Zn efflux when these cells were subsequently chased with 0.1 mM Zn(II) but when the cells were chased with 1 mM Zn(II), efflux was 16.0 ± 0.2 ^{65}Zn cell^{-1} sec^{-1}. CH34 cells chased with 1 mM Zn(II) possessed only 863,000 Zn(II) per cell compared to 2.4 million in strain AE104, and CH34 cells pre-cultivated in 0.1 mM Zn even less, 428,000 Zn(II) per cell (Table 4). These cells carried already 235,000 Zn per cell at the onset of the experiment in ZP1 and nearly no zinc in ZP2 (200 ± 40 zinc per cell) after the uptake period. After a chase with 0.1 mM Zn(II), they kept their zinc content at about 200,000 Zn per cell and only doubled the zinc content when chased with 1 mM zinc.

The plasmid-encoded Czc system is responsible for an enhanced efflux capability of *C. metallidurans* CH34 compared to the plasmid-free strain AE104 (42–44). The pulse-chase experiment (Fig. S7; Tables 2 and 4) clearly demonstrated the outstanding ability of strain CH34 to shield its cells against high zinc concentrations.

DISCUSSION

Zinc homeostasis in *C. metallidurans* is controlled by a flow equilibrium of uptake and efflux reactions

The plasmid-free *C. metallidurans* strain AE104 clearly demonstrated a constant turnover of cell-bound zinc. Uptake of ^{65}Zn ions into zinc-replete cells had been investigated before (21) and occurred at 1 µM Zn(II) with an initial velocity of 166 ± 94 Zn(II) s^{-1} cell^{-1}. This value was reproduced as 162 ± 25 ^{65}Zn cell^{-1} s^{-1}, and also a sevenfold increase in uptake velocity in metal-starved cells. Responsible for this was a lowered magnesium

concentration rather than zinc starvation conditions. Magnesium is a competitive inhibitor of zinc uptake in *C. metallidurans* (21) so up-regulation of magnesium importers was responsible for the increased uptake rate in metal-starved cells.

When the cells, which accumulated ^{65}Zn during an uptake period, were chased with 100 µM non-radioactive zinc, the net efflux of ^{65}Zn was visible (Fig. 2). Adding 100 µM Zn(II) increased the zinc concentration to 101 µM. With a K_m of 137 ± 87 µM of the zinc import, this results according to the Michaelis-Menten equation in a 58.6-fold increase in the import rate from 1/138 v_{max} to 101/238 v_{max} but also in a 101-fold dilution of the radioactive ^{65}Zn so that the uptake velocity should be decreased to less than 58% of the initial value. While non-chased control cells continued to import ^{65}Zn, chased cells exported ^{65}Zn with an initial net efflux rate of 112 ^{65}Zn cell^{-1} s^{-1}, resulting in a decrease of the number of cell-bound ^{65}Zn ions down to 37% of the content before the chase (Table 2). The total zinc content of zinc-replete cells had been 103,000 Zn per cell before the experiment and remained at this number during the uptake phase but 26% of the initially present zinc ions were exchanged for incoming zinc ions during the uptake period (Table 4). During the chase, this number increased to 246,000 Zn per cell due to the higher concentration of zinc ions in the environment but most of the zinc that had been imported during the uptake period was exported again (Table 4).

This demonstrated a continuous turnover of zinc ions in zinc-replete cells of *C. metallidurans*, meaning that zinc uptake and zinc efflux reactions were running simultaneously. A similar turnover was also visible in zinc- and metal-, meaning zinc-magnesium-, starved cells. Metal-starved AE104 cells contained a lower initial zinc content than zinc-replete cells, imported zinc with a seven times higher initial import rate. They reached an equilibrium of the zinc concentration already during the uptake period (Fig. 2) and subsequently exported ^{65}Zn again even in the non-chased control while zinc-replete cells continued to accumulate the radioactive isotope in the control with a small rate of 14 ^{65}Zn cell^{-1} s^{-1} compared to the initial 162 ^{65}Zn cell^{-1} s^{-1} (Table 2). This means that the cells had been able to adjust the zinc import and export rates during the 20-min uptake period.

Regulation of the zinc uptake and efflux activities could have been done by flux control, for example, by binding of metal ions to the regulatory sites of the transporter (35, 36, 45, 46) or by interaction with other proteins, degradation of uptake or *de novo* synthesis of efflux systems. Expression of a gene for a copper-exporting P-type ATPase at 37°C in *Escherichia coli* needed just 2 min to reach an abundance peak for the transcript (47) and 10 min for a *czc* transcript at 30°C in *C. metallidurans* (48). Including the subsequent translation and membrane insertion, this would be just a sufficient time to explain an up-regulation of the efflux activities by protein synthesis. On the other hand, any flux control of the activities of import and export reactions would be a much quicker process and would allow a rapid adjustment of the turnover rate of zinc to changing zinc availability in the environment.

Although a flux control of the transport activities has a lower energetic cost compared to the synthesis and degradation of proteins, a constant turnover of cytoplasmic against environmental zinc is in fact a futile cycle. Efflux of zinc by the P-type ATPase ZntA is driven by ATP hydrolysis (19) and uptake for instance by uniport (5). Many uptake systems have a broad substrate range, for instance, ZupT (49, 50), CorA (51–53), and PitA as metal phosphate importer (54). Most transition metal cations have a similar ionic diameter. When the shell of water molecules has been removed, the radius of Co(II) and Zn(II) is 74 nm that of Mg(II) 65 nm (37). The electronic conformation of Zn(II) and Mg(II) is quite similar, with completely filled 3s and 3d orbitals in the case of Zn(II) and completely filled 2s and 2p orbitals for Mg(II) (55). Discrimination between Zn(II) and Mg(II) requires to explore the small differences in size, and the better ability of Zn(II) to form tetrahedral complexes.

A transport process that discriminates Zn(II) against Mg(II) by complex formation would be a slow process compared to a process that just selects sizes of divalent metal cations because the release of the initially bound cation during the subsequent transport

reaction is an energetic barrier (5). Such discrimination can be easily performed by periplasmic metal-binding proteins of ABC transporters such as ZnuABC for Zn(II) (27, 32) or NikABC (56–58) for Ni(II). These highly substrate-specific import systems are absent in *C. metallidurans* so import of Mg(II) and transition metal cations depends on two P-type ATPases of the Mg/Ca group and secondary import systems (Fig. 1). To allow a high-rate import reaction by these transporters, their substrate discrimination does not allow the formation of tightly bound metal complexes at the substrate binding site but only gating mechanisms that are charge- and size-selective (59–61).

In the case of Mg(II), 12.5 million Mg(II) need to be imported during a generation time, under stress conditions even 40 million (Table S4), compared to 100,000 Zn(II) (Table 4) so that *C. metallidurans* needs 125 times more Mg(II) than Zn(II). The concentration of both metals in an ecosystem such as seawater is 55.5 mM Mg(II) and 153 nM Zn(II) (37), a factor of 363,000. Zinc availability in most environments is much lower than that of magnesium. This means that a high-rate uptake of Mg(II) with a broad substrate specificity automatically provides the cell also with divalent transition metal cations such as Zn(II), Co(II), and Ni(II). If this is not sufficient, many bacteria can produce ABC or ECF-ABC importers such as ZnuABC, NikABC, or CbiMNQO (32, 56, 58, 62–64).

The secondary transport systems such as CorA and Mg-importing P-type ATPases, thus provide Mg(II) to the *C. metallidurans* cell plus a bouquet of transition metal cations. In the second step, surplus metal cations are being removed again. This is done in the plasmid-free strain AE104 by P_{IB2}-type exporters such as ZntA for Zn(II) and CadA for Cd(II) (20). Both proteins have a very similar affinity for Zn(II) and Cd(II) (19) but different MerR-type regulators control the expression of the respective genes, ZntR for *zntA* and CadR for *cadA* (7). This elegantly delegates the time-consuming process of substrate discrimination by complex formation to the regulatory proteins so that ZntA is only expressed at high internal zinc concentrations and CadA, when the Cd-exporting activity of ZntA is not sufficient to remove incoming cadmium. This was clearly demonstrated by the removal of cytoplasmic zinc when the cells were chased with cadmium (Table 3).

Acquisition of divalent metal cations is a very efficient process (5). The secondary import systems plus the P-type Mg importers MgtA and MgtB provide a broad range of metal cations and metal phosphates to the cell. If this is not sufficient for an individual component, in most bacteria, ABC-type importers with periplasmic substrate-binding proteins or ECF-ABC importers are being induced, in *C. metallidurans* just PstABC for phosphate. On the other hand, if too much of an individual metal arrives in the cell, efflux systems are up-regulated removing the specific metal cation again. Theoretically, this could be described as a flow equilibrium of import and export reactions, which adjusts the cytoplasmic availability of an individual metal cation and also the composition of the metal cation bouquet (40). The data presented here provide evidence that such a constant turnover of zinc ions is indeed occurring in *C. metallidurans*.

Metal uptake, efflux, and buffering substances interact to generate the flow equilibrium

As could be expected, the turnover of zinc in *C. metallidurans* strain AE104 was affected in mutants with multiple deletions in the uptake systems Δ7 (*ΔzupT ΔpitA ΔcorA1 ΔcorA2 ΔcorA3 ΔzntB ΔhoxN*) and Δ9 (Δ7 Δ*mgtA ΔmgtB*). Δ7 and Δ9 contained a lower initial zinc content ZP1 connected with a high initial uptake velocity $v_{up}(0)$ than all other strains (Tables 2 and 4). As already mentioned (30, 34), this unambiguously demonstrated the presence of at least one more uptake system "X" for zinc (Fig. 1). While zinc-magnesium-starved cells of Δ7 and Δ9 presented a very low amount of accumulated zinc during the uptake phase, zinc-replete cells of Δ9 but not Δ7 accumulated zinc with a higher rate than the parent; however, an equilibrium was reached after 15 min and the cells subsequently exported the metal again (Fig. 3A). This was a surprise. Search for "X" has been performed in the past by looking at Δ7 and Δ9 cells under metal-starvation conditions. Under these conditions, however, "X" was either down-regulated or on a low activity level.

In addition to the uptake systems, polyphosphate and glutathione also affected zinc uptake and efflux (Fig. 5). While zinc-replete mutant cells without polyphosphate and glutathione were not different from each other, deletion of *gshA* for the first step of glutathione decreased zinc uptake more than an interrupted polyphosphate synthesis in metal-starved cells. This demonstrated that components that should sequester zinc ions in the cytoplasm and subsequently decrease zinc availability in this compartment are also integral parts of zinc homeostasis, especially under metal-starvation conditions. The flow equilibrium of metal uptake and efflux reactions was buffered by cytoplasmic metal-binding components.

It could also be expected that efflux systems influenced the turnover of zinc because they performed the second part of the kinetical flow equilibrium of import and export reactions. Efflux of ^{65}Zn after the uptake period was indeed on a lower level in the efflux mutants Δe2 (Δ*cadA ΔzntA*) and Δe4 (Δe2 Δ*dmeF ΔfieF*) than in the parent strain AE104 (Fig. S6; Fig. 4; Table 2). The initial efflux rates v_{eff} decreased compared to the parent down to 26% in zinc-replete and 27% in metal-starved Δe2 cells, and to 16% in zinc-replete and 9% in metal-starved Δe4 cells (Table 2).

In zinc-replete Δe2 and Δe4 cells, the calculated C_{max} value of the uptake period was much higher than the measured C_{20} value (Table 2), indicating that strains without efflux systems had not reached an equilibrium during the uptake period. The C_{max}/C_{20} value in zinc-replete cells was 5.5 in Δe2 and 8.3 in Δe4 and were the highest values measured in the experiments. This indicated that the activity of the efflux systems was essential to reach a flow equilibrium within 20 min. Other strains with high C_{max}/C_{20} ratios in zinc-replete cells were Δ*ppk* (4.7) > Δ*gshA* = Δ*zupT* (2.7) >parent strain AE104 (2.2; Table 2). Polyphosphate, glutathione, and the zinc importer ZupT were also required to reach an equilibrium within the uptake period.

The data also demonstrated that the secondary efflux systems DmeF and FieF were involved in zinc efflux although their contribution to zinc resistance was neglectable (19). Moreover, reminiscent to "X," still another zinc efflux system, might be present in *C. metallidurans* AE104, although the zinc resistance of the Δe4 mutant is already down to an IC_{50} of 7.1 µM (19).

Strain AE104 as plasmid-free mutant of *C. metallidurans* CH34 wild type

The two plasmids pMOL28 and pMOL30 of *C. metallidurans* CH34 wild type are crowded with metal resistance determinants (e.g., *czc, cnr, chr, cop, pbr, mer*) for cobalt, zinc, cadmium, nickel, copper, lead chromate, and mercury resistance (6, 18, 65–68). Among other genes for periplasmic components and two exporters of the inner membrane, the central product of *czc* is the RND-driven transenvelope pump CzcCBA, which exports Co(II), Zn(II), and Cd(II) from the periplasma across the outer membrane back to the outside (42–44, 69, 70). This adjusts the periplasmic metal concentration for a subsequent import into the cytoplasm and removes cations that just had been exported by inner membrane efflux systems, leading to a high level of zinc, cobalt, and cadmium resistance (18).

This convenient situation was over in the plasmid-free derivative *C. metallidurans* strain AE104 (18), resulting in decreased resistance to all the metals mentioned above. The difference between strains CH34 and AE104 was also evident in the pulse-chase experiments in zinc-replete cells of both strains. In the case of CH34, the cells are additionally pre-incubated in the presence of 100 µM Zn(II) to induce up-regulation of *czc* on plasmid pMOL28. While AE104 and non-induced CH34 cells possessed similar zinc contents at the beginning of the experiment, induced CH34 cells contained about threefold higher zinc content and a down-regulated initial uptake velocity $v_{up}(0)$ (Tables 2 and 4). Despite the similarities in the initial zinc content and $v_{up}(0)$ between AE104 and non-induced CH34 cells, AE104 imported C_{20} = 100,000 ^{65}Zn ions during the uptake phase, CH34 cells under both conditions only 20,000 to 30,000. The CH34 wild-type cells chased with 1 mM Zn(II) were even able to keep the amount of accumulated zinc at a tolerable level, especially, when they were pre-incubated in the presence of 0.1 mM

Zn(II). This demonstrated again the outstanding ability of *C. metallidurans* CH34 wild type to resist high concentrations of external zinc ions and to shield its cell against this metal.

MATERIALS AND METHODS

Bacterial strains and growth conditions

Plasmids and *C. metallidurans* strains (Table 1) in this study were all derivatives of the plasmid-free strain AE104 that lacks pMOL28 and pMOL30 (18), except of course the wild-type CH34. The Δ*ppk::lacZ* strain with *ppk* interrupted by *lacZ*-insertion (40) was produced before the experiment by conjugation of *E. coli* (pLO2::Δ*ppk-lacZ*) and subsequent homologous recombination. Tris-buffered mineral salts medium (18) containing 2 g sodium gluconate/L (TMM) was used to cultivate these strains aerobically with shaking at 30°C. Since the purity of the mineral salts has been steadily improved, the concentration of contaminating zinc chloride and zinc added with the trace element solution SL6 (38) was no longer sufficient to supply sufficient zinc to the cells. Consequently, the zinc content of TMM was determined by ICP-MS (Inductively coupled plasma mass spectrometry) and subsequently adjusted to 200 nM by the addition of zinc chloride. This TMM was designated moderate zinc "mZn medium." Moreover, zinc and metal starvation media were also used. A low zinc (lZn) medium was TMM without added trace element solution SL6 (38). A third medium was a low metal medium (lZn_lMg), TMM without SL6, and 100 µM magnesium chloride instead of 1 mM. Analytical grade salts of transition metal cations were used to prepare 1 M stock solutions, which were sterilized by filtration. Solid Tris-buffered media contained 20 g agar/L.

As determined by inductively coupled plasma mass spectrometry (ICP-MS), the metal contents of all media were 208 ± 15 µM calcium and 3.9 ± 0.2 µM iron (200 µM and 4.3 µM added, respectively). TMM, mZn, and lZn media contained 953 ± 86 µM magnesium (1 mM added) and medium lZn_lMg 85.2 ± 1.4 µM magnesium (0.1 mM added). The content of other metals in media TMM and mZn, which contained trace element solution SL6, were 48.9 ± 4.5 nM Mn(II), 86.3 ± 17.3 nM Co(II), 157 ± 19 nM Ni(II), 16.3 ± 14.0 nM Cu(II) (15.2 nM Mn, 84.1 nM Co, 8.42 nM Ni and 5.87 nM Cu, respectively, coming from a trace element solution), and in media lZn and lZn_lMg without SL6 34.6 ± 0.9 nM Mn(II), 4.6 ± 1.8 nM Co(II), 89.1 ± 2.5 nM Ni(II), and 14.3 ± 5.0 nM Cu(II) coming from contaminations so that the media lZn and lZn_lMg were actually low zinc and low cobalt media, whereas the contaminations were sufficient sources for manganese and nickel. Not-adjusted TMM contained 63.6 ± 9 nM zinc, adjusted mZn-TMM 200 nM. Media without SL6 contained 35.2 ± 30.4 nM zinc. Without SL6, the zinc content of the growth media varied strongly but were always in a range leading to zinc starvation conditions.

Inductively coupled plasma mass spectrometry

For ICP-MS analysis, HNO3 (trace metal grade; Normatom/PROLABO) was added to the samples to a final concentration of 67% (wt/vol) and the mixture was mineralized at 70°C for 2 h. Samples were diluted to a final concentration of 2% (wt/vol) nitric acid. Indium and germanium were added as internal standards at a final concentration of 1 ppb and 10 ppb each. Elemental analysis was performed *via* ICP-MS using Cetac ASX-560 sampler (Teledyne, Cetac Technologies, Omaha, Nebraska), a MicroFlow PFA-100 nebulizer (Elemental Scientific, Mainz, Germany), and an ICAP-RQ ICP-MS instrument (Thermo Fisher Scientific, Bremen) operating with a collision cell and flow rates of 4.5 mL x min-1 of He/H_2 [93%/7% (71)], with an Ar carrier flow rate of 0.76 L × min^{-1} and an Ar make-up flow rate at 15 L x min^{-1}. An external calibration curve was recorded with ICP-multi-element standard solution XVI (Merck) in 2% (vol/vol) nitric acid. The sample was introduced *via* a peristaltic pump and analyzed for its metal content. For blank measurement and quality/quantity thresholds, calculations based on DIN32645 TMM were used. The results were calculated from the ppb data as atoms per cell as described (25).

Pulse-chase experiments with radioactive ^{65}Zn

Cells were incubated in TMM for 17 h at 30°C shaking at 200 rpm, diluted 20-fold into a second pre-culture in the medium that was used for the subsequent main culture (TMM, mZn, lZn, lZn_lMg), and incubated with shaking at 30°C for 24 h. Cells were diluted 50-fold into the main culture, which was incubated with shaking at 30°C at 200 rpm until a turbidity of 150 Klett units was reached (mid-exponential phase of growth). The cells were harvested by centrifugation at 4°C, washed in the same volume of 10 mM TrisHCl (pH 7), suspended in the same volume of 10 mM TrisHCl (pH 7), and kept on ice until needed during the same day. For the experiments, sodium gluconate was added to 6 mL of the cell suspension to a final concentration of 2 g/L directly before the start to provide energy to the cells. At t = 0, radioactive ^{65}Zn was added to the cell suspension to a final concentration of 1 µM Zn(II) and 60 nCi/mL. The $^{65}ZnCl_2$ was supplied by POLATOM (certificate 022–106722-03622-0001).

The cells were incubated with shaking at 30°C. At 0.25, 5, 10, and 15 min, samples of 500 µL were removed, and filtered through a membrane filter (0.2 µm pore size, Whatman cellulose nitrate membrane filters, Cytiva) using a vacuum-driven uptake apparatus. The samples were rapidly washed twice with 5 mL of 50 mM TrisHCl (pH 7) containing 50 mM EDTA. The activity was counted in a Liquid Scintillation Counter (PerkinElmer Tri-Carb 2810 TR) using Ultima Gold (PerkinElmer). The samples were counted twice for 2 min in a window from 0 to 200 keV. In some experiments, ^{63}Ni (Amersham Biosciences) was used instead of ^{65}Zn.

For the chase, non-radioactive zinc was added at t = 20 min to a final concentration of 100 µM or 1 mM. In some experiments, other transition metal chlorides or EDTA were used. Incubation was continued with shaking at 30°C and samples were removed at 20.25, 25, 30, 35, and 40 min. They were treated and analyzed as described above for the samples of the uptake period.

A sample of 100 µL was counted to determine the total radioactivity of the ^{65}Zn in the cell suspension used for the pulse-chase experiment. From this value, the mol zinc per cpm ratio was derived. For each time sample, the mean value and technical deviation of the two 2-min counts were calculated. Two zero controls were subtracted, one for the background radioactivity at the time of the experiment and one for the chemical adsorption of ^{65}Zn by the membrane filter. The resulting value was multiplied by the mol/cpm ration of the respective experiment to give the mol ^{65}Zn per 500 µL time sample. The actual cell number in the sample had been determined *via* an equilibration curve for the turbidity at 600 nm so that the mol ^{65}Zn per cell and subsequently the number of the ^{65}Zn atoms per cell could be calculated.

All experiments were performed at least three times. For each experiment, the zinc content per cell at 7.5 min was calculated from the 5 min and 10 min values. This value was used to correct the number of atoms per cell for all experiments involving the same mutant and the same growth condition. Experiments with large correction factors were removed and the respective experiment was repeated. For each strain and condition, the mean values and deviations of the ^{65}Zn atoms per cell were finally calculated. This value was designated as the cellular metal content C(t) for the respective mutant and growth condition.

Pulse-chase with ^{65}Zn measured: (i) the initial zinc uptake velocity $v_{up}(0)$ at t = 0; (ii) the cellular ^{65}Zn content C_{20} at the end of the uptake period (time point represented in Fig. 2 by the horizontal bar); (iii) the extrapolated maximum zinc content after the uptake period C_{max}; (iv) the efflux velocity v_{eff} at the beginning of the chase at 20 min; (v) the corresponding initial zinc content C_0 used to calculate v_{eff}; and (vi) the final zinc content C_{40} at the end of the chase period (Fig. 2, t = 40 min). To obtain these data, the uptake phase up to 20 min of the pulse-chase experiment was adapted to the equation $C(t) = C_{max} \cdot t/(K_t + t)$ using the Lineweaver-Burk-like plot $1/C(t) = 1/C_{max} + (K_t/C_{max} \cdot 1/t)$. The first deviation by time of the equation $C(t) = C_{max} \cdot t/(K_t + t)$ was $dC(t)/dt = C_{max} \cdot K_t/(K_t + t)^2$. At t = 0, this gave the initial uptake rate $v_{up}(0) = C_{max}/K_t$. After the chase after 20 min, the cell-bound zinc content was modeled by the decay function $C(t) = C_o \cdot e^{\wedge}(-\tau \cdot$

t) using the plot ln C(t) =ln C_o −τ · t. The first deviation by time of the equation C(t) =C_o · e^(−τ · t) was dC(t)/dt = −τ · C_o · e^(−τ · t). And at t = 0, this value was the initial net efflux rate $v_{eff}(0) = -\tau \cdot C_o$. In contrast to the initial uptake rate that was no net rate because the cells did not contain ^{65}Zn at t = 0, $v_{eff}(0)$ was a net rate and the result of the real efflux rate after chase minus the rate of ^{65}Zn re-import at this time.

Experiments with stable ^{67}Zn

Stable enriched ^{67}Zn was employed to determine (vii) the resident zinc pool (ZP) ZP1 at the beginning of the experiment; (viii) the zinc pools ZP1 and ZP2 after the uptake period; and (ix) finally these pools ZP1 and ZP2 after the chase period. The cell suspensions were prepared in the respective media as described for the pulse-chase experiments above; however, the respective growth medium was used instead of the uptake buffer for these experiments. After a zero sample had been removed for the ICP-MS analysis, isotope-enriched ^{67}Zn(II) was added to a final concentration of 1 µM. Incubation was continued with shaking for 20 min, a sample was removed and the remaining cells chased with non-enriched Zn(II) added at a final concentration of 100 µM or 1 mM. In some experiments, other metal chlorides or EDTA were used for the chase. Incubation was continued for 20 min with shaking at 30°C and the third sample was removed. The cells in the respective samples were harvested by centrifugation, washed twice with 50 mM TrisHCl buffer (pH 7.0) containing 50 mM EDTA at 0°C, suspended in 50 mM TrisHCl buffer (pH 7.0), and mineralized for the subsequent ICP-MS analysis. The ^{67}Zn (94% ^{67}Zn) was provided as metal from Nakima Ltd (Savyon, Israel) and oxidized using HCl on ice. The zinc content was verified by ICP-MS.

For the calculation of different zinc pools in the cells, the ratio of ^{67}Zn in the isotope-enriched zinc solution (94%) and non-enriched "usual" zinc [4.1%; (37)] was used. The ICP-MS measurement calculates the quantity of an element from that of its isotopes, thereby correcting for the % of the natural abundance of the respective isotope. The zinc pool 1 (ZP1) was defined as the cellular zinc pool before the addition of isotope-enriched ^{67}Zn and was equal to the ^{64}Zn ICP-MS result [natural abundance 48.6%; (37)]. Similar results were obtained using ^{66}Zn (27.9%) instead of ^{65}Zn. Zinc pool 2 (ZP2) was the zinc pool after incubation of the cells with ^{67}Zn. ZP2 was the ^{67}Zn value coming from the ICP-MS (corrected for a natural abundance of 4.1%) minus the ^{64}Zn value (0.75% in the ^{67}Zn-enriched zinc solution) and the result was divided by 22.2346.

Statistics

Students' *t*-test was used but in most cases the distance (D) value, D, has been used several times previously for such analyses (34, 72, 73). It is a simple, more useful value than Student's *t*-test because non-intersecting deviation bars of two values (D > 1) for three repeats always means a statistically relevant (≥ 95%) difference provided the deviations are within a similar range. At $n = 4$, significance is ≥97.5%, $n = 5 \geq 99\%$ (significant), and $n = 8 \geq 99.9\%$ (highly significant).

ACKNOWLEDGMENTS

We thank Gary Sawers for critically reading this manuscript.

Funding for this work was provided by the Deutsche Forschungsgemeinschaft (Ni262/19).

AUTHOR AFFILIATIONS

[1]Martin-Luther-University Halle-Wittenberg, Institute for Biology/Microbiology, Halle (Saale), Germany
[2]Department of Analytical Chemistry, Helmholtz Centre for Environmental Research – UFZ, Leipzig, Germany

AUTHOR ORCIDs

Dietrich H. Nies http://orcid.org/0000-0002-4516-8267

FUNDING

Funder	Grant(s)	Author(s)
Deutsche Forschungsgemeinschaft (DFG)	Ni262/19	Dietrich H. Nies

ADDITIONAL FILES

The following material is available online.

Supplemental Material

Supplemental material (JB00080-24-s0001.pdf). Tables S1 to S5; Figures S1 to S7.

REFERENCES

1. Waldron KJ, Rutherford JC, Ford D, Robinson NJ. 2009. Metalloproteins and metal sensing. Nature 460:823–830. https://doi.org/10.1038/nature08300
2. Wu FYH, Huang WJ, Sinclair RB, Powers L. 1992. The structure of the zinc sites of *Escherichia coli* DNA-dependent RNA polymerase. J Biol Chem 267:25560–25567. https://doi.org/10.1016/S0021-9258(19)74077-0
3. Markov D, Naryshkina T, Mustaev A, Severinov K. 1999. A zinc-binding site in the largest subunit of DNA-dependent RNA polymerase is involved in enzyme assembly. Genes Dev 13:2439–2448. https://doi.org/10.1101/gad.13.18.2439
4. King RA, Markov D, Sen R, Severinov K, Weisberg RA. 2004. A conserved zinc binding domain in the largest subunit of DNA-dependent RNA polymerase modulates intrinsic transcription termination and antitermination but does not stabilize the elongation complex. J Mol Biol 342:1143–1154. https://doi.org/10.1016/j.jmb.2004.07.072
5. Nies DH. 2016. The biological chemistry of the transition metal "transportome" of *Cupriavidus metallidurans*. Metallomics 8:481–507. https://doi.org/10.1039/c5mt00320b
6. Janssen PJ, Van Houdt R, Moors H, Monsieurs P, Morin N, Michaux A, Benotmane MA, Leys N, Vallaeys T, Lapidus A, Monchy S, Médigue C, Taghavi S, McCorkle S, Dunn J, van der Lelie D, Mergeay M. 2010. The complete genome sequence of *Cupriavidus metallidurans* strain CH34, a master survivalist in harsh and anthropogenic environments. PLoS One 5:e10433. https://doi.org/10.1371/journal.pone.0010433
7. Schulz V, Schmidt-Vogler C, Strohmeyer P, Weber S, Kleemann D, Nies DH, Herzberg M. 2021. Behind the shield of Czc: ZntR controls expression of the gene for the zinc-exporting P-type ATPase ZntA in *Cupriavidus metallidurans*. J Bacteriol 203:e00052-21. https://doi.org/10.1128/JB.00052-21
8. Bütof L, Große C, Lilie H, Herzberg M, Nies DH. 2019. Interplay between the Zur regulon components and metal resistance in *Cupriavidus metallidurans*. J Bacteriol 201:e00192-19. https://doi.org/10.1128/JB.00192-19
9. Bütof L, Schmidt-Vogler C, Herzberg M, Große C, Nies DH. 2017. The components of the unique Zur regulon of *Cupriavidus metallidurans* mediate cytoplasmic zinc handling. J Bacteriol 199:e00372-17. https://doi.org/10.1128/JB.00372-17
10. Mergeay M. 2000. Bacteria adapted to industrial biotopes: metal-resistant *Ralstonia*, p 403–414. In Storz G, Hengge-Aronis R (ed), Bacterial stress responses. ASM Press, Washington DC.
11. Diels L, Mergeay M. 1990. DNA probe-mediated detection of resistant bacteria from soils highy polluted by heavy metals. Appl Environ Microbiol 56:1485–1491. https://doi.org/10.1128/aem.56.5.1485-1491.1990
12. Reith F, Rogers SL, McPhail DC, Webb D. 2006. Biomineralization of gold: biofilms on bacterioform gold. Science 313:233–236. https://doi.org/10.1126/science.1125878
13. Reith F, Brugger J, Zammit CM, Nies DH, Southam G. 2013. Geobiological cycling of gold: from fundamental process understanding to exploration solutions. Minerals 3:367–394. https://doi.org/10.3390/min3040367
14. Van Houdt R, Monchy S, Leys N, Mergeay M. 2009. New mobile genetic elements in *Cupriavidus metallidurans* CH34, their possible roles and occurrence in other bacteria. Antonie Van Leeuwenhoek 96:205–226. https://doi.org/10.1007/s10482-009-9345-4
15. Van Houdt R, Monsieurs P, Mijnendonckx K, Provoost A, Janssen A, Mergeay M, Leys N. 2012. Variation in genomic islands contribute to genome plasticity in *Cupriavidus metallidurans*. BMC Genomics 13:111. https://doi.org/10.1186/1471-2164-13-111
16. Große C, Kohl TA, Niemann S, Herzberg M, Nies DH. 2022. Loss of mobile genomic islands in metal resistant, hydrogen-oxidizing *Cupriavidus metallidurans*. Appl Environ Microbiol 88:e0204821. https://doi.org/10.1128/AEM.02048-21
17. Grosse C, Anton A, Hoffmann T, Franke S, Schleuder G, Nies DH. 2004. Identification of a regulatory pathway that controls the heavy metal resistance system Czc via promoter *czcNp* in *Ralstonia metallidurans*. Arch Microbiol 182:109–118. https://doi.org/10.1007/s00203-004-0670-8
18. Mergeay M, Nies D, Schlegel HG, Gerits J, Charles P, Van Gijsegem F. 1985. *Alcaligenes eutrophus* CH34 is a facultative chemolithotroph with plasmid-bound resistance to heavy metals. J Bacteriol 162:328–334. https://doi.org/10.1128/jb.162.1.328-334.1985
19. Scherer J, Nies DH. 2009. CzcP is a novel efflux system contributing to transition metal resistance in *Cupriavidus metallidurans* CH34. Mol Microbiol 73:601–621. https://doi.org/10.1111/j.1365-2958.2009.06792.x
20. Legatzki A, Grass G, Anton A, Rensing C, Nies DH. 2003. Interplay of the Czc-system and two P-type ATPases in conferring metal resistance to *Ralstonia metallidurans*. J Bacteriol 185:4354–4361. https://doi.org/10.1128/JB.185.15.4354-4361.2003
21. Nies DH, Silver S. 1989. Metal ion uptake by a plasmid-free metal-sensitive *Alcaligenes eutrophus* strain. J Bacteriol 171:4073–4075. https://doi.org/10.1128/jb.171.7.4073-4075.1989
22. Goris J, De Vos P, Coenye T, Hoste B, Janssens D, Brim H, Diels L, Mergeay M, Kersters K, Vandamme P. 2001. Classification of metal-resistant bacteria from industrial biotopes as *Ralstonia campinensis* sp. nov., *Ralstonia metallidurans* sp. nov. and *Ralstonia basilensis* Steinle et al. 1998 emend. Int J Syst Evol Microbiol 51:1773–1782. https://doi.org/10.1099/00207713-51-5-1773
23. Saier MHJ, Tran CV, Barabote RD. 2006. TCDB: the Transporter Classification Database for membrane transport protein analyses and information. Nucleic Acids Res 34:D181–D186. https://doi.org/10.1093/nar/gkj001
24. Busch W, Saier MHJ. 2002. The transporter classification (TC) system. Crit Rev Biochem Mol Biol 37:287–337. https://doi.org/10.1080/-10409230290771528
25. Kirsten A, Herzberg M, Voigt A, Seravalli J, Grass G, Scherer J, Nies DH. 2011. Contributions of five secondary metal uptake systems to metal

homeostasis of *Cupriavidus metallidurans* CH34. J Bacteriol 193:4652–4663. https://doi.org/10.1128/JB.05293-11
26. Schmidt C, Schwarzenberger C, Große C, Nies DH. 2014. FurC regulates expression of *zupT* for the central zinc importer ZupT of *Cupriavidus metallidurans*. J Bacteriol 196:3461–3471. https://doi.org/10.1128/JB.01713-14
27. Patzer SI, Hantke K. 1998. The ZnuABC high-affinity zinc uptake system and its regulator Zur in *Escherichia coli*. Mol Microbiol 28:1199–1210. https://doi.org/10.1046/j.1365-2958.1998.00883.x
28. Gaballa A, Helmann JD. 1998. Identification of a zinc-specific metalloregulatory protein, Zur, controlling zinc transport operons in *Bacillus subtilis*. J Bacteriol 180:5815–5821. https://doi.org/10.1128/JB.180.22.5815-5821.1998
29. Hantke K. 2005. Bacterial zinc uptake and regulators. Curr Opin Microbiol 8:196–202. https://doi.org/10.1016/j.mib.2005.02.001
30. Herzberg M, Bauer L, Kirsten A, Nies DH. 2016. Interplay between seven secondary metal transport systems is required for full metal resistance of *Cupriavidus metallidurans*. Metallomics 8:313–326. https://doi.org/10.1039/c5mt00295h
31. Braun V, Hantke K. 2001. Mechanisms of bacterial iron transport, p 289–311. In Winkelmann G (ed), Microbial transport systems. Wiley-VCH, Weinheim.
32. Patzer SI, Hantke K. 2000. The zinc-responsive regulator Zur and its control of the *znu* gene cluster encoding the ZnuABC zinc uptake system in *Escherichia coli*. J Biol Chem 275:24321–24332. https://doi.org/10.1074/jbc.M001775200
33. Herzberg M, Bauer L, Nies DH. 2014. Deletion of the *zupT* gene for a zinc importer influences zinc pools in *Cupriavidus metallidurans* CH34. Metallomics 6:421–436. https://doi.org/10.1039/c3mt00267e
34. Große C, Herzberg M, Schüttau M, Wiesemann N, Hause G, Nies DH. 2016. Characterization of the Δ7 mutant of *Cupriavidus metallidurans* with deletions of seven secondary metal uptake systems. mSystems 1:e00004-16. https://doi.org/10.1128/mSystems.00004-16
35. Nies DH. 2007. How cells control zinc homeostasis. Science 317:1695–1696. https://doi.org/10.1126/science.1149048
36. Elston R, Mulligan C, Thomas GH. 2023. Flipping the switch: dynamic modulation of membrane transporter activity in bacteria. Microbiology (Reading) 169:0. https://doi.org/10.1099/mic.0.001412
37. Weast RC. 1984. CRC handbook of chemistry and physics. 64th ed. CRC Press, Inc, Boca Raton, Florida, USA.
38. Pfennig N. 1974. *Rhodopseudomonas globiformis*, Sp-N, a new species of *Rhodospirillaceae*. Arch Microbiol 100:197–206. https://doi.org/10.1007/BF00446317
39. Hirth N, Gerlach M-S, Wiesemann N, Herzberg M, Große C, Nies DH. 2023. Full copper resistance in *Cupriavidus metallidurans* requires the interplay of many resistance systems. Appl Environ Microbiol 89:e0056723. https://doi.org/10.1128/aem.00567-23
40. Legatzki A, Franke S, Lucke S, Hoffmann T, Anton A, Neumann D, Nies DH. 2003. First step towards a quantitative model describing Czc-mediated heavy metal resistance in *Ralstonia metallidurans*. Biodegradation 14:153–168. https://doi.org/10.1023/a:1024043306888
41. Große C, Scherer J, Schleuder G, Nies DH. 2023. Interplay between two-component regulatory systems is involved in control of *Cupriavidus metallidurans* metal resistance genes. J Bacteriol 205:e0034322. https://doi.org/10.1128/jb.00343-22
42. Nies DH, Silver S. 1989. Plasmid-determined inducible efflux is responsible for resistance to cadmium, zinc, and cobalt in *Alcaligenes eutrophus*. J Bacteriol 171:896–900. https://doi.org/10.1128/jb.171.2.896-900.1989
43. Nies DH, Nies A, Chu L, Silver S. 1989. Expression and nucleotide sequence of a plasmid-determined divalent cation efflux system from *Alcaligenes eutrophus*. Proc Natl Acad Sci U S A 86:7351–7355. https://doi.org/10.1073/pnas.86.19.7351
44. Nies D, Mergeay M, Friedrich B, Schlegel HG. 1987. Cloning of plasmid genes encoding resistance to cadmium, zinc, and cobalt in *Alcaligenes eutrophus* CH34. J Bacteriol 169:4865–4868. https://doi.org/10.1128/jb.169.10.4865-4868.1987
45. Lunin VV, Dobrovetsky E, Khutoreskaya G, Zhang R, Joachimiak A, Doyle DA, Bochkarev A, Maguire ME, Edwards AM, Koth CM. 2006. Crystal structure of the CorA Mg^{2+} transporter. Nature 440:833–837. https://doi.org/10.1038/nature04642
46. Lu M, Chai J, Fu D. 2009. Structural basis for autoregulation of the zinc transporter YiiP. Nat Struct Mol Biol 16:1063–1067. https://doi.org/10.1038/nsmb.1662
47. Thieme D, Neubauer P, Nies DH, Grass G. 2008. Sandwich hybridization assay for sensitive detection of dynamic changes in mRNA transcript levels in crude *Escherichia coli* cell extracts in response to copper ions. Appl Environ Microbiol 74:7463–7470. https://doi.org/10.1128/AEM.01370-08
48. van der Lelie D, Schwuchow T, Schwidetzky U, Wuertz S, Baeyens W, Mergeay M, Nies DH. 1997. Two component regulatory system involved in transcriptional control of heavy metal homoeostasis in *Alcaligenes eutrophus*. Mol Microbiol 23:493–503. https://doi.org/10.1046/j.1365-2958.1997.d01-1866.x
49. Taudte N, Grass G. 2010. Point mutations change specificity and kinetics of metal uptake by ZupT from *Escherichia coli*. Biometals 23:643–656. https://doi.org/10.1007/s10534-010-9319-z
50. Grass G, Franke S, Taudte N, Nies DH, Kucharski LM, Maguire ME, Rensing C. 2005. The metal permease ZupT from *Escherichia coli* is a transporter with a broad substrate spectrum. J Bacteriol 187:1604–1611. https://doi.org/10.1128/JB.187.5.1604-1611.2005
51. Xia Y, Lundbäck A-K, Sahaf N, Nordlund G, Brzezinski P, Eshaghi S. 2011. Co^{2+} selectivity of *Thermotoga maritima* CorA and its inability to regulate Mg^{2+} homeostasis present a new class of CorA proteins. J Biol Chem 286:16525–16532. https://doi.org/10.1074/jbc.M111.222166
52. Tripathi VN, Srivastava S. 2006. Ni^{2+}-uptake in *Pseudomonas putida* strain S4: a possible role of Mg^{2+}-uptake pump. J Biosci 31:61–67. https://doi.org/10.1007/BF02705236
53. Lohmeyer M, Friedrich CG. 1987. Nickel transport in *Alcaligenes eutrophus*. Arch. Microbiol 149:130–135. https://doi.org/10.1007/BF00425078
54. Jackson RJ, Binet MRB, Lee LJ, Ma R, Graham AI, McLeod CW, Poole RK. 2008. Expression of the PitA phosphate/metal transporter of *Escherichia coli* is responsive to zinc and inorganic phosphate levels. FEMS Microbiol Lett 289:219–224. https://doi.org/10.1111/j.1574-6968.2008.01386.x
55. Housecroft CE, Constable EC. 2006. Chemistry. 3rd ed. Pearson Education Limited, Essex, England.
56. De Pina K, Desjardin V, Mandrand-Berthelot MA, Giordano G, Wu LF. 1999. Isolation and characterization of the *nikR* gene encoding a nickel-responsive regulator in *Escherichia coli*. J Bacteriol 181:670–674. https://doi.org/10.1128/JB.181.2.670-674.1999
57. Rowe JL, Starnes GL, Chivers PT. 2005. Complex transcriptional control links NikABCDE-dependent nickel transport with hydrogenase expression in *Escherichia coli*. J Bacteriol 187:6317–6323. https://doi.org/10.1128/JB.187.18.6317-6323.2005
58. Navarro C, Wu LF, Mandrand-Berthelot MA. 1993. The *nik* operon of *Escherichia coli* encodes a periplasmic binding-protein-dependent transport-system for nickel. Mol Microbiol 9:1181–1191. https://doi.org/10.1111/j.1365-2958.1993.tb01247.x
59. Guskov A, Nordin N, Reynaud A, Engman H, Lundbäck A-K, Jong AJO, Cornvik T, Phua T, Eshaghi S. 2012. Structural insights into the mechanisms of Mg^{2+} uptake, transport, and gating by CorA. Proc Natl Acad Sci U S A 109:18459–18464. https://doi.org/10.1073/pnas.1210076109
60. Nordin N, Guskov A, Phua T, Sahaf N, Xia Y, Lu SY, Eshaghi H, Eshaghi S. 2013. Exploring the structure and function of *Thermotoga maritime* CorA reveals the mechanism of gating and ion selectivity in Co^{2+}/Mg^{2+} transport. Biochem J 451:365–374. https://doi.org/10.1042/BJ20121745
61. Payandeh J, Li C, Ramjeesingh M, Poduch E, Bear CE, Pai EF. 2008. Probing structure-function relationships and gating mechanisms in the CorA Mg^{2+} transport system. J Biol Chem 283:11721–11733. https://doi.org/10.1074/jbc.M707889200
62. Eitinger T, Rodionov DA, Grote M, Schneider E. 2011. Canonical and ECF-type ATP-binding cassette importers in prokaryotes: diversity in modular organization and cellular functions. FEMS Microbiol Rev 35:3–67. https://doi.org/10.1111/j.1574-6976.2010.00230.x
63. Rodionov DA, Hebbeln P, Gelfand MS, Eitinger T. 2006. Comparative and functional genomic analysis of prokaryotic nickel and cobalt uptake transporters: evidence for a novel group of ATP-binding cassette transporters. J Bacteriol 188:317–327. https://doi.org/10.1128/JB.188.1.317-327.2006

64. Siche S, Neubauer O, Hebbeln P, Eitinger T. 2010. A bipartite S unit of an ECF-type cobalt transporter. Res Microbiol 161:824–829. https://doi.org/10.1016/j.resmic.2010.09.010
65. Mergeay M, Monchy S, Vallaeys T, Auquier V, Benotmane A, Bertin P, Taghavi S, Dunn J, van der Lelie D, Wattiez R. 2003. *Ralstonia metallidurans*, a bacterium specifically adapted to toxic metals: towards a catalogue of metal-responsive genes. FEMS Microbiol Rev 27:385–410. https://doi.org/10.1016/S0168-6445(03)00045-7
66. Mergeay M, Van Houdt R. 2021. *Cupriavidus metallidurans* CH34, a historical perspective on its discovery, characterization and metal resistance. FEMS Microbiol Ecol 97:fiaa247. https://doi.org/10.1093/femsec/fiaa247
67. Monchy S, Benotmane MA, Janssen P, Vallaeys T, Taghavi S, van der Lelie D, Mergeay M. 2007. Plasmids pMOL28 and pMOL30 of *Cupriavidus metallidurans* are specialized in the maximal viable response to heavy metals. J Bacteriol 189:7417–7425. https://doi.org/10.1128/JB.00375-07
68. Taghavi S, Lesaulnier C, Monchy S, Wattiez R, Mergeay M, van der Lelie D. 2009. Lead(II) resistance in *Cupriavidus metallidurans* CH34: interplay between plasmid and chromosomally-located functions. Antonie Van Leeuwenhoek 96:171–182. https://doi.org/10.1007/s10482-008-9289-0
69. Tseng T-T, Gratwick KS, Kollman J, Park D, Nies DH, Goffeau A, Saier MHJ. 1999. The RND superfamily: an ancient, ubiquitous and diverse family that includes human disease and development proteins. J Mol Microbiol Biotechnol 1:107–125.
70. Goldberg M, Pribyl T, Juhnke S, Nies DH. 1999. Energetics and topology of CzcA, a cation/proton antiporter of the RND protein family. J Biol Chem 274:26065–26070.
71. Wagegg W, Braun V. 1981. Ferric citrate transport in *Escherichia coli* requires outer membrane receptor protein FecA. J Bacteriol 145:156–163. https://doi.org/10.1128/jb.145.1.156-163.1981
72. Herzberg M, Schüttau M, Reimers M, Große C, Nies DH, Hans-Günther-Schlegel. 2015. Synthesis of nickel-iron hydrogenase in *Cupriavidus metallidurans* is controlled by metal-dependent silencing and un-silencing of genomic islands. Metallomics 7:632–649. https://doi.org/10.1039/c4mt00297k
73. Wiesemann N, Mohr J, Grosse C, Herzberg M, Hause G, Reith F, Nies DH. 2013. Influence of copper resistance determinants on gold transformation by *Cupriavidus metallidurans* strain CH34. J Bacteriol 195:2298–2308. https://doi.org/10.1128/JB.01951-12

Chapter 2 – Intracellular metal handling by COG0523 proteins

I) The metal-binding GTPases CobW2 and CobW3 are at the crossroads of zinc and cobalt homeostasis in *Cupriavidus metallidurans*

Summary of the publication

This publication describes the ability of *C. metallidurans* to survive conditions of zinc starvation, and highlights a novel connection between zinc and cobalt homeostasis. It investigates to which extent cobalt ions can substitute for zinc ions in case of zinc starvation and aims at understanding the role of four proteins with well-established roles in both zinc and cobalt homeostasis: the Zur-regulon ZupT, CobW2 and CobW3, the trio of proteins involved in zinc homeostasis, and the main cobalt efflux system, the CDF protein DmeF.

The cells were exposed to different zinc and cobalt exogenous concentrations, which allowed the creation of various metal conditions, from severe starvation, insufficiency or replete, to abundancy of these ions. The plasmid free parent strain AE104 and combinations of knock-out mutants, of *cobW2, cobW3, zupT* and *dmeF* genes, were created and the effect of the respective encoded gene products was investigated.

When found at the edge of zinc starvation and unable to accumulate the optimal amount of zinc ions, the AE104 cells imported cobalt ions, instead, providing that sufficient cobalt amount is available. The ability to accumulate cobalt ions depends on the presence of both CobW3 and ZupT proteins. Cells containing a deletion of *zupT* accumulated only 7.000 cobalt ions and those with a deletion of *cobW3* gene accumulated 4.000 cobalt ions, while the parent strain accumulated 20.000 cobalt ions.

The increased cobalt uptake also required detoxification of these ions, which is achieved by the CDF efflux system, DmeF. A deletion of *dmeF* gene leads to a considerable sensitivity to cobalt in comparison with the parent strain. ZupT, CobW2 and CobW3 also benefit the cell in withstanding cobalt and cadmium toxicity or handle a general metal starvation situation induced by EDTA. The same three proteins are required to adjust the two cellular zinc pools of the cell.

AMERICAN SOCIETY FOR MICROBIOLOGY | Journal of Bacteriology

| Genetics and Molecular Biology | Full-Length Text

The metal-binding GTPases CobW2 and CobW3 are at the crossroads of zinc and cobalt homeostasis in *Cupriavidus metallidurans*

Diana Galea,[1] **Martin Herzberg,**[1,2] **Dietrich H. Nies**[1]

AUTHOR AFFILIATIONS See affiliation list on p. 25.

ABSTRACT The metal-resistant beta-proteobacterium *Cupriavidus metallidurans* is also able to survive conditions of metal starvation. We show that zinc-starved cells can substitute some of the required zinc with cobalt but not with nickel ions. The zinc importer ZupT was necessary for this process but was not essential for either zinc or cobalt import. The cellular cobalt content was also influenced by the two COG0523-family proteins, CobW2 and CobW3. Pulse-chase experiments with radioactive and isotope-enriched zinc demonstrated that both proteins interacted with ZupT to control the cellular flow-equilibrium of zinc, a central process of zinc homeostasis. Moreover, an antagonistic interplay of CobW2 and CobW3 in the presence of added cobalt caused a growth defect in mutant cells devoid of the cobalt efflux system DmeF. Full cobalt resistance also required a synergistic interaction of ZupT and DmeF. Thus, the two transporters along with CobW2 and CobW3 interact to control cobalt homeostasis in a process that depends on zinc availability. Because ZupT, CobW2, and CobW3 also direct zinc homeostasis, this process links the control of cobalt and zinc homeostasis, which subsequently protects *C. metallidurans* against cadmium stress and general metal starvation.

IMPORTANCE In bacterial cells, zinc ions need to be allocated to zinc-dependent proteins without disturbance of this process by other transition metal cations. Under zinc-starvation conditions, *C. metallidurans* floods the cell with cobalt ions, which protect the cell against cadmium toxicity, help withstand metal starvation, and provide cobalt to metal-promiscuous paralogs of essential zinc-dependent proteins. The number of cobalt ions needs to be carefully controlled to avoid a toxic cobalt overload. This is accomplished by an interplay of the zinc importer ZupT with the COG0523-family proteins, CobW3, and CobW2. At high external cobalt concentrations, this trio of proteins additionally interacts with the cobalt efflux system, DmeF, so that these four proteins form an inextricable link between zinc and cobalt homeostasis.

KEYWORDS zinc, cobalt, *Cupriavidus metallidurans*

Cupriavidus metallidurans is a beta-proteobacterium that is adapted to metal-rich environments such as zinc deserts and auriferous soils (1–4). *C. metallidurans* strain CH34 contains a chromosome, a chromid, and two large plasmids with a variety of metal-resistance determinants (5, 6). The gene products of these determinants export excessively high concentrations of transition metal ions from the cytoplasm to the periplasm, and others from there to the outside. In the case of some metals, reduction and oxidation reactions to less toxic species are also mechanisms employed to decrease the toxic burden of the respective metal ion or complex (7).

Editor Conrad W. Mullineaux, Queen Mary University of London, London, United Kingdom

Address correspondence to Dietrich H. Nies, d.nies@mikrobiologie.uni-halle.de.

The authors declare no conflict of interest.

See the funding table on p. 25.

Received 31 May 2024
Accepted 3 July 2024
Published 23 July 2024

Cobalt and zinc ions can be imported into the *C. metallidurans* cell by a variety of import systems (8–10), for instance, secondary, *proton motive force*-driven members ZupT of the ZIP [ZRT/IRT, TC2.A.5 (11, 12)] and CorA1, CorA2, and CorA3 of the MIT (metal inorganic transport, TC1.A.35) families. The name of these latter transport systems stems from the fact that a deletion of the cognate gene results in increased cobalt tolerance (13, 14). When the cytoplasmic content of zinc or cobalt ions becomes too high, Zn(II) is exported by the P_{IB2}-type ATPases ZntA and CadA, and Co(II) is exported by the CDF (cation diffusion facilitator, TC2.A.4) protein, DmeF (Fig. S1) (15, 16). At even higher concentrations of these ions, the plasmid-encoded transenvelope efflux systems CzcCBA and CnrCBA export Zn(II) and Co(II) to the environment (7). Thus, export and import reactions adjust the cytoplasmic metal zinc concentration in a flow equilibrium, which is buffered by cytoplasmic metal-binding activities (17, 18). The expression "flow equilibrium" was used here to emphasize the importance of metal transport systems to reach the steady state condition of cellular zinc homeostasis.

Despite being a metal-resistant bacterium, *C. metallidurans* is also able to cope with metal-starvation conditions. In the case of zinc ion limitation, the Zur regulon mediates this ability (19–21). Products of this regulon are Zur itself, ZupT, and two metal-binding GTPases of the COG0523 family (20–24), CobW2 and CobW3 (Fig. S1). CobW2 is a zinc-storage compound that binds up to six Zn ions per polypeptide with low affinity at binding sites in the middle of the peptide chain and can unfold in the presence of MgGTP. CobW3 has no a GTPase activity but is able to sequester up to eight Zn ions per polypeptide with decreasing affinity to sites located at the carboxy terminus and equilibrates metal import by ZupT with that of other metal transport systems. When treated with a mixture of metal ions, CobW3 is also able to bind 2 Ni(II), 1 Co(II), and 1 Cd(II) instead of four Zn ions (20). Moreover, under even more extreme zinc starvation conditions, release of Zur from a double binding site at the *cobW1p* promoter allows expression of an operon encoding CobW1 as a third CobW protein, along with several paralogs of zinc-requiring enzymes and the metal-promiscuous GTP cyclohydrolase FolE_IB2 (20, 21, 25). FolE-type enzymes are important for the initiation of folate biosynthesis by cyclo-hydrolyzation of GTP, and synthesis of GTP needs tetrahydrofolate; hence, folate biosynthesis can be described as an "Achilles heel" of bacterial metabolism (26–28).

C. metallidurans possesses three FolE-type enzymes, the strictly zinc-dependent FolE_IA, and the metal-promiscuous FolE_IB1 and FolE_IB2 proteins. FolE_IB1 and IB2 are needed for growth under zinc-starvation conditions (25). The optimally suited cofactors for the two FolE_IBs are Fe(II), Mn(II), and Co(II) (25); however, *C. metallidurans* contains only a very low number of Mn atoms per cell, does not have a NRAMP-type manganese importer (TC2.A.55), and lacks a Mn-dependent superoxide dismutase (8, 29). Iron, on the other hand, is used for a multitude of biochemical reactions (30), but uncontrolled Fe(II) can be extremely detrimental due to its ability to catalyze the Fenton reaction (31–33).

This leaves Co(II) as the most suitable metal cofactor for the metal-promiscuous enzymes in *C. metallidurans* under zinc starvation conditions, besides cobalamin as an important cobalt sink (34). Nevertheless, too high intracellular cobalt concentrations are toxic and damage-nascent iron-sulfur clusters (35–37). If Co(II) can substitute for Zn(II), as discussed for *Salmonella* (38), it should be used only under zinc starvation conditions, and its cellular content must be strictly controlled. In addition to the overall affinity of a metal cation to a protein as defined by its rank in the Irving-Williams series (39), the actual availability controls metalation of a protein by a specific metal cation in competition with another metal cation (40, 41). Although CobW2 has been discussed to be a zinc-storing protein, CobW3 may be capable of sensing metal availability by binding the cations at its carboxy-terminal metal-binding site and use this information to control metal homeostasis by influencing activity of metal transport systems. It is therefore conceivable that the actual availability of cobalt and zinc could control metalation of CobW3 and, subsequently, the import of zinc and other metal cations.

This current study provides evidence for three processes that support the above proposal. First, *C. metallidurans* fills up a part of its cellular zinc pool with cobalt ions. ZupT and CobW3 control this response with a minor contribution from CobW2. Second, these three proteins are also involved in the cellular flow equilibrium of zinc by affecting zinc import rather than efflux. Third, disturbance of the zinc-cobalt homeostasis mediated by these three proteins results in decreased cobalt, cadmium, and metal-starvation tolerance, with DmeF supporting ZupT, CobW3, and CobW2 (Fig. S1) to mediate cobalt resistance.

RESULTS

Experimental strategy

Due to the fact that the GTP cyclohydrolase FolE_IB1 can be activated by Co(II) 50-times more effectively than by Ni(II) (25), *C. metallidurans* may import cobalt rather than nickel under zinc starvation conditions to metalate this enzyme and continue folate biosynthesis. To investigate whether zinc availability influences the cellular cobalt content, the cells were cultivated in Tris-buffered mineral salts medium TMM (5) with gluconate as the carbon source but with different zinc and cobalt concentrations (Table S1). In TMM, trace element solution SL6 (42) provided 35.3 nM Zn(II) and 84.1 nM Co(II) to the medium; however, the actual zinc content varies due to the zinc content of the respective $NaSO_4$ source (25). This fact was used to design six TMM solutions with different zinc and cobalt concentrations exposing the *C. metallidurans* cells to different levels of zinc and cobalt starvation stress (Table S1). All strains used (Table S2) were derivatives of the plasmid-free strain AE104 because a Δ*zupT* deletion results in curing of the plasmid pMOL30 in *C. metallidurans* CH34 wild type (43). All experiments were performed at least as three biological repeats. For most experiments, data points were judged as different if their ratio was at least two and if their deviation bars did not touch or overlap.

Zinc controls cobalt homeostasis in *C. metallidurans*

C. metallidurans strain AE104 was cultivated to the mid-exponential phase of growth (150 Klett units) in three TMM media with 200 nM (aZn), 64 nM (mZn), or 39 nM (lZn) Zn(II), respectively (Table 1). As determined by ICP-MS (inductively coupled plasma mass spectrometry), the zinc content of the cells decreased with the decreasing zinc content of the respective medium from 101,000 Zn per cell via 33,000 down to 7,100 when no

TABLE 1 Metal content of *C. metallidurans* strain AE104 in different TMM media[a]

Addition	Atoms per cell						
	Mg, 10^6	Ca, 10^3	Fe, 10^3	Zn, 10^3	Co, 10^3	Ni, 10^3	Cu, 10^3
TMM 200 nM Zn (aZn)							
0 µM Zn	13.4 ± 0.7	251 ± 9	998 ± 4	101 ± 4	5.3 ± 0.4	4.2 ± 0.2	5.6 ± 0.4
1 µM Zn	14.8 ± 0.6	231 ± 27	1,082 ± 14	128 ± 8	4.7 ± 0.3	4.4 ± 0.2	4.7 ± 0.2
10 µM Zn	14.1 ± 0.3	197 ± 18	1,059 ± 33	124 ± 4	4.4 ± 0.2	4.0 ± 0.0	4.7 ± 0.3
100 µM Zn	17.6 ± 0.4	139 ± 8	834 ± 37	157 ± 19	4.4 ± 0.0	3.4 ± 0.0	5.1 ± 0.2
TMM 64 nM Zn(II) (mZn)							
0 µM Zn	11.2 ± 0.3	269 ± 166	819 ± 28	33.4 ± 5.4	20.5 ± 0.9	5.0 ± 0.6	4.3 ± 0.7
1 µM Zn	11.9 ± 0.2	280 ± 131	874 ± 10	115 ± 1	18.4 ± 1.6	3.6 ± 0.4	4.2 ± 0.4
10 µM Zn	12.6 ± 0.4	209 ± 74	863 ± 33	160 ± 4	21.4 ± 1.3	3.9 ± 0.2	4.1 ± 0.3
100 µM Zn	14.3 ± 0.5	120 ± 66	641 ± 19	155 ± 10	17.7 ± 0.7	2.8 ± 0.3	4.3 ± 1.1
TMM 39 nM Zn(II), no SL6 (lZn)							
0 µM Zn	13.3 ± 0.4	193 ± 43	1,003 ± 40	7.1 ± 1.2	0.3 ± 0.0	4.2 ± 0.1	2.8 ± 0.6
1 µM Zn	13.0 ± 0.5	277 ± 98	850 ± 52	113 ± 8	0.2 ± 0.0	3.3 ± 0.2	5.3 ± 3.4
10 µM Zn	13.9 ± 0.6	187 ± 48	840 ± 45	138 ± 9	0.2 ± 0.0	3.1 ± 0.2	2.4 ± 0.2
100 µM Zn	16.6 ± 0.7	142 ± 43	709 ± 14	186 ± 18	0.2 ± 0.0	2.6 ± 0.1	2.8 ± 0.5

[a]*C. metallidurans* AE104 was cultivated in TMM medium with ambient zinc (aZn) TMM, which leads to fully zinc-replete cells, under moderate zinc starvation (mZn) and under low zinc and cobalt (lZn) to a turbidity of 100 Klett, before mid-exponential phase of growth. Zn(II) was added at the indicated concentration. Incubation was continued with shaking to a turbidity of 150 Klett units reaching the mid-exponential phase and the metal content was determined by ICP-MS. *n* = 3, with the standard deviations indicated.

SL6 was added to the medium. When more zinc (1, 10, and 100 µM) was added to these cells before the mid-exponential phase of growth, their zinc content increased. At high zinc concentrations, the zinc ion content of the cells that had been cultivated under these conditions was similar and reached an intracellular saturation of the zinc repository with on average 150,000 Zn ions per cell, which is comparable with previous studies (17).

Although no important changes between the intracellular content of Mg, Ca, Fe, Ni, and Cu could be observed (Table 1), the cobalt content depended on the medium zinc or cobalt concentration. Cells grown in the presence of the same cobalt concentration (86 nM) with 200 nM (aZn) zinc contained ~5,000 Co ions per cell, but with 64 nM Zn (mZn) about 20,000, and those in low zinc and low cobalt (~2 nM) medium only a few hundred Co atoms per cell were detected. Addition of zinc (1, 10, or 100 µM) before reaching the mid-exponential phase of growth did not change the cobalt content of the cells in this incubation experiment in indirect proportion to the zinc content. The cells seemed to have accumulated more cobalt under zinc starvation condition (mZn) than under zinc-replete conditions (aZn), provided sufficient cobalt (86 nM) was available in these growth media, which was not the case in media without SL6 (lZn) (Table 1). The threshold for the zinc concentration that stimulated increased cobalt accumulation should be between 64 nM and 200 nM Zn(II) but was far below 1 µM Zn(II). Zinc starvation controlled the cobalt level of the cells, but the starvation stress had to be present at the beginning of growth, or even in the pre-cultures. It took some time for the cells to experience starvation conditions and react to them.

To obtain a better measure for the threshold concentration of zinc that governs the cobalt level, strain AE104 was cultivated in standard TMM (160 nM Zn), high-zinc (400 nM Zn), and low zinc-cobalt medium (39 nM Zn) without trace element solution SL6 (Table 2). As published previously (8, 17, 21, 43, 44), the zinc content of the parental strain AE104 remained at about 70,000 to 80,000 Zn ions per cell in standard TMM, which included 160 nM Zn(II) (Table 2). The increased zinc concentration in high zinc medium

TABLE 2 Zinc and cobalt content of *C. metallidurans* strain AE104 and its Δ*zupT* mutant under various growth conditions[a]

Strain	Medium		1,000 Metal atoms per cell	
	Zn (nM)	Co (nM)	Co	Zn
High-zinc TMM (hZn)				
AE104	400	110	3.7 ± 1.1	75.8 ± 7.7
Δ*zupT*	400	110	6.4 ± 0.9	42.8 ± 4.3
Standard TMM				
AE104	160	110	21.3 ± 10.7	68.4 ± 12.4
Δ*zupT*	160	110	7.3 ± 1.9	28.6 ± 4.8
Low-zinc-cobalt, no SL6 (lZn)				
AE104	39	2	0.153 ± 0.045	27.5 ± 11.0
AE104	39	100	40.2 ± 3.6	18.1 ± 9.6
AE104	39	150	40.0 ± 7.4	19.7 ± 5.8
AE104	39	300	57.2 ± 16.5	21.6 ± 8.7
AE104	190	100	25.6 ± 3.6	83.6 ± 6.1
AE104	190	150	20.6 ± 3.5	65.4 ± 4.7
AE104	190	300	24.9 ± 3.2	74.5 ± 8.2
Δ*zupT*	39	2	0.105 ± 0.073	19.9 ± 2.4
Δ*zupT*	39	100	35.2 ± 3.3	14.6 ± 2.2
Δ*zupT*	39	150	44.8 ± 5.9	14.5 ± 6.2
Δ*zupT*	39	300	46.5 ± 19.8	37.1 ± 8.5
Δ*zupT*	190	100	5.4 ± 0.5	32.5 ± 2.8
Δ*zupT*	190	150	8.2 ± 0.8	23.3 ± 3.5
Δ*zupT*	190	300	14.1 ± 4.6	25.8 ± 4.4

[a]Same cultivation conditions as in Table 1. The metal content was verified by ICP-MS and was in the expected range. Data for all metals are presented in Table S3

with 400 nM Zn(II) did not change this number in AE104, although the deviation of this number decreased by half compared with the standard medium.

Again, strain AE104 accumulated approximately 20,000 Zn ions per cell in low Zn-Co medium (lZn) (Tables 1 and 2). This was not surprising because 39 ± 8 nM zinc in low zinc/cobalt medium was distributed among 1.2×10^{12} cells L^{-1} (around the mid-exponential phase of growth), resulting in a maximal number of 19,500 ± 4,000 Zn ions per cell. In low-zinc medium, the zinc content may have been exhausted after growth. A similar calculation for the zinc content of moderate zinc medium of 160 ± 36 nM distributed among the cells calculates to 80,000 ± 18,000 Zn ions per cell. Again, the zinc content of the zinc growth medium was mirrored by that of the cellular zinc content. In contrast, the cellular zinc content remained at 76,000 Zn ions per cell in high zinc medium (400 nM, Table 2). The cells limited their cellular zinc content, e.g., by ZntA-mediated zinc efflux. They were under zinc starvation in low Zn-Co medium, exactly at the edge of zinc starvation at 160 nM zinc but were supplied with sufficient zinc at 400 nM zinc in the medium (Table 2).

A complete distribution of the 2 nM cobalt ions in low zinc/cobalt medium would result in about 1,000 Co ions per cell. The cobalt content of these cells was even below this number (Table 2). In moderate and high zinc media, complete distribution of the approximately 100 nM Co would give 50,000 Co ions per cell. The measured level was below this number, about 21,000 Co ions per cell in moderate zinc and only about 3,700 Co ions per cell in high zinc medium. When on the verge of zinc starvation, the cells accumulated a higher number of Co ions; however, accumulation did not exhaust the cobalt content of the growth medium. Zinc availability in the growth medium did indeed prove to control the cellular cobalt content.

To test this observation further, strain AE104 was cultivated in TMM adjusted to concentrations between 85 nM and 300 nM Zn(II), and the metal content of medium and cells was determined by ICP-MS (Fig. 1A). The cellular zinc content increased with increasing metal availability and followed a curve that reached saturation at 150 nM Zn(II) in the growth medium. The cellular cobalt content, in contrast, followed an inverse

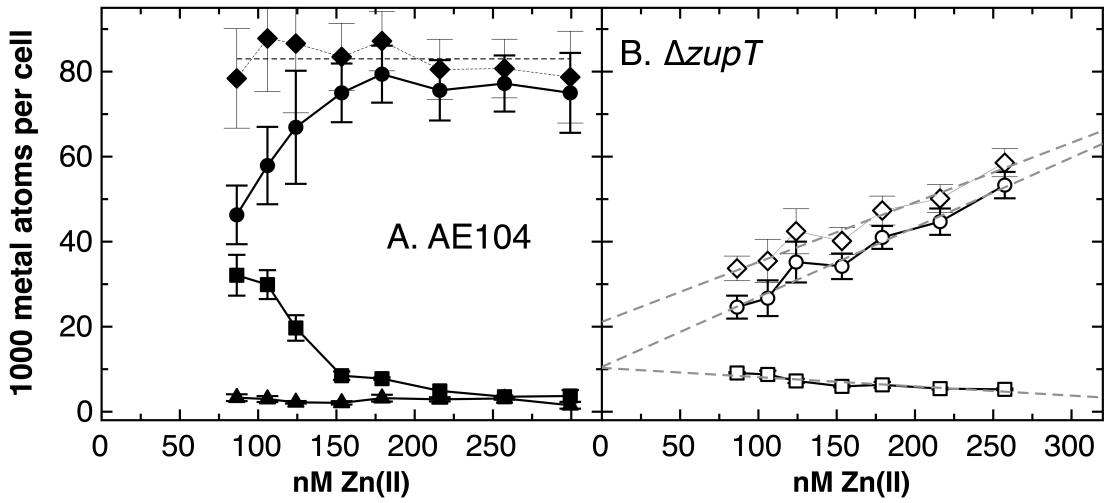

FIG 1 Zinc availability controls the cellular cobalt content in *C. metallidurans* AE104 and ZupT is required for this process. Cells were cultivated in moderate zinc mZn-TMM with an adjusted zinc content to the exponential phase of growth. The cellular zinc (circles), cobalt (squares), and nickel (triangles) contents were measured by ICP-MS. The diamonds represent the sum of the zinc plus cobalt contents per cell. Panel A. The *C. metallidurans* parental strain, AE104. The dashed line indicates the mean value of the sum of the zinc and cobalt content of 83,000 ± 3,900 (Zn + Co)/cell. Panel B. The cellular zinc content of the Δ*zupT* strain (open symbols) was fitted to the zinc availability with 11,300 ± 2,500 Zn/cell + 161 ± 15 zn/cell * nM medium zinc (98%), the cobalt content was 10,600 ± 800 Co/cell – 23 ± 5 Co/cell * nM medium zinc (91%),, and the Zn + Co content was 21,100 ± 3,900 (Zn + Co)/cell + 140 ± 22 (Zn + Co)/cell * nM medium zinc (97%). These functions are shown with dashed gray lines.

curve. The sum of both metal contents was 83,000 ± 3,900 Zn + Co ions per cell. The cells filled up their cobalt content to a level of 83,000 ions per cell minus the zinc content. Interestingly, the nickel content of the cells was not affected (Fig. 1A, triangles). This demonstrated clearly that the zinc availability in the growth medium controlled the cobalt, but not the nickel, content in *C. metallidurans* strain AE104. This may allow cobalt ions to substitute for zinc ions and reflects a possible shared metal pool in the cell.

The zinc importer ZupT of the ZIP protein family is involved in zinc-mediated control of the cellular cobalt content

When the Δ*zupT* mutant was incubated in TMM with adapted zinc concentrations (Fig. 1B), the zinc content of the mutant cells was lower than that of the parent; it did not follow a saturation curve but followed a linear fashion with the zinc content of the medium exhibiting an increase of 161 ± 17 Zn ions per cell per nM exogenously supplied Zn. The cobalt content decreased with the zinc content of the medium, corresponding to a decrease in 23 ± 5 Co ions per cell per nM Zn in the growth medium. Both lines crossed the y-axis at x = 0 with similar numbers, 11,300 ± 2,300 Zn and 10,600 ± 800 Co ions per cell. The total zinc plus cobalt content increased such that 140 ± 22 (Zn + Co) ions per cell per nM Zn represented the sum for the zinc and cobalt ion content (Fig. 1B).

The zinc content of the Δ*zupT* mutant cultivated in moderate zinc and low zinc/cobalt medium (Table 2) was at a value that could be expected from the linear function of the ion (Fig. 1B). In high zinc medium, the cells contained only 42,800 Zn ions per cell, much less than expected from the linear function. This indicated that efflux systems had been activated, for instance, ZntA. Nevertheless, ZupT was also required to adjust the cellular zinc content in high zinc medium. The cobalt content was also at the level expected based on the linear function (Fig. 1B) or from an exhaustive accumulation of the available cobalt in low zinc/cobalt medium (Table 2).

For a more detailed characterization of the role of ZupT in cobalt accumulation, the Δ*zupT* strain and its parent AE104 were cultivated in low zinc-cobalt (lZn) medium, which was supplemented with 100 nM, 150 nM, or 300 nM cobalt chloride, with or without additional 150 nM zinc chloride. This resulted in zinc concentrations in the growth medium of 39 nM or 190 nM (Table 2). At 39 nM Zn(II) in the medium, the cellular zinc content remained at the expected 20,000 Zn ions per cell with no difference between the Δ*zupT* strain and its parent; all available zinc had been accumulated. When Co(II) was added to the cells, both strains accumulated between 37,000 and about 50,000 Co ions per cell at 100 nM, 150 nM, or 300 nM Co(II) (Table 2). Again, the absence of ZupT made no difference with respect to the cellular cobalt content, despite the presence of the remaining import systems for divalent metal cations in the *C. metallidurans* cell. The cobalt content of the medium was not exhausted, although the Zn + Co content of 83,000 ions per cell had not been reached. Strain AE104 substituted Co for Zn only to between 50% and 70% of the total of 83,000 Zn + Co ions, however, not completely. ZupT was not needed under zinc starvation conditions at 39 nM Zn(II) for exhaustive zinc accumulation.

At 190 nM Zn(II), the zinc content of the AE104 parental strain was saturated between 70,000 and 80,000 Zn ions per cell (Fig. 1A; Table 2) but that of the Δ*zupT* mutant accumulated only between 23,000 and 32,000 Zn ions per cell (Table 2). This level was expected based on the linear dependence of the Zn content of Δ*zupT* cells on the zinc availability (Fig. 1B). In contrast to the parental strain, the Co content of Δ*zupT* cells remained very low when Co(II) was added to this medium. The Co content in Δ*zupT* increased in a linear fashion with the cobalt content of the medium but only in the presence of sufficient zinc (Table 2).

Under all these conditions, the cellular content of Ca, Mn, Fe, and Mo remained unchanged with some minor deviations of the copper content (Table S3). The nickel content was decreased at high cobalt concentrations. The magnesium content was increased by a factor of three in the Δ*zupT* mutant when grown in low zinc/cobalt medium that was supplemented with exogenous zinc and cobalt.

The largest difference between the zinc and cobalt content of the Δ*zupT* mutant and its parent was visible in standard TMM without any additions (Table 2). When Co(II) was added (Table 3), strain AE104 did not increase its cellular cobalt content when 1 µM Co(II) was added, but the level increased 2.7-fold when 5 µM Co(II) was added. The Δ*zupT* mutant cells started from a lower cobalt level of 7,000 Co ions per cell when cultivated without added Co and the level increased 3.4-fold and 8.7-fold when 1 µM or 5 µM Co(II) was added, respectively. Thereby, the Δ*zupT* cells attained a similar Co content to the parent cells. The zinc content of these cells decreased 0.42-fold in the Δ*zupT* mutant compared with AE104 when the cells were cultivated without added cobalt and remained at this level when cobalt was added (Table S4).

CobW2 and CobW3 control cobalt homeostasis in *C. metallidurans*

In cells cultivated in standard TMM, the absence of the gene encoding CobW3 resulted in a strongly decreased cobalt content that was at a level of approximately 4,000 Co ions per cell, compared with 20,000 Co ions per cell in the parental strain, AE104 (Table 3). A mutant lacking CobW2 had 13,000 Co ions per cell after growth under the same conditions. A Δ*cobW2* Δ*cobW3* double null mutant did not decrease the Co content any further than what was measured in the Δ*cobW3* single null mutant (Table 3). When 1 µM Co(II) was added to the growth medium, the parental strain increased its cellular cobalt content only slightly. By contrast, compared with the non-amended medium, the three Δ*cobW* mutants increased their intracellular cobalt content between 1.8-fold to 4.5-fold (Table 3). When 5 µM Co(II) was added to the medium, all four strains attained similar cobalt levels of between 39,000 for the double null mutant and 55,000 Co ions per cell for the parental strain.

Deletion of Δ*zupT* resulted in a decreased cobalt content in the cells of 36%, and this decreased number of cobalt ions per cell was not affected by additional deletion of

TABLE 3 Cobalt content of mutant strains cultivated in standard TMM[a]

Added Co(II), µM	0	1	5
Strains	**1,000 Co per cell; Q (D)**		
AE104	20.0 ± 8.7 (1.00; 0.0)	24.1 ± 2.0 (1.20; 0.4)	**54.7 ± 9.1 (2.73; 2.0)**
Δ*cobW3*	**3.9 ± 1.2 (0.19; 1.6)**	**14.9 ± 2.4 (3.84; 3.1)**	**46.3 ± 4.4 (11.9; 7.5)**
Δ*cobW2::dis*	13.3 ± 3.8 (0.66; 0.5)	**24.0 ± 6.4 (1.81; 1.1)**	**42.3 ± 3.2 (3.19; 4.2)**
Δ*cobW3* Δ*cobW2::dis*	**3.6 ± 0.7 (0.18; 1.8)**	**16.1 ± 2.4 (4.50; 4.0)**	**39.0 ± 3.5 (10.9; 8.4)**
Δ*zupT*	**7.3 ± 1.5 (0.36; 1.3)**	**24.9 ± 1.8 (3.42; 5.3)**	**63.4 ± 1.4 (8.70; 19)**
Δ*zupT* Δ*cobW3*	9.9 ± 1.0 (1.35; 1.0)	**30.0 ± 2.8 (3.04; 5.3)**	**62.7 ± 6.0 (6.36; 7.6)**
Δ*zupT* Δ*cobW2::dis*	7.2 ± 1.7 (0.99; 0.0)	**25.5 ± 0.7 (3.54; 7.6)**	**53.6 ± 3.2 (7.43; 9.4)**
Δ*zupT* Δ*cobW3* Δ*cobW2::dis*	7.9 ± 0.7 (1.09; 0.3)	**24.7 ± 2.5 (3.11; 5.2)**	**60.9 ± 4.0 (7.67; 11)**
Δ*dmeF*	20.8 ± 6.6 (1.04; 0.0)	**72.1 ± 7.0 (3.47; 3.8)**	**129.7 ± 13.7 (6.24; 5.4)**
Δ*dmeF* Δ*cobW3*	**5.1 ± 0.7 (0.24; 2.2)**	**42.1 ± 1.1 (8.29; 21)**	**119.0 ± 10.7 (23.4; 10)**
Δ*dmeF* Δ*cobW2::dis*	14.8 ± 4.2 (0.71; 0.6)	**62.6 ± 2.8 (4.24; 6.8)**	**149.9 ± 12.7 (10.2; 8.0)**
Δ*dmeF* Δ*cobW3* Δ*cobW2::dis*	**6.0 ± 1.1 (0.29; 1.9)**	**45.3 ± 1.8 (7.58; 14)**	**140.7 ± 6.7 (23.5; 17)**
Δ*dmeF* Δ*zupT*	16.4 ± 1.9 (0.82; 0.3)	**55.8 ± 5.0 (3.40; 5.7)**	n.d.
Δ*dmeF* Δ*zupT* Δ*cobW3*	18.1 ± 1.2 (1.10; 0.6)	**55.5 ± 3.3 (3.07; 8.5)**	n.d.
Δ*dmeF* Δ*zupT* Δ*cobW2::dis*	13.4 ± 1.5 (0.82; 0.9)	**55.1 ± 8.6 (4.10; 4.1)**	n.d.
Δ*dmeF* Δ*zupT* Δ*cobW3* Δ*cobW2::dis*	12.8 ± 2.4 (0.78; 0.8)	**81.7 ± 7.9 (6.36; 6.7)**	n.d.

[a]The cells were cultivated in standard TMM medium (160 nM Zn) with and without added Co(II). The metal content was measured using the ICP-MS, and the cobalt content of the cells in 1,000 Co per cell is shown. The experiment was repeated with three biological replicates, and standard deviations are indicated. The value is followed by a ratio D of the cobalt contents of the cells followed by a D value in parentheses. In cells cultivated without added cobalt, the Co contents of the Δ*zupT* and the Δ*dmeF* mutants were compared with the value for the parental strain, AE104. The content for the Δ*cobW* deletion mutants was compared with the value of the respective AE104, Δ*zupT,* or Δ*dmeF* strains. For cells cultivated with added Co, the values were compared with that of the respective mutant strain grown without added Co. Given is the ratio Q and the D-value in parentheses. The full metal table is provided in the Supplement. Bold faced values indicate (0.66 < Q OR Q > 1.5) and (D > 1). Three biological repeats were performed; n.d., not done because of the high sensitivity of the respective strains.

either *cobW2, cobW3,* or both genes together (Table 3). All four Δ*zupT* strains had a higher Co ion content in this medium than the AE104 Δ*cobW3* mutant. When 1 µM or 5 µM Co(II) was added, all four Δ*zupT* mutants accumulated similar amounts of cobalt, which were always higher in the Δ*zupT* mutants than in the strains that had a native *zupT* gene.

Thus, CobW3 proved to be essential for the accumulation of cobalt in cells cultivated in standard TMM without added cobalt and depended on the presence of ZupT for accumulation of the cation. The lack of CobW3 caused a stronger decrease in cobalt import in the presence of ZupT than in its absence. CobW3 and ZupT may be involved in a downregulation of cobalt import by other import systems, for example, the CorAs, when sufficient zinc is available. Alternatively or additionally, CobW3 and ZupT together may stimulate efflux of Co under these conditions. CobW2 played a minor role in the control of cobalt accumulation in these cells.

CobW2 and CobW3 control the cellular flow-equilibrium of zinc in *C. metallidurans*

Zinc homeostasis in *C. metallidurans* is based on the control of a flow-equilibrium between uptake and efflux reactions, in addition to an effect caused by the metal-binding cytoplasmic components glutathione and polyphosphate (18). Pulse-chase experiments were performed to investigate how CobW2 or CobW3 affects this flow-equilibrium of zinc. Cells were cultivated in TMM adjusted to 200 nM Zn(II) (ambient Zn, aZn), low zinc (lZn), and metal-starvation medium (lZn_lMg), which is low zinc TMM with 100 µM instead of 1 mM Mg(II) (Table S1) to the exponential phase of growth. Harvest and washed cells were then loaded for 20 min with 1 µM radioactive ^{65}Zn and subsequently chased with 100 µM non-radioactive zinc. The cellular ^{65}Zn content of the cells was measured as described (18), with a control that was not chased. The results obtained for AE104 and Δ*zupT* results have already been published (18) but were obtained in the same experimental series as the data for the Δ*cobW* mutants, and these data are shown again for reference (Fig. 2; Fig. S2 to S4). From the pulse-chase results, the initial uptake rate of ^{65}Zn (v_{up}), the cellular zinc content after the uptake period C_{20}, the ratio of the extrapolated maximum zinc content of the uptake period C_{max} divided by C_{20}, the initial efflux rates v_{eff} of the chase period in the chased and non-chased control cells, and the ratio of the zinc contents at 40 min C_{40} divided by C_{20} were calculated (Table 4).

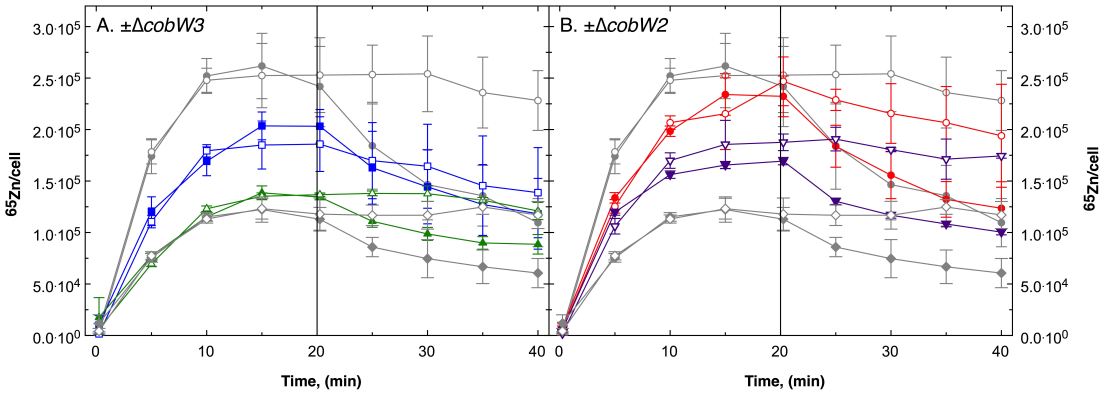

FIG 2 Pulse-chase experiment with *C. metallidurans* strains AE104, and its isogenic Δ*cobW2* and Δ*cobW3* mutants. Cells of strain AE104 (gray circles), Δ*zupT* (grey diamonds), Δ*cobW3* (blue squares), Δ*cobW2* (red circles), Δ*zupT* Δ*cobW2* (purple inverted triangles), and Δ*zupT* Δ*cobW3* (green triangles) were cultivated in low Zn and low Mg (0.1 mM Mg(II)) TMM. Panel A shows the strains without *cobW3*. Panel B those without *cobW2*. After cell-harvest, washing and suspension in uptake buffer, the cells were incubated in the presence of 1 µM ^{65}Zn(II) in the pulse phase and chased at t = 20 min with 100 µM non-radioactive Zn(II) (black symbols), or remained unchased (open symbols). The data for strains AE104 and Δ*zupT* have already been published (18) and were obtained in the same experimental series as the other data.

TABLE 4 Summary of the ^{65}Zn pulse-chase experiments

Medium	Uptake (pulse)			Chase		Pulse continued (control)	
Strains	v_{up} (s^{-1}) , % AE104	C_{20}, 1000 Zn/cell	C_{max}/C_{20}	v_{eff} (s^{-1}), % AE104	C_{40}/C_{20}	v_{eff} (s^{-1}), % AE104	C_{40}/C_{20}
Ambient Zn							
AE104[a]	162 ± 25; 100% ± 15%	96 ± 7; 100% ± 7%	2.20	112.3 ± 1.0; 100.0% ± 0.9%	37.2% ± 6.7%	−14.4 ± −0.2; −12.8% ± −0.2%	127.0% ± 8.8%
Δ*zupT*[a]	94 ± 7; 58% ± 4%	64 ± 4; 66% ± 4%	2.67	38.8 ± 0.3; 34.5% ± 0.2%	46.4% ± 12.7%	2.1 ± 0.0; 1.9% ± 0.0%	102.5% ± 2.5%
Δ*cobW2*	111 ± 4; 69% ± 3%	73 ± 2; 75% ± 2%	2.43	32.2 ± 0.0; 28.6% ± 0.0%	57.2% ± 10.0%	9.3 ± 0.0; 8.3% ± 0.0%	86.3% ± 17.9%
Δ*cobW3*	90 ± 1; 56% ± 0%	54 ± 5; 56% ± 5%	1.99	23.7 ± 0.2; 21.1% ± 0.2%	61.9% ± 11.0%	−4.8 ± 0.0; −4.3% ± 0.0%	120.3% ± 21.6%
Δ*zupT* Δ*cobW2*	96 ± 3; 59% ± 2%	83 ± 4; 87% ± 4%	4.66	15.5 ± 0.0; 13.8% ± 0.0%	82.2% ± 4.4%	−11.1 ± 0.0; −9.9% ± 0.0%	115.2% ± 8.4%
Δ*zupT* Δ*cobW3*	94 ± 4; 58% ± 2%	49 ± 8; 51% ± 8%	1.73	3.2 ± 0.0; 2.8% ± 0.0%	99.6% ± 37.6%	−4.0 ± 0.0; −3.6% ± 0.0%	99.9% ± 53.5%
Low zinc							
AE104[a]	227 ± 17; 100% ± 8%	92 ± 3; 100% ± 3%	1.62	125.4 ± 1.3; 100.0% ± 1.0%	45.2% ± 16.6%	−11.2 ± −0.1; −8.9% ± −0.1%	128.1% ± 10.4%
Δ*zupT*[a]	67 ± 1; 30% ± 0%	63 ± 4; 68% ± 4%	7.44	15.4 ± 0.1; 12.2% ± 0.0%	67.7% ± 2.1%	−6.7 ± 0.0; −5.3% ± 0.0%	118.8% ± 12.9%
Δ*cobW2*	194 ± 34; 86% ± 15%	114 ± 6; 123% ± 6%	1.77	37.6 ± 0.1; 30.0% ± 0.1%	60.2% ± 10.0%	−11.3 ± −0.1; −9.0% ± 0.0%	109.2% ± 23.1%
Δ*cobW3*	113 ± 28; 50% ± 12%	66 ± 5; 72% ± 6%	2.42	24.1 ± 0.0; 19.2% ± 0.0%	71.0% ± 10.5%	−4.8 ± 0.0; −3.8% ± 0.0%	104.0% ± 52.5%
Δ*zupT* Δ*cobW2*	97 ± 2; 43% ± 1%	73 ± 4; 79% ± 4%	3.04	13.4 ± 0.0; 10.6% ± 0.0%	85.1% ± 12.3%	1.3 ± 0.0; 1.1% ± 0.0%	96.1% ± 25.3%
Δ*zupT* Δ*cobW3*	104 ± 13; 46% ± 6%	67 ± 5; 73% ± 6%	2.41	7.1 ± 0.1; 5.6% ± 0.1%	93.2% ± 11.7%	−13.3 ± −0.1; −10.6% ± 0.0%	134.3% ± 33.4%
Low Zn and Mg							
AE104[a]	1147 ± 351; 100% ± 31%	272 ± 28; 100% ± 10%	1.45	314.4 ± 3.0; 100.0% ± 0.9%	40.2% ± 8.6%	27.1 ± 0.1; 8.6% ± 0.0%	83.8% ± 10.7%
Δ*zupT*[a]	509 ± 10; 44% ± 1%	115 ± 4; 42% ± 1%	1.38	53.3 ± 0.2; 16.9% ± 0.1%	52.5% ± 12.3%	−2.1 ± 0.0; −0.7% ± 0.0%	101.4% ± 11.4%
Δ*cobW2*	695 ± 72; 61% ± 6%	240 ± 10; 88% ± 4%	1.49	119.0 ± 0.4; 37.9% ± 0.1%	51.6% ± 10.8%	48.2 ± 0.0; 15.3% ± 0.0%	81.0% ± 20.9%
Δ*cobW3*	677 ± 45; 59% ± 4%	195 ± 12; 71% ± 5%	1.42	86.9 ± 0.3; 27.6% ± 0.1%	60.8% ± 17.7%	46.3 ± 0.1; 14.7% ± 0.0%	71.3% ± 22.5%
Δ*zupT* Δ*cobW2*	788 ± 291; 69% ± 25%	178 ± 13; 66% ± 5%	1.36	65.2 ± 0.3; 20.7% ± 0.1%	56.2% ± 1.5%	16.3 ± 0.0; 5.2% ± 0.0%	97.7% ± 1.2%
Δ*zupT* Δ*cobW3*	382 ± 64; 33% ± 6%	136 ± 2; 50% ± 1%	1.63	44.7 ± 0.2; 14.2% ± 0.1%	65.3% ± 7.0%	14.1 ± 0.0; 4.5% ± 0.0%	89.2% ± 6.1%

[a]Data obtained in the same experimental series and already published (18).

Fully zinc-replete cells of the Δ*zupT*, Δ*cobW2,* Δ*cobW3*, Δ*zupT* Δ*cobW2,* and Δ*zupT* Δ*cobW3* mutants cultivated in aZn-TMM showed insignificant differences between their respective pulse-chase curves (Fig. S2 and S3); however, all mutants accumulated a lower amount of ^{65}Zn than the parent AE104 during the uptake phase, that is, after 20 min (Table 4). Although the parent was fully zinc-saturated after 20 min with 96,000 ^{65}Zn imported, the respective value was only 75% for Δ*cobW2*, 66% for (Δ*zupT),* and 50% for (Δ*cobW3,* Δ*zupT* Δ*cobW3*). The lower zinc contents of the mutant cells led to a decrease of the initial efflux rate in the subsequent chase period, even as low as only 2.8% of the parental value for the Δ*zupT* Δ*cobW3* double null mutant.

Under zinc-starvation conditions (low zinc medium), the pulse-chase curves of the mutant cells were also not significantly different from each other but were different from those of the parent (Fig. S4). The Δ*cobW2* mutant was not different from AE104 with respect to the initial uptake velocity and ^{65}Zn content C_{20} after the pulse period. Also, the Δ*zupT* Δ*cobW2* double mutant accumulated more zinc than the Δ*zupT* mutant and with a higher initial uptake rate (Table 4). Nevertheless, the initial net efflux rate v_{eff} decreased in all mutants, including the Δ*cobW2* strain, in comparison to AE104, and the rate in Δ*zupT* Δ*cobW3* mutant was reduced to 5.6% of the parental value.

Following cultivation under metal-starvation (for Zn, Co, Mg) (lZn_lMg metal-starvation TMM), the parent reached a maximum zinc content after only 15 min during the uptake period and even the non-chased control exported ^{65}Zn after this period, whereas the Δ*zupT* mutant reached a level of zinc that was 60% lower, and the mutant continued to import zinc into un-chased control cells (Fig. 2; Table 4 (18)). Introduction of a *cobW3* deletion into this strain had a stronger negative effect than introduction of a Δ*cobW2* mutation (Fig. 2). The pulse-chase curves of the Δ*zupT* Δ*cobW3* double null mutant (Fig. 2A, green triangles) was similar to that of the Δ*zupT* single mutant, whereas that of the Δ*cobW3* mutant (Fig. 2A, blue squares) lay between the Δ*zupT* mutant and the parental strain. The curve of the Δ*zupT* Δ*cobW2* double null mutant lay between that of the Δ*zupT* mutant and the parental strain and that of the Δ*cobW2* mutant lay between that of the Δ*zupT* Δ*cobW2* double mutant and its parent (Fig. 2B). All mutants accumulated ^{65}Zn with a lower initial uptake rate than AE104 and accumulated lower amounts of zinc after 20 min, except for the Δ*cobW2* mutant (Table 4). All mutants also exported ^{65}Zn with a lower net efflux rate than the parent, with rates between 38% of the parental value in the Δ*cobW2* single mutant and as low as 14% in the Δ*zupT* Δ*cobW3* double null mutant (Table 4).

ZupT, in cooperation with CobW2 and CobW3, influenced the flow-equilibrium of zinc. The effect of a lack of CobW2 was smaller compared with when the gene encoding CobW3 was deleted. In contrast, the effect on the flow-equilibrium was stronger in zinc-replete cells than in zinc- or metal-starved cells. Without these CobW proteins, the initial uptake rates, zinc contents after 20 min incubation with 1 µM Zn(II), and initial net efflux rates were lower compared with the parent. As indicated by the results from metal-starved cells, lack of CobW2 and CobW3 impacted zinc import by ZupT, as well as on other uptake systems (Fig. 2), with a Δ*cobW2* deletion even increasing zinc import in a Δ*zupT* background (Fig. 2B). Thus, these three proteins together seem to control zinc homeostasis in *C. metallidurans* (Table 4), and they also influence the cobalt content of the cells (Table 3).

ZupT, CobW2, and CobW3 control the cellular zinc pools

The pulse-chase experiments with radioactive ^{65}Zn were performed in parallel with experiments using isotope-enriched stable ^{67}Zn solutions (18). This allowed us to differentiate between a zinc pool, ZP1, containing zinc with the natural isotope composition and a ZP2 stemming from the isotope-enriched ^{67}Zn solution. The cells were cultivated in ambient zinc (aZn), zinc-starvation (lZn), and zinc-magnesium-, metal-starvation (lZn_lMg) medium with zinc in the natural isotope composition. Incubation was for 20 min with 1 µM ^{67}Zn(II) and chased for an additional 20 min with 100 µM zinc, again with the natural isotope composition. In this way, ZP2 represented the zinc imported

during the uptake phase, and ZP1 represented zinc that was initially present in the cells and also at the end of the experiment.

As with radioactive zinc, deletion of the genes for ZupT and both CobWs decreased the initial zinc content in ZP1 in zinc-replete cells (Table 5). The strongest effect was measured in the Δ*zupT* Δ*cobW3* double null mutant. Incubation of cells with 1 µM ^{67}Zn resulted in zinc appearing in ZP2, a decrease of zinc in ZP1 but insignificant change in the overall zinc content, that is, ZP1 + ZP2. Zinc ions that were initially present in cells were exchanged against incoming zinc ions, and ZupT, CobW2, and CobW3 were not required for this turnover of zinc (Table 5). During the subsequent chase, zinc was mainly exported or exchanged from ZP2, despite the overall zinc content increasing in the cells. In zinc-replete cells, deletion of either of the three genes *zupT, cobW2,* or *cobW3* individually resulted in a decreased Co and Ni content of the cells (Table S5).

In low-zinc and in low-zinc, low-magnesium media, the cellular zinc content of the cells was lower compared with zinc-replete (aZn) cells, as expected. The high zinc content in the cells of the Δ*zupT* strain after growth in low-zinc medium was twice as high as in all other comparable experimental series and was not considered. Compared with zinc-replete cells, no zinc was exported from ZP1 during the uptake phase in zinc-starved cells, and more zinc remained in ZP2 during the subsequent chase. The exception was the parent in low-zinc, low-magnesium medium. This strain decreased the zinc content in ZP1 during the uptake phase, but its mutant derivatives did not. The zinc content in ZP2 was particularly low in cells of the zinc-starved Δ*zupT* Δ*cobW3* double null mutant compared with the other cells, both before and after the chase (Table 5).

These results allow us to propose that the three proteins ZupT, CobW2, and CobW3 are required to adjust the cellular zinc pools under all conditions examined. The absence of ZupT and CobW3 results in decreased uptake of zinc, whereas efflux of zinc during the chase period was barely affected (Table 5, clearance of ZP2 during the chase period).

TABLE 5 Summary of the experiments with stable ^{67}Zn that accompanied the pulse-chase experiments with radioactive ^{65}Zn[b]

Strains	Initial 10^3 Zn			10^3 Zn after pulse			10^3 Zn after chase (0.1 mM)		
Medium	**ZP1**	**ZP2; %ZPt**	**ZP1 +ZP2**	**ZP1**	**ZP2; %ZPt**	**ZP1 +ZP2**	**ZP1**	**ZP2; %ZPt**	**ZP1 +ZP2**
Ambient Zn									
AE104[a]	103 ± 9	0.0 ± 0.2; 0.0%	103 ± 9	76.6 ± 1.8	27.4 ± 2.2; 26.4%	104 ± 4	240 ± 20	6.1 ± 0.8; 2.5%	246 ± 21
Δ*zupT*[a]	42.8 ± 1.8	<0	42.6 ± 1.7	37.8 ± 2.1	20.5 ± 1.2; 35%	58.3 ± 3.3	226 ± 15	4.1 ± −0.1; 2%	230 ± 14
Δ*cobW2*	73.9 ± 2.6	<0	73.6 ± 2.6	60.9 ± 0.6	21.8 ± 1.3; 26%	82.8 ± 1.9	212 ± 26	3.7 ± 0.3; 2%	215 ± 26
Δ*cobW3*	77.1 ± 2.1	<0	76.8 ± 2.1	64.8 ± 1.6	21.9 ± 1.3; 25%	86.7 ± 2.9	307 ± 44	3.8 ± 0.2; 1%	311 ± 44
Δ*zupT* Δ*cobW2*	57.8 ± 8.8	<0	57.6 ± 8.8	46.9 ± 6.5	20.8 ± 0.4; 31%	67.7 ± 6.9	238 ± 15	4.3 ± 0.1; 2%	243 ± 15
Δ*zupT* Δ*cobW3*	40.3 ± 0.8	<0	40.2 ± 0.8	36.1 ± 1.1	15.1 ± 0.7; 29%	51.1 ± 1.8	168 ± 8	4.1 ± 0.0; 2%	172 ± 7
Low Zn									
AE104[a]	11.0 ± 1.9	0.0 ± 0.0; 0.1%	11.1 ± 1.9	6.7 ± 0.7	79.4 ± 5.3; 92.3%	86.1 ± 6.0	181 ± 17	24.6 ± 1.4; 12.0%	206 ± 19
Δ*zupT*[a]	43.2 ± 1.4	<0	43.0 ± 1.4	37.0 ± 0.8	30.8 ± 2.5; 45%	67.8 ± 3.3	190 ± 8	6.9 ± 0.2; 4%	197 ± 8
Δ*cobW2*	8.9 ± 4.5	0.0 ± 0.0; 0%	8.9 ± 4.5	9.5 ± 3.9	58.4 ± 1.4; 86%	67.9 ± 5.3	180 ± 3	15.5 ± 0.8; 8%	196 ± 4
Δ*cobW3*	8.9 ± 4.6	0.0 ± 0.0; 0%	8.9 ± 4.5	15.4 ± 6.6	42.8 ± 1.7; 74%	58.2 ± 8.3	166 ± 9	15.1 ± 0.3; 8%	182 ± 10
Δ*zupT* Δ*cobW2*	5.3 ± 0.5	0.0 ± 0.0; 1%	5.3 ± 0.5	8.3 ± 3.1	53.5 ± 0.7; 87%	61.8 ± 3.8	161 ± 3	14.1 ± 0.3; 8%	176 ± 4
Δ*zupT* Δ*cobW3*	10.1 ± 6.4	0.0 ± −0.1; 0%	10.1 ± 6.3	8.3 ± 5.5	12.5 ± 0.2; 60%	20.7 ± 5.7	138 ± 13	4.7 ± −0.1; 3%	143 ± 13
Low Zn and Mg									
AE104[a]	29.5 ± 10.2	0.5 ± 0.0; 1.6%	30.0 ± 10.1	6.3 ± 1.3	85.0 ± 3.9; 93.1%	91.3 ± 5.3	201 ± 33	25.4 ± 2.0; 11.2%	226 ± 35
Δ*zupT*[a]	8.3 ± 0.8	<0	8.3 ± 0.8	8.0 ± 0.3	57.4 ± 3.0; 88%	65.4 ± 3.3	169 ± 22	13.9 ± 0.3; 8%	183 ± 22
Δ*cobW2*	21.4 ± 10.4	<0	21.4 ± 10.3	20.0 ± 10.1	56.3 ± 9.0; 74%	76.3 ± 19.1	175 ± 14	14.6 ± 3.0; 8%	190 ± 17
Δ*cobW3*	11.9 ± 1.3	7.0 ± 9.4; 37%	18.9 ± 10.8	10.2 ± 1.2	40.4 ± 2.6; 80%	50.6 ± 3.8	166 ± 22	14.9 ± 0.1; 8%	181 ± 23
Δ*zupT* Δ*cobW2*	12.9 ± 4.0	<0	12.9 ± 4.0	11.4 ± 3.0	57.6 ± 2.0; 83%	69.1 ± 5.0	174 ± 6	13.8 ± 0.8; 7%	188 ± 7
Δ*zupT* Δ*cobW3*	10.4 ± 0.4	<0	10.4 ± 0.4	8.4 ± 0.5	14.2 ± 0.9; 63%	22.6 ± 1.4	171 ± 7	5.5 ± 0.0; 3%	177 ± 7

[a]Data obtained in the same experimental series and already published (18).
[b]The cells of the indicated *C. metallidurans* mutants were incubated in Tris-buffered mineral salts medium adjusted to 200 nM Zn(II) (ambient zinc); the same medium without trace element solution SL6 and 0.1 mM Mg(II) instead of 1 mM Mg(II) (low Zinc and Mg), or TMM medium without SL6 but with 1 mM Mg(II) (low Zn). Zinc coming from SL6 or contaminations was in the natural isotope composition. These cells were incubated with 1 µM enriched stable ^{67}Zn for 20 min (pulse) and subsequently chased with 100 µM Zn(II) (or 1 mM when indicated) with the natural isotope composition. The zinc pools ZP1 and ZP2 were calculated from the ICP-MS measurements and ZPt = ZP1+ZP2 was determined.

ZupT, CobW2, and CobW3 affect Co, Cd, and EDTA resistance

Single or double deletions of *cobW2* and/or *cobW3* in the *C. metallidurans* parental strain AE104 did not decrease zinc or cobalt resistance, but cadmium resistance was decreased (Table 6). In the double mutant resistance to the metal cation-chelator, ethylenediaminetetraacetate (EDTA) was also decreased (Table 6). This decrease in resistance was even stronger in the Δ*zupT* background. Here, cobalt resistance was reduced to 43% in the Δ*zupT* mutant and 8% in the Δ*zupT* Δ*cobW3* double null mutant, whereas a Δ*cobW2* deletion did not decrease any further the low cobalt resistance level of the Δ*zupT* mutant. The pattern of EDTA resistance in the Δ*zupT* mutant was similar to that for its cobalt resistance and accounted for a reduction in resistance to 45% in Δ*zupT* compared with the parent, and a further minor decrease in the Δ*zupT* Δ*cobW2* double mutant, but resistance was decreased to 10% of the Δ*zupT* resistance level in the Δ*zupT* Δ*cobW3* mutant (Table 6).

The effect of these gene deletions in reducing resistance was even stronger with respect to cadmium resistance, where a decrease down to 23% of the parental level in the Δ*zupT* mutant was observed. A further decrease to 23% compared with the level in the Δ*zupT* mutant was observed for the Δ*zupT* Δ*cobW2* double mutant, and an even stronger decrease down to 12% was measured for the Δ*zupT* Δ*cobW3* double mutant (Table 6). Additional deletion of *cobW2* increased the low cobalt and EDTA resistance level of the Δ*zupT* Δ*cobW3* double mutant to approximately the level of the Δ*zupT* mutant. In contrast, cadmium resistance was not affected by the additional deletion of *cobW2* in the Δ*zupT* Δ*cobW3* strain.

These data suggest that CobW2 and CobW3 cooperate to mediate full cadmium resistance in the parental strain and in its Δ*zupT* mutant derivative. On the other hand, the absence of CobW3 decreased cobalt and EDTA resistance in the Δ*zupT* strain, but not in the parent. This strong effect of a Δ*cobW3* deletion in the Δ*zupT* strain with respect to the Co and EDTA resistance, but not the Cd resistance, was reversed again by further deletion of *cobW2*, indicating that CobW2 mediated the low Co and EDTA resistance level in the Δ*zupT* Δ*cobW3* double mutant.

DmeF is an important valve for the release of surplus cobalt ions

The three proteins ZupT, CobW2, and CobW3 control accumulation of cobalt in zinc-starved cells and are involved in resistance to Co, Cd, and EDTA. The main cadmium

TABLE 6 IC_{50} values of mutant strains[a]

Strain	Zn (μM)	Co (μM)	Cd (μM)	EDTA (μM)
AE104	114.2 ± 15.6 (1.00; 0.0)	193 ± 9 (1.00; 0.0)	174 ± 10 (1.00; 0.0)	1,652 ± 58 (1.00; 0.0)
Δ*cobW3*	94.3 ± 2.8 (0.83; 1.1)	176 ± 14 (0.91; 0.7)	**114 ± 15 (0.65; 2.4)**	1,353 ± 180 (0.82; 1.3)
Δ*cobW2::dis*	96.0 ± 7.4 (0.84; 0.8)	182 ± 15 (0.94; 0.5)	**112 ± 5 (0.65; 4.1)**	1,185 ± 156 (0.72; 2.2)
Δ*cobW3* Δ*cobW2::dis*	92.4 ± 4.9 (0.81; 1.1)	174 ± 19 (0.90; 0.6)	**87.5 ± 12.3 (0.50; 3.9)**	**975 ± 276 (0.59; 2.0)**
Δ*zupT*	86.8 ± 3.8 (0.76; 1.4)	**83.8 ± 4.8 (0.43; 7.7)**	**39.1 ± 3.8 (0.23; 9.9)**	**739 ± 154 (0.45; 4.3)**
Δ*zupT* Δ*cobW3*	65.0 ± 5.6 (0.75; 2.3)	**6.6 ± 0.1 (0.08; 15.8)**	**4.8 ± 1.2 (0.12; 6.9)**	**75.5 ± 19 (0.10; 3.8)**
Δ*zupT* Δ*cobW2::dis*	108.2 ± 1.2 (1.25; 4.3)	93.0 ± 9.0 (1.11; 0.7)	**9.0 ± 0.2 (0.23; 7.5)**	548 ± 96 (0.74; 0.8)
Δ*zupT* Δ*cobW3* Δ*cobW2::dis*	78.4 ± 1.7 (0.90; 1.5)	86.1 ± 3.4 (1.03; 0.3)	**4.3 ± 0.0 (0.11; 9.2)**	523 ± 230 (0.71; 0.6)
Δ*dmeF*	106.6 ± 8.7 (0.93; 0.3)	**5.5 ± 0.7 (0.03; 18.7)**	149 ± 25 (0.86; 0.7)	1,343 ± 348 (0.81; 0.8)
Δ*dmeF* Δ*cobW3*	97.6 ± 2.0 (0.92; 0.8)	7.9 ± 0.6 (1.44; 1.8)	132 ± 17 (0.89; 0.4)	1,921 ± 222 (1.43; 1.0)
Δ*dmeF* Δ*cobW2::dis*	98.5 ± 2.1 (0.92; 0.8)	5.2 ± 0.4 (0.95; 0.3)	113 ± 6 (0.76; 1.1)	1,809 ± 164 (1.35; 0.9)
Δ*dmeF* Δ*cobW3* Δ*cobW2::dis*	97.6 ± 2.6 (0.92; 0.8)	6.2 ± 0.3 (1.13; 0.7)	104 ± 11 (0.70; 1.2)	1,721 ± 268 (1.28; 0.6)
Δ*dmeF* Δ*zupT*	78.0 ± 1.7 (0.68; 2.10)	**2.1 ± 0.1 (0.01; 20.1)**	**40.5 ± 1.7 (0.23; 11.5)**	1,263 ± 17 (0.76; 5.19)
Δ*dmeF* Δ*zupT* Δ*cobW3*	77.0 ± 2.3 (0.99; 0.26)	2.6 ± 0.2 (1.22; 1.44)	**72.9 ± 0.9 (1.80; 12.5)**	1,578 ± 34 (1.25; 6.20)
Δ*dmeF* Δ*zupT* Δ*cobW2::dis*	73.6 ± 3.4 (0.94; 0.87)	2.3 ± 0.1 (1.06; 0.47)	**12.9 ± 2.2 (0.32; 7.05)**	1,017 ± 39 (0.81; 4.45)
Δ*dmeF* Δ*zupT* Δ*cobW3* Δ*cobW2::dis*	75.5 ± 1.4 (0.97; 0.81)	2.5 ± 0.0 (1.18; 1.96)	**13.8 ± 4.5 (0.34; 4.30)**	**686 ± 93 (0.54; 5.28)**

[a]Standard TMM. Bold-faced if [(Q > 1.5 OR Q < 0.67) AND D > 1], meaning the ratios of two values are larger than 1.5 and the deviation bars do not overlap. Comparison of the Δ*dmeF* and the Δ*zupT* mutants to AE104 and of the Δ*cobW* mutants to their respective parent.

exporters in *C. metallidurans* are the P_{IB2}-type ATPases ZntA and CadA (15), whereas the CDF protein DmeF is required for cobalt export (15, 16). A Δ*dmeF* mutant showed impaired growth in the presence of 5 µM Co(II) in mZn medium (Fig. 3). The IC_{50} of the mutant was 5.5 µM Co(II) compared with 193 µM in the parental strain, AE104 (Table 6). Resistance to zinc, cadmium, and EDTA was not influenced in the mutant. The CDF protein FieF in AE104 is required for resistance to iron (16, 45). Growth of a Δ*fieF* mutant was only slightly impaired compared with AE104, whereas a Δ*dmeF* Δ*fieF* double mutant had a growth phenotype similar to the Δ*dmeF* single mutant (Fig. 3B). Additional deletion of the genes *cobW2, cobW3,* or both in the Δ*dmeF* strain had limited influence on resistance to Zn, Co, Cd, or EDTA (Table 6).

The cobalt content of cells of the Δ*dmeF* mutant cultivated in standard zinc medium was identical to that of the parent, AE104 (Table 3). When 1 µM or 5 µM Co was added, the level of the cation increased 3.5-fold and 6.2-fold, respectively, to a final level of 130,000 Co per cell, whereas the zinc content of the cells was not influenced (Table S4). These data confirm that DmeF is the major cobalt efflux system of *C. metallidurans* AE104. The CobWs did not mediate any level of cobalt resistance in the absence of DmeF (Table 6).

DmeF supports the function of the ZupT, CobW2, and CobW3 network

All mutants up to the quadruple mutant Δ*dmeF* Δ*zupT* Δ*cobW3* Δ*cobW2::dis* were constructed and characterized. Cobalt resistance of the Δ*zupT* mutant was 43% of the level of the parental strain, AE104, and that of the Δ*dmeF* mutant only 3% of the parent (Table 6). The IC_{50} for Co(II) decreased to 1% of the parental level in the Δ*dmeF* Δ*zupT* double deletion mutant (Table 6). In the presence of 1 µM Co(II), the double mutant grew more slowly than AE104, whereas both single mutants had similar growth rates that ranged between that of the double mutant and that of AE104 (Fig. 4A). In the absence of added Co(II), the Δ*dmeF* mutant grew like its parent, the Δ*zupT* mutant grew more slowly,

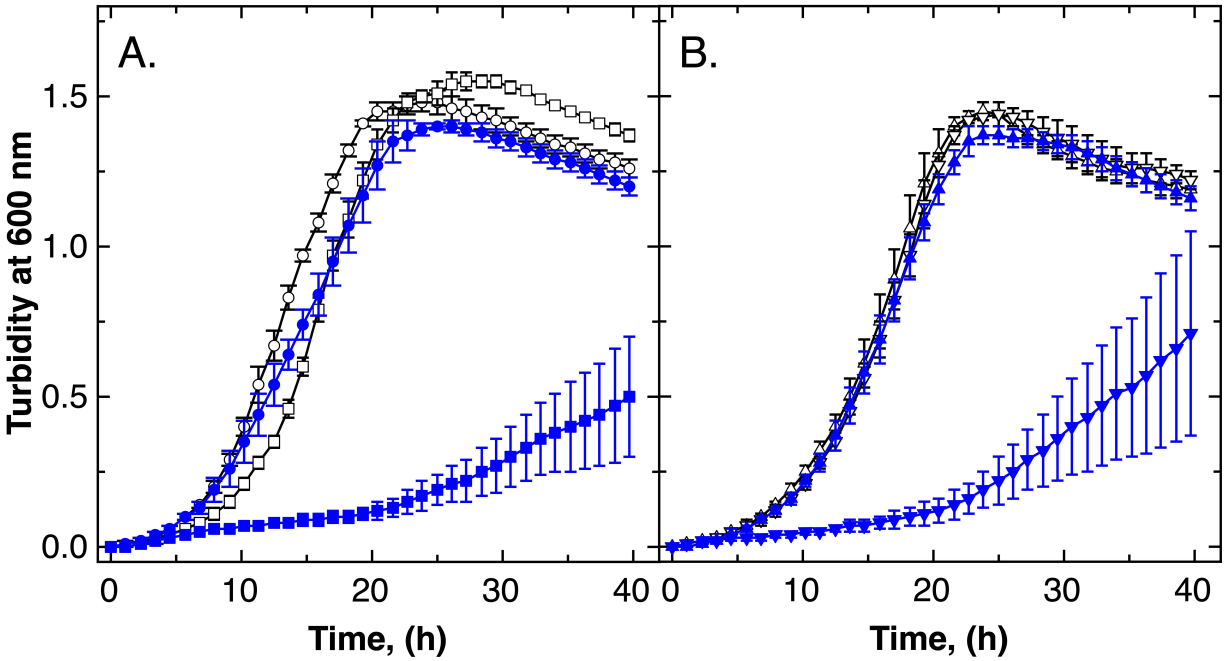

FIG 3 DmeF mediates cobalt resistance in *C. metallidurans*. Panel A shows time-dependent growth of the parental strain, AE104 (circles), and an isogenic Δ*dmeF* mutant (squares). Panel B shows data for a Δ*fieF* (triangles) mutant and a Δ*dmeF* Δ*fieF* (inverted triangles) cultivated with (blue closed symbols) or without (black open symbols) 5 µM co(II) in standard TMM. Data for three biological repeats with standard deviations are shown.

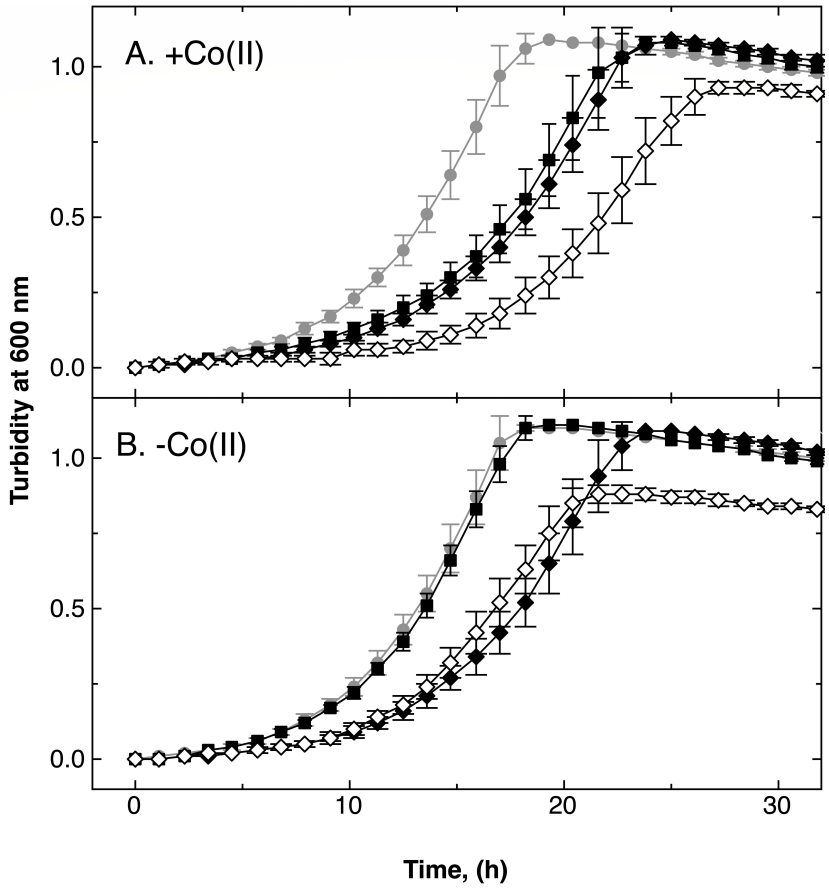

FIG 4 Effect of Co(II) on a Δ*dmeF* Δ*zupT* double null mutant. Time-dependent growth curves of strains Δ*zupT* (closed diamonds), Δ*dmeF* (squares), and Δ*dmeF* Δ*zupT* (open diamonds) in standard TMM medium without (panel B) or with (panel A) addition of 1 µM co(II) are shown. Growth of the parental strain AE104 (closed circles) is shown in gray for reference. Data for three biological repeats with standard deviations were shown.

and the double mutant's growth rate was similar to that of the Δ*zupT* mutant, albeit with a lower growth yield (Fig. 4B). Both transport systems, the ZupT uptake, and the DmeF efflux systems, thus appear to cooperate to mediate cobalt resistance and also to allow the maximum growth yield in the absence of added Co(II) to be attained.

Deletion of *cobW2* or *cobW3* in the Δ*dmeF* isogenic strain increased Co resistance in the case of the Δ*dmeF* Δ*cobW3* strain. The IC_{50} of the Δ*dmeF* Δ*cobW2* strain did not change, however, and the triple mutant exhibited an IC_{50} like that of the Δ*dmeF* strain (Table 6). This effect was more clearly visible in growth curves done in the presence of 2.5 µM Co(II) (Fig. 5). The Δ*cobW3* deletion (Fig. 5, blue triangles) almost restored growth to the parental level, whereas the Δ*cobW2* deletion was less efficient in counteracting the growth delay mediated by the Δ*dmeF* mutation (green inverted triangles). The triple mutant had a growth rate that was between those of the Δ*dmeF* Δ*cobW2* and Δ*dmeF* Δ*cobW3* (magenta diamonds) mutants. This influence on the growth rate was only visible in the Δ*dmeF* mutant background and only in the presence of Co(II) (Fig. S5). Zinc, cadmium, and EDTA resistances were unchanged (Table 6). This suggests that CobW2 and CobW3 were responsible for the growth defect of the Δ*dmeF* mutant in the presence of Co(II). Moreover, both CobW proteins interacted with each other, with loss of CobW3 causing a more severe growth deficiency compared with loss of CobW2.

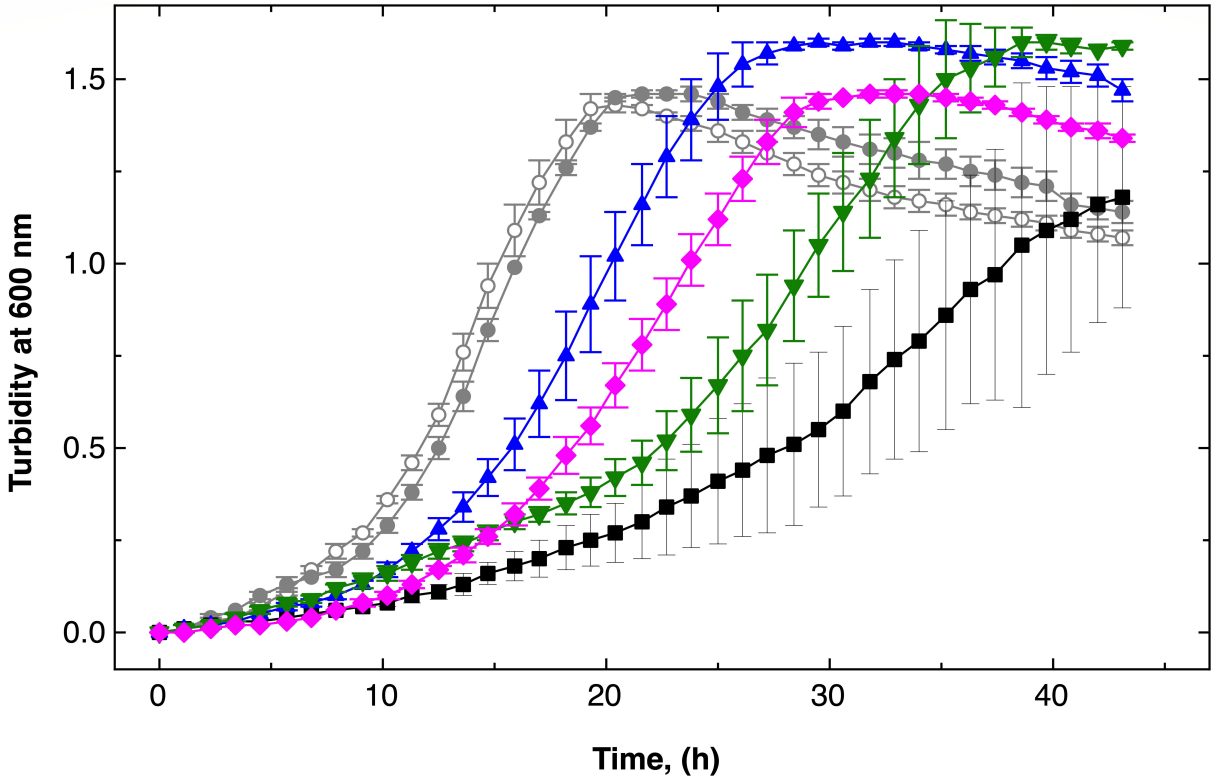

FIG 5 Strains lacking CobW2 and CobW3 show impaired growth in a Δ*dmeF* mutant background. Time-dependent growth of strains Δ*dmeF* (black filled squares), Δ*dmeF* Δ*cobW3* (blue triangles), Δ*dmeF* Δ*cobW2::dis* (green inverted triangles), and the Δ*dmeF* Δ*cobW3* Δ*cobW2::dis* triple mutant (magenta diamonds) in standard TMM in the presence of 2.5 µM co(II). Growth of the parental strain AE104 with (closed circles) and without (open circles) 2.5 µM co(II) is shown in gray for reference. Three biological repeats were performed, and standard deviations are shown. Data for all strains and conditions tested are shown in Supplementary information.

Introduction of a deletion in either the *cobW2* or *cobW3* genes in the Δ*dmeF* Δ*zupT* double mutant background also negatively affected growth in the presence or absence of 1 µM Co(II) (Fig. 6). In the presence of Co(II), the half-logarithmic plot shows that all growth curves were parallel with each other, except that of the parent, AE104 (Fig. S6). Compared with the parent in the presence of Co(II), the deletions affected the length of the lag-phase and the growth rate. Comparing the mutants with each other in the presence of Co(II) and in all comparisons in the absence of Co(II), only the length of the lag-phase was influenced.

When Co(II) was added, Δ*dmeF,* Δ*zupT*, and Δ*dmeF* Δ*zupT* Δ*cobW3* had the same growth delay, which was largest in the Δ*dmeF* Δ*zupT* double mutant and between those of the quadruple mutant and the Δ*dmeF* Δ*zupT* Δ*cobW2* triple mutant (Fig. 6; Fig. S6). As in the Δ*dmeF* mutant, the CobWs were also responsible for the growth delay of the Δ*dmeF* Δ*zupT* double mutant, but the difference in comparison to the Δ*dmeF* single mutant was that CobW2 no longer had any effect. In the absence of added Co(II), Δ*dmeF* mutant grew like the parent AE104, whereas most other mutants had growth phenotypes like the Δ*zupT* mutant, and only the Δ*dmeF* Δ*zupT* Δ*cobW3* strain had a growth phenotype between that of the Δ*zupT* and AE104. A decreased growth yield was only visible in the Δ*dmeF* Δ*zupT* double mutant, and therefore, this was also due to CobW2 or CobW3 (Fig. 6).

Introduction of a Δ*cobW3* mutation into the Δ*dmeF* Δ*zupT* double mutant increased Co resistance slightly, which was reminiscent of the phenotype of the Δ*dmeF* mutant;

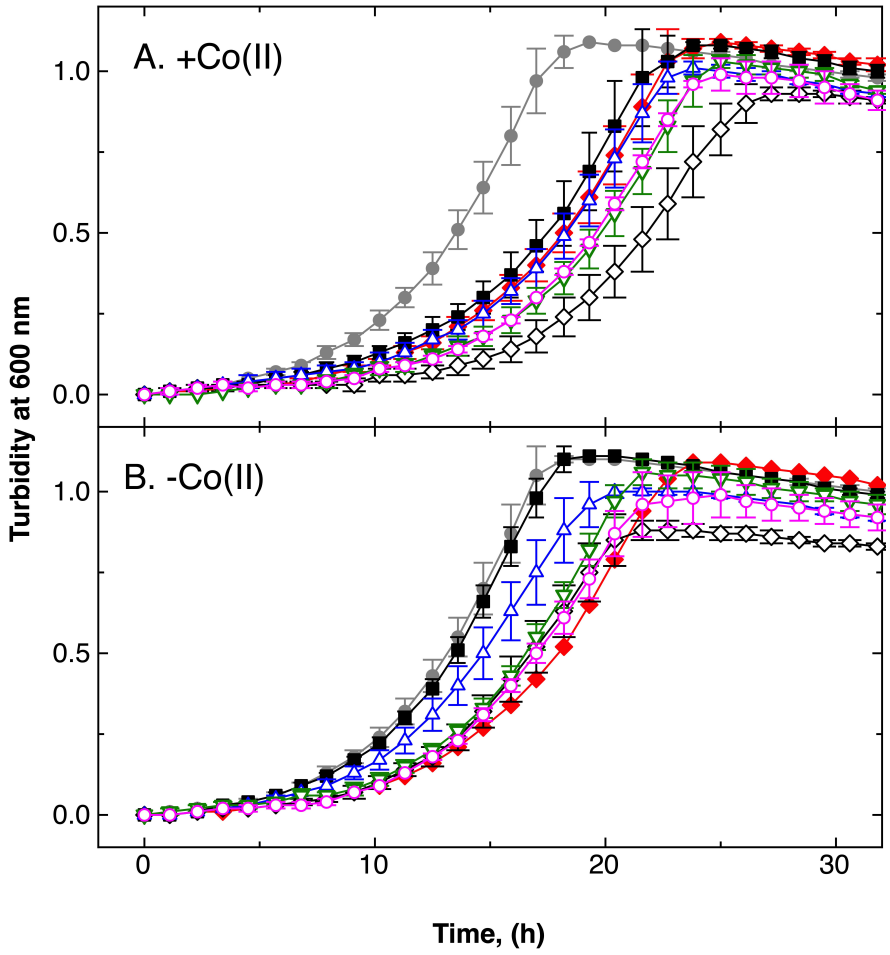

FIG 6 Effect of Co(II) on derivatives of the double deletion strain Δ*zupT* Δ*dmeF*. Time-dependent growth of strains Δ*zupT* (red filled diamonds), Δ*dmeF* (filled squares), Δ*dmeF* Δ*zupT* (open diamonds), Δ*dmeF* Δ*zupT* Δ*cobW2* (green open inverted triangles), Δ*dmeF* Δ*zupT* Δ*cobW3* (blue open triangles), and Δ*dmeF* Δ*zupT* Δ*cobW2* Δ*cobW3* (magenta open circles) in standard TMM medium without (panel B) or with (panel A) 1 µM co(II). Growth of the parent AE104 (closed circles) and is shown in gray for references. Three repeats, deviations indicated.

introducing the Δ*cobW2* allele had no effect (Table 6). Although the Δ*zupT* deletion decreased the cobalt content in standard TMM down to 36% of the parent level, deletion of *zupT* in the Δ*dmeF* mutant barely affected Co levels when compared with those of AE104 (Table 3). DmeF is therefore responsible for maintaining the low cobalt level in the Δ*zupT* strain. Moreover, although deletion of *cobW3* had only a small effect in the Δ*zupT* background, the mutation strongly decreased the cobalt content in the parental strain and its isogenic Δ*dmeF* mutant. However, the *cobW3* mutation had no effect in the Δ*dmeF* Δ*zupT* double null mutant background. Thus, ZupT was responsible for maintaining the low cobalt levels of the parental strain and in a Δ*dmeF* mutant. This means that DmeF, ZupT, and CobW3 cooperate to adjust the cobalt content of the cells in standard TMM.

These effects of the DmeF, ZupT, and CobW3 network on the cobalt level were similar in cells grown in the standard TMM with or without 1 µM Co(II) (Table 3), but the cobalt level increased strongly in the Δ*zupT* Δ*dmeF* Δ*cobW2* Δ*cobW3* quadruple mutant in the presence of 1 µM Co(II). Cobalt resistance of the quadruple mutant was about

2 µM (Table 6) and did not change when CobW2 or CobW3 were present. Neither CobW mediated some degree of cobalt resistance in the absence of ZupT and DmeF. In the presence of DmeF and the Δ*zupT* Δ*cobW2* Δ*cobW3* triple mutant, cobalt resistance increased 3-fold to about 6 µM (Table 6), so that ZupT caused a low degree of cobalt resistance, probably by mediating controlled uptake of Co(II). Again, presence of the CobWs in the Δ*dmeF* mutant background did not increase cobalt resistance, showing the importance of DmeF as central inner membrane efflux system for Co(II). Interestingly, cobalt resistance of the Δ*zupT* Δ*cobW3* double mutant was at the level of that of the Δ*dmeF* mutants and increased again, when *cobW2* was additionally deleted (Table 6). This indicated that CobW2 also has a function in cobalt homeostasis, which may be based on some interplay with the efflux system DmeF.

Although the EDTA resistance was strongly reduced in the Δ*zupT* mutant and even more so in the Δ*zupT* Δ*cobW3* double mutant, it was hardly changed in the Δ*dmeF* single mutant but was decreased in the Δ*dmeF* Δ*zupT* mutant down to 76% of the parental level. It increased again marginally (1.25-fold) when the *cobW3* gene was additionally deleted and was decreased to 81% of the Δ*dmeF* Δ*zupT* level by introduction of a Δ*cobW2* allele and was reduced further to 54% in the Δ*cobW3* Δ*cobW2* mutant. CobW2 and CobW3 synergistically increased EDTA resistance in the presence of ZupT and DmeF, had no effect when DmeF was absent from cells but ZupT was present, and acted antagonistically when either transport system was absent; CobW2 increased and CobW3 decreased resistance. The strongest effect on EDTA resistance was observed in the absence of ZupT but in the presence of DmeF with CobW3 increasing EDTA resistance 10-fold in a CobW2-dependent manner. This indicates that this CobW2-dependent decrease in EDTA resistance in the Δ*zupT* Δ*cobW3* mutant was also DmeF-dependent.

Although both CobWs contributed synergistically to Cd resistance in the presence of both transport systems, they had no effect in the Δ*dmeF* mutant. Deletion of Δ*cobW3* increased Cd resistance nearly 2-fold in the Δ*dmeF ΔzupT* double mutant while the same deletion decreased Cd resistance strongly in the Δ*zupT* strain. This effect was again CobW2-dependent. The IC_{50} for cadmium was similar in the quadruple mutant, the Δ*dmeF* Δ*zupT* Δ*cobW2* triple mutant, and the *ΔzupT* Δ*cobW2* double mutant but was 2-fold higher than in the Δ*zupT ΔcobW3 ΔcobW2* triple and the Δ*zupT* Δ*cobW3* double mutants. DmeF was thus responsible for the strong decrease in cadmium resistance in the Δ*zupT* Δ*cobW3* double mutant (Table 6). This indicated that the ability to adjust the zinc and cobalt content through an interaction between ZupT, CobW2, CobW3, and DmeF is a prerequisite for the bacterium to adapt to metal starvation conditions and also for cadmium resistance. Zinc and cobalt homeostasis and cadmium resistance are linked processes in this bacterium with ZupT, CobW2, CobW3, and DmeF being the main actors in this multiple-ion homeostasis (Fig. S1).

DISCUSSION

The interplay between ZupT, CobW2, CobW3, and DmeF

A complicated interplay between ZupT with CobW2 and CobW3 (Fig. S1) affects the flow-equilibrium of Zn(II) in *C. metallidurans*, along with uptake of other metals, metal efflux systems, and the metal-binding components of the cytoplasm glutathione and polyphosphate (18). This maintains the number of Zn ions per cell at about 70,000 to 80,000 per cell, as previously published (8, 43). To accumulate this number of Zn ions per cell, a zinc content of the growth medium of 140 nM to 160 nM is needed, and indeed, at lower concentrations, all available Zn is accumulated by the cells (Table 2).

If the zinc content of the growth medium does not allow accumulation of 80,000 Zn ions per cell, *C. metallidurans* accumulates Co(II) (Fig. 1). This may allow us to metalate metal-promiscuous enzymes such as FolE_IB1 and FolE_IB2 to substitute Zn-dependent paralogs (25). ZupT and CobW3 are central to this process (Fig. 1; Tables 2 and 3), whereas CobW2 also contributes but in a minor way. The interplay of these three proteins is necessary for *C. metallidurans* to survive metal-starvation conditions, but it also contributes to cadmium and cobalt resistance (Table 3), with the Co efflux system

DmeF (16) also required for full resistance to both metals. DmeF is as important for full cobalt resistance as ZupT (Fig. 4). CobW2 and CobW3 cause delayed growth in a Δ*dmeF* mutant in the presence of ZupT, so that all four proteins are necessary not only to mediate cobalt resistance but also to allow cobalt accumulation in response to zinc starvation.

Cd(II) interacts with all thiol compounds in the cytoplasm, which leads to protein denaturation, limiting levels of glutathione, release of iron from enzymes such as aconitase and subsequently to redox stress (46–49). The influence of ZupT, DmeF, and the CobW proteins in cadmium resistance (Table 6) also indicates that cadmium may disturb zinc homeostasis. Both metals belong to the same group of the periodic system of the elements and are thus chemically related. Disturbance of zinc homeostasis by cadmium has been noted before (50, 51). This would indicate that a primary function of ZupT, DmeF, and the two CobWs would be to protect zinc homeostasis against cadmium by filling-up the zinc pool with available zinc. Under zinc-replete conditions, cadmium cannot outcompete Zn(II) because Cd(II) is a soft metal ion that prefers Cys over His residues, and both metal ions have different ionic radii (52, 53). Only if insufficient Zn(II) is available to fill-up the zinc pool is Cd(II) able to outcompete Zn(II) (40). Filling up the zinc pool with cobalt instead may thus help prevent this toxic effect of Cd(II).

This could be one important reason to fill-up parts of the cellular zinc pool with Co(II) in the event of zinc-limitation. Moreover, metal-promiscuous paralogs of zinc-dependent proteins could be supplied with cobalt to retain functionality (25). This would also explain the role of cobalt in zinc-starved *S. typhimurium* (38) and the link between Zn and Co homeostasis and Cd resistance in *C. metallidurans*. One of the functions of the CzcCBA transenvelope system, but which is absent in the AE104 strain, could be to prevent import of too much of either metal into the plasmid-bearing *C. metallidurans* CH34 cells. Because ZupT is required for the Zn-Co-Cd connection, this would explain why the CzcCBA efflux complex cannot exist in the absence of ZupT (43).

Binding of metals to the CobWs

The homologs of the CobWs are associated with the delivery of Zn(II) to Zn-dependent proteins in bacteria and eukaryotes (22, 23, 54, 55). Metal delivery is aided by GTP- or ZTP-hydrolysis (27) in the case of the CobW-ortholog ZagA. CobW1, which is only needed under extreme zinc-starvation conditions in *C. metallidurans* (20), is related to ZagA, ZNG1 from *Saccharomyces cerevisiae,* and CobW from *Rhodobacter capsulatus* (Fig. S7). All these proteins display the typical Walker A-, B-, switch-, and G-binding motifs of GTPases. The only difference between the GTPases and the ZTPase ZagA could be the Cys residue upstream of the highly conserved Asp residue in the G-binding motif (Fig. S1 and S7). With the exception of CobW3, all of these proteins have an internal metal-binding site between the Walker B and the switch motifs, which is highly conserved (GCI/mCC), strongly selective for soft and borderline transition metal cations, and is probably involved in triggering the GTPase activity (56). More importantly, binding of MgGTP pre-conditions this site for acceptance of the correct metal ions (41). Always in dependence of the extant cytoplasmic metal ion concentration, this, nevertheless, assures the correct metalation of a CobW homolog (40), so that CobW_Rcap from *R. capsulatus* accepts Co(II) but YeiR and YjiA accept Zn(II) (41), delivering it to the internal metal-binding site. This metal preference, modeled under *in vivo* conditions, however, was mirrored to some degree by the relationship between the respective proteins (Fig. S7). CobW_Rcap and YeiR form one deeply branched relationship; ZagA, CobW1, and CobW3 a second; YjiA, CobW2, and ZNG1 the third, which is again deeply branched.

In addition to the missing internal metal binding motif in CobW3, this protein and CobW2 contain large His-rich regions, which AlphaFold2 predicts to form a random coil (Fig. S1 and S7). This region is located at the C-terminus of CobW3 but is internal in CobW2. These motifs could indeed be intrinsically disordered protein (IDP) regions, which organize themselves during binding of metal cations. In this scenario, binding of one metal cation to CobW2 would be to the internal metal-binding site and controlled

by the *in vivo* concentration of a metal cation among those of competing metal cations. With increasing Co and decreasing Zn concentrations, the probability of Co-binding over Zn-binding would consequently increase.

Binding of metal cations to the putative IDP regions would not be controlled directly by MgGTP (41) but by the proportion of a metal among the other cations present in the cell. CobW3 binds about 8 (6.5 to 9) Zn(II) ions with decreasing affinity when only Zn(II) is present. When incubated with a metal mix, 4 Zn(II), 2 to 3 Ni(II), 1 Co(II), and 1 Cd(II) are bound (20). CobW2, with its large internal His-rich region, is present in two different conformations, binding 0.5 Zn(II) or about 7 Zn(II), respectively, when only zinc is present. When offered a mixture of metal cations, CobW2 precipitates (20). This led to the assumption that CobW2 is a zinc-storage protein that binds up to 7 Zn(II) ions in its "open" conformation and one or none Zn ions in its "closed" conformation. CobW2 could therefore act as a zinc buffer but, as shown by the CobW2-dependent decrease of Co resistance of the Δ*zupT* Δ*cobW3* mutant (Table 6), may also interact in some way with DmeF. With about 2,000 copies per cell and 7 Zn(II) ions bound per protein, CobW2 would be able to store 14,000 Zn(II) of the total 70,000 Zn(II) ions in the cell (17, 20), representing 20% of the cellular zinc. CobW3, on the other hand, has a clear influence on metal import (20), and this is further substantiated by the findings of the current study. CobW3 may be capable of determining the relative proportions of metal cations in the metal mix through differential affinities by binding them at its C-terminal His-rich region. This would consequently affect metal transport depending on the actual metal cations bound.

Zinc homeostasis in *C. metallidurans*

As far as is known, zinc is an essential element for all organisms (23, 57). The divalent Zn(II) transition metal cation has a completely filled $3d^{10}$ orbital, which prevents the formation of stable octahedral complexes because no empty 3d orbitals are available to accept free electron pairs from metal ligands (58). Thus, Zn(II) forms tetrahedral complexes. These complexes have the function of stabilizing the conformation of proteins such as in the periplasmic Cu-Zn-dependent superoxide dismutase or in the RpoC (beta-prime) subunit of the RNA polymerase (59, 60). Alternatively, Zn(II) can also act as Lewis acid catalyzing biochemical reactions such as in alcohol dehydrogenase, carbonic anhydrase, or FolE_IA-type GTP-cyclohydrolase I, which initiates biosynthesis of the essential cofactor tetrahydrofolate (25, 61).

As *C. metallidurans* typically contains 70,000 to 80,000 Zn(II) per cell when cultivated in standard TMM (8, 17, 43), high external zinc concentrations cause transient accumulation of zinc resulting in the cation being exported by the P_{IB2}-type ATPase ZntA in the plasmid-free strain AE104, whereas in the CH34 wild-type strain additional plasmid-encoded zinc efflux pumps eject excess zinc ions. Strain AE104 contains a much higher number of zinc-binding proteins, about 110,000 per cell (17), so that after growth in standard TMM, not all zinc-binding sites are occupied. Half of the zinc-binding proteins are involved in genetic information-processing, with two-thirds of these being zinc-binding ribosomal proteins and the remaining one third being zinc-binding proteins of the RNA polymerase. However, only about 4,709 ± 128 copies of RpoC per cell (17) need a zinc ion for correct folding, which is "checked" by the omega subunit RpoZ before final assembly of the RNAP. The lowest cellular zinc content measured in this study was 7,100 ± 1,200 Zn ions per cell (Table 1) in low zinc medium, which would leave about 2,400 Zn for other essential zinc-dependent proteins, for instance, the periplasmic SodC, with 164 ± 43 copies per cell (17).

An operon in *C. metallidurans* contains two Zur-binding sites at the promoter, is only expressed under extreme zinc starvation, and includes a gene encoding the third COG0523-family protein CobW1. The operon also has genes encoding a metal-promiscuous GTP-cyclohydrolase FolE_IB2 that needs Fe, Mn, or Co for activity, and paralogs of the zinc-dependent proteins CysS, QueD, AllB, as well as a carbonic anhydrase (19, 20). The number of the respective paralogs total about 3,700 proteins (17), so that the 7,100

Zn ions per cell might indeed signify the lowest possible zinc content of these cells. As in case of the zinc-dependent GTP cyclohydrolase FolE_IA and its metal-promiscuous substitutes FolE_IB1 and FolE_IB2 (28, 61, 62), other metal cations might act as Lewis acids in an essential biochemical catalysis, substituting for the lack of zinc.

As a consequence of the Debye-Hückel rule (63) and other constraints, Mg(II) and the divalent transition metal cations should form solvent-shared ions-pairs with the Lewis bases inside the cell and form contact ion-pairs whenever a sufficient number and position of Lewis base ligands are available (53). In contrast, the alkali metal cations Na(I) and K(I) should be mostly fully solvated ions, which counteract the negative charges of the proteins and nucleic acids, but otherwise can enter into solvent-shared ions-pairs with these compounds. The proteome of *C. metallidurans* may have a capacity of nearly 6 million binding sites for divalent metal cations, including those in the 110,000 proteins of the zinc repository (17, 53), which might interact with half of the 10 million Mg(II) ions per cell, if Mg(II) is not out-competed by transition metal cations. Moving from protein to protein, Zn(II) might follow the amino acids on their path to the translating ribosome. The ribosomal proteins and the RNA polymerase contain zinc buffers, with RNAP having additional zinc-binding sites besides the essential one in RpoC (17). In this way, Zn(II) is available to be inserted into nascent proteins during translation, which explains the zinc-dependence of translation (64). Proteins such as ZagA might be required for those proteins that did not, or could not, obtain their zinc during translation, or which have lost it.

Should this hypothetical zinc allocation pipeline become limiting for the cation, other metal cations may outcompete the Mg(II) and follow the amino acids to the ribosome. Cd(II), which belongs to the same group of the periodic system as Zn(II) and also has a completely filled d-orbital, may bind to zinc-binding sites in the absence of competing zinc ions, which explains the observed greater cadmium sensitivity of zinc-starved cells. Should Fe(II) enter this allocation pipeline, zinc-dependent proteins would receive the highly redox-active iron. This situation should be prevented by iron-storage proteins or by its rapid sequestration by Fe-dependent proteins, for example, in the form of Fe-S-clusters (30, 65). *C. metallidurans* does not use Mn(II) and handles Cu(I) by a sophisticated periplasmic copper homeostasis and export from the cytoplasm (8, 66). This leaves Co(II) and Ni(II) as the only other possible metal cations that may follow the zinc allocation pathway.

Cobalt and nickel

Ni(II) ions have eight electrons in their 3d orbital (58). An octahedral complex would have six electrons in the non-binding and the remaining two electrons in an anti-bonding 3d orbital, so that four ligands are firmly bound and the axial two are only loosely bound. Such Ni(II) complexes appear as square-planar complexes (41). The CnrCBA transenvelope efflux complex is responsible for nickel resistance in *C. metallidurans* (67). It is regulated by the extracytoplasmic sigma factor CnrH, bound in the absence of nickel by the membrane-bound CnrYX complex with CnrX being the sensor for periplasmic Ni(II) (68–70). CnrX binds Ni(II) in a quasi-octahedral complex (71–74). Two adjacent corners of the Ni(II) complex are occupied by the terminal carboxyl group of a glutamate residue. One anti-bonding d-orbital of the central Ni(II) ion contains the two electrons as an electron pair. This allows Ni(II) to accept one more electron pair from the deprotonated carboxyl group of the Glu ligand. The required pairing energy of the electrons is compensated by the release of energy stemming from the mesomeric overlay of one oxygen donating an electron pair to the Ni(II) as fifth ligand and the other double-bonded oxygen is not bonded by Ni(II) (74). This discriminates strongly against Zn(II) but not Co(II); however, *cnr* is only mildly upregulated by Co(II) compared with Ni(II) (70). In *C. metallidurans* CH34 wild type, the CzcCBA efflux pump keeps the periplasmic Co(II) level low, even in medium with a low metal content (75), so that CnrCBA is only produced at high (low mM) nickel, or even higher cobalt concentrations (5, 76).

In comparison to Ni(II), Co(II) has only seven electrons in the 3d orbital, six in the non-bonding d orbitals and one in an anti-bonding d-orbital. Octahedral complexes are possible, with a switch between the formal Co(II) and Co(III) oxidation states allowing the binding of the 6th beta-ligand or weakening of this bond, as for instance in cobalamin during mutase reactions (77). As outlined elsewhere (7), this provides low-spin Co(III) complexes with a low energetic state due to the half-filled 3d orbitals so that Co(III) complexes are kinetically stable, which traps cobalt in cobalamin complexes so that most of the cell-bound cobalt may reside in these complexes. Derivatives of cobalamin are even used to exchange cobalt between cells, allowing them to keep the concentration of unbound Co(II) in the cytoplasm very low (7).

Trapping of cobalt in cobalamin complexes may lower the concentration of Co(II) available for metalation of CobW3 and other proteins, so that Zn(II) may out-compete cobalt here (41). Indeed, *Pseudomonas denitrificans* strains can be used to produce up to 200 mg/L B_{12} under biotechnological conditions (78). This would calculate to about 150 nM of B_{12} in the growth medium, which would need the same Co(II) concentration to allow biosynthesis. *C. metallidurans* contains the genes for cobalamin biosynthesis or uptake; the respective proteins are there, but none of the genes was up- or down-regulated in *C. metallidurans* strain AE104 under metal stress or starvation conditions (79, 80). Although the abundance of the proteins involved in cobalamin biosynthesis seem not to be regulated under conditions of changing metal availability, product removal by trapping may increase the ratio of cytoplasmic Co bound to cobalamin. On the other hand, none of the tested strains exhausted the cobalt content of the growth medium. That would be expected if a strong cobalamin biosynthesis rate traps all the available cobalt in the center of B_{12}. At this stage, it cannot be concluded how much of the cytoplasmic cobalt is trapped as B_{12} and how this trapping influences binding of Co(II) to CobW3 or the FolE_IBs (41).

CobW3 bound Zn(II), Ni(II), Co(II), and Cd(II), and each metal should form different complexes by binding to the variety of amino acid residues in the large C-terminal His-rich loop of the protein (Fig. S1). This may allow CobW3 to form a variety of conformations of its C-terminal domain, resulting in different actions of CobW3, for instance, during protein-protein interactions. Although Cd(II) should be exported by the P_{IB2}-type ATPases ZntA and CadA (15), *C. metallidurans* cells contain Ni-hydrogenases and maturation proteins like HypB, another member of the COG0523 protein family like the CobWs, even under heterotrophic growth conditions (5), and these proteins should serve as sinks for Ni(II). Therefore, only Co(II) remains to occupy Zn-binding sites and protect them from being bound by Cd(II). To prevent cobalt toxicity, however, the cellular Co(II) level has to be strictly controlled, which is accomplished by the interaction of CobW3, ZupT, DmeF and CobW2 (Fig. S1), and possibly trapping of Co(II) in cobalamin complexes.

MATERIALS AND METHODS

Bacterial strains and growth conditions

Strains used for experiments were derivatives of the plasmid-free derivative AE104 of *C. metallidurans* CH34 (5) and are listed in Table S2. Tris-buffered mineral salts medium (5) containing 2 g sodium gluconate/l (TMM) was used to cultivate these strains aerobically with shaking at 30°C. Modified versions of the standard TMM contained different zinc and magnesium concentrations (Table S1). Solid Tris-buffered media contained 20 g agar/L.

Dose–response growth curves in 96-well plates

Experiments were conducted in TMM. A pre-culture was incubated at 30°C, 200 rpm up to early stationary phase, then diluted 1:20 into fresh medium and incubated for 24 h at 30°C and 200 rpm. Overnight cultures were used to inoculate parallel cultures with increasing metal concentrations in 96-well plates (Greiner). Cells were cultivated for

25 h at 30°C and 1,300 rpm in a neoLab Shaker DTS-2 (neoLab, Heidelberg, Germany) and the optical density was determined at 600 nm in a TECAN Infinite M Nano reader (Tecan Group Ltd., Männedorf, Switzerland) as indicated. To calculate the IC_{50} values (inhibitory concentration: metal concentration that led to turbidity reduction by half) and the corresponding *b*-value (measure of the slope of the sigmoidal dose–response curve), the data were adapted to the formula $OD(c) = OD0/\{1 + \exp((c - IC_{50})/b)\}$, which is a simplified version of a Hill-type equation as introduced by Pace and Scholtz (81) as published (82). OD(*c*) is the turbidity at a given metal concentration, OD0 that had no added metal, and *c* is the metal concentration.

Time-dependent growth curves in 48-well plate

Experiments were conducted in TMM. A pre-culture was incubated at 30°C, 200 rpm up to early stationary phase, then diluted 1:20 into fresh medium and incubated for 24 h at 30°C and 200 rpm. Overnight cultures were diluted 50-fold in fresh medium with or without additions in 48-well plates (TPP). The kinetic loop consisted of 90 cycles and was performed in TECAN Spark microplate reader (TECAN, Switzerland). Shaking duration was 2,000 seconds, in orbital mode with an amplitude of 4 mm and frequency of 150 rpm. Optical density was measured at 600 nm at the end of each cycle.

Genetic techniques

Standard molecular genetic techniques were used (83, 84). For conjugative gene transfer, overnight cultures of donor strain *E. coli* S17/1 (85) and of the *C. metallidurans* recipient strains grown at 30°C in Tris- buffered medium were mixed (1:1) and plated onto nutrient broth agar. After 2 d, the bacteria were suspended in TMM, diluted, and plated onto selective media as previously described (83). Primer sequences are provided in Table S2.

Gene deletions

Primer sequences are also provided in Table S2. Plasmid pECD1002, a derivate of plasmid pCM184 (86), was used to construct deletion mutants. These plasmids harbor a kanamycin resistance cassette flanked by *loxP* recognition sites. Plasmid pECD1002 additionally carries alterations of 5 bp at each *loxP*-site. Using these mutant *lox* sequences, multiple gene deletions within the same genome are possible without interferences by secondary recombination events (87, 88). Fragments of 300 bp upstream and downstream of the target gene were amplified by PCR, cloned into vector pGEM T-Easy (Promega), sequenced, and further cloned into plasmid pECD1002. The resulting plasmids were used in a double-crossover recombination in *C. metallidurans* strains to replace the respective target gene by the kanamycin-resistance cassette, which was subsequently also deleted by transient introduction of *cre* expression plasmid pCM157 (86). Cre recombinase is a site-specific recombinase from the phage P1 that catalyzes the *in vivo* excision of the kanamycin resistance cassette at the *loxP* recognition sites. The correct deletions of the respective transporter genes were verified by Southern DNA-DNA hybridization. For construction of multiple deletion strains, these steps were repeated. The resulting mutants carried a small open reading frame instead of the wild-type gene to prevent polar effects.

Inductively-coupled plasma mass spectrometry (ICP-MS)

Cells were incubated in TMM for 20 h at 30°C with shaking at 200 rpm, diluted 20-fold into fresh TMM medium, and shaking was continued at 30°C for 24 h. Cells were diluted 66-fold into fresh medium until 100 Klett was reached (mid-exponential phase of growth). Metals were added, and the cells were left growing until they reached 150 Klett. Ten milliliters of the cells were harvested by centrifugation, washed twice with 50 mM TrisHCl buffer (pH 7.0) containing 10 mM EDTA, and 150 mM NaCl at 4°C. For ICP-MS analysis, HNO3 (trace metal grade; Normatom/PROLABO) was added to the samples to a final concentration of 67% (wt/vol), and the mixture was mineralized at

70°C for 2 h. Samples were diluted to a final concentration of 2% (wt/vol) nitric acid. Indium and germanium were added as internal standards at a final concentration of 1 ppb and 10 ppb each. Elemental analysis was performed via ICP-MS using Cetac ASX-560 sampler (Teledyne, Cetac Technologies, Omaha, Nebraska), a MicroFlow PFA-100 nebulizer (Elemental Scientific, Mainz, Germany), and an ICAP-RQ ICP-MS instrument (Thermo Fisher Scientific, Bremen) operating with a collision cell and flow rates of 4.5 mL × min^{-1} of He/H_2 [93%/7% (89)], with an Ar carrier flow rate of 0.76 L × min^{-1} and an Ar make-up flow rate at 15 L × min^{-1}. An external calibration curve was recorded with ICP-multi-element standard solution XVI (Merck) in 2% (vol/vol) nitric acid. The sample was introduced via a peristaltic pump and analyzed for its metal content. For blank measurement and quality/quantity thresholds, calculations based on DIN32645 TMM were used. The results were calculated from the ppb data as atoms per cell as described (8).

Pulse-chase experiments with radioactive ^{65}Zn

Cells were incubated in TMM for 17 h at 30°C shaking at 200 rpm, diluted 20-fold into a second pre-culture in the medium that was used for the subsequent main culture (TMM, aZn, lZn, and lZn_lMg) and incubated with shaking at 30°C for 24 h. Cells were diluted 50-fold into the main culture, which was incubated with shaking at 30°C at 200 rpm until a turbidity of 150 Klett units was reached (mid-exponential phase of growth). The cells were harvested by centrifugation at 4°C, washed in the same volume of 10 mM TrisHCl (pH 7), suspended in the same volume of 10 mM TrisHCl (pH 7), and kept on ice until needed during the same day. For the experiments, sodium gluconate was added to 6 mL of the cell suspension to a final concentration of 2 g/L directly before the start. At t = 0, radioactive ^{65}Zn was added to the cell suspension to a final concentration of 1 µM Zn(II) and 60 nCi/mL. The $^{65}ZnCl_2$ was supplied by POLATOM (certificate 022–106722-03622-0001).

The cells were incubated with shaking at 30°C. At 0.25, 5, 10, and 15 min, samples of 500 µL were removed and filtered through a membrane filter (0.2-µm pore size, Whatman cellulose nitrate membrane filters, Cytiva) using a vacuum-driven uptake apparatus. The samples were rapidly washed twice with 5 mL of 50 mM TrisHCl (pH 7) containing 50 mM EDTA. The activity was counted in a Liquid Scintillation Counter (PerkinElmer Tri-Carb 2810 TR) using Ultima Gold (PerkinElmer). The samples were counted twice for 2 min in a window from 0 to 200 keV.

For the chase, non-radioactive zinc was added at t = 20 min to a final concentration of 100 µM. Incubation was continued with shaking at 30°C, and samples were removed at 20.25, 25, 30, 35, and 40 min. They were treated and analyzed as described above for the samples of the uptake period.

A sample of 100 µL was counted to determine the total radioactivity of the ^{65}Zn in the cell suspension used for the pulse-chase experiment. From this value, the mol zinc per cpm ratio was derived. For each time sample, the mean value and technical deviation of the two 2 min counts were calculated. Two zero controls were subtracted, one for the background radioactivity at the time of the experiment and one for the chemical adsorption of ^{65}Zn by the membrane filter. The resulting value was multiplied with the mol/cpm ration of the respective experiment to give the mol ^{65}Zn per 500 µL time sample. The actual cell number in the sample had been determined via an equilibration curve for the turbidity at 600 nm, so that the mol ^{65}Zn per cell and subsequently the number of the ^{65}Zn atoms per cell could be calculated.

All experiments were performed at least three times. For each individual experiment, the zinc content per cell at 7.5 min was calculated from the 5 min and 10 min values. This value was used to correct the number of atoms per cell for all experiments involving the same mutant and the same growth condition. Experiments with large correction factors were removed and the respective experiment repeated. For each strain and condition, the mean values and deviations of the ^{65}Zn atoms per cell were finally calculated. This

value was designated as the cellular metal content C(t) for the respective mutant and growth condition.

Pulse-chase with ^{65}Zn measured: (i) the initial zinc uptake velocity $v_{up}(0)$ at t = 0; (ii) the cellular ^{65}Zn content C_{20} at the end of the uptake period (time point represented in Fig. 2 by the horizontal bar); (iii) the extrapolated maximum zinc content after the uptake period C_{max}; (iv) the efflux velocity v_{eff} at the beginning of the chase at 20 min; (v) the corresponding initial zinc content C_0 used to calculate v_{eff}; and (vi) and the final zinc content C_{40} at the end of the chase period (Fig. 2, t = 40 min). To obtain these data, the uptake phase up to 20 min of the pulse-chase experiment was adapted to the equation $C(t) = C_{max} \cdot t/(K_t + t)$ using the Lineweaver-Burk-like plot $1/C(t) = 1/C_{max} + K_t/C_{max} \cdot 1/t$. The first deviation by time of the equation $C(t) = C_{max} \cdot t/(K_t + t)$ was $dC(t)/dt = C_{max} \cdot K_t/(K_t + t)^2$. At t = 0, this gave the initial uptake rate $v_{up}(0) = C_{max}/K_t$. After the chase after 20 min, the cell-bound zinc content was modeled by the decay function $C(t) = C_o \cdot e^{(-t \cdot t)}$ using the plot $\ln C(t) = \ln C_o - t \cdot t$. The first deviation by time of the equation $C(t) = C_o \cdot e^{(-t \cdot t)}$ was $dC(t)/dt = -t \cdot C_o \cdot e^{(-t \cdot t)}$. However, at t = 0, this value was the initial net efflux rate $v_{eff}(0) = -t \cdot C_o$. In contrast to the initial uptake rate that was no net rate because the cells did not contain ^{65}Zn at t = 0, $v_{eff}(0)$ was a net rate, and the result of the real efflux rate after chase minus the rate of ^{65}Zn re-import at this time.

Experiments with stable ^{67}Zn

Stable enriched ^{67}Zn was employed to determine (vii) the resident zinc pool (ZP) ZP1 at the beginning of the experiment; (viii) the zinc pools ZP1 and ZP2 after the uptake period; and (ix) finally, these pools ZP1 and ZP2 after the chase period. The cell suspensions were prepared in the respective media as described for the pulse-chase experiments above; however, the respective growth medium was used instead of uptake buffer for these experiments. After a zero sample had been removed for the ICP-MS analysis, isotope-enriched ^{67}Zn(II) was added to a final concentration of 1 µM. Incubation was continued with shaking for 20 min, a sample was removed, and the remaining cells were chased with non-enriched Zn(II) added at a final concentration of 100 µM. Incubation was continued for 20 min with shaking at 30°C, and the third sample was removed. The cells in the respective samples were harvested by centrifugation, washed twice with 50 mM TrisHCl buffer (pH 7.0) containing 50 mM EDTA at 0°C, suspended in 50 mM TrisHCl buffer (pH 7.0), and mineralized for the subsequent ICP-MS analysis. The ^{67}Zn (94% ^{67}Zn) was provided as metal from Nakima Ltd (Savyon, Israel) and oxidized using HCl on ice. The zinc content was verified by ICP-MS.

For the calculation of different zinc pools in the cells, the ratio of ^{67}Zn in the isotope-enriched zinc solution (94%) and non-enriched "usual" zinc [4.1% (90)] was used. The ICP-MS measurement calculates the quantity of an element from that of its isotopes, thereby correcting for the % of the natural abundance of the respective isotope. The zinc pool 1 (ZP1) was defined as the cellular zinc pool before addition of isotope-enriched ^{67}Zn and was equal to the ^{64}Zn ICP-MS result [natural abundance 48.6% (90)]. Similar results were obtained by using ^{66}Zn (27.9%) instead of ^{65}Zn. Zinc pool 2 (ZP2) was the zinc pool after incubation of the cells with ^{67}Zn. ZP2 was the ^{67}Zn value coming from the ICP-MS (corrected for a natural abundance 4.1%) minus the ^{64}Zn value (0.75% in the ^{67}Zn-enriched zinc solution) and the result was divided by 22.2346.

Statistics

Students' *t*-test was used, but in most cases, the distance (D) value, D, has been used several times previously for such analyses (10, 91, 92). It is a simple, more useful value than Student's *t*-test because non-intersecting deviation bars of two values (D > 1) for three repeats always mean a statistically relevant (≥ 95%) difference, provided the deviations are within a similar range. At $n = 4$, significance is ≥97.5%, at $n = 5$ ≥ 99% (significant), and at $n = 8$ ≥ 99.9% (highly significant).

ACKNOWLEDGMENTS

Funding for this work was provided by the Deutsche Forschungsgemeinschaft (Ni262/19).

We thank Gary Sawers for critically reading the manuscript and Grit Schleuder for expert technical support.

AUTHOR AFFILIATIONS

[1]Molecular Microbiology, Institute for Biology/Microbiology, Martin-Luther-University Halle-Wittenberg, Halle (Saale), Germany
[2]Department of Environmental Analytical Chemistry, Helmholtz Centre for Environmental Research – UFZ, Leipzig, Germany

AUTHOR ORCIDs

Dietrich H. Nies http://orcid.org/0000-0002-4516-8267

FUNDING

Funder	Grant(s)	Author(s)
Deutsche Forschungsgemeinschaft (DFG)	NI262/19-2	Dietrich H. Nies

ADDITIONAL FILES

The following material is available online.

Supplemental Material

Supplemental material (JB00226-24-s0001.pdf). Tables S1 to S5; Figures S1 to S7.

REFERENCES

1. Janssen PJ, Morin N, Mergeay M, Leroy B, Wattiez R, Vallaeys T, Waleron K, Waleron M, Wilmotte A, Quillardet P, de Marsac NT, Talla E, Zhang C-C, Leys N. 2010. Genome sequence of the edible *Cyanobacterium arthrospira* sp. PCC 8005. J Bacteriol 192:2465–2466. https://doi.org/10.1128/JB.00116-10
2. Diels L, Mergeay M. 1990. DNA probe-mediated detection of resistant bacteria from soils highy polluted by heavy metals. Appl Environ Microbiol 56:1485–1491. https://doi.org/10.1128/aem.56.5.1485-1491.1990
3. Stiers M, Mergeay M, Pinson H, Janssen L, Voets E, De Cauwer H, Schepens T. 2021. Individualized mechanical ventilation in a shared ventilator setting: limits, safety and technical details. J Clin Monit Comput 35:1299–1309. https://doi.org/10.1007/s10877-020-00596-7
4. Reith F, Rogers SL, McPhail DC, Webb D. 2006. Biomineralization of gold: biofilms on bacterioform gold. Science 313:233–236. https://doi.org/10.1126/science.1125878
5. Mergeay M, Nies D, Schlegel HG, Gerits J, Charles P, Van Gijsegem F. 1985. *Alcaligenes eutrophus* CH34 is a facultative chemolithotroph with plasmid-bound resistance to heavy metals. J Bacteriol 162:328–334. https://doi.org/10.1128/jb.162.1.328-334.1985
6. diCenzo GC, Finan TM. 2017. The divided bacterial genome: structure, function, and evolution. Microbiol Mol Biol Rev 81:e00019-17. https://doi.org/10.1128/MMBR.00019-17
7. Nies DH. 2016. The biological chemistry of the transition metal "Transportome" of *Cupriavidus metallidurans*. Metallomics 8:481–507. https://doi.org/10.1039/c5mt00320b
8. Kirsten A, Herzberg M, Voigt A, Seravalli J, Grass G, Scherer J, Nies DH. 2011. Contributions of five secondary metal uptake systems to metal homeostasis of *Cupriavidus metallidurans* CH34. J Bacteriol 193:4652–4663. https://doi.org/10.1128/JB.05293-11
9. Herzberg M, Bauer L, Kirsten A, Nies DH. 2016. Interplay between seven secondary metal transport systems is required for full metal resistance of *Cupriavidus metallidurans*. Metallomics 8:313–326. https://doi.org/10.1039/c5mt00295h
10. Große C, Wolff-Menzler C. 2016. Analysis and assessment of modifications of the PEPP system introduced by the PEPP catalogue 2015. Gesundheitswesen 78:446–451. https://doi.org/10.1055/s-0035-1548850
11. Busch W, Saier MHJ. 2002. The transporter classification (TC) system. Crit Rev Biochem Mol Biol 37:287–337. https://doi.org/10.1080/-10409230290771528
12. Saier MHJ, Tran CV, Barabote RD. 2006. TCDB: the transporter classification database for membrane transport protein analyses and information. Nucleic Acids Res 34:D181–D186. https://doi.org/10.1093/nar/gkj001
13. Abelson PH, Aldous E. 1950. Ion antagonisms in microorganisms - interference of normal magnesium metabolism by nickel, cobalt, cadmium, zinc, and manganese. J Bacteriol 60:401–413. https://doi.org/10.1128/jb.60.4.401-413.1950
14. Nelson DL, Kennedy EP. 1971. Magnesium transport in *Escherichia coli* - inhibition by cobaltous ion. J Biol Chem 246:3042–3049.
15. Scherer J, Nies DH. 2009. CzcP is a novel efflux system contributing to transition metal resistance in *Cupriavidus metallidurans* CH34. Mol Microbiol 73:601–621. https://doi.org/10.1111/j.1365-2958.2009.06792.x
16. Munkelt D, Grass G, Nies DH. 2004. The chromosomally encoded cation diffusion facilitator proteins DmeF and FieF from *Wautersia metallidurans* CH34 are transporters of broad metal specificity. J Bacteriol 186:8036–8043. https://doi.org/10.1128/JB.186.23.8036-8043.2004
17. Herzberg M, Dobritzsch D, Helm S, Baginsky S, Nies DH. 2014. The zinc repository of *Cupriavidus metallidurans*. Metallomics 6:2157–2165. https://doi.org/10.1039/c4mt00171k
18. Nies DH, Schleuder G, Galea D, Herzberg DH. 2024. A flow equilibrium of zinc in cells of *Cupriavidus metallidurans*. J Bacteriol 206:e00080-24. https://doi.org/10.1128/jb.00395-23

19. Schmidt C, Schwarzenberger C, Große C, Nies DH. 2014. Furc regulates expression of *zupT* for the central zinc importer zupT of *Cupriavidus metallidurans*. J Bacteriol 196:3461–3471. https://doi.org/10.1128/JB.01713-14
20. Bütof L, Große C, Lilie H, Herzberg M, Nies DH. 2019. Interplay between the zur regulon components and metal resistance in *Cupriavidus metallidurans*. J Bacteriol 201:e00192-19. https://doi.org/10.1128/JB.00192-19
21. Bütof L, Schmidt-Vogler C, Herzberg M, Große C, Nies DH. 2017. The components of the unique zur regulon of *Cupriavidus metallidurans* mediate cytoplasmic zinc handling. J Bacteriol 199:e00372-17. https://doi.org/10.1128/JB.00372-17
22. Chen YY, O'Halloran TV. 2022. A zinc chaperone mediates the flow of an inorganic commodity to an important cellular client. Cell 185:2013–2015. https://doi.org/10.1016/j.cell.2022.05.012
23. Maret W. 2022. Escort proteins for cellular zinc ions. Nature 608:38–39. https://doi.org/10.1038/d41586-022-01988-2
24. Haas CE, Rodionov DA, Kropat J, Malasarn D, Merchant SS. 2009. A subset of the diverse COG0523 family of putative metal chaperones is linked to zinc homeostasis in all kingdoms of life. BMC Genomics 10:470. https://doi.org/10.1186/1471-2164-10-470
25. Schulz V, Galea D, Herzberg M, Nies DH. 2024. Protecting the Achilles heel: three FolE_I-type GTP-cyclohydrolases needed for full growth of metal resistant *Cupriavidus metallidurans* under a variety of conditions. J Bacteriol 206
26. Nies DH. 2019. The ancient alarmone ZTP and zinc homeostasis in *Bacillus subtilis*. Mol Microbiol 112:741–746. https://doi.org/10.1111/mmi.14332
27. Chandrangsu P, Huang X, Gaballa A, Helmann JD. 2019. *Bacillus subtilis* fole is sustained by the ZagA zinc Metallochaperone and the alarmone ZTP under conditions of zinc deficiency. Mol Microbiol 112:751–765. https://doi.org/10.1111/mmi.14314
28. Sankaran B, Bonnett SA, Shah K, Gabriel S, Reddy R, Schimmel P, Rodionov DA, Helmann JD, Iwata-Reuyl D, Swairjo MA. 2009. Zinc-independent folate biosynthesis: genetic, biochemical, and structural investigations reveal new metal dependence for GTP cyclohydrolase IB. J Bacteriol 191:6936–6949. https://doi.org/10.1128/JB.00287-09
29. Roux M, Covés J. 2002. The iron-containing superoxide dismutase of *Ralstonia metallidurans* CH34. FEMS Microbiol Lett 210:129–133. https://doi.org/10.1111/j.1574-6968.2002.tb11171.x
30. Braun V, HantkeK. 2007 Acquisition of iron by bacteria, p 189–217. In Nies DH, Silver S (ed), Molecular Microbiology of heavy metals. Vol. 6. Springer-Verlag, Berlin-Heidelberg.
31. Massey V, Strickland S, Mayhew SG, Howell LG, Engel PC, Matthews RG, Schuman M, Sullivan PA. 1969. The production of superoxide anion radicals in the reaction of reduced flavins and flavoproteins with molecular oxygen. Biochem Biophys Res Commun 36:891–897. https://doi.org/10.1016/0006-291x(69)90287-3
32. Haber F, Weiss J. 1932. Über die katalyse des hydroperoxydes. Naturwissenschaften 20:948–950. https://doi.org/10.1007/BF01504715
33. Liochev SI, Fridovich I. 2002. The haber-weiss cycle - 70 years later: an alternative view. Redox Rep. 7:55–57; https://doi.org/10.1179/135100002125000190
34. Fazzio TG, Roth JR. 1996. Evidence that the CysG protein catalyzes the first reaction specific to B-12 synthesis in *Salmonella typhimurium*, insertion of cobalt. J Bacteriol 178:6952–6959. https://doi.org/10.1128/jb.178.23.6952-6959.1996
35. Ranquet C, Ollagnier-de-Choudens S, Loiseau L, Barras F, Fontecave M. 2007. Cobalt stress in *Escherichia coli*. J Bio Chem 282:30442–30451. https://doi.org/10.1074/jbc.M702519200
36. Thorgersen MP, Downs DM. 2007. Cobalt targets multiple metabolic processes in *Salmonella enterica*. J Bacteriol 189:7774–7781. https://doi.org/10.1128/JB.00962-07
37. Fantino JR, Py B, Fontecave M, Barras F. 2010. A genetic analysis of the response of *Escherichia coli* to cobalt stress. Environ Microbiol 12:2846–2857. https://doi.org/10.1111/j.1462-2920.2010.02265.x
38. Ammendola S, Ciavardelli D, Consalvo A, Battistoni A. 2020. Cobalt can fully recover the phenotypes related to zinc deficiency in *salmonella typhimurium*. Metallomics 12:2021–2031. https://doi.org/10.1039/d0mt00145g
39. Irving H, Williams RJP. 1948. Order of stability of metal complexes. Nature 162:746–747. https://doi.org/10.1038/162746a0
40. Osman D, Robinson NJ. 2023. Protein metalation in a nutshell. FEBS Lett 597:141–150. https://doi.org/10.1002/1873-3468.14500
41. Young TR, Martini MA, Foster AW, Glasfeld A, Osman D, Morton RJ, Deery E, Warren MJ, Robinson NJ. 2021. Calculating metalation in cells reveals CobW ACQUIRES Co(II) for vitamin B(12) biosynthesis while related proteins prefer Zn(II). Nat Commun 12:1195. https://doi.org/10.1038/s41467-021-21479-8
42. Pfennig N. 1974. *Rhodopseudomonas globiformis*, Sp-N, a new species of *Rhodospirillaceae*. Arch Microbiol 100:197–206. https://doi.org/10.1007/BF00446317
43. Herzberg M, Bauer L, Nies DH. 2014. Deletion of the *zupT* gene for a zinc importer influences zinc pools in *Cupriavidus metallidurans* CH34. Metallomics 6:421–436. https://doi.org/10.1039/c3mt00267e
44. Schulz V, Schmidt-Vogler C, Strohmeyer P, Weber S, Kleemann D, Nies DH, Herzberg M. 2021. Behind the shield of czc: ZntR controls expression of the gene for the zinc-exporting P-type ATPase ZntA in *Cupriavidus metallidurans*. J Bacteriol 203:e00052-21. https://doi.org/10.1128/JB.00052-21
45. Grass G, Otto M, Fricke B, Haney CJ, Rensing C, Nies DH, Munkelt D. 2005. Fief (YiiP) from *Escherichia coli* mediates decreased cellular accumulation of iron and relieves iron stress. Arch Microbiol 183:9–18. https://doi.org/10.1007/s00203-004-0739-4
46. Helbig K, Grosse C, Nies DH. 2008. Cadmium toxicity in glutathione mutants of *Escherichia coli*. J Bacteriol 190:5439–5454. https://doi.org/10.1128/JB.00272-08
47. Helbig K, Bleuel C, Krauss GJ, Nies DH. 2008. Glutathione and transition metal homeostasis in *Escherichia coli*. J Bacteriol 190:5431–5438. https://doi.org/10.1128/JB.00271-08
48. Wang ZJ, Zhang Y, Chen YH, Han FY, Shi YX, Pan S, Li Z. 2024. Competition of CD(II) and Pb(II) on the bacterial cells: a new insight from bioaccumulation based on nanosims imaging. Appl Environ Microbiol 90. https://doi.org/10.1128/aem.01453-23
49. Cornejo FA, Muñoz-Villagrán C, Luraschi RA, Sandoval-Díaz MP, Cancino CA, Pugin B, Morales EH, Piotrowski JS, Sandoval JM, Vásquez CC, Arenas FA. 2023. Soft-metal(loid)s induce protein aggregation in *Escherichia coli*. Front Microbiol 14. https://doi.org/10.3389/fmicb.2023.1281058
50. Begg SL, Eijkelkamp BA, Luo Z, Couñago RM, Morey JR, Maher MJ, Ong C-LY, McEwan AG, Kobe B, O'Mara ML, Paton JC, McDevitt CA. 2015. Dysregulation of transition metal ion homeostasis is the molecular basis for cadmium toxicity in *Streptococcus pneumoniae*. Nat Commun 6:6418. https://doi.org/10.1038/ncomms7418
51. Wang AY, Crowley DE. 2005. Global gene expression responses to cadmium toxicity in *Escherichia coli*. J Bacteriol 187:3259–3266. https://doi.org/10.1128/JB.187.9.3259-3266.2005
52. Nies DH. 2022. Edited by C. J. Hurst. Microbial metabolism of metals and metalloids, Vol. 10, p 21–52. Vol. 10. Springer, Heidelberg.
53. Nies DH. 2022. How is a zinc ion correctly allocated to a zinc-dependent protein?, p 579–659. In HurstCJ (ed), Microbial metabolism of metals and metalloids. Vol. 10. Springer, Heidelberg.
54. Weiss A, Murdoch CC, Edmonds KA, Jordan MR, Monteith AJ, Perera YR, Rodríguez Nassif AM, Petoletti AM, Beavers WN, Munneke MJ, Drury SL, Krystofiak ES, Thalluri K, Wu H, Kruse ARS, DiMarchi RD, Caprioli RM, Spraggins JM, Chazin WJ, Giedroc DP, Skaar EP. 2022. Zn-regulated GTPase metalloprotein activator 1 modulates vertebrate zinc homeostasis. Cell 185:2148–2163. https://doi.org/10.1016/j.cell.2022.04.011
55. Pasquini M, Grosjean N, Hixson KK, Nicora CD, Yee EF, Lipton M, Blaby IK, Haley JD, Blaby-Haas CE. 2022. Zng1 is a GTP-dependent zinc transferase needed for activation of methionine aminopeptidase. Cell Rep 39:110834. https://doi.org/10.1016/j.celrep.2022.110834
56. Sydor AM, Jost M, Ryan KS, Turo KE, Douglas CD, Drennan CL, Zamble DB. 2013. Metal binding properties of *Escherichia coli* YjiA, a member of the metal homeostasis-associated COG0523 family of GTPases. Biochemistry 52:1788–1801. https://doi.org/10.1021/bi301600z
57. Krężel A, Maret W. 2016. The biological inorganic chemistry of zinc ions. Arch Biochem Biophys 611:3–19. https://doi.org/10.1016/j.abb.2016.04.010
58. HousecroftCE, ConstableEC. 2006. *Chemistry (Weinheim an der Bergstrasse, Germany)*. 3rd ed. Pearson Education Limited, Essex, England.

59. Markov D, Naryshkina T, Mustaev A, Severinov K. 1999. A zinc-binding site in the largest subunit of DNA-dependent RNA polymerase is involved in enzyme assembly. Genes Dev 13:2439–2448. https://doi.org/10.1101/gad.13.18.2439
60. Huang WJ, Sinclair RB, Powers L. 1992. The structure of the zinc sites of *Escherichia coli* DNA-dependent RNA polymerase. J Biol Chem 267:25560–25567. https://doi.org/10.1016/S0021-9258(19)74077-0
61. Rebelo J, Auerbach G, Bader G, Bracher A, Nar H, Hösl C, Schramek N, Kaiser J, Bacher A, Huber R, Fischer M. 2003. Biosynthesis of pteridines. reaction mechanism of GTP cyclohydrolase I. J Mol Biol 326:503–516. https://doi.org/10.1016/s0022-2836(02)01303-7
62. Auerbach G, Herrmann A, Bracher A, Bader G, Gütlich M, Fischer M, Neukamm M, Garrido-Franco M, Richardson J, Nar H, Huber R, Bacher A. 2000. Zinc plays a key role in human and bacterial GTP cyclohydrolase I. Proc Natl Acad Sci U S A 97:13567–13572. https://doi.org/10.1073/pnas.240463497
63. Debye P, Hückel E. 1923. Zur Theorie der Elektrolyte I. Gefrierpunktserniedrigung und verwandte Erscheinungen. Physikal Zeitschr 24:185–206.
64. Hensley MP, Tierney DL, Crowder MW. 2011. Zn(II) binding to *Escherichia* coli 70s ribosomes. Biochemistry 50:9937–9939. https://doi.org/10.1021/bi200619w
65. Layer G, Ollagnier-de Choudens S, Sanakis Y, Fontecave M. 2006. Iron-sulfur cluster biosynthesis: characterization of *Escherichia coli* CyaY as an iron donor for the assembly of [2Fe-2S] clusters in the scaffold IscU. J Biol Chem 281:16256–16263. https://doi.org/10.1074/jbc.M513569200
66. Hirth N, Gerlach M-S, Wiesemann N, Herzberg M, Große C, Nies DH. 2023. Full copper resistance in *Cupriavidus metallidurans* requires the interplay of many resistance systems. Appl Environ Microbiol 89:e0056723. https://doi.org/10.1128/aem.00567-23
67. Liesegang H. 1993. Characterization of the inducible nickel and cobalt resistance determinant cnr from pMOL28 of *Alcaligenes eutrophus* CH34. J Bacteriol 175:767–778. https://doi.org/10.1128/jb.175.3.767-778.1993
68. Tibazarwa C, Wuertz S, Mergeay M, Wyns L, van Der Lelie D. 2000. Regulation of the *cnr* cobalt and nickel resistance determinant of *Ralstonia eutropha* (*Alcaligenes eutrophus*) CH34. J Bacteriol 182:1399–1409. https://doi.org/10.1128/JB.182.5.1399-1409.2000
69. Grass G, Fricke B, Nies DH. 2005. Control of expression of a periplasmic nickel efflux pump by periplasmic nickel concentrations. Biometals 18:437–448. https://doi.org/10.1007/s10534-005-3718-6
70. Grass G, Grosse C, Nies DH. 2000. Regulation of the *cnr* cobalt/nickel resistance determinant from *Ralstonia* sp. CH34. J Bacteriol 182:1390–1398. https://doi.org/10.1128/JB.182.5.1390-1398.2000
71. Pompidor G, Maillard AP, Girard E, Gambarelli S, Kahn R, Covès J. 2008. X-ray structure of the metal-sensor CnrX in both the apo- and copper-bound forms. FEBS Lett 582:3954–3958. https://doi.org/10.1016/j.febslet.2008.10.042
72. Trepreau J, Girard E, Maillard AP, de Rosny E, Petit-Haertlein I, Kahn R, Covès J. 2011. Structural basis for metal sensing by CnrX. J Mol Biol 408:766–779. https://doi.org/10.1016/j.jmb.2011.03.014
73. Maillard AP, Künnemann S, Große C, Volbeda A, Schleuder G, Petit-Härtlein I, de Rosny E, Nies DH, Covès J. 2015. Response of CnrX from *Cupriavidus metallidurans* CH34 to nickel binding. Metallomics 7:622–631. https://doi.org/10.1039/c4mt00293h
74. Trepreau J, Grosse C, Mouesca J-M, Sarret G, Girard E, Petit-Haertlein I, Kuennemann S, Desbourdes C, de Rosny E, Maillard AP, Nies DH, Covès J. 2014. Metal sensing and signal transduction by CnrX from *Cupriavidus metallidurans* CH34: role of the only methionine assessed by a functional, spectroscopic, and theoretical study. Metallomics 6:263–273. https://doi.org/10.1039/c3mt00248a
75. Schromm TM, Grosse CU. 2023. From 2D projections to the 3D rotation matrix: an attempt for finding a machine learning approach for the efficient evaluation of mechanical joining elements in X-ray computed tomography volume data. SN Appl Sci 5:18. https://doi.org/10.1007/s42452-022-05220-8
76. Nies DH, Rehbein G, Hoffmann T, Baumann C, Grosse C. 2006. Paralogs of genes encoding metal resistance proteins in *Cupriavidus metallidurans* strain CH34. Microb Physiol 11:82–93. https://doi.org/10.1159/000092820
77. Takahashi-Iñiguez T, García-Hernandez E, Arreguín-Espinosa R, Flores ME. 2012. Role of vitamin B12 on methylmalonyl-coA mutase activity. J Zhejiang Univ Sci B 13:423–437. https://doi.org/10.1631/jzus.B1100329
78. Xia W, Chen W, Peng W, Li K. 2015. Industrial vitamin B production by *Pseudomonas denitrificans* using maltose syrup and corn steep liquor as the cost-effective fermentation substrates. Bioprocess Biosyst Eng 38:1065–1073. https://doi.org/10.1007/s00449-014-1348-5
79. Große C, Kohl TA, Niemann S, Herzberg M, Nies DH. 2022. Loss of mobile genomic islands in metal resistant, hydrogen-oxidizing *Cupriavidus metallidurans*. Appl Environ Microbiol 88:e0204821. https://doi.org/10.1128/AEM.02048-21
80. Große C, Grau J, Große I, Nies DH. 2022. Importance of RpoD- and non-RpoD-dependent expression of horizontally acquired genes in *Cupriavidus metallidurans*. Microbiol Spectr 10:e0012122. https://doi.org/10.1128/spectrum.00121-22
81. Pace CN, Scholtz MJ. 1997. Edited by T. Creighton. Protein structure: a practical approach, p 299–322. IRL press, Oxford, UK.
82. Anton A, Weltrowski A, Haney CJ, Franke S, Grass G, Rensing C, Nies DH. 2004. Characteristics of zinc transport by two bacterial cation diffusion facilitators from *Ralstonia metallidurans* and *Escherichia coli*. J Bacteriol 186:7499–7507. https://doi.org/10.1128/JB.186.22.7499-7507.2004
83. Nies D, Mergeay M, Friedrich B, Schlegel HG. 1987. Cloning of plasmid genes encoding resistance to cadmium, zinc, and cobalt in *Alcaligenes eutrophus* CH34. J Bacteriol 169:4865–4868. https://doi.org/10.1128/jb.169.10.4865-4868.1987
84. Sambrook J, Fritsch EF, Maniatis T. 1989. Molecular cloning, a laboratory manual. 2nd ed. Cold Spring Harbor Laboratory, Cold Spring Harbor, N.Y.
85. Simon R, Priefer U, Pühler A. 1983. A broad host range mobilization system for *in vivo* genetic engineering: transposon mutagenesis in gram-negative bacteria. Nat Biotechnol 1:784–791. https://doi.org/10.1038/nbt1183-784
86. Marx CJ, Lidstrom ME. 2002. Broad-host-range *CRE-Lox* system for antibiotic marker recycling in Gram-negative bacteria. Biotechniques 33:1062–1067. https://doi.org/10.2144/02335rr01
87. Suzuki N, Nonaka H, Tsuge Y, Inui M, Yukawa H. 2005. New multiple-deletion method for the *Corynebacterium glutamicum* genome, using a mutant *Lox* sequence. Appl Environ Microbiol 71:8472–8480. https://doi.org/10.1128/AEM.71.12.8472-8480.2005
88. Albert H, Dale EC, Lee E. 1995. Site-specific integration of DNA into wild-type and mutant *Lox* sites placed in the plant genome. Plant J 7:649–659. https://doi.org/10.1046/j.1365-313x.1995.7040649.x
89. Wagegg W, Braun V. 1981. Ferric citrate transport in *Escherichia coli* requires outer membrane receptor protein FECA. J Bacteriol 145:156–163. https://doi.org/10.1128/jb.145.1.156-163.1981
90. Weast RC. 1984. CRC handbook of chemistry and physics. 64th ed. CRC Press, Inc., Boca Raton, Florida, USA.
91. Herzberg M, Schüttau M, Reimers M, Große C, Nies DH. 2015. Synthesis of nickel-iron hydrogenase in *Cupriavidus metallidurans* is controlled by metal-dependent silencing and UN-silencing of genomic Islands. Metallomics 7:632–649. https://doi.org/10.1039/c4mt00297k
92. Wiesemann N, Mohr J, Grosse C, Herzberg M, Hause G, Reith F, Nies DH. 2013. Influence of copper resistance determinants on gold transformation by *Cupriavidus metallidurans* strain CH34. J Bacteriol 195:2298–2308. https://doi.org/10.1128/JB.01951-12

Chapter 3 – The metal homeostasis response seen at the proteome level

I) Linking the transcriptome to physiology: response of the proteome of *Cupriavidus metallidurans* to changing metal availability

Summary of the publication

This publication investigates the adaptation of *C. metallidurans* to changing metal availability. The plasmid-containing strain CH34 and the plasmid-free derivative AE104 were challenged with a toxic metal mix or were cultivated under conditions of general metal starvation. The proteome of both strains was identified and quantified, and further coupled with the regulation of gene transcription *via* anti-sense RNA (asRNA) (Große *et al*., 2024).

Out of the 6.364 gene products encoded in the theoretical proteome of CH34, 3.540 proteins changed abundance as a specific response to changing metal availability. The proteome of *C. metallidurans* in conditions of multiple metal shock was composed of the products of the multiple metal resistance determinants, that react to Zn^{2+}, Cu^{2+}, Co^{2+}, Ni^{2+}, Cd^{2+}, As^{5+}, Cr^{3+}, Hg^{2+}. In metal starvation conditions, the prevalent gene products were associated with iron homeostasis and starvation, particularly the TonB-dependent siderophore receptors, found both in CH34 and AE104. Additionally, in strain CH34 components of the Zni and Zne systems were enhanced under general metal starvation.

Among abundant polypeptides were products of the plasmid-encoded metal-resistance determinants of CH34, particularly the RND system CzcCBA, in presence of the multiple metal shock. This supports the essential role of transport reactions in maintaining metal homeostasis. In this case, the CzcCBA efflux system is responsible for decreasing the cellular zinc content in CH34.

Metallomics, 16, 2024, mfae058
https://doi.org/10.1093/mtomcs/mfae058
Advance access publication date: 19 November 2024
Paper

Linking the transcriptome to physiology: response of the proteome of *Cupriavidus metallidurans* to changing metal availability

Diana Galea[1], Martin Herzberg[1,2], Dirk Dobritzsch[3], Matt Fuszard[3], Dietrich H. Nies[1,*]

[1]Institute for Biology/Microbiology, Martin-Luther-University Halle-Wittenberg, 06099 Halle (Saale), Germany, [2]Department of Analytical Chemistry, Helmholtz Centre for Environmental Research—UFZ, Leipzig 04318, Germany and [3]Core Facility—Proteomic Mass Spectrometry, Charles Tanford Center, Martin-Luther-University Halle-Wittenberg, 06099 Halle (Saale), Germany
*Corresponding author. Martin-Luther-University Halle-Wittenberg, Institute for Biology/Microbiology, Kurt-Mothes-Str. 3, 06099 Halle (Saale), Germany. E-mail: d.nies@mikrobiologie.uni-halle.de

Abstract

Cupriavidus metallidurans CH34 is a metal-resistant bacterium. Its metal homeostasis is based on a flow equilibrium of metal ion uptake and efflux reactions, which adapts to changing metal concentrations within an hour. At high metal concentrations, upregulation of the genes for metal efflux systems occurs within minutes. Here, we investigate the changes in the bacterial proteome accompanying these genetic and physiological events after 1.5 cell duplications, which took 3 h. To that end, *C. metallidurans* CH34 and its plasmid-free derivative, AE104, either were challenged with a toxic metal mix or were cultivated under metal-starvation conditions, followed by bottom-up proteomics. When metal-shocked or -starved cells were compared with their respective controls, 3540 proteins changed in abundance, with 76% appearing in one, but not the other, condition; the remaining 24% were up- or downregulated. Metal-shocked *C. metallidurans* strains had adjusted their proteomes to combat metal stress. The most prominent polypeptides were the products of the plasmid-encoded metal-resistance determinants in strain CH34, particularly the CzcCBA transenvelope efflux system. Moreover, the influence of antisense transcripts on the proteome was also revealed. In one specific example, the impact of an asRNA on the abundance of gene products could be demonstrated and this yielded new insights into the function of the transmembrane efflux complex ZniCBA under conditions of metal starvation.

Keywords: transenvelope efflux systems; zinc; metal homeostasis; *Cupriavidus metallidurans*; metal starvation; proteomics

Graphical abstract

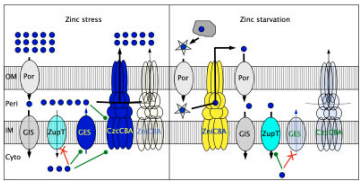

The transenvelope pump ZniCBA was upregulated under metal-starvation conditions and an antisense RNA was involved in regulation of this process. This suggests a possibly novel function of these efflux systems.

Introduction

Cupriavidus metallidurans CH34 is a master in metal ion homeostasis [1–3]. In mesophilic environments, this β-proteobacterium is able to adjust its zinc ion homeostasis to external zinc concentrations from the lower nM to the mM range, as well as being capable of handling low or high concentrations of other divalent metal cations. Determinants on its chromosome are responsible for conferring this resistance and include a chromid and the two large plasmids pMOL28 and pMOL30 [4–8].

Resistance to the transition metal cations of Co(II), Zn(II), Ni(II), and Cd(II) is based on efflux by members of the P_{IB}-ATPases [9, 10], CDF proteins [11], or other protein families, and takes place from the cytoplasm to the periplasm [2]. From the periplasm, large transenvelope efflux systems, such as CzcCBA or CnrCBA, export these ions out of the cell [2, 12]. While the central CzcA or related proteins are able to transport cations across a proteolipid membrane *in vitro* [13–16], biochemical and genetic studies making use of multiple deletion mutants clearly indicate that the *in vivo* function of these efflux complexes is export from the periplasm to the outside of the cell [17–24].

While at high metal concentrations redox changes plus metal efflux are the predominant homeostatic processes, a flow

Received: August 29, 2024. **Accepted:** November 16, 2024

equilibrium of import and export processes governs metal homeostasis at more ambient metal concentrations (e.g. zinc concentrations between 150 nM and 100 µM) [25, 26]. The flow equilibrium transforms the energy used for the simultaneously occurring transport processes of numerous cations into the appropriate composition of the cytoplasmic, and presumably also the periplasmic, metal cation pools, which subsequently determine the competition between these cations for the metal-binding sites of the proteins in these compartments [27, 28]. Pulse-chase experiments revealed that *C. metallidurans* cells needed 15 min to 1 h at 30°C to adapt its physiology to changing metal availability [25].

Uptake of Zn(II) and related cations, such as Co(II) and Cd(II), is accomplished by at least 10 import systems with broad substrate specificity [29–31]. In contrast, metal ion efflux or removal by other mechanisms is a metal-specific process, which is not based on the substrate specificity of the efflux system but on the regulation of the expression of the respective gene(s). Efflux of zinc ions is mediated by the P_{IB2}-type ATPase, ZntA [18, 32]. While ZntA and the related proteins CadA and PbrA export zinc and cadmium ions with similar substrate specificities [18], the respective MerT-type regulators ZntR, CadR, and PbrR are metal selective [33–40]. Similarly, metal specificity of the regulation of expression of nickel resistance is based on the discrimination between nickel and cobalt and zinc ions by the nickel sensor, CnrX [41–45].

Consequently, Zn(II) is exported by the inner membrane exporters ZntA, CdfX, CzcD, and CzcP and further from the periplasm to the outside by CzcCBA. The inner membrane efflux systems all have slightly different functions with respect to zinc export [46]. Expression of their cognate genes is controlled by ZntR or the two-component system CzcRS [18, 47], depending on the cytoplasmic or periplasmic metal ion concentration, respectively. Export of Co(II) is by DmeF to the periplasm and out of the cell by CzcCBA and CnrCBA, while export of Cd(II) is by ZntA, CadA, and CzcCBA, and that of Ni(II) by DmeF, CnrT, and CnrCBA. Copper resistance is a special case and results from an interplay of periplasmic oxidation of the more toxic Cu(I) to Cu(II), efflux of Cu(I) from the cytoplasm to the periplasm by P_{IB1}-type ATPases, efflux from the cell by transenvelope protein complexes such as CusCBA, with a minor contribution by other factors [19]. Chromate resistance is also based on efflux [48–51], arsenate resistance on reduction to arsenite followed by efflux [52–54], and mercury resistance on uptake of Hg(II) and reduction to the volatile metallic Hg(0) [55]. Since the environments of *C. metallidurans* contain not one but metal mixtures with different contents of individual metals [56], this allows this bacterium to export metal cations via parallel export routes with specific rates adjusted to the content of this individual metal, which is sensed by cytoplasmic, two-component or other regulatory systems.

As anticipated, expression of the various metal-resistance determinants of *C. metallidurans* (e.g. *czc*, *cnr*, *cop1*, *cop2*, *chr*, *ars*, and *mer*) was upregulated when exponentially growing cells were challenged for 10 min with a toxic mixture of metal ions [7, 8, 57, 58]. Moreover, in many cases, also antisense transcripts of these determinants were changed in expression. While the physiological adaptation of the cells to changing metal concentration occurs in the time range of 15–40 min [25], gene expression peaks at 2–30 min and returns to the initial expression level after 1 h [59, 60].

This current study investigates the outcome of the physiological and transcriptomic changes of *C. metallidurans* during its adaptation to changing metal availability. We analyze the proteome of this bacterium after these processes have occurred and demonstrate that altered abundances of sense and antisense RNAs also result in changes to the proteome. One example demonstrates how an antisense RNA is involved in reassignment of the function of a transenvelope efflux complex. Consequently, this proteome study completes on a different timescale the previous investigation of metal homeostasis of *C. metallidurans* at the onset of the adaptation process by transcriptomics and during this process by pulse-chase experiments, thereby linking the transcriptome to physiology.

Results

Experimental strategy

Exponentially growing cells of *C. metallidurans* CH34 wild-type and its plasmid-free derivative AE104 were challenged with a strain-specific mixture of toxic metals, or EDTA (Ethylenediaminetetraacetic acid) as done for the transcriptome analysis [58]. These strain-specific mixtures contained the individual metals in the ratio of their toxicity for strains CH34 and AE104, respectively. The concentration of the mixture used was equal to the IC_{50} value of this mixture for the respective strain. Similarly, EDTA was also applied at the respective IC_{50} value for either strain. To give the cells time to produce the gene products and to possibly dilute out no longer useful gene products by growth, exponentially growing cells were incubated in the presence of their metal mix for 1.5 duplications, which took approximately 3 h in an aerobic incubation at 30°C.

All experiments were performed in triplicate, yielding six data sets after whole proteome analysis by tandem mass spectrometry (CH34_0, CH34 control; CH34_M, metal-shocked CH34; CH34_E, metal-starved CH34; and similarly AE104_0, AE104_M and AE104_E for strain AE104). The quantities of each protein in the supernatant and solubilized ultracentrifugation sediment were normalized to an overall number of 1.86 million proteins per cell as derived from the experimentally determined average protein content [61]. This gave a copy number per cell for the respective protein. For the six data sets, the mean values and deviations of the copy numbers were calculated and these values compared for CH34 cells with and without toxic metal treatment (CM0), and with EDTA (CME) treatment. The same was done for AE104 cells (AM0, AME) and a comparison between CH34 and AE104 under nonchallenging conditions was done. The full data set for the measurements under the six conditions and the five calculations is provided in the supplement, together with additional data, for instance the KEGG orthology category [62, 63] of the respective proteins. The overall results are provided as Supplementary Data Set.

Of the 6755 annotated open reading frames [1], 3502 proteins were identified at least once under one condition; however, 3253 proteins were never detected (Supplementary Data Set). From the 369 open reading frames, which were found on all four replicons with Rmet tags from Rmet_6403 and higher, annotated in a later annotation process, only 7 were found at least once as proteins. About half of the predicted proteins were identified, primarily those originally annotated. This matched the published result from a first determination of the proteome of nonchallenged cells of the plasmid-free strain AE104 [61] (Supplementary Fig. S1). The 10 proteins identified to have the highest copy numbers ranged between 18 000 and 66 500 copies per cell (Supplementary Table S1).

Furthermore, the protein abundances given in copy numbers between metal-shocked and -starved (EDTA-treated) CH34 or similarly treated AE104 cells compared to the control (Supplementary Table S2) yielded five distinct comparison categories, which were then evaluated (Table 1). Only values with $Q \geq 2$

Table 1. Overview of the number of proteins up- or downregulated in the comparisons[a]

Comparison	Total	(Dis)-appearing	Regulated		
			Quantitatively	Significantly	Q_sense ≥2
CM0: up	490	346	144	53	18
CM0: down	470	315	155	76	0
CE0: up	193	79	114	61	3
CE0: down	393	320	73	27	1
0AC: up	387	339	48	14	nfc
0AC: down	330	263	67	19	nfc
AM0: up	244	190	54	25	9
AM0: down	472	375	97	29	4
AE0: up	327	296	31	10	2
AE0: down	234	176	58	13	0
Sum	3540	2699	841	327	37

[a] The total number of proteins upregulated/appearing or downregulated/disappearing is recorded in the second column. The first column lists the comparisons CM0 (CH34 metal-shocked to the control), CE0 (metal-starvation to the control), 0AC (AE104 to CH34 under nonchallenging conditions), AM0 (AE104 metal-shocked to the control), and AE0 (metal-starvation to the control). The proteins that disappeared or appeared and were not found in one of the conditions but in the other are listed in the third column. Quantitative results were defined as those with at least a single determination in each of the two conditions, with a two-fold ratio and a distance value >1. Significant results were those that came from at least two determinations in each of the two conditions, with a two-fold ratio and a distance value >1. The last column lists the significantly regulated proteins, which could be correlated with a significantly changed abundance of their sense RNA. The comparison between CH34 and AE104 control cells was not considered for correlation with the transcriptome data (nfc, not further considered).

or Q ≤0.5 and D >1 were considered. This yielded an overall number of 3540 changes in which polypeptides were either increased or decreased in abundance (Table 1). In 2699 cases, the identified proteins were found only under one condition. In these cases, a ratio Q could not be calculated. In 841 instances (designated 'quantitatively regulated'), proteins were found at least once under both conditions, which allowed calculation of a Q value and classification of the proteins into the groups 'upregulated' and 'downregulated', if the distance value D was >1. This indicated in the case of a single appearance of a protein under one condition that this value was outside the deviation span of the mean value of the result in the other condition. In the event of two single appearances, a D value could not be calculated because this would have been a division by zero. These comparisons were not further considered. Only in 327 instances ('significantly regulated'), a protein could be measured at least twice under both conditions, which allowed the calculation of its up- or downregulation if D >1. Most of the measured changes of the proteome were simply appearances or disappearances of proteins under one condition. Only in 9.2% of the cases was a significant change in the copy number per cell determined (Table 1).

As outlined in the Supplementary data, which details further constraints of the method used, small proteins of 100 amino acid residues or less in size (see Supplementary Fig. S2) and membrane-bound proteins without large hydrophilic domains (examined with the F_1F_0 ATPase subunits, Supplementary Table S3) were strongly underrepresented in this proteomic approach. The smallest number of proteins per cell that was measured at least twice under a particular condition was about 10 copies per cell. This indicated that for small proteins a copy number of about 50 should represent the lower detection limit, and for membrane-integral proteins without large hydrophilic extensions between 70 and 350 copies per cell should apply.

Metal-challenged CH34 cells compared to the control and the products of metal-resistance determinants

In *C. metallidurans* CH34 wild-type cells treated with a toxic metal mixture, the abundance of 960 proteins changed, with 346 proteins appearing and 315 proteins disappearing in metal-treated cells compared to the control (Table 1). The 10 proteins with the highest copy numbers that appeared in metal-shocked cells (Supplementary Table S4) and the 10 up-regulated ones with the highest Q ratios (Supplementary Table S5) were in most cases products of metal-resistance determinants. Upregulation of the transcription of these genes measured after 10 min [58] showed a corresponding higher copy number of their products after 3 h under these conditions.

The *czc* determinant on plasmid pMOL30 mediated high-level resistance to cobalt, zinc, and cadmium. The RND protein CzcA and the membrane fusion protein CzcB could be found and quantified in CH34 cells under all three cultivation conditions, including EDTA-mediated overall metal starvation (Table 2). This indicated that the CzcCBA complex has an important function in metal homeostasis in *C. metallidurans*, even at low metal concentrations. Nevertheless, the copy numbers of both proteins were clearly upregulated ~10-fold following metal shock. Unexpectedly, the copy number of the outer membrane factor CzcC was only 46% of that of CzcA (Table 2). Either CzcC was underrepresented or only half of the CzcCBA complexes contained CzcC. CzcC was also strongly upregulated (23-fold) after metal stress, it was not found after EDTA treatment, or was determined only in one set of the control cells. Thus, CzcC may be even more underrepresented in metal-starved or control cells than in metal-shocked cells.

Among the other Czc proteins, the response regulator CzcR was also found under all conditions and was upregulated 8.5-fold following metal stress. Its associated sensory histidine kinase CzcS, the P_{IB4}-type ATPase CzcP, and the periplasmic CzcE protein were also found in metal-stressed cells. Other *czc* products could not be determined (Table 2).

Cupriavidus metallidurans also has on its chromid an ancient and interrupted czc_2 paralog with the gene encoding the central zinc- and cadmium-exporting P_{IB2}-type ATPase ZntA in its vicinity (Supplementary Table S2). Interestingly, the $CzcC_2$ outer membrane factor was also present in metal-shocked CH34 and AE104 cells although the interrupted $czcB_2$ and the $czcA_2$ gene products could not be identified. This indicated the possibility that $CzcC_2$ may also interact with CzcBA to form an alternative transenvelope efflux complex $CzcC_2BA$.

Table 2. Products of the plasmid-encoded metal-resistance determinants[a]

Locus tag	Gene	CH34_0	CH34_M	CH34_E	Description
Plasmid pMOL28:					
pMOL28 *mer*: not found *merR, merT, merD,* and *merE*					
Rmet_6346	*merP*	NF	3 935 ± 1757	48	Periplasmic mercury-binding protein
Rmet_6183	*merA*	NF	11 249 ± 2 250	NF	A6UXG5 Mercuric reductase
chr*: not found *chrZ, chrP, chrF1, chrA1,* and *chrI					
Rmet_6195	*chrY*	NF	263 ± 152	NF	Q1L9 X 2 Putative uncharacterized protein
Rmet_6197	*chrN*	NF	129 ± 77	NF	Q1L9 X 0 Putative uncharacterized protein
Rmet_6198	*chrO*	NF	727 ± 239	17	Q1L9W9 Putative uncharacterized protein
Rmet_6200	*chrE*	NF	314 ± 199	NF	Q5NUZ8 Superoxide dismutase SodM
Rmet_6201	*chrC*	104	1 318 ± 1 154 (12.7; 1.1)	NF	P17550 Superoxide dismutase (Fe)
Rmet_6203	*chrB1*	NF	649 ± 516	NF	P17552 Protein ChrB
cnr*: not found *cnrY, cnrC,* and *cnrA					
Rmet_6206	*cnrX*	44	388 ± 176	NF	P37975 Nickel sensor of the antisigmafactor complex
Rmet_6207	*cnrH*	67	NF	NF	P37978 RNA polymerase sigma factor CnrH
Rmet_6209	*cnrB*	207	1 235 ± 272	NF	P37973 Nickel and cobalt-resistance protein CnrB
Rmet_6211	*cnrT*	11	NF	NF	Q9L3G0 CnrT protein
Plasmid pMOL30: neither *ncc* nor *sil* products found					
pbr*: not found *pbrU, pbrR, pbrA, pbrB/C,* and *pbrD					
Rmet_5945	*pbrT*	206 ± 156	223 ± 47 (1.1; 0.1)	847 ± 353 (4.1; 1.3)	Q58AJ4 PbrT protein (iron permease FTR1)
czc* region: not found *flgB, ompP, czcJ, czcD, czcI, czcN,* and *czcM					
Rmet_5970	*czcP*	31 ± 19	76	NF	Q1LAJ7 Heavy metal translocating P-type ATPase
Rmet_5976	*czcE*	NF	96	NF	Q1LAJ1 Putative uncharacterized protein
Rmet_5977	*czcS*	NF	313 ± 270	NF	Q44007 Sensor protein CzcS
Rmet_5978	*czcR*	67	566 ± 539 (8.5; 0.9)	89 ± 52 (1.3; 0.4)	Q44006 Transcriptional activator protein CzcR
Rmet_5980	*czcA*	95	854 ± 489 (9.0; 1.4)	75 ± 50 (0.8; 0.2)	P13511 Cobalt–zinc–cadmium-resistance protein CzcA
Rmet_5981	*czcB*	146 ± 104	1 509 ± 607 (10.4; 1.9)	113 ± 26 (0.8; 0.2)	P13510 Cobalt–zinc–cadmium-resistance protein CzcB
Rmet_5982	*czcC*	17	391 ± 207 (22.7; 1.8)	NF	P13509 Cobalt–zinc–cadmium-resistance protein CzcC
cop1*: not found *copV, copT, copM, copK, copD1, copJ, copG, copL, copQ, copE,* and *copW					
Rmet_6109	*copN*	NF	112 ± 25	NF	Q1LA58 Putative uncharacterized protein
Rmet_6110	*copS1*	NF	467 ± 471	NF	Q58AD4 Sensor protein
Rmet_6111	*copR1*	21 ± 9	322 ± 125	22 ± 8 (1.0; 0.1)	Q58AD5 Two-component regulator
Rmet_6112	*copA1*	NF	1 054 ± 623	NF	Q58AD6 Copper-resistance protein CopA
Rmet_6113	*copB1*	NF	1 559 ± 870	NF	Q58AD7 CopB protein (copper-resistance B)
Rmet_6114	*copC1*	NF	704 ± 120	NF	Q1LA53 Copper-resistance protein CopC
Rmet_6116	*copI*	NF	2 274 ± 982	NF	Q58AE0 Putative oxydoreductase
Rmet_6119	*copF*	195 ± 116	768 ± 701 (3.9; 0.7)	46 ± 21 (0.2; 1.1)	Q58AE3 Heavy metal translocating P-type ATPase
Rmet_6122	*copH*	NF	5 301 ± 2 837	36	Q58AE5 CopH protein
pMOL30 *mer1*: no products found					
pMOL30 *mer2*: not found *merT, merD,* and *merE*					
Rmet_6171	*merR*	117 ± 68	151 ± 102 (1.3; 0.2)	146 ± 38 (1.3; 0.3)	P69413 Mercuric-resistance operon regulatory protein
Rmet_6173	*merP*	NF	3 935 ± 1 757	48	Q58AI1 Periplasmic mercuric ion-binding protein
Rmet_6174	*merA*	NF	249 ± 147	NF	Q1L9Z3 Mercuric reductase MerA

[a]The copy numbers per cell of the products of plasmid-encoded metal-resistance determinants are given for *C. metallidurans* strain CH34 cultivated without added substance (CH34_0), metal-shocked (CH34_M) and metal-starvation conditions (CH34_E) with the mean values and deviations. Numbers without deviations indicate proteins determined just once in the respective triplicate determination. The copy numbers are followed by the ratios Q and the distance value D for the comparison of CH34_M and of CH34_E with CH34_0. These values were not provided when the respective protein could not be measured in CH34_0. NF, not found.

Only the membrane fusion protein CnrB of the pMOL28-encoded nickel-resistance determinant *cnr* was found, while the nickel sensor CnrX, and single appearances of the sigma factor CnrH and the inner membrane efflux system CnrT were identified (Table 2). Although CnrB had a similar abundance in metal-shocked CH34 cells as CzcB, neither CnrC nor CnrA could be quantified.

Two more RND-driven transenvelope efflux systems were encoded on the chromid by the *zni/zne* region (Supplementary Table S2). Unexpectedly, the subunits of both transenvelope complexes, ZniCBA and ZneCBA, were found, or were upregulated in their synthesis in EDTA-treated CH34 cells. ZniCBA were also present in metal-shocked and CH34 control cells but were not upregulated when these two conditions were

compared. With the exception of ZniA, AE104 control cells revealed that ZniCBA were also present under all conditions tested, and were indeed upregulated in EDTA-treated but not in metal-shocked AE104 cells; however, the copy numbers were lower in EDTA-treated AE104 than in EDTA-treated CH34 cells. This suggests that, unexpectedly, the ZniCBA system has a role under metal-starvation conditions rather than in dealing with metal stress, for instance being part of a cycling process required to route metal cations to their target proteins, as shown for copper [64]. The copy numbers of the Zne proteins were lower than those of the Zni proteins. Zne could possibly support or enhance the function(s) of Zni. Among the remaining components for possible transenvelope exporters of divalent metal cations, only the outer membrane factor NimC and the membrane fusion protein NimB were found, but there was no indication of any regulation in response to metal availability.

The CusCBA components, which are responsible for efflux of the monovalent cations Cu(I) and Ag(I), were only identified in metal-shocked AE104 cells (Supplementary Table S2). The SilCBA components were not found. This suggested that transenvelope efflux of Cu(I) was of lower significance in CH34 than in strain AE104. Indeed, metal-shocked CH34 cells revealed an upregulation in the synthesis of the periplasmic Cu(I) oxidases $CopA_1$, encoded on plasmid pMOL30 (Table 2), and its chromid paralog $CopA_2$ (Supplementary Table S2), each with similar copy numbers. In addition to $CopA_1$, the other pMOL30-encoded proteins CopN, $CopB_1$, $CopC_1$, CopI, and CopH were also detected, or were found to be upregulated in metal-stressed CH34 cells. Moreover, $CopC_2$, two-component regulatory systems $CopS_1$ and $CopR_1$, $CopS_2$ and $CopR_2$ were also present in metal-shocked CH34 and AE104 cells. Because CH34 cells contained a variety of factors supporting the synthesis and function of the two periplasmic Cu(I) oxidases, $CopA_1$ and $CopA_2$, CH34 cells may be able to remove Cu(I) efficiently by oxidation to the less toxic Cu(II), which decreased the need to remove periplasmic Cu(I) by Cus-mediated export. In contrast, export of Cu(I) by Cus seemed to be more important in the plasmid-free strain AE104, which contains only the Cop_2 system [19].

Six components of the plasmid pMOL28-encoded chromate-resistance determinant were found in metal-treated CH34 cells, but not under the other conditions, with the exception of a single determination of the superoxide dismutase-like ChrC in CH34 control cells (Table 2). Two products of the second, smaller and chromid-encoded chr_2 determinant were found in metal-treated CH34 and AE104 cells (Supplementary Table S2). Products of the chromosomal arsenate-resistance and the various mercury-resistance proteins were also upregulated after treatment of the strains CH34 and AE104 with a toxic metal mixture.

GshA and GshB, which are required for glutathione biosynthesis, were not upregulated in synthesis following metal treatment of CH34 or AE104 cells, but proteins required for iron–sulfur cluster biosynthesis, namely IscR, IscA and IscU, were shown to increase in abundance (Supplementary Table S2). This agrees to the fact that iron–sulfur clusters are the primary intracellular targets of copper toxicity [65]. Additionally, the regulatory proteins of the phosphate response, PhoB and PhoU, and the periplasmic phosphate-binding protein PstS of the PstABC import system were upregulated under metal-stressed conditions. This indicated that the synthesis of proteins required for assembly of iron–sulfur clusters and phosphate supply were both responsive to metal stress. Phosphate-stressed polypeptides were possibly induced in response to the presence of arsenate in the challenging metal mix [52, 66, 67].

Among the metal efflux systems of the inner membrane, the chromosomal ZntA was found to be highly abundant, with 3425 ± 2300 copies, but only in metal-stressed CH34 cells (Table 3); the exception were 502 copies identified in unchallenged AE104 cells, but in a single determination (Supplementary Table S2). The cadmium exporter, CadA, could not be identified, nor was the plasmid-encoded lead efflux system PbrA found under any of the conditions tested. While lead was not a component of the toxic metal mixture, cadmium was. The plasmid-encoded P_{IB4}-type ATPase CzcP, a high-rate exporter of zinc ions [18], made two single appearances in metal-treated CH34, as well as in untreated CH34 control cells. The Cu(I)–exporter CupA was upregulated in its synthesis in metal-stressed CH34 (Table 3) and in AE104 (Supplementary Table S2) cells, although the latter result was not significant due to a high deviation in the measurements made in metal-shocked AE104 cells. This was also the case for the plasmid-encoded CopF ATPase (Table 3). Like CupA, CopF was upregulated four-fold in metal-treated CH34 cells but the deviation was high. While DmeF could only be determined in CH34 control cells, no upregulation was detected in metal-treated CH34 or AE104 cells, the abundance of this cobalt-exporting CDF protein was two-fold higher in AE104 than in CH34 control cells. The Fe(II) exporter FieF was present in all cells but appeared not to be regulated. RdxI, CtpA1, CnrT, AtmA were each identified once, while CzcD was not found in either cell or under any of the conditions tested (Table 3 and Supplementary Table S2).

Genes with upregulated transcription following metal treatment generally showed a correlation with increased copy numbers of their respective products. Since metal-resistance determinants often encoded membrane-bound products such as metal efflux systems, the low detection efficiency of membrane-bound proteins together with a possible low copy number of these proteins limited their successful determination in many cases. Nevertheless, the proteome of *C. metallidurans* was clearly changed to combat the effects of metal toxicity. Upregulated transcription of genes involved in metal resistance resulted in most cases to an upregulated copy number of the respective gene products.

Downregulated gene products following metal stress

Following metal shock, *C. metallidurans* not only upregulated the expression of many genes of metal-resistance determinants, but also downregulated expression of many genes encoding ribosomal proteins, proteins involved in the initiation and elongation of translation, transcription, motility, synthesis of hydrogenases, and the components of the F_1F_0 ATPase [58]. The corresponding proteins involved in hydrogenase synthesis were only found in CH34 control cells and not in metal-shocked or -starved CH34 cells (Supplementary Table S2). Among the chemotaxis proteins, 26 were not found at all and only 12 were identified in CH34-untreated control cells, half of which were only detected in a single sample. These six proteins were either not downregulated in abundance in metal-treated CH34 cells or appeared only as single measurements under this condition. The levels of the components of the F_1F_0 ATPase were not regulated under any of the conditions or in either strain tested (Supplementary Table S3). The components of the RNA polymerase, including the various sigma factors, were also not regulated in CH34 cells after metal shock, with the exception of a 50% reduction in RpoB and a 40% reduction in the termination factor Rho; however, the anticipated upregulation of the sigma factor associated with *cnr* expression,

Table 3. Efflux systems of the inner membrane in *C. metallidurans* strain CH34[a]

Locus tag	Gene	CH34_0	CH34_M	CH34_E	Description
Rmet_4594	*zntA*	NF	3425 ± 2300	NF	Q1LEH0 P_{IB2}-type ATPase
Rmet_5970	*czcP*	31 ± 19	76 (2.4; 2.4)	NF	Q1LAJ7 P_{IB4}-type ATPase
Rmet_3524	*cupA*	309 ± 184	2640 ± 1113 (8.6; 1.8)	142 (0.5; 0.9)	Q1LHI0 P_{IB1}-type ATPase
Rmet_6119	*copF*	195 ± 116	768 ± 701 (3.9; 0.7)	46 ± 21 (0.2; 1.1)	Q58AE3 P_{IB1}-type ATPase
Rmet_2046	*rdxI*	155	NF	NF	Q1LLQ1 P_{IB1}-type ATPase
Rmet_0198	*dmeF*	221 ± 129	NF	NF	Q1LRZ2 CDF protein
Rmet_3406	*fieF*	209 ± 93	258 ± 150 (1.2; 0.2)	201 ± 116 (1.0; 0.0)	Q1LHU8 CDF protein
Rmet_6211	*cnrT*	11	NF	NF	Q9L3G0 CnrT protein
Rmet_0391	*atmA*	54	NF	NF	Q1LRE9 ABC-type transporter

[a]The copy numbers per cell of the products of various metal-resistance determinants are given for *C. metallidurans* strain CH34 cultivated without added substance (CH34_0), metal-shocked (CH34_M) and metal-starvation conditions (CH34_E) with the mean values and deviations. Numbers without deviations indicate proteins determined just once in the respective triplicate determination. The copy numbers are followed by the ratios Q and the distance value D for the comparison of CH34_M and of CH34_E with CH34_0. These values were not provided when the respective protein could not be measured in CH34_0. NF, not found. Not found in any of the cells were the products of the genes *cadA*, *pbrA*, and *czcD*. The copper-exporting P_{IB1}-type ATPase CtpA1 (Rmet_2379) was found only once with 917 copies in nonchallenged AE104 cells.

CnrH, was noted. The abundance of the starvation sigma RpoS did not change under these any of the conditions. The total number of ribosomal proteins was 444 000 ± 159 000 in CH34 control cells and 80% of this number, 356 000 ± 141 000, was still found in metal-shocked cells (Supplementary Table S2). This demonstrated that the downregulated transcriptional activity of these genes after 10 min did not manifest as a measurable decrease in the amount of the gene products after 3 h. The cells were able to adapt to the altered conditions within 1.5 cell duplications.

Metal starvation

About 200 proteins were either upregulated in their abundance or appeared in metal-starved CH34 cells, and about 400 were downregulated or were no longer detectable (Table 1). The numbers of upregulated proteins or proteins making an appearance in metal-starved AE104 cells were ∼300 and 200, respectively. Among the proteins making an appearance in metal-starved CH34 cells, and which had the highest copy number, were the TonB-dependent siderophore receptor Rmet_0837, the periplasmic binding protein HmuT of an ABC-type importer, and Rmet_1115 involved in siderophore biosynthesis (Supplementary Table S4). These proteins also appeared in metal-starved AE104 cells. In CH34 cells, the proteins that were no longer detectable included those involved in the synthesis of the soluble hydrogenase, while in strain AE104 included were the three systems ZntA, DmeF, and CtpA1 for Zn, Co, and Cu ions efflux, respectively (Supplementary Table S4); however, it should be emphasized that all three were only identified in one of the AE104 control cell samples.

The most strongly upregulated proteins in metal-starved CH34 cells were the Zni and Zne components, the cysteine synthase CysK, other components involved in siderophore biosynthesis and ExbB1, which was needed to drive TonB-dependent transport processes (Supplementary Table S5). CysK, a TonB-dependent outer membrane receptor, and ZniC were also upregulated in strain AE104 under the same condition.

These results indicated that uptake of iron was primarily affected in EDTA-treated CH34 cells. Indeed, the proteins involved in siderophore biosynthesis were significantly upregulated or appeared in metal-starved CH34 and AE104 cells (Supplementary Table S2). The TonB-dependent outer membrane receptor Rmet_0123 was downregulated in metal-shocked but upregulated in both strains upon metal starvation. The sigma factor RpoI, which controlled expression of the siderophore biosynthesis cluster, appeared in metal-starved CH34 cells, as did its membrane-bound anti-sigma factor, RsiA. Moreover, the anti-sigma factors RsjA and RskA of the sigma factors RpoJ and RpoK, respectively, both of which are related to RpoI, were also identified in metal-starved CH34 cells, although their cognate sigma factors were not found. The membrane-bound iron importer FeoB was significantly upregulated in metal-starved CH34 cells, but was also present in metal-shocked CH34 as well as the untreated control cells (Table 4). FeoB was also present in AE104 cells in slightly higher copy numbers in comparison to CH34 cells under the same conditions, but the differences were not significant (Table 4). The associated small (100 aa) FeoA protein could also be quantified in metal-starved CH34 and AE104 cells (Table 4). In contrast to the proteomic response measured after 3 h, transcription of the respective genes was not upregulated after 10 min [58].

Of the other metal uptake systems, ZupT, HoxN, and MgtB were not found and the metal inorganic phosphate importer PitA was identified just once in AE104 control cells (Table 4). The MgtA P-type Mg/Ca importer was present under five of the six conditions, but its synthesis was not regulated in response to metals or a lack thereof. The four representatives of the CorA-type uptake systems for Mg(II) and other divalent cations were found in some of the cells but could not be detected in all of them. Only ZntB, which might be an importer or exporter of Zn ions, showed a 2.3-fold upregulation in metal-shocked AE104 cells, but this result was based upon only a single determination in these cells. Otherwise, FeoB was the only upregulated metal uptake system.

Proteins involved in either uptake of phosphate by the PstABC importer or synthesis or degradation of polyphosphate were not changed in abundance under any condition (Supplementary Table S2), nor were GshA and GshB, which are required for glutathione biosynthesis. Concerning the biosynthesis of iron–sulfur clusters, the abundance of the Isc proteins did not change under metal starvation conditions, with a downregulation of 40% for the cysteine desulfurase IscS being detected in metal-starved CH34 cells. While the important zinc importer, ZupT, could not be found, the remaining proteins produced under control of the zinc uptake regulator Zur were identified, including Zur. CobW2 and CobW3 were present under all conditions. The abundance of CobW3 was not changed—a 2.2-fold higher level of the zinc storage protein CobW2 was noted in metal-starved CH34 cells. The copy number of CobW2 in metal-starved AE104 cells was also slightly higher than in AE104 and in CH34 control cells but the differences were not significant. The third CobW protein, CobW1, which is produced only under strong zinc starvation conditions, was

Table 4. Metal uptake systems[a]

Locus tag	Gene	Control (Q, D)	Metal-shocked (Q, D)	Metal-starved (Q, D)	Description
Strain CH34					
Rmet_3052	*corA1*	394 ± 242	NF	NF	Q1LIV2 Mg and Co transport protein CorA1
Rmet_0036	*corA2*	391	NF	NF	Q1LSF4 Mg and Co transport protein CorA2
Rmet_3287	*corA3*	162 ± 96	180; (1.1; 0.2)	108 ± 63 (0.7; 0.3)	Q1LI67 Mg and Co transport protein CorA3
Rmet_1973	*pitA*	NF	NF	NF	Q1LLX4 Phosphate transporter
Rmet_5396	*mgtA*	29 ± 17	32 (1.1; 0.2)	26 ± 15 (0.9; 0.1)	Q1LC71 ATPase, E1–E2 type
Rmet_0549	*zntB*	82 ± 22	79 (1.0; 0.2)	68 ± 19 (0.8; 0.3)	Q1LQZ1 Mg and Co transport protein ZntB
Rmet_5890	*feoB*	212 ± 69	292 ± 75 (1.4; 0.6)	**1176 ± 699 (5.6; 1.3)**	Q1LAS7 Ferrous iron transport protein FeoB
Rmet_5891	*feoA*	194	NF	246 ± 142 (1.3; 0.4)	Q1LAS6 Ferrous iron transport protein FeoA
Strain AE104					
Rmet_3052	*corA1*	371	NF	NF	Q1LIV2 Mg and Co transport protein CorA1
Rmet_0036	*corA2*	195 ± 128 (0.5; 1.5)	NF	229 (1.2; 0.3)	Q1LSF4 Mg and Co transport protein CorA2
Rmet_3287	*corA3*	67 (0.4; 1.0)	41 ± 26 (0.6; 1.0)	127 ± 77 (1.9; 0.8)	Q1LI67 Mg and Co transport protein CorA3
Rmet_1973	*pitA*	209	NF	NF	Q1LLX4 Phosphate transporter
Rmet_5396	*mgtA*	22 (0.8; 0.4)	NF	28 ± 17 (1.3; 0.4)	Q1LC71 ATPase, E1–E2 type
Rmet_0549	*zntB*	80 ± 52 (1.0; 0.0)	**186 (2.3; 2.0)**	51 ± 30 (0.6; 0.3)	Q1LQZ1 Mg and Co transport protein ZntB
Rmet_5890	*feoB*	311 ± 118 (1.5; 0.5)	443 ± 432 (1.4; 0.2)	588 ± 216 (1.9; 0.8)	Q1LAS7 Ferrous iron transport protein FeoB
Rmet_5891	*feoA*	NF	178	125 ± 72	Q1LAS6 Ferrous iron transport protein FeoA

[a]The number of the products per cell of the respective gene with deviations, plus the comparisons CH34 with metal mix to without, and CH34 with EDTA to without, same for strain AE104 and for nonchallenged control cells AE104/CH34. The ratios Q and the distance values follow these numbers in parentheses. Single values indicate a result only in one out of the three determinations. NF is 'not found' in any of the three replicates. Comparisons to NF values were not done. Bold-faced Q ratios with D >1 and at least two-fold up- und downregulation of the abundance.

Table 5. Transcriptomic data for the gene-encoded proteins with different changes in the sense-to-antisense ratios[a]

		Before the change			After the change			Comparison			
Locus tag	Gene	Mean	Mean_AST	S/AS	MEAN	Mean_AST	S/AS	Comp	Q_sense	Q_AST	QS_AS
Data with QS_AS ratios >50											
Rmet_3525	*cupC*	184 ± 37	334 ± 45	0.55	7 912 ± 912	255 ± 28	31.0	CM0+	42.9	0.77	56.1
Rmet_0333	*arsR*	47 ± 4	3 ± 2	14.2	17 327 ± 1 563	20 ± 3	852	AM0+	366	6.10	60.0
Rmet_0333	*arsR*	61 ± 3	5 ± 3	13.0	20 485 ± 2 242	23 ± 2	878	CM0+	338	5.00	67.5
Rmet_0331	*arsC2*	11 ± 1	3 ± 1	3.40	5 969 ± 277	20 ± 3	294	AM0+	527	6.10	86.3
Rmet_3525	*cupC*	145 ± 19	306 ± 38	0.48	6 767 ± 1 554	153 ± 17	44.3	AM0+	46.6	0.50	93.2
Rmet_3620	*degP*	28 ± 1	105 ± 10	0.26	3 680 ± 424	116 ± 8	31.7	CM0+	133	1.10	121
Rmet_0123		6 ± 1	102 ± 12	0.06	132 ± 20	1.7 ± 1.1	79.0	AE0+	23.2	0.02	1 417
Data with QS_AS ratios between 1.2 and 20 (selected data points)											
Rmet_5319	*zniA*	57 ± 3	4 ± 1	13.1	147 ± 3	3 ± 1	49	CE0+	2.6	0.69	3.7
Rmet_5320	*zniB*	116 ± 8	29 ± 3	3.94	291 ± 56	44 ± 4	6.6	CE0+	2.5	1.49	1.7
Data with QS_AS ratios <0.25											
Rmet_5673	*copS2*	5 ± 1	Not found	39 ± 3	43 ± 4	0.91	CM0+	7.38			
Rmet_5321	*zniC*	46 ± 4	1 ± 1	46.3	110 ± 7	156 ± 9	0.71	AE0+	2.37	157	0.02
Rmet_1195	*bfrB*	315 ± 5	157 ± 20	2.01	110 ± 9	681 ± 93	0.16	AM0–	0.35[b]	4.35	0.08
Rmet_1026	*iscU*	545 ± 36	2.3 ± 0.6	233	1 724 ± 72	65 ± 9	26.5	AM0+	3.17	27.9	0.11
Rmet_0506	*purK*	125 ± 24	0.3 ± 0.6	375	62 ± 9	1.3 ± 0.6	46.2	AM0–	0.49 [b]	4.00	0.12
Rmet_0970	*ggt*	235 ± 17	2.3 ± 0.6	101	37 ± 3	2.7 ± 1.1	14.0	AM0–	0.16 [b]	1.14	0.14
Rmet_1026	*iscU*	506 ± 17	4 ± 0	127	1 728 ± 146	63 ± 5	27.3	CM0+	3.41	15.8	0.22
Rmet_1027	*iscA*	556 ± 59	4 ± 0	139	2 015 ± 421	63 ± 5	31.8	CM0+	3.62	15.8	0.23

[a]The published transcriptomic data [58] for genes with strongly increased (>50) or decreased (<0.25) sense-to-antisense RNA ratios in the comparisons CH34 metal-shocked to the control (CM0; CMO+ up- and CM0– down-regulated), same for AE104 (AM0), metal-starved CH34 cells to the control (CE0) and the same for strain AE104 (AE0). The abundances as NPKM values of the RNAs before and after application of the changed condition are listed, Mean for sense RNA, Mean_AST for antisense RNA, S/AS for the ratio of sense-to-antisense RNA plus the changes of the sense, antisense abundances and that of the sense-to-antisense ratios.
[b]The ratios Q are given while the associated figures are using the 1/Q values. Down-regulated genes on a gray field.

identified in metal-starved CH34 and AE104 cells, and this was also true for the product of the second gene of the *cobW1* operon, the GTP (Guanosine triphosphate) cyclohydrolase FolE_IB2, which is a metal-promiscuous enzyme [68]. The two paralogs of FolE_IB2, the metal-promiscuous FolE_IB1 and the zinc-dependent FolE_IA, were present under all conditions but showed no upregulation of their abundance, except for a 2.1-fold increase in FolE_IB1 levels in metal-treated AE104 cells.

These findings demonstrated that *C. metallidurans* primarily reacted to EDTA-mediated metal starvation by upregulation of the capacity to import iron ions directly, or associated with its siderophore. This seemed to be sufficient to supply iron to the Isc iron–sulfur cluster biogenesis apparatus. An upregulation of the storage capacity for zinc and for a Zn-independent GTP hydrolase involved in folate biosynthesis were additional adjustments of the proteome to EDTA-mediated zinc starvation conditions.

Relationship between protein abundance and associated transcripts

To determine the relationship between protein abundance and the expression levels of its associated sense transcript mRNA and antisense asRNAs, we measured the abundance in proteins per cell encoded by a gene and matched this with the abundance of the respective mRNA in NPKM (nucleotide activities per kilobase of exon model per million mapped reads, a measure of RNA abundance), as published [58]. This was done for all six conditions (strain CH34 or AE104, control, metal-shocked, and -starved cells). In a second step, the proteome mRNA data points were sorted into six groups, which now depended on the abundance of the asRNA, given in NPKM as published [58]. These groups included AST0, which were genes/transcripts with no associated asRNA, as the first group, whereas the groups AST1 and AST5 were between or above the boundaries when NPKM = 3, 10, 30, or 100 (groups AST1 to AST5).

For all conditions, the asRNA-grouped protein abundances were plotted against that of their mRNA in a double-$\log_{10}$ plot (Supplementary Fig. S3). Although the distribution of the data points was scattered, the protein abundances increased with measured increases of their cognate sense RNA. In all comparisons, the data points of the group AST1, associated with low asRNA abundances (green in S3), represented genes expressed on a low level and subsequently a low copy number of the corresponding gene product. On the other hand, a group with a high, but not the highest, asRNA abundance (AST4, red data points in S3, 30 < NPKM ≤ 100) was associated with strong expression events and subsequently high copy numbers of those gene products. This demonstrated that a change in the transcriptome at the onset of a cellular adaptation process indeed resulted in a subsequently altered proteome composition.

For all asRNA groups and conditions, a linear curve fit was employed, which usually had low regression coefficients ~50% due to the large scattering of the data points. When the resulting functions were plotted (Fig. 1, Supplementary Fig. S3, and Supplementary Table S6), the slopes of the functions increased with the asRNA abundances. The functions had the form $\lg_{10}(\text{protein}) = \lg_{10}(a) + \lg_{10}(b) \times \lg_{10}(\text{senseRNA})$ so that the protein abundance $P = a \times b^{\lg(\text{sRNA})}$. The abundance of the sense RNA was between 1 and 10 000, so that $\lg_{10}(\text{sRNA})$ was between 0 and 4. For all conditions, the a values decreased from class AST0 to AST4 whereas the slope (b values) increased. This indicates that the influence of the mRNA abundance on the protein abundance increased with the asRNA abundance. Exceptions were the data points in class AST5 with NPKM >100 for the asRNA. They displayed higher a but lower b values again, so that here a high asRNA abundance negatively affected the protein-to-mRNA ratios. These data indicated a global positive effect of asRNAs on gene expression at low asRNA abundances, but a negative effect at high values. On a global scale, asRNAs enhanced the copy number of the gene products at low abundances but seem to have a destabilizing function at high asRNA abundances. Antisense transcripts thus influenced the proteome composition.

Influence of transcriptome on proteome changes

The data points resulting from the plot of a protein abundance to that of its sense RNA were scattered (Supplementary Fig. S3). This may mirror the fact that the abundance of a protein depends on many factors, for instance that of the associated mRNA, translation initiation and elongation efficiency, degradation and dilution by growth of the cell. A comparison of the ratios Q of the up- or

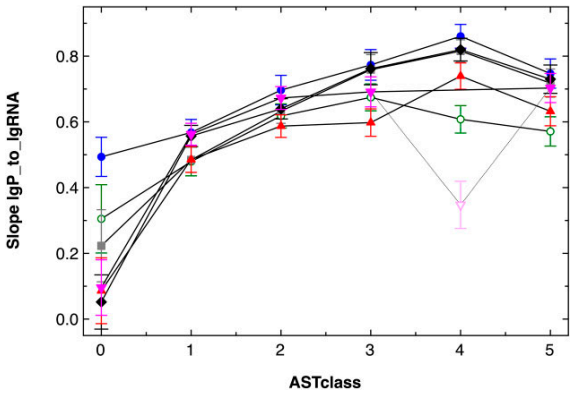

Figure 1. The abundance of antisense RNAs influenced the protein yield from the associated sense RNA. The abundance of proteins (copy number per cell) was plotted as decadic logarithm against that of the abundance of its transcript (NPKM values as published [58]). Closed circles are CH34 control cells, open circles metal-, squares EDTA-treated cells of strain CH34. Diamonds are AE104 control cells, triangles metal- and inverted triangles EDTA-treated AE104 cells. Data points were grouped according to the abundance (NPKM values as published [58]) of the respective asRNA into six groups: no asRNA (0), NPKM ≤3 (1), 3 < NPKM ≤ 10 (2), 10 < NPKM ≤ 30 (3), 30 < NPKM ≤ 100 (4), and NPKM > 100 (5). A linear curve fit was performed for the six groups (Supplementary Fig. S3) to the function $\lg_{10}(\text{protein}) = \lg_{10}(a) + \lg_{10}(b) \times \lg_{10}(\text{senseRNA})$. Shown here is the slope $\lg_{10}(b)$ for the six asRNA groups per condition. The color code has no meaning and was used for contrast. The pale inverted triangle was a slope outside of the remaining data.

downregulation of the abundance of a protein and its associated sense RNA may negate (or nullify) the influence of the other factors and highlight that of the sense RNA abundance. Moreover, great changes in asRNA abundance should be reflected in linearly correlated changes in inhibition rate of the sense RNA [69]. Thus, the Q values for the regulation of the significantly regulated 327 proteins (Table 1) were plotted against the changes of their associated sense RNAs, using 1/Q values for downregulated proteins (Fig. 2, gray and colored symbols). The comparison of control cells of AE104 with those from strain CH34 was omitted from this analysis because asRNA-dependent regulatory events vary between bacterial strains [70].

Seven proteins were upregulated, despite showing no or only a very low upregulation of their sense RNA (gray filled squares in parallel with the vertical zero line in Fig. 2) but only for two proteins was the upregulation of the sense RNA abundance significant (blue filled squares). These were ZniA and ZniB with ~2.5-fold upregulation of the sense RNA resulting in a >10-fold higher protein abundance in EDTA-treated CH34 cells (Fig. 3). This highlighted the importance of the ZniCBA transenvelope complex in handling metal starvation conditions.

For all data points, the double-$\log_{10}$ plots followed linear functions with regression coefficients of 75% and 85% for genes upregulated following metal stress in strain CH34 or AE104, respectively (Fig. 2). The regression coefficients for upregulated genes in metal-starved CH34 or AE104 cells were 20% and 40%, and much lower than those for upregulated metal-stressed cells, for both strains. For downregulated genes, the regression coefficients were 19% for metal-stressed CH34 cells, and close to, at or below zero for genes down-regulated in metal-starved or unchallenged CH34 cells. However, the lower abundance of the downregulated proteins did not correlate with the downregulation of the associated mRNAs.

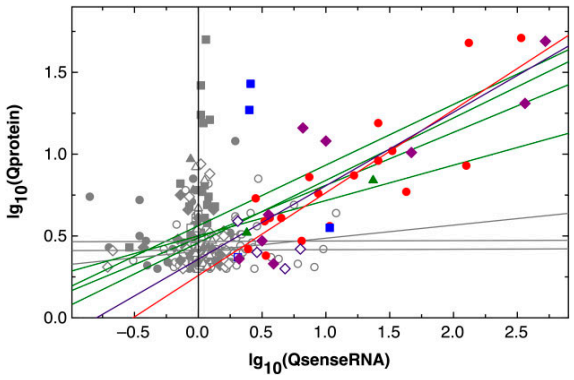

Figure 2. Changes in abundance of proteins correlated with changes in abundance of the associated sense RNA. The 327 proteins with a significantly changed abundance following metal-stressed or starvation in CH34 and AE104 cells were plotted against the changes of the associated sense RNA. Filled symbols represent upregulated protein copy numbers, open symbols the inverse ratio Q of downregulated proteins. Circles are the comparison of metal-shocked CH34 to the control (CM0), squares metal-starved CH34 cells to the control (CE0), diamonds metal-shocked AE104 cells to the control (AM0), and triangles metal-starved AE104 cells (AE0). Colors indicate data points with significant changes (Q ≥2 for up- and 1/Q ≥2 for downregulated RNAs, D >1). CM0 red, CE0 blue, AM0 purple, and the two values for AE0 in green. Gray symbols are the results with significant changes in the proteome but not the transcriptome. The lines are linear curve fittings for the subsequent functions:
CM0+, all data: lg10(Qprotein) = 0.487 ± 0.034 + 0.323 ± 0.042 × lg10(QsenseRNA), R^2 = 74.8%
CM0+, Qs ≥2: lg10(Qprotein) = 0.258 ± 0.100 + 0.506 ± 0.077 × lg10(QsenseRNA), R^2 = 75.5%
CM0−, all data: lg10(Qprotein) = 0.406 ± 0.017 + 0.079 ± 0.049 × lg10(QsenseRNA), R^2 = 19.0%
CE0+, all data: lg10(Qprotein) = 0.562 ± 0.042 + 0.371 ± 0.233 × lg10(QsenseRNA), R^2 = 20.4%
CE0−, all data: lg10(Qprotein) = 0.413 ± 0.017 + 0.003 ± 0.246 × lg10(QsenseRNA), R^2 = 2.2%
AM0+, all data: lg10(Qprotein) = 0.459 ± 0.044 + 0.381 ± 0.049 × lg10(QsenseRNA), R^2 = 85.0%
AM0+, Qs ≥ 2: lg10(Qprotein) = 0.358 ± 0.143 + 0.449 ± 0.098 × lg10(QsenseRNA), R^2 = 86.7%
AM0−, all data: lg10(Qprotein) = 0.467 ± 0.032 + 0.002 ± 0.102 × lg10(QsenseRNA), R^2 = 0%
AE0+, all data: lg10(Qprotein) = 0.500 ± 0.079 + 0.261 ± 0.176 × lg10(QsenseRNA), R^2 = 39.8%
Upregulated items in the comparisons are indicated by a '+' and green lines, downregulated (1/Q values) by a '−' and gray lines. For AE0−, R^2 was <null and this function is not given. Functions in italic letters have regression coefficient <20%. The bold-faced equations are those for the data points with QsenseRNA ≥2 with CM0+ in red and AMO+ in purple.

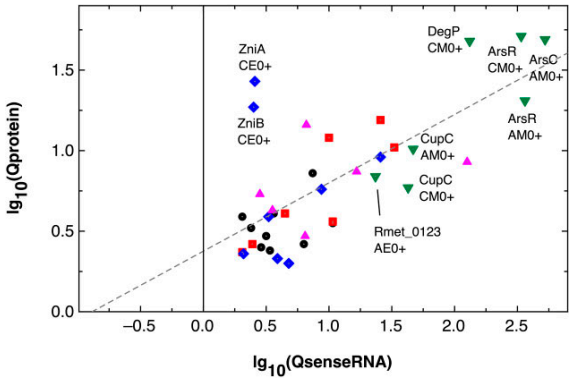

Figure 3. Changes in abundance of proteins correlated with changes in abundance of the associated sense RNA. The figure shows the same data points as that in Fig. 1 but uses another symbol and color code to group these points according to the associated changes in the sense-to-antisense ratios QS_AS. Group 1, no QS_AS ratio or QS_AS <0.25 (black circles); group 2, 0.5 < QS_AS < 1.2 (red squares); group 3, 1.2 ≤ QS_AS < 4 (blue diamonds); group 4, 4 ≤ QS_AS < 20 (magenta triangles); and group 5, QS_AS > 50 (green inverted triangles). Dashed lines come from the fitting of all values (small gray dot within the symbols), lg_{10}(Qprotein) = 0.376 ± 0.084 + 0.424 ± 0.069 × lg_{10}(QsenseRNA), R^2 = 72.1%, or Qprotein = 2.38 × $2.66^{QsenseRNA}$. Data points for group 5 and two *zni* data points from other groups are labelled with the protein and the respective comparison.

To analyze the effect of antisense RNAs on the effect of changed sense RNA abundances and consequently altered protein abundances, only the data points with both significantly changed protein and sense RNA abundances were further considered (Table 1 and Fig. 2, colored data points). This resulted in 37 data points, mostly from upregulated metal-shocked CH34 and AE104 cells. The curve fittings of these double-log plots gave regression coefficients similar to those from the plot using all data points. This was the consequence of the strong influence of highly upregulated protein abundance on the sense RNA plots and the fact that all data points with Q values below 2 ($log_{10}(2) = 0.301$) were below the threshold so that all functions started in the region of the data point 0.3/0.3 (Fig. 2).

The 37 data points were subsequently regrouped into 5 clusters with increasing ratios of the sense to the associated antisense RNAs (Fig. 3, Table 5). Two clusters of data points were separated from each other. A strong increase (>50-fold) of the sense RNA compared to its antisense RNA represented highly upregulated sense RNAs, leading to an increase in the abundance of the gene products (Fig. 3, green inverted triangles). A second group included data points with decreased sense-to-antisense ratios (≤0.23-fold) and upregulation of the sense RNAs and their product on a low level (Fig. 3, black closed circles). The other groups, which contained events with no change in the sense-to-antisense ratios (red squares), a small (blue diamonds) or medium (magenta triangles) increase in the sense-to-antisense ratios, fell between these two groupings.

Despite the differences in the changes of the sense-to-antisense ratios, the data points could be fitted to a linear function with a regression coefficient of 72% (Fig. 3). This means that the abundance of the sense mRNA had a stronger effect on the subsequent increase or decrease of the protein copy number than that of the sense-to-antisense ratios. Group 1 of these data points contained gene products without asRNA or with a >four-fold decrease of the sense-to-antisense ratios, meaning much more asRNA relative to the associated sense RNA (Fig. 3, black dots). A stronger impact of the asRNA abundance would lead to the appearance of two additional clusters in these data points, one generated in the absence of asRNA, in which no stabilizing effect could be exerted by the asRNA molecule on the already destabilizing sense RNA, and the second, in which there is an increasing effect of the asRNA on its sense RNA, whether one of stabilization or destabilization. These data sets with a decrease in the sense-to-antisense ratios (Fig. 3, black circles) contained data points associated with downregulation of three genes: *purK* encoding a subunit of the phosphoribosylaminoimidazole carboxylase, *ggt* encoding a γ-glutamyl transferase, and *bfrB* encoding a bacterioferritin (Table 5). The upregulated genes encoded the chromid-located copper-sensing histidine kinase $CopS_2$, ZniC for the ZinCBA transenvelope efflux system and components of the Isc system for the synthesis of iron–sulfur clusters.

Some of the data points were simultaneously associated with the strongest increase in the sense-to-antisense ratios, an increase in abundance of sense RNA and of the copy numbers of the respective gene product (Fig 3, green inverted triangles). Found in metal-shocked conditions were the regulator of arsenate-resistance ArsR, appearing in CH34 as well as AE104 cells, while the arsenate reductase ArsC appeared only in AE104, but the copper chaperone CupC was present again in both strains. The protease DegP was only found in metal-shocked CH34 cells and representative for EDTA-starved AE104 cells was an outer membrane TonB-dependent receptor Rmet_0123 that is encoded downstream of the *zur-cobW2-cobW3* genes in the same operon Op0032r.

Two data points stood out that were above the function that represented the double-$\log_{10}$ plot (Fig. 3, blue diamonds). They showed a higher abundance of their copy number in comparison with that of the sense RNA. These were ZniA and ZniB in EDTA-treated CH34 cells. Such an effect may be due to a stabilizing effect, for instance by an asRNA.

Discussion

Changes in the proteome of *C. metallidurans* following metal stress

Metal resistance in *C. metallidurans* CH34 wild type is mediated by resistance determinants on the two plasmids pMOL28 and pMOL30 [71], resulting in upregulation of these genes following metal shock, and indeed, the gene products can be found in the proteome of this bacterium. Prominent are the components of the transenvelope efflux complexes CzcCBA (cobalt, zinc, and cadmium resistance) and CnrCBA (cobalt and nickel resistance), and proteins involved in copper and chromate resistance. The CzcCBA proteins were also present in control cells cultivated without added metals so that Czc has also a function in metal homeostasis in the absence of high metal concentrations.

Transenvelope efflux complexes are composed of an RND (resistance, nodulation, cell division protein family [72, 73]) inner membrane protein that extends into the periplasm, an outer membrane factor OMF that also reaches into the periplasm [74], and a membrane fusion MFP or adaptor protein [72, 75, 76], named CzcA, CzcC, and CzcB, respectively. For the CusCBA copper-exporting system from *Escherichia coli*, a subunit composition $CusC_3B_6A_3$ was determined [15]. This subunit ratio was prominent among the RND-driven transenvelope efflux systems for metals and organic substances [77]. In our data set, the ratio of CzcA to CzcB was 1:1.8 so that a $CzcA_3B_6$ complex structure could be concluded but the OMF CzcC was only present in metal-challenged CH34 cells in a ratio of CzcA:CzcC = 1:0.46 (Table 2, Fig. 4). Since membrane-integral proteins were not efficiently quantified in the proteomic approach used, this could be the consequence of an underrepresentation of the OMF with its membrane-integral hydrophobic β-barrel. The related OMF CnrC was not even detectable in metal-shocked CH34 cells, whereas CnrB was present in a similar abundance as CzcB, 1235 ± 272 versus 1509 ± 607 copies per cell, respectively, suggesting potentially 200 copies of the $CnrC_3B_6A_3$ and 250 copies of the $CzcC_3B_6A_3$ complexes per cell.

The chromid-encoded transenvelope efflux system ZniCBA was interestingly found with increased abundance in EDTA-treated CH34 cells, indicating some role in metal ion supply and not resistance (Fig. 4). By looking at the abundance of the three proteins, a subunit composition of $ZniC_3B_6A_{4.5}$ with ~413 copies per cell could be derived from the number of the B subunits. Adjacent to the *zni* region on the chromid is the *zne* region. The related ZneCBA complex was also upregulated under metal-starvation rather than under metal-resistance conditions. The subunit ratio of ZneA:ZneB was 1:1.5, with ZneC being present in lower copy numbers as determined from the result of a single determination in these cells. The total number of ZneCBA complexes was 77 per cell and thus much lower than that of the ZniCBA complexes. Abundance of ZniCBA and ZneCBA complexes was also upregulated in metal-starved AE104 cells, leading to ~76 and 3 complexes, respectively (Supplementary Table S2). Zni and Zne could have a specific function in periplasmic metal homeostasis under metal-starvation conditions in CH34 cells with their sophisticated periplasmic metal-resistance components.

Appearance of CzcCBA and an even 12-fold upregulation of ZniCBA in metal-starved cells was not expected (Fig. 4). One explanation would be that CzcCBA is continuously present to counteract any sudden increase in Co(II), Zn(II), and Cd(II) concentrations, but this does not explain the upregulation of ZniCBA. ZniA is an export system of divalent transition metal cations as judged by a conserved motif ('DFG—D—EN') in the membrane-integral α-helix, which is essential for import of protons into the cytoplasm and subsequently proton-driven export of metal cations from the periplasm to the outside [12, 13]. ZniCBA is thus a transenvelope protein complex for export of divalent transition metal cations. The difference between CzcCBA and ZniCBA is the presence of additional metal-binding sites in CzcA and CzcB, which may allow a flux control of the efflux activity of CzcCBA driven by the cytoplasmic or periplasmic Zn(II) or Co(II) concentrations [12, 20, 78], with an additional control of this activity by the periplasmic protein CzcI [33]. Under certain metal-starvation conditions, CzcCBA may export its substrate metal cations only with a low rate and ZniCBA may be needed to compensate for the loss of transport activity by CzcCBA.

In marine environments, zinc is found in inorganic pools that include biogenic silica, clays, and various metal oxides [79]. *Cupriavidus metallidurans* most likely encounters such zinc speciations also in its environment. Such particular zinc-containing substances may generate fragments or species able to cross the outer membrane, for instance driven by TonB-dependent outer membrane proteins. It could be hypothesized that CzcCBA, ZniCBA, and other RND-driven transenvelope systems may have a second function in addition to mediating metal resistance: mobilization of essential transition metal cations from various inorganic and organic complexes (Fig. 4). The cation would be sequestered by the efflux system, exported to the outside, able to re-enter the periplasm as 'free' ions just complexed by water, and subsequently imported into the cytoplasm. That way, a cycling of metal ions occurs that may assist their allocation to a target protein [64]. Such a function of CzcCBA or ZniCBA as a substitute in release of Zn(II) or Co(II) from organic or inorganic complexes would explain the upregulation of the copy numbers of the ZniCBA components under those metal-starvation conditions that lead to downregulated activity of CzcCBA by flux control [78].

Metal-shocked *C. metallidurans* cells induced a large variety of metal-resistance genes, and for many of them, the gene products could be found in the proteome (Supplementary Table S2). Following metal shock, *C. metallidurans* also downregulated genes for ribosomal proteins, proteins involved in the initiation and elongation of translation, transcription, motility, synthesis of hydrogenases, and the components of the F_1F_0 ATPase [58]. A downregulation of the respective gene products after 1.5 cell duplications, however, was not measured (Supplementary Table S2). The abundance of a protein depends not only on *de novo* synthesis but also

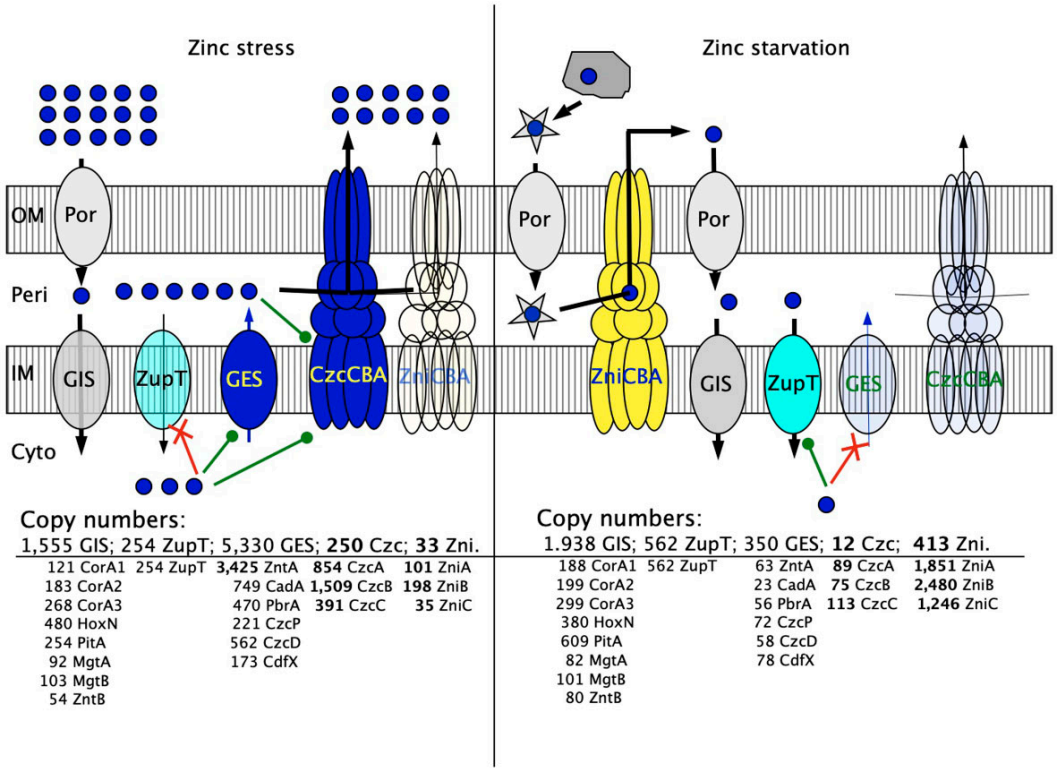

Figure 4. Model of Zn(II) transport under stress and starvation conditions. Under conditions of zinc (small circles) stress, Zn(II) is imported into the periplasm by porins and either immediately exported by 250 CzcCBA systems to the outside, or imported by 1555 general import systems (GIS) or 254 ZupT into the cytoplasm. Due to the flow equilibrium [25], Zn(II) is exported back into the periplasm by 5330 general export systems (GES) such as ZntA. Under zinc-starvation conditions (right hand), hypothetical zinc-containing particles (gray irregular field) might generate zinc-containing fragments or species (stars), which are also imported into the periplasm. A total of 413 ZniCBA complexes might release the zinc ion from these fragments by export to the outside. Subsequently, Zn(II) is reimported into the periplasm and further on into the cytoplasm. Below, the copy numbers of the transport proteins are shown, bold-faced when measured, otherwise the numbers are generated from the transcript abundance using the functions generated in Supplementary Fig. S3. The arrows indicate transport, lines with crosses possible downregulatory, lines with balls upregulatory effects of transport activities. Lower intensities of the colors of the transport systems indicate a lower abundance of the respective proteins.

on degradation and dilution by growth. With a doubling time of *C. metallidurans* of ~4 h and a period of 3 h between challenge of the cells and their harvest, growth of the cell should dilute the abundance of a protein down to 60%. To keep the abundance of a protein constant during growth and reduce its subsequent dilution, ~40% have to be newly synthesized during the period of 3 h. A decrease in the abundance of the mRNA by half would consequently mean that only 20% of a given protein would have been synthesized, resulting in a coverage of 80% on the protein abundance after the experimental period of 3 h compared to time zero. Indeed, 80% of the total number of ribosomal proteins were found in metal-challenged CH34 cells compared to the control, but with respect of a general deviation of 0.4-fold of the proteome determination, this difference is most likely purely a coincidence. This means that the downregulation of all these genes at the onset of a metal shock did not ultimately lead to a lower protein content, indicating that the cells had adjusted to the high metal concentration, reached metal homeostasis again, and proceeded with growth after 1.5 cell duplications.

These results demonstrated that upregulated genes in metal-challenged *C. metallidurans* cells indeed led to an increased abundance of proteins involved in metal resistance. Moreover, these increased abundances were interrelated at the transcriptional and translational levels. This could be anticipated but now has been demonstrated.

Connecting the proteome and the handling of zinc cations in *C. metallidurans*

Pulse-chase experiments demonstrated continuous import and export of zinc ions into *C. metallidurans* cells [25]. In standard Tris-buffered mineral salt medium containing 200 nM Zn(II), the cells rapidly accumulated radioactive ^{65}Zn as well as isotope-enriched stable ^{67}Zn, and exported these ions quickly when chased with 100 µM nonradioactive or nonenriched zinc. In the wild-type *C. metallidurans* CH34, which contained the plasmid-encoded *czc* determinant, zinc import was strongly reduced, especially when the cells were preincubated in the presence of 100 µM Zn(II) [25]. In agreement with previous results [80, 81], it was concluded that CzcCBA was responsible for this decreased accumulation of zinc. The proteomic data supported this conclusion. As judged from the number of CzcB subunits, nonchallenged CH34 cells contained on average 24 CzcCBA complexes, metal-induced cells 250, and metal-starved cells only 12 complexes (Table 2, Fig. 4). The plasmid-free strain AE104 does not contain *czc* [71] and consequently produces no CzcCBA complexes. None of the

chromosomal or chromid-encoded paralogs of the RND protein CzcA were found in strain AE104 (Supplementary Table S2) and, with the exception of *zniA* and *zneA*, the respective genes were inactivated [7, 8, 82]. From the number of B-proteins, 22 ZniCBA complexes could be present in nonchallenged AE104 cells, so that Zni might have had some influence on the flow equilibrium of zinc under the condition that ZniA had also been produced in strain AE104. Unchallenged CH34 cells contained ZniA and even ZneA leading to 22 ZniCBA and 3 ZneCBA, in addition to the 24 CzcCBA complexes. However, the strong differences between zinc import into CH34 and AE104 cells during the uptake period of the pulse-chase experiment [25] indicated that the presence of CzcCBA had the strongest influence on zinc accumulation, especially when *czc* was upregulated under metal stress.

While the CzcCBA components could be quantified in the proteome of *C. metallidurans*, most of the other zinc transport systems were not, or at least not under all conditions (Tables 3 and 4). This was probably the result of the underrepresentation of membrane proteins in the proteomic analysis, as demonstrated by the subunits of the F_1F_0 ATPase (Supplementary Table S3), which was present in about ~1500 copies per cell as judged from the α-subunit. The functions that describe the dependence of the protein abundance under the six conditions from the abundance of the sense and antisense transcripts (Supplementary Table. S6) allow a rough estimation of the numbers of these proteins (Fig. 4). These numbers were in the same range as the determined copy numbers, when these data were available. Nonchallenged CH34 cells, for instance, contained 394 ± 242 $CorA_1$ (estimate 170), 391 $CorA_2$ as single result (estimate 195), 162 ± 96 $CorA_3$ (estimate 293), 29 ± 17 MgtA (estimate 71), and 82 ± 22 ZntB (estimate 73, Table 4 and Supplementary Table S6). These data demonstrated that a wide range of import systems [29–31, 83], mainly for the macrobioelements phosphate and magnesium, did not change much in abundance under varying conditions. These systems are able to transport the ionic or phosphate-bound forms of various transition metal cations including Zn(II), leaving it to the subsequently acting efflux systems to adjust the cytoplasmic concentration and composition of these ions [2, 25].

The determined and estimated copy numbers of general metal import systems did not change much between metal-stressed and -starved *C. metallidurans* cells (Fig. 4), with the exception of a predicted two-fold upregulation of ZupT, which was in agreement with previous results [31, 83–85]. ZupT was responsible for 42% of the initial zinc import rate in nonchallenged cells (68 $^{65}Zn\ cell^{-1}\ s^{-1}$) and 70% in zinc-starved cells (160 $^{65}Zn\ cell^{-1}\ s^{-1}$) [25], which agrees with a duplication of the copy numbers.

In comparison to the zinc uptake system, the number of those able to export zinc ions across the inner membrane was strongly upregulated, from 350 general export systems for zinc (all estimated numbers) to 5330 (3425 ZntA measured, others estimated, Fig. 4). The numbers clearly emphasized the importance of efflux systems for metal homeostasis, which supports conclusions from biochemical, gene deletion and physiological studies [18, 25, 32, 33, 86, 87]. In total, the proteomic data close the knowledge gap between these studies and the investigation of the transcriptome of *C. metallidurans*.

Role of the asRNAs as shown for the *zniBA* genes

In contrast to *czcCBA*, these *zni* genes are oriented as *zniBA* on one DNA strand and *zniC* on the other, both operons starting at the same promoter regions (Fig. 5). A strong transcriptional interference occurs at the divergent *zniB–zniC* region. The 5′ untranslated regions (5′UTRs) of both genes overlap, with each other and extend even into the opposing gene. The promoter *zniCp* depends on the main sigma factor RpoD, as found in a published and recently performed determination of the transcriptional start sites (TSS) in *C. metallidurans* [8]. In contrast, the additional RpoD-dependent and published *zniBp* [8] was no longer found in the recent measurement. Instead, the 5′UTR of *zniC* extended more deeply into *zniB* as in the previous measurements (Fig. 5). This is all in agreement with a heavy transcriptional interference in the *zniB–zniC* region, based on RNAP competition and asRNA effects by overlapping 5′UTRs [88, 89]. This interaction may be required to express *zniB* and *zniC* in such a way that the resulting subunit ratio is 2:1.

Moreover, the location of the genes of the *zni–zne* region switches between both DNA strands, resulting in an excludon effect [90]. Most intriguingly, and indicated by the position of ZniB and ZniA in Fig. 3, transcription of *zniBA* was upregulated eight-fold in metal-challenged *C. metallidurans* CH34 cells compared to the control, but this results only in a meager and not significant 50% increase in the copy number of the respective gene products (Fig. 5). Obviously, Zni might not be required in metal-stressed *C. metallidurans* CH34 cells with their active Czc system.

On the other hand, expression of *zniBA* was upregulated 2.5-fold in metal-starved CH34 cells but the protein copy number increased 10-fold. In control and metal-starved cells, a TSS in the middle of *zniA* resulted in one or two short asRNAs, respectively, of *zniBA*. These might represent RNAse III-mediated degradation products of double-stranded RNA [91]. But in metal-challenged cells with their comparably low protein synthesis yield despite an eight-fold upregulation of transcription, the activity of this promoter doubles, which leads to an asRNA with a much higher abundance that starts in the middle of *zniA* and continues into the already busy *zniB–zniC* divergent region. Half way, yet another TSS appears [58]. This asRNA seems to be responsible for the comparably low translation yield of ZniCBA. It seems as if during evolution of *C. metallidurans* and following acquisition of the *czc* determinant, *zni–zne* became subordinate. It turned from a zinc-exporting transenvelope system into one that only mediates zinc export under conditions when CzcCBA is not able to function, namely under metal-starvation conditions. An asRNA appears to have been central in mediating this subordination.

Experimental

Bacterial strains and growth conditions

Cupriavidus metallidurans strains used in this study were CH34 (wild type) and its plasmid-free derivative AE104, which lacks pMOL28 and pMOL30 [71]. Tris-buffered mineral salt medium [71] containing 2-g sodium gluconate/L (TMM) was used to cultivate these strains aerobically with shaking at 30°C. Analytical grade salts of cation chlorides, potassium chromate, and potassium arsenate were used to prepare 1 M stock solutions, which were sterilized by filtration. Tris-buffered media were solidified by incorporating 20-g agar/L.

To challenge *C. metallidurans* CH34 and AE104 simultaneously with several transition metal cations, a MultiTox metal mix optimized for the transcriptome determination [58] was employed. The CH34-specific MultiTox metal mix was 3.35 mM, composed of 461 µM Zn(II), 241 µM Cu(II), 1503 µM arsenate, 0.37 µM Hg(II), 19 µM chromate, 15 µM Cd(II), 761 µM Ni(II), and 347 µM Co(II). Strain AE104 was challenged with 1000 µM of its specific MultiTox mixture comprising 5 µM Zn(II), 120 µM Cu(II), 849 µM arsenate, 0.18 µM Hg(II), 7 µM chromate, 3 µM Cd(II), 9 µM Ni(II), and 7 µM Co(II). These MultiTox metal mixes should lead to a comparable

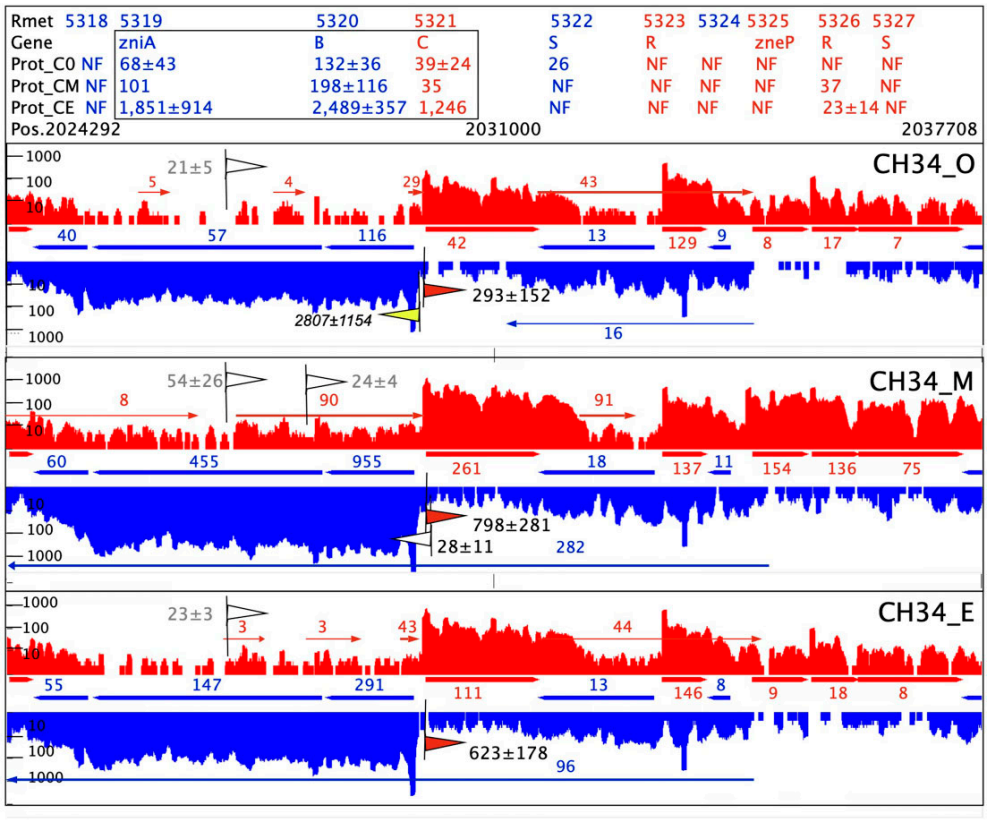

Figure 5. Dependence of the protein copy number on the transcriptional activities. The figure shows the RNASeq results of the chromid region ~2 012 000 base pairs in metal-challenged (CH34_M), -starved (CH34_E), or control cells (CH34_0), transcripts of the forward strand in red, in reverse direction in blue. Arrows between the abundance plots show the position of the open reading frames and the NPKM values of the gene-specific sense RNA transcripts. Above or below the abundance plots are the position of the annotated asRNAs and their NPKM values. The header on the top gives the Rmet locus number, the gene name, the copy number of the gene product under the three conditions plus a position marker. Flags indicate transcriptional start sites (TSS), white not associated to a sigma factor yet, and red RpoD-dependent. The yellow flag indicates the published TSS *zniBp* [8], which was, however, no longer found in recent experiments. The TSS signal score is given adjacent to the flags, the no longer found *zniBp* in italics. The genes *zniB*, *zniC*, their 5′ untranslated regions and TSSs are strongly overlapping. Coordinates annotated to position 2 030 000 of the chromid sequence are from the left to the right −165 (*zniC*-5′UTR), −105 (3′ of *zniB*), −77 (old *zniBp*), +10 (*zniCp*), +16 (previously published *zniC*-5′UTR), +59 (new found *zniBp*), +64 (5′ of *zniC*) and +109 (*zniB*-5′UTR). This indicates a lively interaction between transcription initiation of *zniC* and *zniB*.

toxicity of each metal in the cells of the strains CH34 and in AE104. To obtain general metal starvation conditions, CH34 was treated with 1576 µM EDTA and AE104 was treated with 306 µM EDTA, which were the respective IC_{50} values of EDTA for these strains.

Quantitative proteome analysis

For the quantitative proteome analysis, the strains were cultivated to the mid-exponential phase, challenged at 100 Klett units with MultiTox or EDTA, harvested at 150 Klett units, and crude extract was prepared by ultra-sonication as published [92]. After low-touring centrifugation (30 min, 4500 × *g*), ultracentrifugation (1 h, 540 000 × *g*) was used to separate soluble and membrane proteins. Protein concentration was determined using the BCA Protein Assay Kit (Sigma-Aldrich, Germany). Protein digestion was performed using the SP3 protocol [93]. Briefly, 100-µg proteins of both fractions were incubated with Sera-Mag Speedbeads Carboxylate-Modified Magnetic Particles (1 µM GE Healthcare) for subsequent protein binding, washing, and in solution digestion. Protein binding on the magnetic beads was induced using 70% ACN (v/v, acetonitrile), followed by 20-min incubation at RT (room temperature) with shaking at 400 rpm in a ThermoMixer C (Eppendorf). Two additional washing steps with 70% EtOH were performed, followed by resuspension of the magnetic beads in 100% ACN, and complete lyophilization of the beads. Afterwards, the beads were resuspended in 50-µl 50 mM ammonium bicarbonate. The reduction reaction was carried out by using 10 mM DTT (Dithiothreitol) at 80°C while shaking for 15 min. The alkylation of the cysteine residues was done using 20 mM CAA (chloracetamide) at room temperature in the dark. The supernatant was discarded and 50-µl 50 mM ammonium bicarbonate was added to resuspend the magnetic beads. Protein digestion was carried out with 2-µg trypsin/Lys-C Mix (Promega, USA) overnight at 37°C; 10-µg peptide solution was further purified using the Pierce C18 spin tips (Thermo Fisher Scientific, USA). The peptide solution was adjusted to a pH below 4 using 2.5% trifluoroacetic acid and scaled up to 20 µl using 0.1% trifluoroacetic acid. Prior use, the tips were first wetted using 20-µl 0.1% trifluoroacetic acid in 80% ACN, and then equilibrated only with 0.1% trifluoroacetic acid, three times. After each step, the tips were centrifuged for 1 min at 1000 × *g*; 20 µl of the peptide solution was applied to the C18 spin tips followed by centrifugation, and the same centrifugation conditions were applied throughout the purification

procedure. Washing of the bound peptides was done using 20-µl 0.1% trifluoroacetic acid twice, and elution was achieved with 20-µl 0.1% trifluoroacetic acid in 80% ACN, performed twice to elute all bound peptides. Last, the peptides were dried with a SpeedVac vacuum concentrator. Peptides were resuspended in 25-µl 0.1% fluoroacetic acid and sonicated in a water bath for 15 min. Nano-ESI-LC-MS-MS (nano electrospray ionisation liquid chromatography tandem mass spectrometry) was performed downstream for whole proteome analysis.

Liquid chromatography-coupled mass spectrometry

Approximately 200 ng of peptides for each sample and replicate were initially trapped (PepMap100 5 µm, 3 × 5 mm Thermo Scientific #160454) and separated on a Waters M-Class C18 25-cm analytical column (Acquity UPLC® M-Class Peptide BEH 130 Å, 1.7 µm, 75 µm × 250 mm, Waters #186007484) over 180 min with an increasing gradient of ACN (3%–22%) at 240 nl/min on a Dionex UltiMate 3000 RSCLnano System before being injected in to a Thermo Scientific Orbitrap Exploris 480 mass spectrometer. Peptides were ionized in positive mode with 1800 V and a transfer capillary temperature of 300°C. Samples were subjected to further separation with FAIMS Pro with three compensation voltages (CVs: −40, −55, and −65) resulting in three separate MS experiments within one data file. Each experiment had the following settings: MS resolution of 120 000 at 200 m/z, a scan range of 350–1400 m/z, MS AGC (automatic gain control) target of 300% for max IT (injection time) of 50 ms; MSMS (tandem mass spectrometry) of all the most intense peaks for a total cycle time of 1 s with the following settings: isolation window of 2-m/z normalized collision energy of 30%, resolution of 15 000 with an AGC target of 100%, and a max 30-ms IT. Every fragmented precursor within ±10 ppm was immediately excluded from reanalysis for 45 s.

Data analysis

Raw files were analyzed by MaxQuant software [94] version 2.0.3.0 and searched against the *C. metallidurans* Uniprost FASTA database (UniProt ID: UP000002429). Generally, the already set parameters were kept. *N*-terminal acetylation and methionine oxidation were added as variable modification. False discovery rate was set to 0.01 for peptides (minimum length of seven amino acids). For protein identification, unique and razor peptides were set to 1. Group-specific parameters for the instrument were set to Orbitrap and 2-ppm peptide search tolerance. Match between runs was enabled and protein quantification was set to LFQ (label-free quantification), with classic normalization type.

Statistical analysis, reference protein mixtures, and data normalization

The accumulated LFQ intensity for the identified protein in each of the three technical repeats was used to calculate the mean values and deviations of the protein amounts per biological repeat and bacterial strain. These values were not normalized to 1 million proteins per bacterial cell but instead to 1.88 million proteins per cell. This number was calculated from the number of bacterial cells before harvest and the protein concentration in the crude extract, which gave an average protein content of 115 fg/cell. This number was divided by the average protein mass of 37.2 kDa of the synthesized proteome, $\Sigma\{(\text{fmol}(\text{protein}_i)/\Sigma\text{fmol}(\text{allproteins})\cdot\text{mass}(\text{protein}_i)\}$, yielding 3.088 amol protein per cell, which was multiplied with the Avogadro number. The resulting 1.86 million proteins per cell were lower than the number of 2.6 million proteins per *E. coli* cell, although *E. coli* has a 1.5-fold lower cell volume and should have a lower dry mass [86, 95–97].

The resulting cellular numbers and deviations for each protein per biological repeat and bacterial strain were used to calculate the mean protein numbers per bacterial cell and strain. The deviation was the mean value of the deviations of the biological repeats. Finally, the protein numbers of the strains were compared. A protein number was judged as up- or downregulated if the quantities were at least two-fold lower or higher in the mutant-derived extract, respectively. Additionally, a 'D' value was calculated as a measure of the significance of the difference. The 'D' value gives the difference in the protein numbers, mutant minus parent, divided by the sum of the deviation of these mean values. If D >1, the deviation bars of the mean values do not overlap, leading to a significant result (>95%) if n >3 as published [98]. If a protein was up- or downregulated and the difference between the protein numbers was significant (D ≥1), the value was judged as significantly different. All values are provided in the Supplementary Data Set.

To verify compatibility and reproducibility of the method used for the determination of the proteome, the protein content of unchallenged cells of *C. metallidurans* strain AE104 was plotted against the already published data [61] (Supplementary Fig. S1). The data points were on a line with a regression coefficient of 100% and a slope of $1.0000 \pm 3.16\times10^{-16}$. A number of 2816 proteins were found in both data sets.

For the six data sets, the mean values and deviations of the copy numbers were calculated if a protein was quantified in two or three of the samples of one data set. Proteins found only once in a data set were not excluded but noted with a '0' as deviation, which served as a flag for such a result. From the six data sets, the ratios Q of the copy numbers for each protein in the comparisons CH34 cells with compared to without toxic metals (CM0), with or without EDTA (CME), and the same for AE104 cells (AM0, AME) plus the comparison AE104 with CH34 (0AC) and the distance value D (= absolute[value1 − value2]/[deviation1 + deviation2]) as a measure of significance, were calculated. Comparisons that included only one result in a data point give a D value of 0 or a calculation error, indicating that a respective comparison was not a significant result. Proteins not found were annotated with a copy number of 1 per cell to allow subsequent mathematical operations, for instance calculation of the ratio Q of the copy numbers of two conditions. The full data set is provided as the Supplementary Data Set.

Acknowledgments

We thank Gary Sawers for critically reading this manuscript and Grit Schleuder for skillful technical assistance for nearly 30 years. We also thank Dr Henning Großkopf for providing help in setting up the MaxQuant calculation.

Supplementary data

Supplementary data are available at *Metallomics* online.

Conflict of interest

None declared.

Funding

Funding for this work was provided by the Deutsche Forschungsgemeinschaft (Ni262/19).

Data availability

The mass spectrometry proteomics data have been deposited to the ProteomeXchange Consortium via the PRIDE (www.ebi.ac.uk/pride) partner repository with the data set identifier PXD057750.

Reference

1. Janssen PJ, Van Houdt R, Moors H *et al.* The complete genome sequence of *Cupriavidus metallidurans* strain CH34, a master survivalist in harsh and anthropogenic environments. *PLoS One* 2010;**5**:e10433. https://doi.org/10.1371/journal.pone.0010433
2. Nies DH. The biological chemistry of the transition metal "transportome" of *Cupriavidus metallidurans*. *Metallomics* 2016;**8**:481–507. https://doi.org/10.1039/C5MT00320B
3. Mergeay M, Van Houdt R. *Cupriavidus metallidurans* CH34, a historical perspective on its discovery, characterization and metal resistance. *FEMS Microbiol Ecol* 2021;**97**:fiaa247. https://doi.org/10.1093/femsec/fiaa247
4. Van Houdt R, Monsieurs P, Mijnendonckx K *et al.* Variation in genomic islands contribute to genome plasticity in *Cupriavidus metallidurans*. *BMC Genomics* 2012;**13**:111. https://doi.org/10.1186/1471-2164-13-111
5. Van Houdt R, Monchy S, Leys N *et al.* New mobile genetic elements in *Cupriavidus metallidurans* CH34, their possible roles and occurrence in other bacteria. *Antonie Van Leeuwenhoek* 2009;**96**:205–26. https://doi.org/10.1007/s10482-009-9345-4
6. Monchy S, Benotmane MA, Janssen P *et al.* Plasmids pMOL28 and pMOL30 of *Cupriavidus metallidurans* are specialized in the maximal viable response to heavy metals. *J Bacteriol* 2007;**189**:7417–25. https://doi.org/10.1128/JB.00375-07
7. Große C, Kohl T, Herzberg M *et al.* Loss of mobile genomic islands in metal resistant, hydrogen-oxidizing *Cupriavidus metallidurans*. *Appl Environ Microb* 2022;**88**:e0204821. https://doi.org/10.1128/aem.02048-21
8. Große C, Grau J, Große I *et al.* Importance of RpoD- and non-RpoD-dependent expression of horizontally acquired genes in *Cupriavidus metallidurans*. *Microbiol Spectr* 2022;**10**:e0012122. https://doi.org/10.1128/spectrum.00121-22
9. Argüello JM, Eren E, Gonzalez-Guerrero M. The structure and function of heavy metal transport P-1B-ATPases. *Biometals* 2007;**20**:233–48. https://doi.org/10.1007/s10534-006-9055-6
10. Fagan MJ, Saier MH, Jr. P-type ATPases of eukaryotes and bacteria: sequence comparisons and construction of phylogenetic trees. *J Mol Evol* 1994;**38**:57–99. https://doi.org/10.1007/BF00175496
11. Paulsen IT, Saier MH, Jr. A novel family of ubiquitous heavy metal ion transport proteins. *J Membr Biol* 1997;**156**:99–103. https://doi.org/10.1007/s002329900192
12. Nies DH. RND-efflux pumps for metal cations. In: Yu EW, Zhang Q Brown MHs (eds), *Microbial Efflux Pumps: Current Research*. Norfolk: Caister Academic Press, 2013, 79–122.
13. Goldberg M, Pribyl T, Juhnke S *et al.* Energetics and topology of CzcA, a cation/proton antiporter of the RND protein family. *J Biol Chem* 1999;**274**:26065–70. https://doi.org/10.1074/jbc.274.37.26065
14. Zgurskaya HI, Nikaido H. Bypassing the periplasm: reconstitution of the AcrAB multidrug efflux pump of *Escherichia coli*. *Proc Natl Acad Sci USA* 1999;**96**:7190–5. https://doi.org/10.1073/pnas.96.13.7190
15. Su CC, Long F, Zimmermann MT *et al.* Crystal structure of the CusBA heavy-metal efflux complex of *Escherichia coli*. *Nature* 2011;**470**:558–62. https://doi.org/10.1038/nature09743
16. Long F, Su CC, Zimmermann MT *et al.* Crystal structures of the CusA efflux pump suggest methionine-mediated metal transport. *Nature* 2010;**467**:484–8. https://doi.org/10.1038/Nature09395
17. Grass G, Rensing C. Genes involved in copper homeostasis in *Escherichia coli*. *J Bacteriol* 2001;**183**:2145–7. https://doi.org/10.1128/JB.183.6.2145-2147.2001
18. Scherer J, Nies DH. CzcP is a novel efflux system contributing to transition metal resistance in *Cupriavidus metallidurans* CH34. *Mol Microbiol* 2009;**73**:601–21. https://doi.org/10.1111/j.1365-2958.2009.06792.x
19. Hirth N, Gerlach MS, Wiesemann N *et al.* Full copper resistance in *Cupriavidus metallidurans* requires the interplay of many resistance systems. *Appl Environ Microb* 2023;**89**:e0056723. https://doi.org/10.1128/aem.00567-23
20. Kim E-H, Nies DH, McEvoy M *et al.* Switch or funnel: how RND-type transport systems control periplasmic metal homeostasis. *J Bacteriol* 2011;**193**:2381–7. https://doi.org/10.1128/JB.01323-10
21. Ucisik MN, Chakravorty DK, Merz KM. Models for the metal transfer complex of the N-terminal region of CusB and CusF. *Biochemistry* 2015;**54**:4226–35. https://doi.org/10.1021/acs.biochem.5b00195
22. Padilla-Benavides T, Thompson AMG, McEvoy MM *et al.* Mechanism of ATPase-mediated Cu^{+} export and delivery to periplasmic chaperones: the interaction of *Escherichia coli* CopA and CusF. *J Biol Chem* 2014;**289**:20492–501. https://doi.org/10.1074/jbc.M114.577668
23. Bagai I, Rensing C, Blackburn NJ *et al.* Direct metal transfer between periplasmic proteins identifies a bacterial copper chaperone. *Biochemistry* 2008;**47**:11408–14. https://doi.org/10.1021/bi801638m
24. Loftin IR, Franke S, Roberts SA *et al.* A novel copper-binding fold for the periplasmic copper resistance protein CusF. *Biochemistry* 2005;**44**:10533–40. https://doi.org/10.1021/bi050827b
25. Nies DH, Schleuder G, Galea D *et al.* A flow equilibrium of zinc in cells of *Cupriavidus metallidurans*. *J Bacteriol* 2024;**206**:e0008024. https://doi.org/10.1128/jb.00080-24
26. Kwiatos N, Waldron KJ. In a state of flux: new insight into the transport processes that maintain bacterial metal homeostasis. *J Bacteriol* 2024;**206**:e0014624.https://doi.org/10.1128/jb.00146-24
27. Osman D, Robinson NJ. Protein metalation in a nutshell. *FEBS Lett* 2023;**597**:141–50. https://doi.org/10.1002/1873-3468.14500
28. Waldron KJ, Rutherford JC, Ford D *et al.* Metalloproteins and metal sensing. *Nature* 2009;**460**:823–30. https://doi.org/10.1038/nature08300
29. Herzberg M, Bauer L, Kirsten A *et al.* Interplay between seven secondary metal transport systems is required for full metal resistance of *Cupriavidus metallidurans*. *Metallomics* 2016;**8**:313–26. https://doi.org/10.1039/C5MT00295H
30. Grosse C, Herzberg M, Schüttau M *et al.* Characterization of the Δ7 mutant of *Cupriavidus metallidurans* with deletions of seven secondary metal uptake systems. *mSystems* 2016;**1**:e00004–16. https://doi.org/10.1128/mSystems.00004-16
31. Kirsten A, Herzberg M, Voigt A *et al.* Contributions of five secondary metal uptake systems to metal homeostasis of

Cupriavidus metallidurans CH34. *J Bacteriol* 2011;**193**:4652–63. https://doi.org/10.1128/JB.05293-11
32. Legatzki A, Anton A, Grass G *et al.* Interplay of the Czc-system and two P-type ATPases in conferring metal resistance to *Ralstonia metallidurans*. *J Bacteriol* 2003;**185**:4354–61. https://doi.org/10.1128/JB.185.15.4354-4361.2003
33. Schulz V, Schmidt-Vogler C, Strohmeyer P *et al.* Behind the shield of Czc: ZntR controls expression of the gene for the zinc-exporting P-type ATPase ZntA in *Cupriavidus metallidurans*. *J Bacteriol* 2021;**203**:e00052–21. https://doi.org/10.1128/JB.00052-21
34. Huang S, Liu X, Wang D *et al.* Structural basis for the selective Pb(II) recognition of metalloregulatory protein PbrR691. *Inorg Chem* 2016;**55**:12516–9. https://doi.org/10.1021/acs.inorgchem.6b02397
35. Taghavi S, Lesaulnier C, Monchy S *et al.* Lead(II) resistance in *Cupriavidus metallidurans* CH34: interplay between plasmid and chromosomally-located functions. *Antonie Van Leeuwenhoek* 2009;**96**:171–82. https://doi.org/10.1007/s10482-008-9289-0
36. Julian DJ, Kershaw CJ, Brown NL *et al.* Transcriptional activation of MerR family promoters in *Cupriavidus metallidurans* CH34. *Antonie Van Leeuwenhoek* 2009;**96**:149–59. https://doi.org/10.1007/s10482-008-9293-4
37. Borremans B, Hobman JL, Provoost A *et al.* Cloning and functional analysis of the *pbr* lead resistance determinant of *Ralstonia metallidurans* CH34. *J Bacteriol* 2001;**183**:5651–8. https://doi.org/10.1128/JB.183.19.5651-5658.2001
38. Outten CE, O'Halloran TV. Femtomolar sensitivity of metalloregulatory proteins controlling zinc homeostasis. *Science* 2001;**292**:2488–92. https://doi.org/10.1126/science.1060331
39. Outten CE, Outten FW, O'Halloran TV. DNA distortion mechanism for transcriptional activation by ZntR, a Zn(II)-responsive MerR homologue in *Escherichia coli*. *J Biol Chem* 1999;**274**:37517–24. https://doi.org/10.1074/jbc.274.53.37517
40. Brocklehurst KR, Hobman JL, Lawley B *et al.* ZntR is a Zn(II)-responsive MerR-like transcriptional regulator of *zntA* in *Escherichia coli*. *Mol Microbiol* 1999;**31**:893–902. https://doi.org/10.1046/j.1365-2958.1999.01229.x
41. Trepreau J, Girard E, Maillard AP *et al.* Structural basis for metal sensing by CnrX. *J Mol Biol* 2011;**408**:766–79. https://doi.org/10.1016/j.jmb.2011.03.014
42. Pompidor G, Maillard AP, Girard E *et al.* X-ray structure of the metal-sensor CnrX in both the apo- and copper-bound forms. *FEBS Lett* 2008;**582**:3954–8. https://doi.org/10.1016/j.febslet.2008.10.042
43. Tibazarwa C, Wuertz S, Mergeay M *et al.* Regulation of the *cnr* cobalt and nickel resistance determinant of *Ralstonia eutropha* (*Alcaligenes eutrophus*) CH34. *J Bacteriol* 2000;**182**:1399–409. https://doi.org/10.1128/JB.182.5.1399-1409.2000
44. Maillard AP, Kuennemann S, Grosse C *et al.* Response of CnrX from *Cupriavidus metallidurans* CH34 to nickel binding. *Metallomics* 2015;**7**:622–31. https://doi.org/10.1039/c4mt00293h
45. Trepreau J, Grosse C, Mouesca J-M *et al.* Metal sensing and signal transduction by CnrX from *Cupriavidus metallidurans* CH34: role of the only methionine assessed by a functional, spectroscopic, and theoretical study. *Metallomics* 2014;**6**:263–73. https://doi.org/10.1039/C3MT00248A
46. Schulz V, Galea D, Schleuder G *et al.* The efflux system CdfX exports zinc that cannot be transported by ZntA in *Cupriavidus metallidurans*. *J Bacteriol* 2024;**206**:e0029924. https://doi.org/10.1128/jb.00299-24
47. Große C, Scherer J, Schleuder G *et al.* Interplay between two-component regulatory systems is involved in control of *Cupriavidus metallidurans* metal resistance genes. *J Bacteriol* 2023;**205**:e0034322. https://doi.org/10.1128/jb.00343-22
48. Juhnke S, Peitzsch N, Hübener N *et al.* New genes involved in chromate resistance in *Ralstonia metallidurans* strain CH34. *Arch Microbiol* 2002;**179**:15–25. https://doi.org/10.1007/s00203-002-0492-5
49. Nies DH, Koch S, Wachi S *et al.* CHR, a novel family of prokaryotic proton motive force-driven transporters probably containing chromate/sulfate transporters. *J Bacteriol* 1998;**180**:5799–802. https://doi.org/10.1128/JB.180.21.5799-5802.1998
50. Nies A, Nies DH, Silver S. Nucleotide sequence and expression of a plasmid-encoded chromate resistance determinant from *Alcaligenes eutrophus*. *J Biol Chem* 1990;**265**:5648–53. https://doi.org/10.1016/S0021-9258(19)39411-6
51. Cervantes C, Silver S. Plasmid chromate resistance and chromium reduction. *Plasmid* 1992;**27**:65–71. https://doi.org/10.1016/0147-619X(92)90007-W
52. Bhattacharjee H, Rosen BP. Arsenic metabolism in prokaryotic and eukaryotic microbes. In: Nies DH Silver SS (eds), *Molecular Microbiology of Heavy Metals*. Berlin: Springer-Verlag, 2007, 371–406.
53. Oden KL, Gladysheva TB, Rosen BP. Arsenate reduction mediated by the plasmid-encoded ArsC protein is coupled to glutathione. *Mol Microbiol* 1994;**12**:301–6. https://doi.org/10.1111/j.1365-2958.1994.tb01018.x
54. Tisa LS, Rosen BP. Molecular characterization of an anion pump. The ArsB protein is the membrane anchor for the ArsA protein. *J Biol Chem* 1990;**265**:190–4. https://doi.org/10.1016/S0021-9258(19)40214-7
55. Silver S, Hobman JL. Mercury microbiology: resistance systems, environmental aspects, methylation, and human health. In: Nies DH SS Silver (eds), *Molecular Microbiology of Heavy Metals*. Berlin: Springer, 2007, 357–70.
56. Wiesemann N, Bütof L, Herzberg M *et al.* Synergistic toxicity of copper and gold compounds in *Cupriavidus metallidurans*. *Appl Environ Microb* 2017;**83**:e01679–17. https://doi.org/10.1128/AEM.01679-17
57. Große C, Poehlein A, Blank K *et al.* The third pillar of metal homeostasis in *Cupriavidus metallidurans* CH34: preferences are controlled by extracytoplasmic functions sigma factors. *Metallomics* 2019;**11**:291–316. https://doi.org/10.1039/C8MT00299A
58. Große C, Grau J, Herzberg M *et al.* Antisense transcription is associated with expression of metal resistance determinants in *Cupriavidus metallidurans* CH34. *Metallomics* 2024;**16**:mfae057. https://doi.org/10.1093/mtomcs/mfae057
59. Thieme D, Neubauer P, Nies DH *et al.* Sandwich hybridization assay for sensitive detection of dynamic changes in mRNA transcript levels in crude *Escherichia coli* cell extracts in response to copper ions. *Appl Environ Microb* 2008;**74**:7463–70. https://doi.org/10.1128/aem.01370-08
60. van der Lelie D, Schwuchow T, Schwidetzky U *et al.* Two component regulatory system involved in transcriptional control of heavy metal homoeostasis in *Alcaligenes eutrophus*. *Mol Microbiol* 1997;**23**:493–503. https://doi.org/10.1046/j.1365-2958.1997.d01-1866.x
61. Herzberg M, Dobritzsch D, Helm S *et al.* The zinc repository of *Cupriavidus metallidurans*. *Metallomics* 2014;**6**:2157–65. https://doi.org/10.1039/C4MT00171K
62. Kanehisa M, Goto S, Hattori M *et al.* From genomics to chemical genomics: new developments in KEGG. *Nucleic Acids Res* 2006;**34**:D354–7. https://doi.org/10.1093/nar/gkj102

63. Kanehisa M, Sato Y. KEGG Mapper for inferring cellular functions from protein sequences. *Protein Sci* 2020;**29**:28–35. https://doi.org/10.1002/pro.3711
64. Waldron KJ, Firbank SJ, Dainty SJ *et al.* Structure and metal loading of a soluble periplasm cuproprotein. *J Biol Chem* 2010;**285**:32504–11. https://doi.org/10.1074/jbc.M110.153080
65. Macomber L, Imlay JA. The iron-sulfur clusters of dehydratases are primary intracellular targets of copper toxicity. *Proc Natl Acad Sci USA* 2009;**106**:8344–9. https://doi.org/10.1073/Pnas.0812808106
66. Mobley HLT, Rosen BP. Energetics of plasmid-mediated arsenate resistance in *Escherichia coli*. *Proc Natl Acad Sci USA* 1982;**79**:6119–22. https://doi.org/10.1073/pnas.79.20.6119
67. Chen CM, Misra TK, Silver S *et al.* Nucleotide sequence of the structural genes for an anion pump. The plasmid-encoded arsenical resistance operon. *J Biol Chem* 1986;**261**:15030–8. https://doi.org/10.1016/S0021-9258(18)66824-3
68. Schulz V, Galea D, Herzberg M *et al.* Protecting the Achilles heel: three FolE_I-type GTP-cyclohydrolases needed for full growth of metal resistant *Cupriavidus metallidurans* under a variety of conditions. *J Bacteriol* 2024;**206**:e0039523. https://doi.org/10.1128/jb.00395-23
69. Wagner EGH, Altuvia S, Romby P. Antisense RNAs in bacteria and their genetic elements. *Homology Effects* 2002;**46**:361–98. https://doi.org/10.1016/S0065-2660(02)46013-0
70. Eckweiler D, Häussler S. Antisense transcription in. *Microbiology (Reading)* 2018;**164**:889–95. https://doi.org/10.1099/mic.0.000664
71. Mergeay M, Nies D, Schlegel HG *et al. Alcaligenes eutrophus* CH34 is a facultative chemolithotroph with plasmid-bound resistance to heavy metals. *J Bacteriol* 1985;**162**:328–34. https://doi.org/10.1128/jb.162.1.328-334.1985
72. Saier MH, Tam R, Reizer A *et al.* Two novel families of bacterial membrane proteins concerned with nodulation, cell division and transport. *Mol Microbiol* 1994;**11**:841–7. https://doi.org/10.1111/j.1365-2958.1994.tb00362.x
73. Tseng T-T, Gratwick KS, Kollman J *et al.* The RND superfamily: an ancient, ubiquitous and diverse family that includes human disease and development proteins. *J Mol Microbiol Biotechnol* 1999;**1**:107–25.
74. Dinh T, Paulsen IT, Saier MHJ. A family of extracytoplasmic proteins that allow transport of large molecules across the outer membranes of gram-negative bacteria. *J Bacteriol* 1994;**176**:3825–31. https://doi.org/10.1128/jb.176.13.3825-3831.1994
75. Higgins MK, Bokma E, Koronakis E *et al.* Structure of the periplasmic component of a bacterial drug efflux pump. *Proc Natl Acad Sci USA* 2004;**101**:9994–9. https://doi.org/10.1073/pnas.0400375101
76. De Angelis F, Lee JK, O'Connell JD *et al.* Metal-induced conformational changes in ZneB suggest an active role of membrane fusion proteins in efflux resistance systems. *Proc Natl Acad Sci USA* 2010;**107**:11038–43. https://doi.org/10.1073/Pnas.1003908107
77. Klenotic PA, Yu EW. Structural analysis of resistance-nodulation cell division transporters. *Microbiol Mol Biol Rev* 2024;**88**:e0019823. https://doi.org/10.1128/mmbr.00198-23
78. Nies DH. How cells control zinc homeostasis. *Science* 2007;**317**:1695–6. https://doi.org/10.1126/science.1149048
79. Duan J, Cloete R, Loock JC *et al.* Biogenic-to-lithogenic handoff of particulate Zn affects the Zn cycle in the Southern Ocean. *Science* 2024;**384**:1235–40. https://doi.org/10.1126/science.adh8199
80. Nies DH, Silver S. Plasmid-determined inducible efflux is responsible for resistance to cadmium, zinc, and cobalt in *Alcaligenes eutrophus*. *J Bacteriol* 1989;**171**:896–900. https://doi.org/10.1128/jb.171.2.896-900.1989
81. Nies DH, Nies A, Chu L *et al.* Expression and nucleotide sequence of a plasmid-determined divalent cation efflux system from *Alcaligenes eutrophus Proc Natl Acad Sci USA* 1989;**86**:7351–5. https://doi.org/10.1073/pnas.86.19.7351
82. Nies DH, Rehbein G, Hoffmann T *et al.* Paralogs of genes encoding metal resistance proteins in *Cupriavidus metallidurans* strain CH34. *J Mol Micobiol Biotechnol* 2006;**11**:82–93.
83. Herzberg M, Bauer L, Nies DH. Deletion of the *zupT* gene for a zinc importer influences zinc pools in *Cupriavidus metallidurans* CH34. *Metallomics* 2014;**6**:421–36. https://doi.org/10.1039/C3MT00267E
84. Bütof L, Schmidt-Vogler C, Herzberg M *et al.* The components of the unique Zur regulon of *Cupriavidus metallidurans* mediate cytoplasmic zinc handling. *J Bacteriol* 2017;**199**:e00372–17. https://doi.org/10.1128/JB.00372-17
85. Schmidt C, Schwarzenberger C, Grosse C *et al.* FurC regulates expression of *zupT* for the central zinc importer ZupT of *Cupriavidus metallidurans*. *J Bacteriol* 2014;**196**:3461–71. https://doi.org/10.1128/JB.01713-14
86. Legatzki A, Franke S, Lucke S *et al.* First step towards a quantitative model describing Czc-mediated heavy metal resistance in *Ralstonia metallidurans*. *Biodegradation* 2003;**14**:153–68. https://doi.org/10.1023/A:1024043306888
87. Munkelt D, Grass G, Nies DH. The chromosomally encoded cation diffusion facilitator proteins DmeF and FieF from *Wautersia metallidurans* CH34 are transporters of broad metal specificity. *J Bacteriol* 2004;**186**:8036–43. https://doi.org/10.1128/JB.186.23.8036-8043.2004
88. Thomason MK, Storz G. Bacterial antisense RNAs: how many are there, and what are they doing? *Annu Rev Genet* 2010;**44**:167–88. https://doi.org/10.1146/annurev-genet-102209-163523
89. Georg J, Hess WR. *cis*-antisense RNA, another level of gene regulation in bacteria. *Microbiol Mol Biol Rev* 2011;**75**:286–300. https://doi.org/10.1128/Mmbr.00032-10
90. Sesto N, Wurtzel O, Archambaud C *et al.* The excludon: a new concept in bacterial antisense RNA-mediated gene regulation. *Nat Rev Micro* 2013;**11**:75–82. https://doi.org/10.1038/nrmicro2934
91. Lasa I, Toledo-Arana A, Dobin A *et al.* Genome-wide antisense transcription drives mRNA processing in bacteria. *Proc Natl Acad Sci USA* 2011;**108**:20172–7. https://doi.org/10.1073/pnas.1113521108
92. Rensing C, Kües U, Stahl U *et al.* Expression of bacterial mercuric ion reductase in *Saccharomyces cerevisiae*. *J Bacteriol* 1992;**174**:1288–92. https://doi.org/10.1128/jb.174.4.1288-1292.1992
93. Hughes CS, Moggridge S, Muller T *et al.* Single-pot, solid-phase-enhanced sample preparation for proteomics experiments. *Nat Protoc* 2019;**14**:68–85. https://doi.org/10.1038/s41596-018-0082-x
94. Tyanova S, Temu T, Cox J. The MaxQuant computational platform for mass spectrometry-based shotgun proteomics. *Nat Protoc* 2016;**11**:2301–19. https://doi.org/10.1038/nprot.2016.136
95. Sundararaj S, Guo A, Habibi-Nazhad B *et al.* The CyberCell Database (CCDB): a comprehensive, self-updating, relational database to coordinate and facilitate in silico modeling of *Escherichia coli*. *Nucleic Acids Res* 2004;**32**:D293–5. https://doi.org/10.1093/nar/gkh108
96. Neidhardt FC, Umbarger HE. Chemical composition of *Escherichia coli*. In: Neidhardt FCS (ed), *Escherichia coli and Salmonella: Cellular and Molecular Biology*. Washington: American Society of Microbiology, 1996.

97. Goris J, De Vos P, Coenye T *et al.* Classification of metal-resistant bacteria from industrial biotopes as *Ralstonia campinensis* sp. nov., *Ralstonia metallidurans* sp. nov. and *Ralstonia basilensis* Steinle et al. 1998 emend. *Int J Syst Evol Microbiol* 2001;**51**:1773–82. https://doi.org/10.1099/00207713-51-5-1773

98. Wiesemann N, Mohr J, Grosse C *et al.* Influence of copper resistance determinants on gold transformation by *Cupriavidus metallidurans* strain CH34. *J Bacteriol* 2013;**195**:2298–308. https://doi.org/10.1128/JB.01951-12

Received: August 29, 2024. **Accepted:** November 16, 2024

Discussion

5. The physiological range of zinc homeostasis in *Cupriavidus metallidurans*

5.1 Adjustment of the cellular zinc content

The zinc resistant betaproteobacterium *C. metallidurans* is a survivalist in zinc-contaminated environments, but is nevertheless able to maintain its zinc homeostasis. Three different aspects are pivotal to zinc homeostasis in this betaproteobacterium: i) the cellular zinc content, ii) the transportome, and iii) the zinc repository. *C. metallidurans* AE104 is able to accumulate intracellularly various zinc quotas over a wide range of extracellular zinc concentrations. The zinc quota, or the cellular zinc content, referred to is defined as the intracellular total zinc concentration, which is measured by inductively-coupled mass-spectrometry (ICP-MS), and is quantified and expressed in units of concentrations, in this case atoms per cell (Outten and O'Halloran, 2001; Chandrangsu *et al.,* 2017). The zinc quota does not offer any information on the intracellular bioavailability of the zinc ions, zinc-protein associations, binding affinities or coordination geometries, but gives the total amount of this transition metal cation that has accumulated at a given timepoint inside the cell.

In the studies presented in this thesis, the zinc quotas were determined in the middle of the exponential phase of growth, both for wild-type strain CH34, and AE104 as parent strain for the respective mutant derivatives. Cells were cultivated in Tris-buffered minimal medium provided with different zinc chloride concentrations, from low nanomolar zinc concentrations of ≈35 nM $ZnCl_2$ to 200 nM $ZnCl_2$, or they were additionally challenged with micromolar zinc concentrations. AE104 cells accumulate 20.000 to 30.000 zinc atoms per cell when the exogenous zinc concentration provided in the Tris minimal medium is 35 nM $ZnCl_2$ (Nies *et al*., 2024; Galea *et al*., 2024; Schulz *et al*., 2024). The Δ*zupT* cells accumulated 14.000 to 30.000 zinc ions per cell, and in one instance 7.000 ions per cell, which can indicate the minimum amount of zinc ions needed by *C. metallidurans* (Galea *et al*., 2024). At the other end of the spectrum, the zinc content of AE104 cells could be increased to 120.000 - 150.000 - 250.000 zinc atoms per cell, when the cells are challenged with 1, 10 or 100 µM $ZnCl_2$ (Herzberg *et al*., 2014; Nies *et al*., 2024). Reaching an intracellular zinc concentration of 250.000 zinc atoms is possible in a knock-out mutant, Δ*e4*, which lacks the Zn^{2+}/Cd^{2+}- exporting P-type ATPases ZntA,

CadA and the Co^{2+}/Fe^{2+}-exporting CDF proteins, and when challenged with 10 µM exogenous $ZnCl_2$ (Herzberg *et al*., 2014). This zinc quota indicates the maximum amount of zinc ions *C. metallidurans* is able to handle intracellularly (Herzberg *et al*., 2014).

The overall zinc concentration gradient and the resulting intracellular metal ion states this betaproteobacterium is able to deal with is more nuanced (Galea *et al*., 2024) and will be discussed in more detail below. However, the abovementioned cellular zinc contents describe two extremes that the AE104 strain is able to deal with and defines the upper and lower limits of its zinc homeostatic spectrum. Nevertheless, *C. metallidurans* AE104 cells accumulate 70.000 to 80.000 zinc atoms per cell when the supplemented zinc concentration in the Tris minimal medium is 200 nM $ZnCl_2$. This is described as an optimum zinc quota and can be understood as the zinc-replete or zinc-sufficient state of *C. metallidurans* (Herzberg *et al*., 2014; Nies *et al*., 2024; Galea *et al*., 2024; Schulz *et al*., 2024).

C. metallidurans AE104 is thus able to handle different external zinc concentrations and adjusts its cellular zinc content accordingly. Zinc-insufficiency results in an accumulation of a minimum of 20.000 zinc atoms per cell, while a maximum zinc content is reached at 250.000 zinc atoms. Ideally, however, the zinc content of AE104 cells in zinc-sufficiency is in the range of 70.000 zinc atoms per cell. It is important to emphasize that *C. metallidurans* does not accumulate only zinc ions intracellularly and the quota of transition metals it accumulates is represented by: 10.000.000 Mg; 700.000 Fe; 70.000 Zn; 7.000 Cu; 4.000 Co; 3.000 Ni; and 300 Mn ions per cell (Galea *et al*., 2024).

The association of the cognate metal ion and its target protein is vital for any living cell. This process, known as metalation, happens ideally if optimum bioavailable concentrations are maintained intracellularly. As seen in *C. metallidurans*, and in other bacteria, the cytosol is a heterogenous environment for divalent transition metal cations. As a consequence, cells need to ensure optimal concentrations for each one of these. How does then, a metal resistant betaproteobacterium like *C. metallidurans* CH34, isolated from, and adapted to survive in, metal-contaminated environments ensure an optimal and efficient metalation process, and avoid mis-metalation reactions?

5.2 Transport *via* a kinetical flow-equilibrium – pivotal to zinc homeostasis

The primary goal of the homeostatic processes is to control intracellular metal ion concentrations within narrow limits. This should be, on the one hand, optimal for supplying enough metal ions to fulfil the requirements of metalloproteins, but, on the other hand, should not exceed an upper limit that would result in unspecific and deleterious effects when bound to other metalloproteins, in the process known as mis-metalation. This control involves distinct activities: i) cells need to sense whether their internal metal ion concentration is kept within narrow limits or when changes occur; and ii) they need to use several strategies to attain and then maintain these concentrations. In the homeostatic control of metal ions, metal sensors, metal transporters and cytosolic metal-binding proteins take central roles.

Metalation and mis-metalation reactions are especially ruled by the Irving-Williams, which dictates a preferential order for certain divalent metal cations to bind to proteins, at least *in vitro*. Cellular systems have solved this problem by employing a homeostatic control for each metal ion, which places metalloregulatory proteins at the apex of metal homeostasis. Metalloregulatory proteins function by using a mechanism known as “the set-point model”, which involves a fine-tuning of the intracellular metal concentrations that keeps their bioavailability in inverse proportion to the tightest binding metal ions dictated by the Irving-William series (Osman *et al*., 2019).

Thus, copper will be found in very low concentrations inside the cytosol, since its chemistry is prone to bind and mis-metalate metalloproteins with high affinity. This is why copper homeostasis in many bacteria, including *C. metallidurans* relies mainly on periplasmic processes in which combined sequestration, oxidation of Cu^{+} to Cu^{2+}, and export processes actively remove excess copper ions from the cytoplasm as soon as they might be imported into this cellular compartment (Hirth *et al*., 2023). Zinc and cupric ions are close to each other in the Irving Williams series and they have similar high affinity for proteins. However, in contrast to copper, the intracellular requirement for zinc, is significantly higher (Outten and O’Halloran, 2001).

Along with their capacity to sense intracellular metal ion concentrations and modulate gene expression, metalloregulatory proteins additionally show preferences for certain amino acids that form the metal-binding sites for their cognate metal ion to solve the

problem of compatibility and competition of cognate and noncognate metal ions for the same metalloregulator (Lenner *et al.,* 2025). This allows them in return, to control the expression of those genes which encode proteins needed to maintain the homeostasis of the metal they have evolved to bind. The transcriptional regulation of genes encoding transport systems is tightly linked with the set point model of the metalloregulatory proteins. Metal sensors are, thus, placed at the apex of metal homeostasis because their affinity for their cognate metal ions defines the intracellular metal availabilities (Osman *et al*., 2019). I

In the case of zinc homeostasis, these affinities have been experimentally determined in several organisms and follow the same principle. This principle is that both prokaryotic and eukaryotic cells contain sensors whose affinities for zinc ions are generally low, ranging from the femtomolar to the low nanomolar range. For instance, the ZAP1 sensor regulates zinc homeostasis in the case of zinc deficiency in *Saccharomyces cerevisiae* and is a transcription factor that has three functional domains, and seven C_2H_2 zinc fingers (ZF) motifs, two of which bind Zn^{2+} ions with low nanomolar affinities with measured K_D of ≈0.2 nM and ≈4 nM (Lyons *et al*., 2000; Qiao *et al*., 2006). Another example is the zinc-responsive transcriptional repressor protein SmtB from the unicellular cyanobacterium *Synechococcus* PCC7942, which binds Zn^{2+} with an affinity in the 10^{-11} – 10^{-12} M range, indicating that cytosolic bioavailable zinc ion levels should be maintained at a low level (VanZile *et al*., 2000*).* In *A. baumannii*, the zinc uptake regulator Zur was reported to bind zinc in its regulatory metal site with a determined dissociation constant K_{Zn} of 6.0 ± 2.2 x 10^{-12} M and defining a low bioavailable cytosolic Zn^{2+} concentration of ≈ 6 x 10^{-13} M (Kim *et al*., 2024). In *E. coli*, the bioavailable zinc concentration for a half-maximum transcriptional response was determined to be ≈ 10^{-15} M and both zinc regulators, ZntR and Zur, become saturated when the intracellular zinc concentrations reach femtomolar levels, 2.0 ± 0.1 x 10^{-16} M for Zur, and 11.5 ± 1.3 x 10^{-16} M for ZntR (Outten and O'Halloran, 2001).

C. metallidurans also has several metal sensors to set the levels of zinc to optimal concentrations. The metalloregulatory proteins Zur, ZntR and CadR are responsible for the cytoplasmic zinc sensing and handling of zinc, whereas the two-component system CzcRS is operational in the wild-type CH34 strain to sense high periplasmic zinc concentrations (Schmidt *et al*., 214; Schulz *et al*., 2021). Zur is responsible for inducing high affinity uptake for zinc ions in the event of zinc starvation, and ZntR is responsible

for inducing efflux of zinc ions in the case of zinc excess in the plasmid-free strain AE104. Both of these metalloregulatory proteins are operational and ensure a state of zinc repletion when cells are cultivated in the presence of 200 nM $ZnCl_2$ in Tris minimal medium, where the cells accumulate an optimum zinc quota of 70.000 zinc atoms (Galea *et al*., 2024; Große *et al*., 2024). Transport processes across the inner membrane are essential to maintaining zinc homeostasis in bacterial cells and their main control is achieved through transcriptional regulation of gene expression, augmented by other processes, such as flux control, or post-transcriptional modifications (Elston *et al*., 2023).

In *C. metallidurans* it has been demonstrated that a kinetical flow-equilibrium of zinc ions is at the core of zinc homeostasis (Nies *et al*., 2024). This means that zinc ions are continuously transported across the inner membrane, simultaneously in both directions (Nies *et al*., 2024). The kinetical flow-equilibrium, which is based on combined import and efflux reactions, is responsible for adjusting the cellular zinc content of zinc-replete AE104 cells. Physiological data generated by studying a multitude of knock-out mutants has clarified the roles of each uptake and efflux system, which contribute to the metal homeostasis of this bacterium. Moreover, the flow-equilibrium also adjusts the zinc content of cells that suffer from zinc starvation or zinc and magnesium starvation, as well. This makes the kinetical flow-equilibrium of zinc ions a core process among the processes governing zinc homeostatic control in this betaproteobacterium. The rates of import and efflux of ^{65}Zn were determined in zinc-replete AE104 cells, cultivated in the presence of 200 nM $ZnCl_2$, in a “pulse-chase” procedure (Nies *et al.,* 2024). These data indicated that zinc-replete AE104 cells continuously imported and exported ^{65}Zn in order to adjust its cellular zinc content. A kinetical flow equilibrium enabled AE104 cells to adjust the cytosolic zinc levels, irrespective of the external zinc availability they encountered. The broad-substrate, low-specificity import systems, as well as the high-affinity zinc importer ZupT, influence import of zinc ions (Nies *et al*., 2024). Our findings show that ZupT is responsible for 42% of the initial zinc import in zinc-replete AE104 cells, whereas its contribution increased to 70% in zinc-starved cells.

In conclusion, transport reactions are essential for the adjustment of the cellular zinc pool. In addition to other mechanisms, which regulate and control transport, *C. metallidurans* additionally uses a kinetical flow-equilibrium based on continuous import and export of zinc ions to adjust its cellular zinc content in response to the changing metal availability and they achieve this in a relatively short period of time. This allows gene expression and

protein production to become rapidly activated upon encountering higher metal concentrations, for instance (Galea *et al*., 2024).

5.3 Intracellular zinc pools

Irrespective of the zinc availability *C. metallidurans* encounters, the zinc cellular content is adjusted and managed in such a way that the metalation of zinc-dependent proteins is maintained, as well as the metalation of other metalloproteins that require different metal ion cofactors. It is widely accepted that a large portion of metalloproteins acquire their cognate metal ion from cellular metal pools in the cytosol. Thus, in these cellular metal pools optimal bio-availabilities need to be maintained, to avoid mis-metalation reactions in case the bioavailable concentration exceeds the optimum one, or the lack of the cognate metal ion cofactors when the bioavailability is below the optimal threshold. As zinc quotas, or those of any other transition metal, change when cells are exposed to different metal concentrations, the bioavailability of that metal pool is also subjected to change. This means that the bioavailable concentration in these cellular metal pools is not static, but undergoes dynamic, transient changes. Intracellular fluctuations of zinc ions, nevertheless, mean that for a certain time the cytosolic metal concentration needs to be buffered. To avoid such a potentially detrimental effect, cells need to sustain these two parallel processes: one is the perpetual metalation of zinc-proteins, or other metalloproteins, while maintaining the optimal bioavailable zinc concentrations in the cytosol. For instance, *C. metallidurans* distributes its zinc ions into two functional zinc pools that aid in maintenance of zinc homeostasis (Herzberg *et al*., 2014). One zinc pool has low-specificity for incoming zinc ions and can be filled with zinc imported by any importer of the zinc transportome, while the second zinc pool serves for the metalation of zinc-dependent proteins.

Experimental evidence that advances the understanding of zinc pools and the intracellular fluctuations of zinc ions in *C. metallidurans* has been provided (Nies *et al*., 2024). This was achieved by incubating AE104 cells with isotope-enriched ^{67}Zn to discriminate between zinc ions which are present in the cell with a natural isotope composition, and isotope-enriched ^{67}Zn that is imported and accumulated into the cell during the pulse phase. AE104 cells were incubated with various concentrations of isotope-enriched ^{67}Zn and the cellular zinc content was measured by ICP-MS. Addition of 1 µM, 10 µM, and 100 µM ^{67}Zn to cells in the middle of the exponential growth phase

differentiated between the zinc contents with different isotope configurations. Unchallenged zinc-replete AE104 cells contained 90.000 zinc ions in their natural composition. Following the addition of the ^{67}Zn, the resident zinc quota decreased to approximately 40.000 to 50.000 atoms per cell, and it remained unchanged even when the cells were challenged with 1 µM or 100 µM ^{67}Zn. The incoming ^{67}Zn ions were imported and accumulated within the cell, such that a technical ^{67}Zn pool was measured, which contained 55.000 to 135.000 atoms per cell with increasing ^{67}Zn concentrations. As a result, the total zinc content increased from 109.000 atoms to 178.000 atoms.

Two zinc contents were measured in zinc-starved AE104 cells, as well, by using the same incubation with isotope-enriched ^{67}Zn. In this case, however, some differences were noticed. Zinc-starved AE104 cells accumulated a cellular zinc content of around 10.000 zinc atoms per cell (Nies *et al*., 2024). Incoming ^{67}Zn ions were accumulated by zinc-starved AE104 cells in larger numbers than zinc-replete cells, which accounted for 94.000 atoms to 144.000 atoms into ZP2. The overall zinc content of the zinc-starved cells reached 107.000 to 155.000 atoms. However, in zinc starvation conditions, the amount of zinc ions residing in ZP1 did not decrease, but was maintained at a low level of 10.000 atoms, irrespective of the ^{67}Zn concentrations used in the pulse phase. This effect was different when compared with zinc-replete AE104 that firstly decreased approximately 40% of their residing zinc content, and then retained it at similar levels during accumulation of ^{67}Zn ions. Zinc- and magnesium- starved cells showed the same response as the zinc-starved cells (Nies *et al*., 2024). This means that in zinc starvation, 90% of the total cellular zinc content was represented by incoming ^{67}Zn ions while the amount originally measured in ZP1 remained at constant levels of 10.000 ^{64}Zn atoms per cell.

Taken together, two zinc contents could be quantified by measuring the natural residing zinc and incoming ^{67}Zn in all conditions, zinc-replete, zinc-starved, and metal-starved AE104 cells. Residing zinc was measured in the zinc pool 1 and imported ^{67}Zn during the pulse with isotope-enriched ^{67}Zn led to the measurement of the technical zinc pool 2 (ZP2). Additionally, an income of the ^{67}Zn ions resulted in 40% exchange of the residing zinc in the cytosol with the incoming ^{67}Zn ions for zinc-replete cells (Nies *et al*., 2024).

More insight about fluctuations of the zinc ions in *C. metallidurans* was obtained when cells were chased with 100µM non-enriched zinc following incubation with ^{67}Zn. Zinc-

replete AE104 contained 103.000 resident zinc atoms in ZP1 when unchallenged with isotope-enriched zinc. Addition of 1 µM ^{67}Zn led to the accumulation of 27.000 ^{67}Zn ions per cell. Incoming ^{67}Zn ions were accumulated into ZP2 and represented 26% of the total cellular zinc content, while ZP1 was kept at 76.600 zinc atoms per cell. An additional chase with the non-isotope-enriched zinc solution increased the total cellular zinc content to 246.000 zinc atoms. The amount of ZP1 increased considerably from 76.600 to 240.000 atoms per cell and the level of zinc ions in ZP2 decreased from 27.000 to 6.100 zinc atoms. A subsequent export of the zinc ions from ZP2 was noticed also during the chase phase. Zinc -replete AE104 exported 78% of the zinc ions from ZP2 during the chase phase, and zinc-starved cells 70%. This data set indicated the presence of loosely-bound zinc ions that are destined to be exported, and that there is a constant turnover of zinc ions in the cell (Nies *et al*., 2024).

5.3.1 Binding of zinc ions in the cell

In contrast to the zinc ions residing in the low-specificity zinc pool, which can be imported by any general import system, the accumulation and allocation of zinc ions in the tightly-bound zinc pool is strictly dependent on the high-affinity zinc importer ZupT (Herzberg *et al*., 2014). Some zinc-dependent proteins that need to be obligatorily metalated with zinc ions are, for instance, the β' subunit of the DNA-dependent RNA polymerase core (RpoC), certain ribosomal proteins, or essential enzymes such as the GTP-cyclohydrolase I, FolE_1A (Herzberg *et al*., 2014; Schulz *et al*., 2024). In *E. coli*, the RNAP core enzyme contains 5 subunits, RpoA (α), RpoB (β), RpoC (β') and RpoZ (ω), in the following composition $\alpha_2\beta\beta'\omega$, and contains one tightly bound Zn^{2+} in RpoC, and one loosely bound in RpoB (Chen and Powers, 1995). Zinc ions bind tightly to the RpoC subunit in a tetrahedral coordination formed by four cysteine residues, and is necessary as a structural ion to convert a denatured subunit into a compact conformation, and promote assembly with the other RNAP subunits (Markov *et al*., 1999). The 70S ribosome of *E. coli* binds 8 equivalent of zinc per ribosome, four ions are bound by the proteins of the large subunit, L2, L13, L31 and L36, and another four are bound by the ribosomal proteins of the small subunit, S2 and S15-S17 (Hensley *et al*., 2011). *C. metallidurans* contains five zinc-binding ribosomal proteins, one in the large subunit, L2, and the other four in the small subunit, S2, S9, S15 and S17. These were identified in a bottom-up proteomics experiment and quantified to a total number of 40.000 copies per cell, in the proteome of zinc-replete AE104 cells (Galea *et al*., 2024). The zinc-binding ribosomal proteins are a

major intracellular sink for zinc in *C. metallidurans*, and they need available zinc to allow the synthesis of zinc-dependent proteins, for instance, RpoC (Herzberg *et al*., 2014). The GTP-cyclohydrolase type I, FolE_IA, is a strictly zinc-dependent enzyme that plays a central role in the biosynthesis of the essential cofactor tetrahydrofolate (Nichol *et al*., 1985). FolE_1A binds 0.6 Zn per mol per protomer, and the zinc ion binds tightly to this protein because it is not freely exchangeable when the protomer is incubated with the zinc-complexing compound TPEN (Schulz *et al*., 2024). In *E. coli*, the catalytically active zinc is coordinated in FolE_1A to Cys-Cys-His and a water molecule, and presumably in *C. metallidurans*, too, due to the conserved amino acids (Rebelo *et al*., 2003; Schulz *et al*., 2024). Zinc-replete AE104 synthesizes this protein constitutively, and a copy number of 119 proteins per cell was found (Galea *et* al., 2024). This zinc-enzyme might acquire the zinc cofactor as it is being synthesized by the 70S ribosome in this bacterium. The 10.000 zinc atoms measured in ZP1 in zinc-starved AE104 cells might indicate the kinetically-trapped zinc ions in zinc-dependent enzymes at the time of measurement.

The buffering capacity of the cytosol is one vital factor which influences the bioavailable zinc concentrations (Maret, 2011). The other one is transport, and in *C. metallidurans* transport is very specialized with a multitude of transport proteins, and several regulatory mechanisms for transport. The zinc ions that are “labile” need to be buffered accordingly. In a cell characterized by a strong buffering capacity, transiently metal ion concentrations return quickly to optimal conditions. A weaker buffering capacity needs to be complemented by transport reactions, which take on a dominant role in modulating these changes through elevated import or export (Colvin *et al*., 2010; Maret, 2011). In *C. metallidurans*, buffering is achieved by the zinc repository. The zinc repository is the “container” of the cytoplasmic zinc pool, and it was identified and quantified using a bottom-up proteomic approach of mid-exponentially growing AE104 cells (Herzberg *et al*., 2014).

The zinc proteome of *C. metallidurans* was predicted to contain 109.000 zinc-binding or -containing proteins. However, this number might be even larger, between 200.000 and 300.000, if more zinc-binding sites per protein and the theoretical number of proteins per cell are considered (Herzberg *et al*., 2014). Experimentally, between 110.000 and 120.000 zinc-binding proteins were identified. This number exceeds the optimum 70.000 zinc atoms per cell, for instance, that the AE104 strain accumulates in zinc-replete conditions. The zinc repository is able to accommodate at least 110.000 incoming zinc ions, but

possibly many more, thus the repository takes on an important role in intracellular zinc buffering in this bacterium. Using proteins of the zinc repository as a major sink for zinc ions is beneficial for the cell because proteins are flexible, highly abundant, can bind divalent transition metal divalent with varying affinities. In this scenario, the incoming ^{67}Zn ions of ZP2 would be firstly accommodated by components of the zinc repository through weaker interactions, which would make them subjected to export upon the chase with non-isotope enriched zinc. In addition to the zinc-binding proteins of the zinc repository, other cytosolic metal-binding molecules can bind metal ions. These can be glutathione or polyphosphate and are part of a general binding component. Glutathione, in *C. metallidurans*, is also important for copper homeostasis (Hirth *et al.*, 2023). Nevertheless, it also influences zinc homeostasis, along with polyphosphates (Nies *et al.*, 2024).

By distributing incoming zinc ions between the two zinc pools, *C. metallidurans* can sustain the two parallel processes, of metalating zinc-dependent proteins and of maintaining optimal intracellular concentrations of bioavailable zinc (Fig. 1).

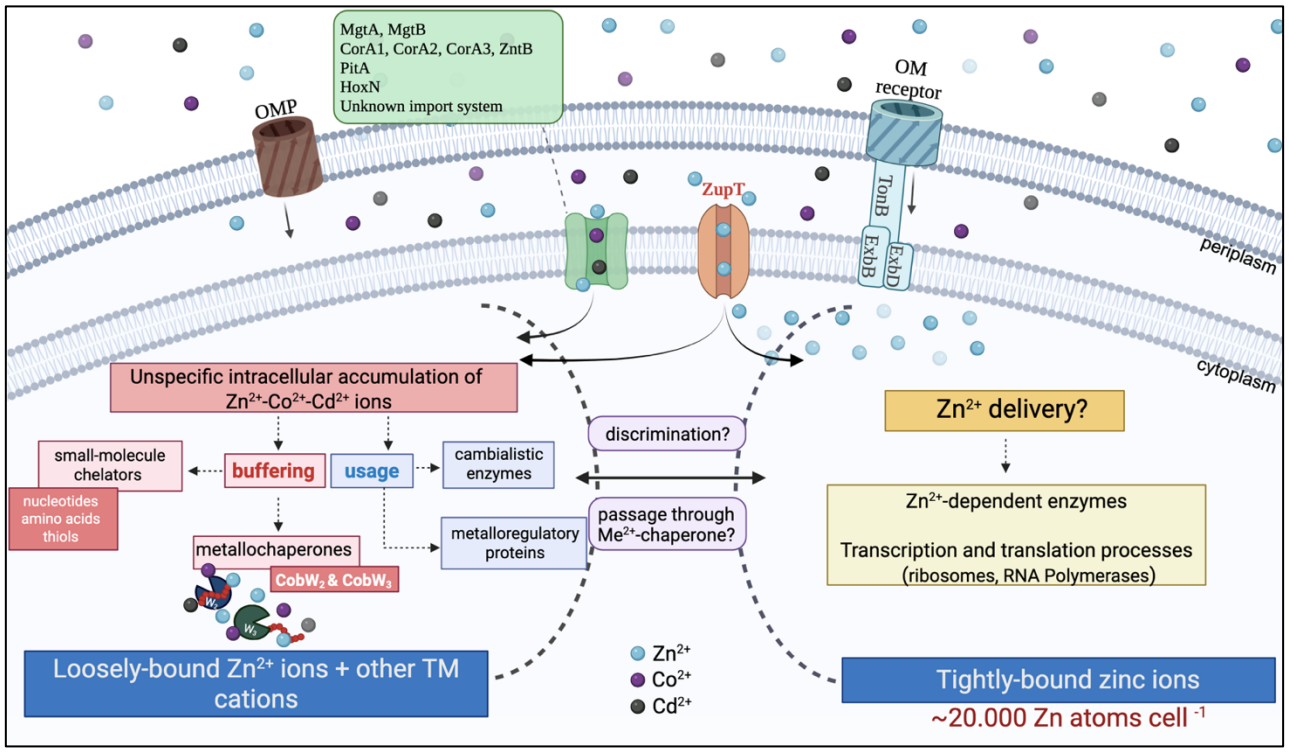

Fig. 1. Zinc pools in *Cupriavidus metallidurans* AE104. Two distinct zinc pools have been described *C. metallidurans*. The pool of tightly-bound zinc can be accounted for in the transcription and translation machinery. The loosely-bound Zn pool can accommodate more incoming zinc ions and possibly accept other divalent transition metal cations. ZupT and the other secondary import systems are responsible for the import of the metal ions across the inner membrane into the cytoplasm. Efflux mediated by ZntA, CadA, and CdfX is not represented (original illustration adapted from Herzberg *et al.*, 2014).

6. Interplay between zinc and cobalt homeostasis

6.1 The zinc starvation response in *C. metallidurans*

When *C. metallidurans* faces conditions of low zinc availability, it is not able to achieve a zinc-repletion state in the cytosol. This means that the cell is not able to fill the cellular zinc content to the optimum quota of 70.000 zinc atoms per cell. In this situation, Zur senses the depletion of the zinc ions in the cytosol and activates a Zur-regulated response. The Zur regulon in *C. metallidurans* contains the *zupT* gene, *cobW*$_1$ operon and *zur-cobW*$_2$ *operon* and the *cobW*$_3$ gene (Fig. 2) (Bütof *et al*., 2017). Zinc starvation conditions can be created by incubating cells with metal-complexing compounds, like EDTA. Incubation of AE104 zinc-replete cells with 100 µM EDTA decreases their zinc cellular content to 50.000 zinc atoms per cell, in comparison with the 70.000 zinc ion-quota they accumulate under zinc repletion (Schulz *et al.*, 2024). Cultivation of AE104 cells in the presence of 80-100 nM $ZnCl_2$ decreases the cellular content to 40.000 - 50.000 zinc atoms per cell, indicating intracellular zinc starvation (Galea *et al*., 2024). The expression of the *zupT* gene is strictly regulated by zinc starvation through Zur and can be up-regulated in the presence of 100-200 µM EDTA (Kirsten *et al*., 2011, Schmidt *et al*., 2014). Although it is not the only zinc importer responsible for importing zinc ions, this transport system is needed for efficient import and allocation of zinc ions to the zinc pool where zinc-dependent proteins are metalated (Herzberg *et al*., 2014).

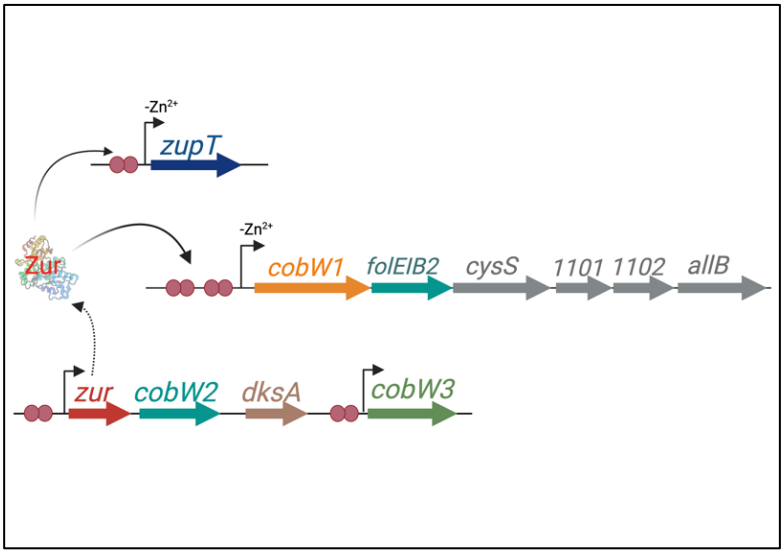

Fig. 2. Zur regulon in *Cupriavidus metallidurans*. The Zur regulon ensures maintenance of zinc homeostasis in conditions of low zinc availability. It contains genes encoding for the high-affinity zinc importer ZupT (ZRT/IRT-like protein ZIP family), Zur regulator (Zinc Uptake Regulator of the Fur family of metalloregulators), three COG0523-family metallochaperones of the G3E Family of P-loop GTPases CobW1, CobW2 and CobW3 and an operon region which includes paralogs of important zinc-dependent enzymes (FolE_IB2), adjacent to the *cobW1* gene (modified from Bütof *et al*., 2017).

In addition to the high-affinity zinc importer, *C. metallidurans* synthesizes paralogs of zinc-dependent proteins under zinc-starvation situations. It is common for cells in metal-starvation situations to reduce the dependency on particular elements by expressing alternative pathways, which leads to a functional substitution for the limiting element. This substitution may use a metal ion that is more abundantly available to the cell than one which is scarce and essential to other metabolic pathways (Merchant and Helmann, 2012). Proteins encoded by the *cobW₁* operon have been found and quantified in the proteome of *C. metallidurans* AE104 cells challenged with the metal-complexing compound, EDTA (Galea *et al*., 2024). Zinc-starved cells synthesize 614 ± 368 copies of the $CobW_1$ protein per cell, and 85 copies of FolE_IB2, whereas these proteins were never found in the proteome of zinc-replete cells. Despite the low copy number of the FolE_IB2, transcriptome data strongly suggests up-regulation of expression of the entire *cobW₁* operon under conditions of zinc-starvation (Herzberg *et al*., 2015; Bütof *et al*., 2017). Expression of the *folE_IB1* gene is not under the transcriptional control of Zur and is not influenced by zinc starvation. The *folE_IB1* gene was expressed in zinc-replete cells, too, from promoters that are not dependent on the house-keeping sigma factor, RpoD (Schulz *et al*., 2024). FolE_IB1 was synthesized at a total copy number of 1042 ± 632 proteins per cell in EDTA-challenged AE104 cells, while under non-challenging conditions 738 ± 54 copies per cell were measured (Galea *et al*., 2024).

Both FolE_IB1 and FolE_IB2 are metal-cambialistic enzymes, which can catalyze the hydrolysis of GTP with other metal cofactors such as Fe^{2+}, Co^{2+}, Ni^{2+} or Mn^{2+}. Both enzymes showed GTPase activity when their apo-proteoforms were incubated with Co^{2+} as the metal cofactor (Schulz *et al*., 2024). *C. metallidurans* does not have a Mn-dependent superoxide dismutase, does not contain a Mn-specific importer of the NRAMP protein family and accumulates Mn^{2+} only at very low levels (Kirsten *et al*., 2011). Increased import of Mn ions has been observed only under iron-starvation conditions, whereas zinc insufficiency had no influence on the generally low cellular Mn content (Schulz *et al*., 2024; Galea *et al*., 2024). In this case, the intracellular manganese concentration is insufficient to activate these two enzymes. Nickel ions were also not imported by zinc-starved AE104 cells neither and thus only an increased concentration of cobalt could suffice to activate the FolE_IBs (Schulz *et al*., 2024; Galea *et al*., 2024).

6.2 Usage of cobalt ions

It has been shown that cells import elevated amounts of cobalt ions when they faced conditions of zinc insufficiency (Galea *et al*., 2024). The cobalt quotas increased from 10.000 to 30.000 cobalt atoms per cell, in correlation with a decrease in the zinc quota. In contrast, under zinc-sufficiency conditions, when the optimum zinc quota is filled, AE104 cells accumulate only low amounts of cobalt atoms per cell, between 3.000 to 7.000. The zinc concentrations in the Tris minimal medium were adjusted to the low nM range, from a minimum of 85 nM to 300 nM provided exogenous $ZnCl_2$. The concentrations of the other divalent transition metal cations, or macroelements, were not altered and guaranteed that any effect noted on the bacterial cells were dependent on zinc availability. Cultivation of the cells with 200 nM $ZnCl_2$, or above, replenishes their optimum cellular zinc content, whereas when faced with a zinc starvation situation, AE104 cells import cobalt ions. With the subsequent increase of the cobalt content under zinc insufficiency conditions, an intracellular handling is necessary to ensure homeostasis of the higher intracellular concentrations of cobalt. On the one hand, cobalt ions follow the uptake pathway, since they are used as cofactors for certain metalloproteins. On the other hand, buffering reactions in the cytosol are essential in order to avoid mis-metalation events caused by an inadvertent increase in the cobalt concentration.

A positive effect of cobalt ions has been reported in the case of zinc starvation. For instance, *Salmonella* Typhimurium substitutes zinc ions with cobalt ions to recover phenotypes associated to zinc deficiency (Ammendola *et al*., 2020). It was shown that cobalt ions were imported in cells suffering from a zinc shortage, and were used for the metalation of zinc-dependent enzymes, or to rescue other pathways or proteins in this bacterium affected by a shortage of zinc. The growth behaviour of a *znuABC* mutant, which is unable to import zinc ions to the same level as the wild type strain, was rescued by supplementation with cobalt and exhibited higher cobalt content intracellularly compared with the wild-type strain. Under these conditions, a portion of the imported cobalt quota was associated with the ribosomes, both in the wild-type strain and the *znuABC* mutant strain. For example, the cobalt ion was incorporated into the Cu, Zn SodCII when cells were cultivated in Zn-limited conditions, and additionally supplemented with cobalt (Ammendola *et al*., 2020). The purified Cu,Co SOD retained activity comparable to the enzyme metalated with zinc. This work provided evidence for cobalt

import and *in vivo* incorporation of this cation into normally Zn-dependent enzymes to rescue phenotypes related to zinc starvation in *Salmonella*.

In vitro, cobalt ions can also substitute zinc ions in zinc enzymes. The divalent transition metal cations of cobalt and zinc possess similar ionic radii of around 740 pm (Weast, 1984). Common methods to obtain information on metal coordination environments and catalytic mechanisms of metalloenzymes are based on substituting *in vitro* the zinc ion, which is spectroscopically silent, with cobalt, due to its good spectroscopic properties (Maret and Vallee, 1993). Yeast cells are able to replace *in vivo* zinc with cobalt in zinc-containing alcohol dehydrogenase when they are grown in synthetic medium that is zinc-deprived and cobalt-enriched (Curdel and Iwatsubo, 1968). It is known that Co^{3+} can be kinetically trapped in cobalamin and form stable complexes (Young *et al*., 2021). *C. metallidurans* contains the genes needed for both cobalamin biosynthesis and its uptake, but the synthesis of the gene products is not influenced by changing metal availability, or by zinc starvation (Große *et al.,* 2022). However, a portion of the imported cobalt ions would be trapped in cobalamin complexes, and subsequently lower its available intracellular concentrations.

To conclude, the inability of *C. metallidurans* to achieve an intracellular zinc-replete state leads the cell to increase its cellular cobalt content and substitute cell-bound zinc ions with cobalt ions. Although zinc starvation responses differ between *C. metallidurans* and *Salmonella*, the advantageous usage of cobalt in the case of zinc starvation makes it plausible for *C. metallidurans* to benefit from such an adaptation. However, rather than metalating the zinc-dependent FolE_IA with zinc ions, which might be needed for the transcription-translation machinery, *C. metallidurans* preferentially metalates the cambialistic paralogs, FolE_IBI or FolE_IB2. This would allow *C. metallidurans* to rely on these two enzymes under conditions of zinc starvation, either using iron *in vivo* or cobalt ions if iron is required for other key cellular processes, and maintain biosynthesis of tetrahydrofolate (Schulz *et al*., 2024). Another portion of the cobalt ions might reside in cobalamin complexes (Young *et al*., 2021). Nevertheless, the concentration of the cobalt ions needs to be tightly regulated in order to prevent mis-metalation reactions, a task which can be taken on by cytosolic metal-binding compounds.

7. Intracellular handling of zinc and cobalt ions

7.1 The COG0523 proteins

The COG0523-family of P-loop GTPases is ubiquitously spread across the tree of life. The number of protein sequences that are associated with this family of GTPases is most likely still increasing today. In 2021, a comprehensive study based on genomic enzymology segregated 80.000 protein sequences related to a COG0523 protein into 40 distinct sequence-similarity network (SSN) clusters (Edmonds *et al*., 2021). This study emphasized their prevalence and diverse functionality of this protein family. However, the number of characterized proteins is significantly lower, and the knowledge regarding their specific roles in metal homeostasis is still expanding. The commonly accepted view is that they are involved in cofactor insertion and metallocenter maturation of various metalloproteins, indicating that they form integral parts in the metal homeostasis of an organism (Haas *et al*., 2009).

C. metallidurans CH34 encodes for three COG0523-family proteins, termed in this organism $CobW_1$, $CobW_2$ and $CobW_3$ (Haas *et al*., 2009; Bütof *et al*., 2019). The genes encoding for these proteins, *cobW₁*, *cobW₂* and *cobW₃*, are located on chromosome 1 and are members of the Zur regulon in this betaproteobacterium (Bütof *et al*., 2017). However, some notable differences are present among these three G3E-class of GTPases regarding their genomic organization, transcriptional activity and biochemical roles, suggesting a segregation in their functionality. The *cobW1* gene is found in a locus with seven additional genes, which are co-transcribed in an operon, with expression being strictly Zur-dependent due to the presence of two Zur-binding boxes found upstream of its promoter (Bütof et al., 2017; Schulz et al., 2024). The genes of the *cobW₁* operon are transcribed only in zinc-starved cells, under conditions that have been elaborated in more detail in Chapter 2. Repression of *cobW₁* expression under zinc-replete conditions, the presence of the two Zur-binding motifs in the regulatory region of the operon, and its adjacent location to the *folE_IB2* gene places $CobW_1$ in the same protein cluster with other strictly Zur-regulated COG0523-proteins.

Although their ubiquitous prevalence and functional characterization points to somewhat distinct possible roles in metal homeostasis as metallochaperones, the COG0523-GTPases possess similar structural motifs. The conserved sequence features of SIMIBI class GTPases are located at their N-termini and are characterized by the canonical

Walker A [GxxGxGK] and Walker B [hhhExxG] motifs, a guanine recognition motif [NKxD] and residues in the Switch I, which bind the γ-phosphate of the nucleotide (Leipe *et al*., 2002; Khil *et al*., 2004; Haas *et al*., 2009). Moreover, members of the G3E family possess a glutamate residue in place of an aspartate in the Walker B motif, which is responsible for coordinating the catalytically essential Mg^{2+} ion (Leipe *et al*., 2022). The GTPase domain is thus retained at the N-terminus and is responsible for GTP hydrolysis, an activity essential for metallochaperone activity, as shown, for examples, for the metallocentre biosynthesis of hydrogenase and urease (Mehta *et al*., 2003; Olson and Maier, 2000) and substantiated by biochemical studies performed on COG0523 proteins (Osterberg *et al*., 2024; Jordan *et al*., 2019; Sydor *et al*., 2013). A distinct feature of the COG0523 proteins is the internal metal-binding site [CxCC] between the Walker A and Walker B motifs (Haas *et al*., 2009). The Zur-regulated COG0523 subfamily is the most prevalent within the COG0523-family. This subfamily acquired its representative name from the presence of Zur-binding sites preceding genes encoding for the COG0523 proteins (Haas *et al*., 2009). The proteins of this cluster are suggested to act as zinc metallochaperones under conditions of severe zinc starvation (Herzberg et al., 2015; Bütof *et al*., 2019; Edmonds et al., 2021).

B. subtilis has one COG0523 representative and analysis of zinc-dependent repression of the encoding gene mediated by Zur of the encoding gene confirms its clustering within the Zur-regulated COG0523 subfamily (Gaballa and Helmann, 1998; Gabriel *et al*., 2008). This COG0523 protein was originally named YciC, it was initially found as a highly abundant protein in a Δ*zur* mutant, and the amino-terminal region of YciC displayed significant similarity to the CobW from *P. denitrificans* (Crouzet *et al*., 1991; Gaballa and Helmann, 1998). Moreover, cells lacking the high-affinity zinc transport system and including an additional *yciC* mutation showed growth impairment under conditions of severe zinc limitation. This growth defect was phenotypically complemented by adding exogenous zinc. It was only several years later, that the YciC protein was postulated to function as a metallochaperone, either for zinc or for one or more metal cations (Gabriel *et* al., 2008). Consequently, it has been proposed that Zur-regulated proteins have putative roles under zinc-limitation conditions and act as zinc metallochaperones, which couple *in vitro* GTP hydrolysis with delivery of the zinc ion to an apo-protein (Haas *et al*., 2009).

The YciC protein has been renamed ZagA (ZTP-activated GTPase A) and appears to support *de novo* folate biosynthesis under conditions of zinc limitation (Chandrangsu *et al*., 2019). Under zinc deficiency, folate biosynthesis is impaired in *B. subtilis* due to a decrease in the activity of FolE, which requires a zinc ion as cofactor. This decrease in zinc is simultaneously associated with accumulation of Z-nucleotide monophosphate (ZMP), which is subsequently phosphorylated to Z-nucleotide triphosphate (ZTP) and acts as an alarmone of folate limitation (Bochner and Ames, 1982; Kim *et al*., 2015). The accumulation of the alarmone ZTP activates the ZagA metallochaperone to bind FolE, an interaction that would promote the delivery of the zinc ion to the zinc-dependent FolE in order to further sustain folate biosynthesis (Chandrangsu *et al*., 2019).

Experimentally, the ZagA-FolE interaction was verified in a bacterial two-hybrid assay, but molecular-level insights are still lacking, as is the metal-binding capacity of the ZagA protein. There was no interaction detectable between ZagA and its zinc-independent paralog FolEB. The suggested model in *B. subtilis* places ZagA as a zinc chaperone, which delivers zinc to the zinc-dependent FolE in a ZTP-dependent manner. ZagA is able to hydrolyse GTP, too, but induction of the Z nucleotide accumulation is crucial for the interaction between ZagA and FolE to occur.

Other examples of Zur-regulated COG0523-family proteins are the ZigA (Zinc-induced GTPase A) proteins from *A. baumannii* ATCC 17978 and *Staphylococcus aureus*. In the Gram-negative opportunistic pathogen *A. baumannii*, the *zigA* gene was the most significantly up-regulated gene revealed by RNA sequencing performed on a ∆*zur* mutant, under conditions of calprotectin (CP)-, an antimicrobial with metal-binding properties, or TPEN- treatment (Mortensen *et al*., 2014). The same expression pattern was obtained for the *zigA* gene in *S. aureus*, whereby up-regulation of expression occurred under CP-treatment in a ∆*zur* mutant, while its expression remained fully repressed under conditions Zn^{2+} excess (Jordan *et al*., 2019). Detailed studies in *A. baumannii* proposes a model in which ZigA functions as a metallochaperone for the metalation of the Zn^{2+}-binding histidine ammonia-lyase, HutH, in order to mobilize zinc through catabolism of His intracellular reservoirs; however, there is currently no evidence for a stable interaction between ZigA and its suggested target protein (Mortensen *et al*., 2014).

ZigA from *A. baumannii* is able to bind two zinc ions per monomer, one with high affinity and one with lower affinity. It also binds one molar equivalent of Co^{2+}. Zn^{2+}-bound ZigA

showed increased GTPases activity in comparison with its apo-form and the protein from *S. aureus* binds three zinc ions, one with high affinity and two with a lower affinity. Its GTPase activity was investigated and shown to increase in presence of Zn^{2+} (Jordan *et al*., 2019). The GTPase activity of both proteins was dependent on metal-binding to the CxCC motif. The currently proposed mechanism for the activation of GTP hydrolysis involves a thermodynamic coupling between the metal and nucleotide-binding events. The zinc ion is bound by all three Cys residues of the CxCC motif in a typical tetrahedral coordination (Osterberg *et al*., 2024). Protein structure and folding is tightly coupled to nucleotide binding, in agreement with the poor GTP-hydrolysis activity of the free protein, which is also considered a non-functional state of the protein and thus leads to protein degradation relative to the GTP-bound form.

A model based on this data set proposes as a mechanism of action for the ZigA protein governed by 'on' and 'off' states. Briefly, after translation and folding, ZigA is found as apo-ZigA intracellularly, which can bind a cognate G-nucleotide and become functionally activated. GTP-bound *Ab*ZigA is able to scavenge Zn^{2+} from buffered pools of bio-available Zn^{2+} and binds this ion at the CxCC motif, which makes the protein optimal for recognition of the client protein. Binding of the client protein stimulates the GTP hydrolysis and, as a consequence of the lower-affinity for Zn^{2+} by the GDP-bound ZigA, a favourable thermodynamic gradient will be formed and the zinc ion can be delivered to the apo-client protein (Osterberg *et al*., 2024). Similarly, the Co^{2+} chaperone, CobW from *Rhodobacter capsulatus,* may mediate metal delivery through a favourable thermodynamic gradient that is established only upon GTP hydrolysis (Young *et al*., 2023).

In light of these working models, in *C. metallidurans* $CobW_1$ is proposed to act as a metallochaperone with the role of maturating metal-dependent proteins in conditions of zinc starvation (Bütof *et al*., 2019). $CobW_1$ exhibits binding capacity for several divalent transition metal cations. The incubation of the apo-form with zinc yielded one zinc per monomer with high affinity, which is bound at the CxCC motif. Upon incubation of the apo-protein with a metal ion mix containing equimolar concentrations of zinc, nickel, cobalt and cadmium, $CobW_1$ was able to bind 1 Zn^{2+} ion, 1.5 Ni^{2+} ions and 1 Co^{2+} ion to sites with lower metal affinity. When only zinc was added to the protein, $CobW_1$ bound a total of 2.5 zinc ions per monomer, with high or low affinity. $CobW_1$ exhibited GTPase activity in the presence or absence of zinc, with stimulating effects when zinc was present (Bütof *et al*., 2019). In *C. metallidurans,* a zinc-dependent interaction between $CobW_1$ and the

metal-cambialistic FolEI_B2 was determined in a pulldown assay in which the Strep-tagged FolEI_B2 protein was incubated with His-tagged $CobW_1$ (Bütof *et al*., 2019). There is, however, a lack of experimental evidence regarding the ability of these Zur-regulated proteins to catalyze GTP hydrolysis with other transition metal divalent cations. Given the interaction of $CobW_1$ with the metal-cambialistic FolE_IB2, which can be activated with Mn^{2+}, Fe^{2+} or Co^{2+}, and the ability of $CobW_1$ to bind other metal ions, it is debatable whether $CobW_1$ is able to transfer other metal cofactors and metalate zinc-independent enzymes, like FolE_IB2 or even FolE_IB1, when cells are challenged by zinc starvation.

In addition to $CobW_1$, which might take the role of metalating zinc-independent enzymes in the case of zinc starvation, the $CobW_2$ and $CobW_3$ proteins have unique physiological roles in *C. metallidurans* (Galea *et al*., 2024). The *cobW₂* gene is found in a dicistronic *zur-cobW₂* operon (Bütof *et al*., 2019). One Zur binding sequence is found upstream of the *zur* gene and the expression of this operon starts from a strong transcriptional start site (TSS) located in the regulatory region of *zur*. Expression of the *zur-cobW₂* operon is never fully repressed and high transcriptional levels measured by reporter gene assays were confirmed in the plasmid-free strain AE104. The gene activity of *cobW₂* was measured and calculated in a beta-galactosidase assay to be 119 U/mg d.w. The downstream gene, *dksA1*, is not transcribed with *cobW₂* and is not part of the Zur regulon. The *cobW₃* gene is located downstream of *dksA1*, and possesses both its own TSS, as well as a Zur-binding sequence. Its gene activity assessed by a beta-galactosidase assay was calculated to 88 U/mg d.w. The expression of both *cobW₂* and *cobW₃* genes is up-regulated approximately 2-fold in metal-starved cells upon incubation with EDTA, and is slightly down-regulated by exogenous zinc addition in the same parental strain AE104. Expression levels of *cobW₂* and *cobW₃* remained unchanged in the zinc-starved Δ*zupT* mutant strain (Bütof et al., 2017; Bütof et al., 2019). Although both *cobW₂* and *cobW₃* genes are responsive to zinc starvation, the expression patterns differ from that of the *cobW₁* cluster, which shows the strongest up-regulation in zinc starvation conditions. Different physiological roles distinguish them from the Zur-regulated representatives, as well as amino acid peculiarities in their primary structure.

It is also common for other bacterial species to encode for one or more homologs of COG0523-family of proteins, suggesting different roles within different environments. *A.* baumannii has two COG0523 proteins, but only ZigA is Zur-regulated and is up-regulated under CP treatment, while the gene encoding another member, A1S_0934, was not

expressed under these conditions (Mortensen *et* al., 2014; Nairn *et* al., 2016). Similarly, *S. aureus* possesses three members of the COG0534 family, but only the *zigA* gene was investigated in the context of zinc starvation (Jordan *et al*., 2019). Further information on the other COG0523 proteins from either *A. baumannii* or *S. aureus* is currently lacking.

7.2 $CobW_2$ proteins: Intracellular metal storage

$CobW_2$ proteins have a direct influence on the flow-equilibrium of zinc ions in *C. metallidurans*. Mutant cells lacking the *cobW₂* gene exhibited lower initial uptake rates for ^{65}Zn, a 25% decrease in zinc content after 20 minutes of incubation with radioactive zinc, and lower initial efflux rates, when compared with their zinc-replete parent strain (Nies *et* al., 2024; Galea *et al*., 2024). Since the kinetical flow-equilibrium of zinc ions is a central process of zinc homeostasis in *C. metallidurans*, this makes $CobW_2$ proteins important components in maintaining zinc homeostasis (Nies *et al*., 2024). Moreover, these proteins are required for the adjustment of the cellular zinc pools (Galea *et al*., 2024). Mutant strains lacking the $CobW_2$ proteins were not able to accumulate ^{67}Zn in ZP2 to the same extent as AE104 cells. Zinc-replete and zinc-starved knock-out mutants accumulated 20% less zinc ions after they were pulsed with 1 µM ^{67}Zn, whereas in metal-starved cells the difference increased to 35% when compared with their isogenic parent. This indicates that more zinc ions were readily available for export from this zinc pool by members of the efflux transportome, such as the P-type ATPase ZntA, when $CobW_2$ protein was missing.

The cells maintain a constant cellular content of both zinc and cobalt ions at 83.000 ± 3.900 atoms per cell in the AE104 strain. Both the intracellular zinc and cobalt concentrations need to be buffered properly to ensure the metalation of the zinc proteome, as well as the cobalt proteome. Proteins of the zinc repository are available to accommodate incoming divalent transition metal cations, such as zinc, cobalt, or even cadmium (Herzberg *et al*., 2014). The $CobW_2$ protein is part of the zinc repository. Approximately 1.600 copies of $CobW_2$ are produced intracellularly, and metal-starved conditions can increase this number 2-fold (Galea *et al*., 2024).

The primary structure of $CobW_2$ has some particular features. Like the other COG0523 GTP-ases, $CobW_2$ contains the motifs at its N-terminus, the internal CxCC binding motif and the G-nucleotide-binding motif. Additionally, starting from position D221 to H265,

$CobW_2$ has an internal His-binding motif. The His stretch in the $CobW_2$ protein contains 22 His residues, 7 Asp residues and 5 Glu residues. Additionally, 2 Cys, 6 Gly and 1 Thr can be found within this motif. In comparison with $CobW_1$, $CobW_2$ is able to bind more zinc ions per monomer (Bütof *et al*., 2019). Incubation of the apo-proteoform with $ZnCl_2$ yielded two outcomes. It was able to bind 0.5 Zn / monomer with high affinity, perhaps through a monomer-bridging site, or it could bind 6 Zn / monomer, all with lower affinity. Addition of MgGTP was able to stabilize the zinc-bound proteoform, which had 6 Zn / monomer. The higher binding capacity of $CobW_2$ for zinc ions assigns this protein the role of a zinc storage or a zinc-buffering protein as part of the zinc repository (Bütof *et* al., 2019).

Some other representatives of the G3E family can also possess a histidine-rich stretch, internally or distally located, to increase the metal binding capacity of the protein (Haas *et* al., 2009). The $CobW_2$ protein is co-localized in the same cluster with two related COG0523 GTPases from *E. coli* (Edmonds *et al*., 2019). *E*. *coli* has two COG0523 GTPases, YeiR and YjiA. The YjiA protein does not have a clearly assigned function to date. It has been suggested that this GTPase has a role in the cellular response to DNA damage following the genotoxic stress induced by mitomycin C as it was found among the novel genes up-regulated after treatment with this substance (Khil *et al*., 2002). At the same time, the YjiA protein was also found in high abundance in *E. coli* cells in which ppGpp-peptide conjugates were used to capture ppGpp-binding proteins, suggesting a role in adaptation to cellular stress, since (p)ppGpp is a cellular alarmone which accumulates as part of the stringent response to nutrient-poor conditions and other stressors (Wang *et al*., 2019). Its encoding gene is neither preceded by Zur-binding sites, nor is it co-localized with *folE* genes (Haas *et al*., 2009). The YeiR protein, on the other hand, has been studied both physiologically and biochemically in the context of zinc homeostasis (Blaby-Haas *et al*., 2012). The *yeiR* gene is not under the control of the Zur transcriptional regulator and expression is not induced under zinc starvation (Panina *et al*., 2003; Sigdel *et al*., 2006; Graham *et al*., 2009). However, the phenotypes caused by deleting the *yeiR* gene have linked this gene product to zinc homeostasis (Blaby-Haas *et al*., 2012). Deletion of either *yeiR* alone, or in combination with the genes encoding the high-affinity zinc import system ZnuABC led to EDTA- and cadmium-sensitive phenotypes of the mutants, whereas the double deletion Δ*yeiR* Δ*znuABC* strain exhibited the most significant growth defect towards these two compounds. Notably, both phenotypes could be rescued by exogenous zinc supplementation (Blaby-Haas *et al*., 2012).

The YeiR from *E. coli* was shown to bind up to three zinc ions, with high affinity at the CxCC motif; however, the presence of the poly-histidine motif (HxHxH) at the C-terminus might also aid zinc-binding (Blaby-Haas *et al*., 2012). The YjiA protein can bind cobalt, nickel or four zinc ions, while two zinc ions can be bound with high-affinity and the other two zinc ions are bound with lower affinity. Its GTPase activity is inhibited by the addition of Co^{2+}, and Ni^{2+}, while Zn^{2+} addition completely inhibits enzyme activity (Sydor *et al*., 2013).

The cobalt proteome of *C. metallidurans* consists of 1.302 putative Co^{2+}-binding proteins (Herzberg *et al*., 2014). Under zinc sufficiency AE104 cells accumulate approximately 3.000 cobalt ions (Galea *et* al., 2024). Under zinc starvation conditions, the cell increases its cobalt import and accommodates 10.000 to 30.000 cobalt ions (Galea *et al*., 2024). $CobW_2$, as part of the zinc repository and based on its primary structure and zinc-binding capacity, can act as an intracellular cobalt-binding protein. In a triple knock-out mutant, Δ*dmeF* Δ*zupT* c*obW2*::dis, the cells were able to accumulate 20.000 to 30.000 zinc ions, which are guided to the tightly-bound zinc pool of the cell, and to strictly zinc-dependent enzymes. Any resident cobalt ions can be buffered by components of the zinc repository, including $CobW_2$ proteins. In this way, $CobW_2$ proteins would be able to accommodate between 10.000 to 20.000 cobalt atoms, given their copy number. $CobW_2$ is not only needed to bind and buffer cobalt ions, but could interact, in this case, with DmeF and ensure both a buffering role and an export pathway for detoxification of surplus cobalt ions.

DmeF is the main cobalt efflux system of *C. metallidurans* AE104 cells (Scherer *et al*. 2009; Galea *et al*., 2024). DmeF is a transmembrane protein including a cytoplasmic domain between transmembrane domains TM4 and TM5 that contains a large His-rich stretch, from position H125 to H195. The metal-binding His residues enable this protein to form an internal loop to bind additional cobalt ions. In the absence of both $CobW_2$ and DmeF, cobalt ions need to be mobilized by different binding compounds in the cytosol or be exported to the outside.

It has been noted that correct metalation of several members of the COG0523 proteins is dependent on the cytosolic metal concentrations, although these proteins are able to bind several metal cofactors, as described above. A study in which *E. coli* strains were engineered for B_{12} production by containing functional B_{12} pathways from *Rhodobacter*

capsulatus, which included the CobW chaperone, showed that CobW can bind *in vitro* both Co^{2+} or Zn^{2+} to the CxCC motif with high affinity, as long as MgGTP is bound. However, the cognate cofactor for CobW is in fact Co^{2+}, whereas YeiR and YjiA prefer to bind Zn^{2+} as their cofactor (Young *et al.,* 2021*)*. Nevertheless, in order for the cognate metal cofactor to be bound to the CobW protein, it was necessary that the concentrations of these two cations in the cytosol enabled Co^{2+} to outcompete Zn^{2+} for binding (Young *et al*., 2021). Similarly, *in vivo* zinc-cobalt occupancy would dictate whether $CobW_2$ in *C. metallidurans* binds zinc or cobalt ions. It is only in a cytosolic environment where high cobalt and low zinc concentrations are present, that $CobW_2$ is able to bind cobalt ions and would therefore also have a buffering role for cobalt ions.

C. metallidurans might adapt to fluctuating intracellular availabilities of zinc and cobalt by using metallochaperones such as the $CobW_2$ proteins. They are an integral part of the zinc repository, acting as zinc-binding proteins. They are able to bind several zinc ions per monomer and they influence the flow-equilibrium, as well as the zinc pools, of the cell. Given a decrease in zinc and increase in cobalt availability in the cytosol, the $CobW_2$ protein can be envisioned as metallochaperones able to bind cobalt ions *in vivo*, too, and to support the cobalt storage capacity of *C. metallidurans*.

7.3 $CobW_3$ proteins influence metal import

At this outset of this work, there was a significant gap in our knowledge concerning the role of the $CobW_3$ protein in metal distribution, sensing, or storage. The $CobW_3$ protein is different from the other CobW proteins regarding its primary structure and its discernible biochemical features. Its primary structure lacks the internal metal-binding site CxCC metal-binding motif between the Switch and the Walker B motif. $CobW_3$ does not exhibit GTP hydrolysis *in vitro*, either for the Zn-bound or the apo-protein (Bütof *et al*., 2019). A distinct feature, however, is the presence of a metal-binding histidine-rich stretch at the C-terminus, from D367 to H391. The poly-histidine stretch is formed by nine Asp residues, eight His residues, four Gly residues, two Cys residues, one Pro residue and one Ala residue.

This is congruent with a highly versatile metal-binding capacity of this protein. Incubation of the apo-form with $ZnCl_2$ yielded eight Zn atoms bound per mol of protein. *In vitro*

experiments showed that $CobW_3$ bound four Zn atoms, 2 Ni atoms, 1 Co atoms and 1 Cd atoms per mol of protein when the apo-form was treated with a metal mix of equimolar concentrations of Zn, Ni, Co and Cd. The eight zinc atoms were bound to the $CobW_3$ protein with different affinities, which suggests a potential role of the $CobW_3$ protein in titrating cytoplasmic zinc concentrations (Bütof *et al*., 2019).

Titrating and binding zinc ions with different affinities might aid in controlling the zinc availability over the range of its intracellular concentration. For instance, such a control of zinc availability is known for human metallothioneins, which are proteins involved in zinc storage in the event of intracellular zinc excess. These metal-binding proteins can bind up to seven zinc ions, but with different binding affinities. These binding affinities range from nanomolar to picomolar, a feature that enables them to exert a control over the zinc availability in the cytosol, despite a broad concentration range (Krezel and Maret, 2007; Krezel and Maret, 2008).

Given the fact that $CobW_3$ is also able to bind other divalent transition metal cations, it cannot be excluded that such a titrating function could also be used for other cations. Since this protein does not possess the characteristic internal metal-binding motif of the CobW protein family, nor does it catalyze GTP hydrolysis *in vitro*, its role as a zinc metallochaperone, such as that of $CobW_1$, can essentially be excluded. On the other hand, $CobW_3$ has been previously suggested to have an influence on metal import (Bütof *et al*., 2019).

In this thesis, additional evidence is provided supporting this proposed function, and it shows that this protein directly influences cobalt import in AE104 cells, in addition to being a part of the zinc homeostatic control system (Galea *et al*., 2024). A knock-out mutant that lacks the $CobW_3$ protein was unable to accumulate as many cobalt ions as its parent strain, and showed a considerable (5-fold) decrease in its cellular cobalt content. To corroborate this observation, a Δ*dmeF* knock-out mutant was cultivated in the presence of cobalt, and was negatively affected due to cobalt toxicity. An additional deletion of the *cobW*$_3$ gene in this background led to a positive growth effect in the presence of exogenous cobalt. Lack of the $CobW_3$ protein in the Δ*dmeF* mutant also led to a decrease in the cellular cobalt content; 5-fold in unchallenged cells and 1.7-fold in cells challenged with exogenous cobalt.

Based on these observations, $CobW_3$ appears to have a direct influence on the import of cobalt ions. As it is able to bind both zinc or cobalt ions, the mechanism that enables this protein to modulate metal import could stem from the presence of the *C*-terminal His-rich region and binding of metal cations to the amino acids of this region, through different affinities. Different metal-binding affinity might enable the $CobW_3$ to "sense" the relative proportion of either intracellular zinc or cobalt and consequently affect metal transport, or overall cellular content, of the actual metal cation bound to the protein. $CobW_3$ is also part of the zinc repository, as well, and is found in the loosely-bound pool of zinc (Herzberg *et al*., 2014).

As already described, in a zinc starvation situation, the intracellular zinc ions are found within the tightly-bound zinc pool of the cell, to be allocated to zinc-dependent proteins. A depletion of the zinc ions from the loosely-bound zinc pool of the cell and the zinc "sensing" ability of $CobW_3$, would require an elevated zinc uptake, primarily achieved through ZupT. Indeed, the absence of both ZupT and $CobW_3$ proteins affected zinc uptake of the knock-out strains when compared to their parent. Import of ^{67}Zn into ZP2 was significantly lowered in a knock-out mutant lacking both *zupT* and *cobW₃* genes, especially in zinc-starved cells (Nies *et* al., 2024; Galea *et al*., 2024). Insufficiency of exogenous zinc led to an increase in cobalt import by AE104 cells. In this scenario, $CobW_3$ could act as a "sensing" molecule for intracellular cobalt concentrations.

In zinc-replete AE104 cells, there are 329 copies of the $CobW_3$ protein. Metal-starved cells do not significantly increase their $CobW_3$ protein synthesis, and 397 copies are present (Galea *et al*., 2024). If these proteins would bind 8 cations per monomer, it would mean approximately 4.000 cobalt ions are bound intracellularly to the $CobW_3$ proteins. Cells without the $CobW_3$ proteins accumulated approximately 4.000 cobalt ions in comparison with AE104 cells, which contained 20.000 cobalt ions per cell. Consequently, the amount of 16.000 cobalt ions that is not imported by the cell cannot be solely due to the binding capacity for cobalt ions to the His-rich stretches of the $CobW_3$ proteins. An additional mechanism must compensate for this effect.

The binding of Zn^{2+}, Ni^{2+}, Co^{2+} or Cd^{2+} to the $CobW_3$ in the different amino acids of the His- rich motif would enable the protein to adopt different conformations. This in return, would influence the ways in which the $CobW_3$ protein might act through protein-protein interactions, for instance. Cells did not accumulate any cadmium ions under the

conditions tested (Galea *et al*., 2024). Nevertheless, cells are able to accommodate cadmium ions and they contain a repertoire of efflux systems to export these cations: the P_{IB2}-type ATPases, ZntA and CadA, or the newly identified CDF protein, CdfX (Scherer *et al.*, 2009; Schulz *et al*., 2024). In *C. metallidurans* the sink for nickel ions is represented by the Ni-hydrogenases and the HypB maturation proteins (Meargeay *et al*., 1985). Moreover, the cells do not increase nickel uptake under zinc starvation and the nickel content of mutant cells devoid of $CobW_3$ remained comparable to the parental strain (Galea *et al*., 2024).

This leaves as candidates for binding to the $CobW_3$ proteins the zinc and cobalt ions. Whereas ZupT is the high affinity import system for zinc ions, *C. metallidurans* imports cobalt ions through transport proteins from the battery of the low-affinity, broad-substrate-specificity importers, such as PitA, or the $CorA_{123}$ (Kirsten *et al*., Herzberg *et al*., 2016). With the clear function of the $CobW_3$ protein influencing zinc and cobalt import, it remains to be investigated which members of the inner membrane transportome might act as interaction partners for this protein, or which molecular mechanism $CobW_3$ adopts. Uptake of cobalt ions still occurs in mutant cells lacking the $CobW_3$ protein, when they are were challenged with 1 µM or 5 µM $CoCl_2$ (Galea *et al*., 2024). $CobW_3$ exhibited an effect only in the nM range, indicating also that the conditions in which the role of $CobW_3$ should be further investigated are undoubtedly pivotal to understanding its real physiological role. The ability of $CobW_3$ to mediate either zinc or cobalt uptake might be a result of the *in vivo* occupancy of these two cations, similar to the case of metalating CobW with Co^{2+} (Young *et al.,* 2021).

A protein-protein interaction between $CobW_2$ and $CobW_3$ cannot be excluded neither at this point, and the physiological data is indicative of such an interaction. $CobW_2$ possesses a zinc-independent *in vitro* GTPase activity that is proposed to aid this protein in changing between a non-binding dimer and a zinc-binding dimer (Bütof *et al*., 2019). In a scenario in which $CobW_3$ functions as an intracellular “sensing” molecule of zinc and cobalt ions, $CobW_3$ might be the unknown signal that triggers the GTPase activity of $CobW_2$ to enhance the cellular buffering capacity. The knock-out mutant lacking both ZupT and $CobW_3$ exhibited a considerably lower resistance to cobalt, which was similar to that of a Δ*dmeF* knock-out mutant, despite both $CobW_2$ and DmeF proteins being present in the cell. A scenario in which $CobW_2$ would not be able to exert its cobalt-binding function, and additionally, not be able to interact with DmeF to support the detoxification

of cobalt ions, might explain such a low resistance of the cells to cobalt. Further research is needed to explore this proposal. Nevertheless, it seems clear that in *C. metallidurans* the $CobW_2$ protein and DmeF are nearer the end in the sequence of zinc and cobalt homeostasis events, through their buffering and efflux actions, while ZupT and $CobW_3$ influence the import and the intracellular distribution of these two cations (Fig. 3).

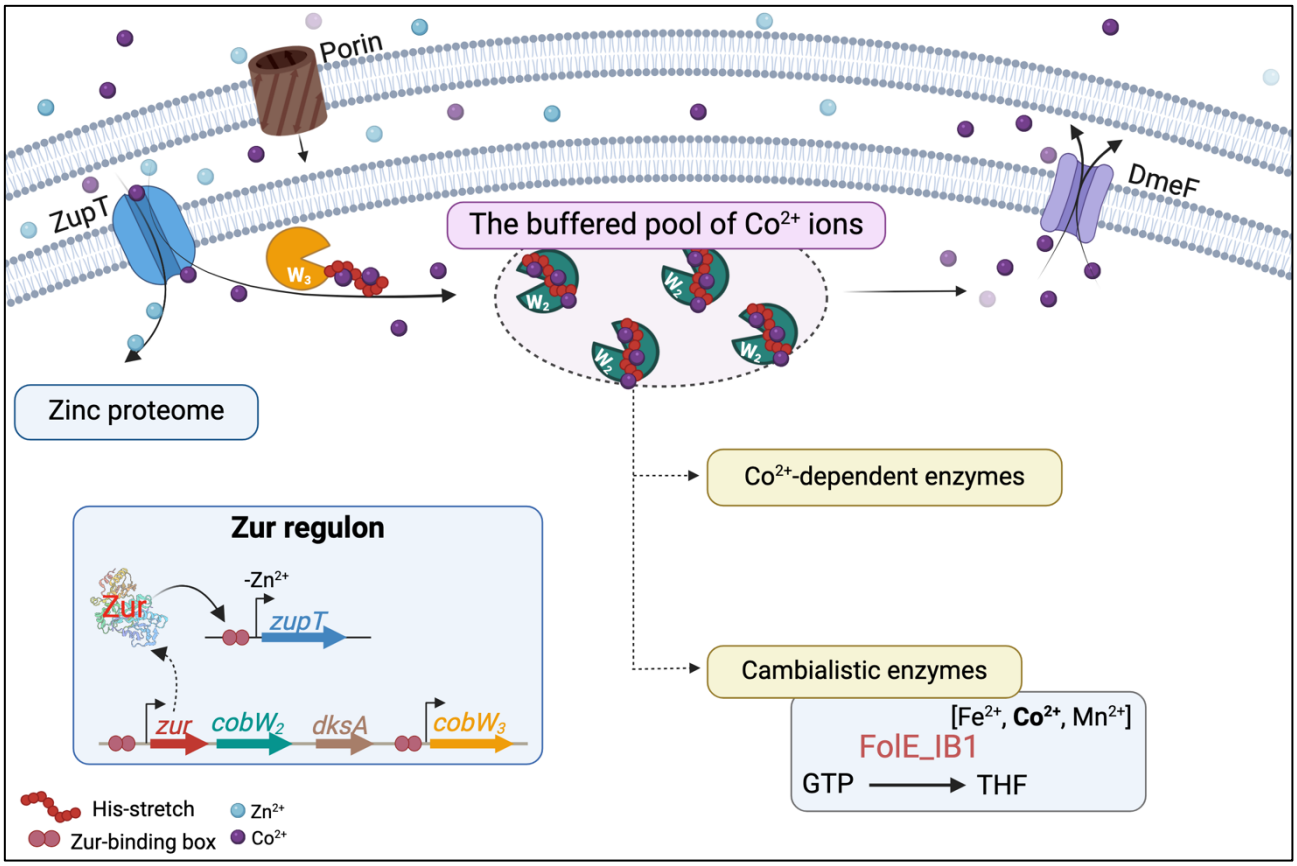

Fig. 3. Model of cobalt homeostasis under zinc insufficiency conditions. Elevated cobalt amounts are accumulated by *Cupriavidus metallidurans* when the zinc availability is decreasing. As a consequence, the cobalt pool within the cell must be buffered so that the Co^{2+}-dependent enzymes can be metalated with this cofactor, while avoiding mis-metalation reactions. Additionally, Co^{2+} ions might also be incorporated in cambialistic enzymes. Maintenance of an appropriate cobalt intracellular concentration emerges from the action of the two transporters ZupT and DmeF, as well as the two intracellular COG0523 metallochaperones $CobW_2$ and $CobW_3$ (original illustration adapted from Galea *et al*., 2024; Schulz *et al*., 2024; Bütof *et al*., 2019).

Summary

The focus of this work was to investigate the contribution of the COG0523 proteins belonging to the SIMIBI P-loop GTPases to the intracellular metal reservoirs and broaden the knowledge of how a metal-resistant bacterium maintains zinc homeostasis, by using *Cupriavidus metallidurans* as a model organism:

i) The core strategy of maintaining zinc homeostasis is based on a kinetical flow equilibrium of zinc ions, in which both import and export reactions run simultaneously. This generates a continuous flow of zinc ions through the cell adjusting the zinc concentration and overall composition of the transition metal pool.

ii) Zinc ions in the cytosol can be kinetically trapped and incorporated into zinc-dependent proteins, or form labile, readily-exchangeable pools with other cytosolic ligands, such as metallochaperones and glutathione. The formation of intracellular zinc pools could be measured using stable isotope-enriched zinc.

iii) An increased cellular content of cobalt ions is a direct consequence of zinc starvation. Subsequently, cobalt ions can be used for zinc sparing reactions such as metalation of paralogs of zinc-dependent enzymes, FolE_IBI and FolE_IB2.

iv) *C. metallidurans* maintains a constant divalent transition metal cation quota of 80.000 zinc and cobalt ions per cell. The zinc repository may be responsible for the intracellular binding of both zinc and cobalt cations.

v) The COG0523 metallochaperones $CobW_2$ and $CobW_3$ aid in maintenance of both zinc and cobalt homeostasis. $CobW_2$ acts as a zinc storage protein, and additionally assists the intracellular buffering of cobalt ions. $CobW_3$ is at the helm of an import pathway of cobalt ions, as well as influencing accumulation of zinc ions. The uniqueness of $CobW_2$ and $CobW_3$ in the metal-resistant bacterium *C. metallidurans* contributes to its layered zinc homeostasis.

Outlook

New functional roles of the ubiquitous family of COG0523 metallochaperones that contribute to zinc and cobalt homeostasis of *C. metallidurans* were elucidated in this thesis. Nevertheless, future studies should unravel the mechanisms through which these two proteins contribute to the homeostasis. These include:

i) The role of $CobW_3$ to mediate import of zinc and cobalt ions could be further investigated by *in vivo* cross-linking to discover any potential interaction partners, either from the inner membrane transportome or cytosolic proteins. Moreover, localization of the $CobW_3$ protein at the inner membrane, as a consequence of a direct protein-protein interaction with transmembrane proteins, could be confirmed by immunogold labelling.

ii) FRET studies could be applied to study the conformations of the $CobW_2$ protein, when found as a non-binding or zinc-binding dimer. The *in vivo* binding capacity of $CobW_2$ for cobalt ions could be tested in Tris minimal medium with minimum zinc availability and sufficient cobalt availability, in a knock-out mutant combination with DmeF. Biochemical studies can be further applied to assess the binding of cobalt ions *in vitro*, as well as other conformations of $CobW_2$ when bound with Co^{2+}.

List of figures

References

Aguilar-Barajas, E., Diaz-Perez, C., Ramirez-Diaz, M. I., Riveros-Rosas, H., & Cervantes, C. (2011). Bacterial transport of sulfate, molybdate, and related oxyanions. *Biometals*, 24(4), 687-707.

Ammendola, S., Ciavardelli, D., Consalvo, A., & Battistoni, A. (2020). Cobalt can fully recover the phenotypes related to zinc deficiency in *Salmonella* Typhimurium. *Metallomics*, 12(12), 2021-2031.

Anbar, A. D. (2008). Elements and evolution. *Science*, 322(5907), 1481-1483.

Andreini, C., Bertini, I., & Rosato, A. (2004). A hint to search for metalloproteins in gene banks. *Bioinformatics*, 20(9), 1373-1380.

Andreini, C., Banci, L., Bertini, I., & Rosato, A. (2006). Zinc through the three domains of life. *J Proteome Res*, 5(11), 3173-3178.

Andreini, C., Banci, L., Bertini, I., & Rosato, A. (2006). Counting the zinc-proteins encoded in the human genome. *J Proteome Res*, 5(1), 196-201.

Andreini, C., Bertini, I., Cavallaro, G., Holliday, G. L., & Thornton, J. M. (2008). Metal ions in biological catalysis: from enzyme databases to general principles. *J Biol Inorg Chem*, 13(8), 1205-1218.

Andrews, S. C., Robinson, A. K., & Rodriguez-Quinones, F. (2003). Bacterial iron homeostasis. *FEMS Microbiol Rev*, 27(2-3), 215-237.

Anton, A., Große, C., Reissmann, J., Pribyl, T., & Nies, D. H. (1999). CzcD is a heavy metal ion transporter involved in regulation of heavy metal resistance in *Ralstonia* sp. strain CH34. *J Bacteriol*, 181(22), 6876-6881.

Argüello, J. M. (2003). Identification of ion-selectivity determinants in heavy-metal transport P1B-type ATPases. *J Membr Biol*, 195(2), 93-108.

Argüello, J. M., Eren, E., & Gonzalez-Guerrero, M. (2007). The structure and function of heavy metal transport P1B-ATPases. *Biometals*, 20(3-4), 233-248.

Bagai, I., Rensing, C., Blackburn, N. J., & McEvoy, M. M. (2008). Direct metal transfer between periplasmic proteins identifies a bacterial copper chaperone. *Biochemistry*, 47(44), 11408-11414.

Barwinska-Sendra, A., & Waldron, K. J. (2017). The role of intermetal competition and mis-metalation in metal toxicity. *Adv Microb Physiol*, 70, 315-379.

Beinert, H., Holm, R. H., & Munck, E. (1997). Iron-sulfur clusters: nature's modular, multipurpose structures. *Science*, 277(5326), 653-659.

Bhattacharjee, H., & Rosen, B. P. (2007). Arsenic metabolism in prokaryotic and eukaryotic microbes. In *Molecular microbiology of heavy metals* (pp. 371-406). Berlin, Heidelberg: Springer Berlin Heidelberg.

Blaby-Haas, C. E., Flood, J. A., Crecy-Lagard, V., & Zamble, D. B. (2012). YeiR: a metal-binding GTPase from *Escherichia coli* involved in metal homeostasis. *Metallomics*, 4(5), 488-497.

Braun, V. (1995). Energy-coupled transport and signal transduction through the gram-negative outer membrane via TonB-ExbB-ExbD-dependent receptor proteins. *FEMS Microbiol Rev*, 16(4), 295-307.

Bütof, L., Schmidt-Vogler, C., Herzberg, M., Große, C., & Nies, D. H. (2017). The components of the unique Zur regulon of *Cupriavidus metallidurans* mediate cytoplasmic zinc handling. *J Bacteriol*, 199(21), 10-1128.

Bütof, L., Große, C., Lilie, H., Herzberg, M., & Nies, D. H. (2019). Interplay between the Zur Regulon components and metal resistance in *Cupriavidus metallidurans*. *J Bacteriol*, 201(15), 10-1128.

Bochner, B. R., & Ames, B. N. (1982). ZTP (5-amino 4-imidazole carboxamide riboside 5'-triphosphate): a proposed alarmone for 10-formyl-tetrahydrofolate deficiency. *Cell*, 29(3), 929-937.

Boer, J. L., Mulrooney, S. B., & Hausinger, R. P. (2014). Nickel-dependent metalloenzymes. *Arch Biochem Biophys*, 544, 142-152.

Borgstahl, G. E., Parge, H. E., Hickey, M. J., Beyer, W. F., Jr., Hallewell, R. A., & Tainer, J. A. (1992). The structure of human mitochondrial manganese superoxide dismutase reveals a novel tetrameric interface of two 4-helix bundles. *Cell*, 71(1), 107-118.

Borremans, B., Hobman, J. L., Provoost, A., Brown, N. L., & van Der Lelie, D. (2001). Cloning and functional analysis of the pbr lead resistance determinant of *Ralstonia metallidurans* CH34. *J Bacteriol*, 183(19), 5651-5658.

Campbell, A. K. (1990). Calcium as an intracellular regulator. *Proc Nutr Soc*, 49(1), 51-56.

Capdevila, D. A., Rondon, J. J., Edmonds, K. A., Rocchio, J. S., Dujovne, M. V., & Giedroc, D. P. (2024). Bacterial metallostasis: metal sensing, metalloproteome remodeling, and metal trafficking. *Chem Rev*, 124(24), 13574-13659.

Cervantes, C., & Campos-García, J. (2007). Reduction and efflux of chromate by bacteria. In *Molecular microbiology of heavy metals* (pp. 407-419). Berlin, Heidelberg: Springer Berlin Heidelberg.

Chandrangsu, P., Rensing, C., & Helmann, J. D. (2017). Metal homeostasis and resistance in bacteria. *Nat Rev Microbiol*, 15(6), 338-350.

Chandrangsu, P., Huang, X., Gaballa, A., & Helmann, J. D. (2019). *Bacillus subtilis* FolE is sustained by the ZagA zinc metallochaperone and the alarmone ZTP under conditions of zinc deficiency. *Mol Microbiol*, 112(3), 751-765.

Changela, A., Chen, K., Xue, Y., Holschen, J., Outten, C. E., O'Halloran, T. V., & Mondragon, A. (2003). Molecular basis of metal-ion selectivity and zeptomolar sensitivity by CueR. *Science*, 301(5638), 1383-1387.

Chao, Y., & Fu, D. (2004). Kinetic study of the antiport mechanism of an *Escherichia coli* zinc transporter, ZitB. *J Biol Chem*, 279(13), 12043-12050.

Chen, D., & Powers, L. (1995). Synthesis and structures of Zn (C6H12OS2) 2 (ClO4) 2 and Zn (C3H6NS2) 2 (C3H4N2)—Model compounds for the Zn sites in RNA polymerase. *Journal of inorganic biochemistry*, *58*(4), 245-253.

Choi, S. H., Lee, K. L., Shin, J. H., Cho, Y. B., Cha, S. S., & Roe, J. H. (2017). Zinc-dependent regulation of zinc import and export genes by Zur. *Nat Commun*, 8(1), 15812.

Cobine, P., Wickramasinghe, W. A., Harrison, M. D., Weber, T., Solioz, M., & Dameron, C. T. (1999). The *Enterococcus hirae* copper chaperone CopZ delivers copper(I) to the CopY repressor. *FEBS Lett*, 445(1), 27-30.

Cobine, P. A., George, G. N., Jones, C. E., Wickramasinghe, W. A., Solioz, M., & Dameron, C. T. (2002). Copper transfer from the Cu(I) chaperone, CopZ, to the repressor, Zn(II) CopY: metal coordination environments and protein interactions. *Biochemistry*, 41(18), 5822-5829.

Collard, J. M., Provoost, A., Taghavi, S., & Mergeay, M. (1993). A new type of *Alcaligenes eutrophus* CH34 zinc resistance generated by mutations affecting regulation of the *cnr* cobalt-nickel resistance system. *J Bacteriol*, 175(3), 779-784.

Colvin, R. A., Holmes, W. R., Fontaine, C. P., & Maret, W. (2010). Cytosolic zinc buffering and muffling: their role in intracellular zinc homeostasis. *Metallomics*, 2(5), 306-317.

Cowan, J. A. (1991). Metallobiochemistry of magnesium. Coordination complexes with biological substrates: site specificity, kinetics and thermodynamics of binding, and implications for activity. *Inorg Chem*, 30(13), 2740-2747.

Cowan, J. A. (2002). Structural and catalytic chemistry of magnesium-dependent enzymes. *Biometals*, 15(3), 225-235.

Christians, S., & Kaltwasser, H. (1986). Nickel-content of urease from *Bacillus pasteurii*. *Arch Microbiol*, 145(1), 51-55.

Crouzet, J., Levy-Schil, S., Cameron, B., Cauchois, L., Rigault, S., Rouyez, M. C., Blanche, F., Debussche, L., & Thibaut, D. (1991). Nucleotide sequence and genetic analysis of a 13.1-kilobase-pair *Pseudomonas denitrificans* DNA fragment containing five *cob* genes and identification of structural genes encoding Cob(I)alamin adenosyltransferase, cobyric acid synthase, and bifunctional cobinamide kinase-cobinamide phosphate guanylyltransferase. *J Bacteriol*, 173(19), 6074-6087.

Curdel, A., & Iwatsubo, M. (1968). Biosynthetic incorporation of cobalt into yeast alcohol dehydrogenase. *FEBS letters*, 1(3), 133-136.

Culotta, V. C., Klomp, L. W., Strain, J., Casareno, R. L., Krems, B., & Gitlin, J. D. (1997). The copper chaperone for superoxide dismutase. *J Biol Chem*, 272(38), 23469-23472.
Diels, L., & Mergeay, M. (1990). DNA probe-mediated detection of resistant bacteria from soils highly polluted by heavy metals. *Appl Environ Microbiol*, 56(5), 1485-1491.

Dixon, N. E., Gazzola, T. C., blakeley, R. L., & Zermer, B. (1975). Letter: Jack bean urease (EC 3.5.1.5). A metalloenzyme. A simple biological role for nickel? *J Am Chem Soc*, 97(14), 4131-4133.

Dominguez, D. C. (2004). Calcium signalling in bacteria. *Mol Microbiol*, 54(2), 291-297.

Dudev, T., & Lim, C. (2014). Competition among metal ions for protein binding sites: determinants of metal ion selectivity in proteins. *Chem Rev*, 114(1), 538-556.

Dupont, C. L., Yang, S., Palenik, B., & Bourne, P. E. (2006). Modern proteomes contain putative imprints of ancient shifts in trace metal geochemistry. *Proc Natl Acad Sci U S A*, 103(47), 17822-17827.

Edmonds, K. A., Jordan, M. R., & Giedroc, D. P. (2021). COG0523 proteins: a functionally diverse family of transition metal-regulated G3E P-loop GTP hydrolases from bacteria to man. *Metallomics*, 13(8), mfab046.

Eide, D. J. (1998). The molecular biology of metal ion transport in *Saccharomyces cerevisiae*. *Annu Rev Nutr*, 18(1), 441-469.

Eitinger, T., Suhr, J., Moore, L., & Smith, J. A. (2005). Secondary transporters for nickel and cobalt ions: theme and variations. *Biometals*, 18(4), 399-405.

Ellefson, W. L., Whitman, W. B., & Wolfe, R. S. (1982). Nickel-containing factor F430: chromophore of the methylreductase of Methanobacterium. *Proc Natl Acad Sci U S A*, 79(12), 3707-3710.

Elston, R., Mulligan, C., & Thomas, G. H. (2023). Flipping the switch: dynamic modulation of membrane transporter activity in bacteria. *Microbiology*, 169(11), 001412.

Ferreira, K. N., Iverson, T. M., Maghlaoui, K., Barber, J., & Iwata, S. (2004). Architecture of the photosynthetic oxygen-evolving center. *Science*, 303(5665), 1831-1838.

Fiedor, L., Kania, A., Mysliwa-Kurdziel, B., Orzel, L., & Stochel, G. (2008). Understanding chlorophylls: central magnesium ion and phytyl as structural determinants. *Biochim Biophys Acta*, 1777(12), 1491-1500.

Fillat, M. F. (2014). The FUR (ferric uptake regulator) superfamily: diversity and versatility of key transcriptional regulators. *Arch Biochem Biophys*, 546, 41-52.

Finney, L. A., & O'Halloran, T. V. (2003). Transition metal speciation in the cell: insights from the chemistry of metal ion receptors. *Science*, 300(5621), 931-936.

Frieden, E. (1985). New perspectives on the essential trace elements. *J Chem Educ*, 62(11), 917-923.

Fong, Y. H., Wong, H. C., Yuen, M. H., Lau, P. H., Chen, Y. W., & Wong, K. B. (2013). Structure of UreG/UreF/UreH complex reveals how urease accessory proteins facilitate maturation of *Helicobacter pylori* urease. *PLoS Biol*, 11(10), e1001678.

Foster, A. W., Osman, D., & Robinson, N. J. (2014). Metal preferences and metallation. *J Biol Chem*, 289(41), 28095-28103.

Gaballa, A., & Helmann, J. D. (1998). Identification of a zinc-specific metalloregulatory protein, Zur, controlling zinc transport operons in *Bacillus subtilis*. *J Bacteriol*, 180(22), 5815-5821.

Gabriel, S. E., Miyagi, F., Gaballa, A., & Helmann, J. D. (2008). Regulation of the *Bacillus subtilis yciC* gene and insights into the DNA-binding specificity of the zinc-sensing metalloregulator Zur. *J Bacteriol*, 190(10), 3482-3488.

Galea, D., Herzberg, M., & Nies, D. H. (2024). The metal-binding GTPases CobW2 and CobW3 are at the crossroads of zinc and cobalt homeostasis in *Cupriavidus metallidurans*. *J Bacteriol*, 206(8), e00226-24.

Galea, D., Herzberg, M., Dobritzsch, D., Fuszard, M., & Nies, D. H. (2024). Linking the transcriptome to physiology: response of the proteome of *Cupriavidus metallidurans* to changing metal availability. Metallomics, 16(12), mfae058.

Gerstenberg, C., Friedrich, B., Schlegel, H. G. (1982). Physical evidence for plasmids in autotrophic, especially hydogen-oxidizing bacteria. *Arch Microbiol*, 133(2), 90-96.

Ghosh, M., Grunden, A. M., Dunn, D. M., Weiss, R., & Adams, M. W. (1998). Characterization of native and recombinant forms of an unusual cobalt-dependent proline dipeptidase (prolidase) from the hyperthermophilic archaeon *Pyrococcus furiosus*. *J Bacteriol*, 180(18), 4781-4789.

Goris, J., De Vos, P., Coenye, T., Hoste, B., Janssens, D., Brim, H., Diels, L., Mergeay, M., Kersters, K., & Vandamme, P. (2001). Classification of metal-resistant bacteria from industrial biotopes as *Ralstonia campinensis* sp. nov., *Ralstonia metallidurans* sp. nov. and *Ralstonia basilensis* Steinle et al. 1998 emend. *Int J Syst Evol Microbiol*, 51(5), 1773-1782.

Gouaux, E., & MacKinnon, R. (2005). Principles of selective ion transport in channels and pumps. *Science*, *310*(5753), 1461-1465.

Graham, A. I., Hunt, S., Stokes, S. L., Bramall, N., Bunch, J., Cox, A. G., McLeod, C. W., & Poole, R. K. (2009). Severe zinc depletion of *Escherichia coli*: roles for high affinity zinc binding by ZinT, zinc transport and zinc-independent proteins. *J Biol Chem*, 284(27), 18377-18389.

Grass, G., Große, C., & Nies, D. H. (2000). Regulation of the *cnr* cobalt and nickel resistance determinant from *Ralstonia* sp. strain CH34. *J Bacteriol*, 182(5), 1390-1398.

Grass, G., Fricke, B., & Nies, D. H. (2005). Control of expression of a periplasmic nickel efflux pump by periplasmic nickel concentrations. *Biometals*, 18(4), 437-448.

Grass, G., Otto, M., Fricke, B., Haney, C. J., Rensing, C., Nies, D. H., & Munkelt, D. (2005). FieF (YiiP) from *Escherichia coli* mediates decreased cellular accumulation of iron and relieves iron stress. *Arch Microbiol*, 183(1), 9-18.

Gray, H. B., Malmstrom, B. G., & Williams, R. J. (2000). Copper coordination in blue proteins. *J Biol Inorg Chem*, 5(5), 551-559.

Große, C., Grass, G., Anton, A., Franke, S., Santos, A. N., Lawley, B., Brown, N. L., & Nies, D. H. (1999). Transcriptional organization of the *czc* heavy-metal homeostasis determinant from *Alcaligenes eutrophus*. *J Bacteriol*, 181(8), 2385-2393.

Große, C., Anton, A., Hoffmann, T., Franke, S., Schleuder, G., & Nies, D. H. (2004). Identification of a regulatory pathway that controls the heavy-metal resistance system Czc via promoter *czcNp* in *Ralstonia metallidurans*. *Arch Microbiol*, 182(2-3), 109-118.

Große, C., Kohl, T. A., Niemann, S., Herzberg, M., & Nies, D. H. (2022). Loss of mobile genomic islands in metal-resistant, hydrogen-oxidizing *Cupriavidus metallidurans*. *Appl Environ Microbiol*, 88(4), e0204821.

Große, C., Grau, J., Herzberg, M., & Nies, D. H. (2024). Antisense transcription is associated with expression of metal resistance determinants in *Cupriavidus metallidurans* CH34. *Metallomics*, 16(12), mfae057.

Guffanti, A. A., Wei, Y., Rood, S. V., & Krulwich, T. A. (2002). An antiport mechanism for a member of the cation diffusion facilitator family: divalent cations efflux in exchange for K+ and H+. *Mol Microbiol*, 45(1), 145-153.

Gumataotao, N., Lankathilaka, K. P., Bennett, B., & Holz, R. C. (2017). The iron-type nitrile hydratase activator protein is a GTPase. *Biochem J*, 474(2), 247-258.

Haas, C. E., Rodionov, D. A., Kropat, J., Malasarn, D., Merchant, S. S., & de Crecy-Lagard, V. (2009). A subset of the diverse COG0523 family of putative metal chaperones is linked to zinc homeostasis in all kingdoms of life. *BMC Genomics*, 10(1), 470.

Halle, B., & Denisov, V. P. (1998). Water and monovalent ions in the minor groove of B-DNA oligonucleotides as seen by NMR. *Biopolymers: Original Research on Biomolecules*, 48(4), 210-233.

Hantke, K. (2005). Bacterial zinc uptake and regulators. *Curr Opin Microbiol*, 8(2), 196-202.

Hensley, M. P., Tierney, D. L., & Crowder, M. W. (2011). Zn (II) binding to *Escherichia coli* 70S ribosomes. *Biochemistry*, 50(46), 9937-9939.

Herzberg, M., Dobritzsch, D., Helm, S., Baginsky, S., & Nies, D. H. (2014). The zinc repository of *Cupriavidus metallidurans*. *Metallomics*, 6(11), 2157-2165.

Herzberg, M., Bauer, L., & Nies, D. H. (2014). Deletion of the zupT gene for a zinc importer influences zinc pools in Cupriavidus metallidurans CH34. *Metallomics*, 6(3), 421-436.

Herzberg, M., Bauer, L., Kirsten, A., & Nies, D. H. (2016). Interplay between seven secondary metal uptake systems is required for full metal resistance of *Cupriavidus metallidurans*. *Metallomics*, 8(3), 313-326.

Higgins, K. A., Carr, C. E., & Maroney, M. J. (2012). Specific metal recognition in nickel trafficking. *Biochemistry*, 51(40), 7816-7832.

Higgs, P. I., Myers, P. S., & Postle, K. (1998). Interactions in the TonB-dependent energy transduction complex: ExbB and ExbD form homomultimers. *J Bacteriol*, 180(22), 6031-6038.

Himelblau, E., & Amasino, R. M. (2001). Nutrients mobilized from leaves of *Arabidopsis thaliana* during leaf senescence. *J Plant Physiol*, 158(10), 1317-1323.

Hirth, N., Gerlach, M. S., Wiesemann, N., Herzberg, M., Große, C., & Nies, D. H. (2023). Full copper resistance in *Cupriavidus metallidurans* requires the interplay of many resistance systems. *Appl Environ Microbiol*, 89(6), e0056723.

Hood, M. I., Mortensen, B. L., Moore, J. L., Zhang, Y., Kehl-Fie, T. E., Sugitani, N., Chazin, W. J., Caprioli, R. M., & Skaar, E. P. (2012). Identification of an *Acinetobacter baumannii* zinc acquisition system that facilitates resistance to calprotectin-mediated zinc sequestration. *PLoS Pathog*, 8(12), e1003068.

Horn, D., & Barrientos, A. (2008). Mitochondrial copper metabolism and delivery to cytochrome c oxidase. *IUBMB Life*, 60(7), 421-429.

Huang, D. L., Tang, D. J., Liao, Q., Li, H. C., Chen, Q., He, Y. Q., Feng, J. X., Jiang, B. L., Lu, G. T., Chen, B., & Tang, J. L. (2008). The Zur of *Xanthomonas campestris* functions as a repressor and an activator of putative zinc homeostasis genes via recognizing two distinct sequences within its target promoters. *Nucleic Acids Res*, 36(13), 4295-4309.

Irving, H. M. N. H., & Williams, R. J. P. (1948). Order of stability of metal complexes. *Nature*, 162(4123), 746-747.

Jack, D. L., Yang, N. M., & Saier, M. H., Jr. (2001). The drug/metabolite transporter superfamily. *Eur J Biochem*, 268(13), 3620-3639.

Janssen, P. J., Van Houdt, R., Moors, H., Monsieurs, P., Morin, N., Michaux, A., Benotmane, M. A., Leys, N., Vallaeys, T., Lapidus, A., Monchy, S., Medigue, C., Taghavi, S., McCorkle, S., Dunn, J., van der Lelie, D., & Mergeay, M. (2010). The complete genome sequence of *Cupriavidus metallidurans* strain CH34, a master survivalist in harsh and anthropogenic environments. *PLoS One*, 5(5), e10433.

Johnson, D. C., Dean, D. R., Smith, A. D., & Johnson, M. K. (2005). Structure, function, and formation of biological iron-sulfur clusters. *Annu Rev Biochem*, 74(1), 247-281.

Jordan, M. R., Wang, J., Weiss, A., Skaar, E. P., Capdevila, D. A., & Giedroc, D. P. (2019). Mechanistic insights into the metal-dependent activation of Zn(II)-dependent metallochaperones. *Inorg Chem*, 58(20), 13661-13672.

Kaluarachchi, H., Chan Chung, K. C., & Zamble, D. B. (2010). Microbial nickel proteins. *Nat Prod Rep*, 27(5), 681-694.

Keilin, D., & Mann, T. (1940). Carbonic anhydrase. Purification and nature of the enzyme. *Biochem J*, 34(8-9), 1163-1176.

Khil, P. P., & Camerini-Otero, R. D. (2002). Over 1000 genes are involved in the DNA damage response of *Escherichia coli*. *Mol Microbiol*, 44(1), 89-105.

Khil, P. P., Obmolova, G., Teplyakov, A., Howard, A. J., Gilliland, G. L., & Camerini-Otero, R. D. (2004). Crystal structure of the *Escherichia coli* YjiA protein suggests a GTP-dependent regulatory function. *Proteins*, 54(2), 371-374.

Kim, P. B., Nelson, J. W., & Breaker, R. R. (2015). An ancient riboswitch class in bacteria regulates purine biosynthesis and one-carbon metabolism. *Mol Cell*, 57(2), 317-328.

Kim, M., Le, M. T., Fan, L., Campbell, C., Sen, S., Capdevila, D. A., Stemmler, T. L., & Giedroc, D. P. (2024). Characterization of the Zinc Uptake Repressor (Zur) from *Acinetobacter baumannii*. *Biochemistry*, 63(5), 660-670.

Kirsten, A., Herzberg, M., Voigt, A., Seravalli, J., Grass, G., Scherer, J., & Nies, D. H. (2011). Contributions of five secondary metal uptake systems to metal homeostasis of *Cupriavidus metallidurans* CH34. *J Bacteriol*, 193(18), 4652-4663.

Klomp, L. W., Lin, S. J., Yuan, D. S., Klausner, R. D., Culotta, V. C., & Gitlin, J. D. (1997). Identification and functional expression of HAH1, a novel human gene involved in copper homeostasis. *J Biol Chem*, 272(14), 9221-9226.

Kobayashi, M., & Shimizu, S. (1999). Cobalt proteins. *Eur J Biochem*, 261(1), 1-9.

Koronakis, V., Sharff, A., Koronakis, E., Luisi, B., & Hughes, C. (2000). Crystal structure of the bacterial membrane protein TolC central to multidrug efflux and protein export. *Nature*, 405(6789), 914-919.

Krezel, A., & Maret, W. (2006). Zinc-buffering capacity of a eukaryotic cell at physiological pZn. *J Biol Inorg Chem*, 11(8), 1049-1062.

Krezel, A., & Maret, W. (2007). Dual nanomolar and picomolar Zn(II) binding properties of metallothionein. *J Am Chem Soc*, 129(35), 10911-10921.

Krezel, A., & Maret, W. (2008). Thionein/metallothionein control Zn(II) availability and the activity of enzymes. *J Biol Inorg Chem*, 13(3), 401-409.

Kuchar, J., & Hausinger, R. P. (2004). Biosynthesis of metal sites. *Chem Rev*, 104(2), 509-525.

Kunkle, D. E., & Skaar, E. P. (2023). Moving metals: How microbes deliver metal cofactors to metalloproteins. *Mol Microbiol*, 120(4), 547-554.

Kwiatos, N., & Waldron, K. J. (2024). In a state of flux: new insight into the transport processes that maintain bacterial metal homeostasis. *J Bacteriol*, 206(5), e00146-24.

Leach, M. R., & Zamble, D. B. (2007). Metallocenter assembly of the hydrogenase enzymes. *Curr Opin Chem Biol*, 11(2), 159-165.

Legatzki, A., Grass, G., Anton, A., Rensing, C., & Nies, D. H. (2003). Interplay of the Czc system and two P-type ATPases in conferring metal resistance *to Ralstonia metallidurans*. *J Bacteriol*, 185(15), 4354-4361.

Leipe, D. D., Wolf, Y. I., Koonin, E. V., & Aravind, L. (2002). Classification and evolution of P-loop GTPases and related ATPases. *J Mol Biol*, 317(1), 41-72.

Lenner, N., Chariker, L., & Leibler, S. (2025). Compatibility of intracellular binding: Evolutionary design principles for metal sensors. *Proc Natl Acad Sci U S A*, 122(18), e2427151122

Lin, S. J., & Culotta, V. C. (1995). The ATX1 gene of *Saccharomyces cerevisiae* encodes a small metal homeostasis factor that protects cells against reactive oxygen toxicity. *Proc Natl Acad Sci U S A*, 92(9), 3784-3788.

Lin, S. J., Pufahl, R. A., Dancis, A., O'Halloran, T. V., & Culotta, V. C. (1997). A role for the *Saccharomyces cerevisiae* ATX1 gene in copper trafficking and iron transport. *J Biol Chem*, 272(14), 9215-9220.

Lu, J., Zheng, Y., Yamagishi, H., Odaka, M., Tsujimura, M., Maeda, M., & Endo, I. (2003). Motif CXCC in nitrile hydratase activator is critical for NHase biogenesis in vivo. *FEBS Lett*, 553(3), 391-396.

Lyons, T. J., Gasch, A. P., Gaither, L. A., Botstein, D., Brown, P. O., & Eide, D. J. (2000). Genome-wide characterization of the Zap1p zinc-responsive regulon in yeast. *Proc Natl Acad Sci U S A*, 97(14), 7957-7962.

Makarova, K. S., Ponomarev, V. A., & Koonin, E. V. (2001). Two C or not two C: recurrent disruption of Zn-ribbons, gene duplication, lineage-specific gene loss, and horizontal gene transfer in evolution of bacterial ribosomal proteins. *Genome Biol*, 2(9), research0033.1-0033.14.

Maret, W., & Vallee, B. L. (1993). Cobalt as probe and label of proteins. *Methods Enzymol*, 226, 52-71.

Maret, W. (2011). Metals on the move: zinc ions in cellular regulation and in the coordination dynamics of zinc proteins. *Biometals*, 24(3), 411-418.

Markov, D., Naryshkina, T., Mustaev, A., & Severinov, K. (1999). A zinc-binding site in the largest subunit of DNA-dependent RNA polymerase is involved in enzyme assembly. *Genes & Dev*, 13(18), 2439-2448.

Mauzerall, D. (1976). Chlorophyll and photosynthesis. *Phil Trans R Soc London B,* 273(924), 287-294.

Mehta, N., Benoit, S., & Maier, R. J. (2003). Roles of conserved nucleotide-binding domains in accessory proteins, HypB and UreG, in the maturation of nickel-enzymes required for efficient *Helicobacter pylori* colonization. *Microb Pathog*, 35(5), 229-234.

Merchant, S. S., & Helmann, J. D. (2012). Elemental economy: microbial strategies for optimizing growth in the face of nutrient limitation. *Adv Microb Physiol*, 60, 91-210.

Mergeay, M., Nies, D., Schlegel, H. G., Gerits, J., Charles, P., & Van Gijsegem, F. (1985). *Alcaligenes eutrophus* CH34 is a facultative chemolithotroph with plasmid-bound resistance to heavy metals. *J Bacteriol*, 162(1), 328-334.

Mikolay, A., & Nies, D. H. (2009). The ABC-transporter AtmA is involved in nickel and cobalt resistance of *Cupriavidus metallidurans* strain CH34. *Antonie Van Leeuwenhoek*, 96(2), 183-191.

Morbach, S., & Krämer, R. (2002). Body shaping under water stress: osmosensing and osmoregulation of solute transport in bacteria. *Chembiochem*, 3(5), 384-397.

Monchy, S., Benotmane, M. A., Janssen, P., Vallaeys, T., Taghavi, S., van der Lelie, D., & Mergeay, M. (2007). Plasmids pMOL28 and pMOL30 of *Cupriavidus metallidurans* are specialized in the maximal viable response to heavy metals. *J Bacteriol*, 189(20), 7417-7425.

Mortensen, B. L., Rathi, S., Chazin, W. J., & Skaar, E. P. (2014). *Acinetobacter baumannii* response to host-mediated zinc limitation requires the transcriptional regulator Zur. *J Bacteriol*, 196(14), 2616-2626.

Munkelt, D., Grass, G., & Nies, D. H. (2004). The chromosomally encoded cation diffusion facilitator proteins DmeF and FieF from *Wautersia metallidurans* CH34 are transporters of broad metal specificity. *J Bacteriol*, 186(23), 8036-8043.

Munson, G. P., Lam, D. L., Outten, F. W., & O'Halloran, T. V. (2000). Identification of a copper-responsive two-component system on the chromosome of *Escherichia coli* K-12. *J Bacteriol*, 182(20), 5864-5871.

Murakami, S., Nakashima, R., Yamashita, E., & Yamaguchi, A. (2002). Crystal structure of bacterial multidrug efflux transporter AcrB. *Nature*, 419(6907), 587-593.

Nairn, B. L., Lonergan, Z. R., Wang, J., Braymer, J. J., Zhang, Y., Calcutt, M. W., Lisher, J. P., Gilston, B. A., Chazin, W. J., de Crecy-Lagard, V., Giedroc, D. P., & Skaar, E. P. (2016). The Response of *Acinetobacter baumannii* to zinc starvation. *Cell Host Microbe*, 19(6), 826-836.

Nichol, C. A., Smith, G. K., & Duch, D. S. (1985). Biosynthesis and metabolism of tetrahydrobiopterin and molybdopterin. *Ann Rev Biochemy*, 54(1), 729-764.

Nies, D., Mergeay, M., Friedrich, B., & Schlegel, H. G. (1987). Cloning of plasmid genes encoding resistance to cadmium, zinc, and cobalt in *Alcaligenes eutrophus* CH34. *J Bacteriol*, 169(10), 4865-4868.

Nies, D. H., Nies, A., Chu, L., & Silver, S. (1989). Expression and nucleotide sequence of a plasmid-determined divalent cation efflux system from *Alcaligenes eutrophus*. *Proc Natl Acad Sci U S A*, 86(19), 7351-7355.

Nies, A., Nies, D. H., & Silver, S. (1989). Cloning and expression of plasmid genes encoding resistances to chromate and cobalt in *Alcaligenes eutrophus*. *J Bacteriol*, 171(9), 5065-5070.

Nies, A., Nies, D. H., & Silver, S. (1990). Nucleotide sequence and expression of a plasmid-encoded chromate resistance determinant from *Alcaligenes eutrophus*. *J Biol Chem*, 265(10), 5648-5653.

Nies, D. H., & Silver, S. (1995). Ion efflux systems involved in bacterial metal resistances. *J Ind Microbiol*, 14(2), 186-199.

Nies, D. H., Koch, S., Wachi, S., Peitzsch, N., & Saier, M. H., Jr. (1998). CHR, a novel family of prokaryotic proton motive force-driven transporters probably containing chromate/sulfate antiporters. *J Bacteriol*, 180(21), 5799-5802.

Nies, D. H., Rehbein, G., Hoffmann, T., Baumann, C., & Große, C. (2006). Paralogs of genes encoding metal resistance proteins in *Cupriavidus metallidurans* strain CH34. J *Mol Microbiol Biotechnol*, 11(1-2), 82-93.

Nies, D. H. (2016). The biological chemistry of the transition metal "transportome" of *Cupriavidus metallidurans*. *Metallomics*, 8(5), 481-507.

Nies, D. H., Schleuder, G., Galea, D., & Herzberg, M. (2024). A flow equilibrium of zinc in cells of *Cupriavidus metallidurans*. *J Bacteriol*, e00080-24.

Noinaj, N., Guillier, M., Barnard, T. J., & Buchanan, S. K. (2010). TonB-dependent transporters: regulation, structure, and function. *Annu Rev Microbiol*, 64, 43-60.

Nojiri, M., Yohda, M., Odaka, M., Matsushita, Y., Tsujimura, M., Yoshida, T., Dohmae, N., Takio, K., & Endo, I. (1999). Functional expression of nitrile hydratase in *Escherichia coli*: requirement of a nitrile hydratase activator and post-translational modification of a ligand cysteine. *J Biochem*, 125(4), 696-704.

Olson, J. W., & Maier, R. J. (2000). Dual roles of *Bradyrhizobium japonicum* nickelin protein in nickel storage and GTP-dependent Ni mobilization. *J Bacteriol*, 182(6), 1702-1705.

Osman, D., Patterson, C. J., Bailey, K., Fisher, K., Robinson, N. J., Rigby, S. E., & Cavet, J. S. (2013). The copper supply pathway to a *Salmonella* Cu, Zn-superoxide dismutase (SodCII) involves P1B-type ATPase copper efflux and periplasmic CueP. *Mol Microbiol*, 87(3), 466-477.

Osman, D., Martini, M. A., Foster, A. W., Chen, J., Scott, A. J. P., Morton, R. J., Steed, J. W., Lurie-Luke, E., Huggins, T. G., Lawrence, A. D., Deery, E., Warren, M. J., Chivers, P. T., & Robinson, N. J. (2019). Bacterial sensors define intracellular free energies for correct enzyme metalation. *Nat Chem Biol*, 15(3), 241-249.

Osterberg, M. K., Smith, A. K., Campbell, C., Deredge, D. J., Stemmler, T. L., & Giedroc, D. P. (2024). Coupling of zinc and GTP binding drives G-domain folding in *Acinetobacter baumannii* ZigA. *Biophys J*, 123(8), 979-991.

Outten, C. E., & O'Halloran, T. V. (2001). Femtomolar sensitivity of metalloregulatory proteins controlling zinc homeostasis. *Science*, 292(5526), 2488-2492.

Padilla-Benavides, T., Thompson, A. M. G., McEvoy, M. M., & Argüello, J. M. (2014). Mechanism of ATPase-mediated Cu+ export and delivery to periplasmic chaperones: the interaction of *Escherichia coli* CopA and CusF. *J Biol Chem*, 289(30), 20492-20501.

Padovani, D., Labunska, T., & Banerjee, R. (2006). Energetics of interaction between the G-protein chaperone, MeaB, and B12-dependent methylmalonyl-CoA mutase. *J Biol Chem*, 281(26), 17838-17844.

Panina, E. M., Mironov, A. A., & Gelfand, M. S. (2003). Comparative genomics of bacterial zinc regulons: enhanced ion transport, pathogenesis, and rearrangement of ribosomal proteins. *Proc Natl Acad Sci U S A*, 100(17), 9912-9917.

Parr, R. G., & Pearson, R. G. (1983). Absolute hardness: companion parameter to absolute electronegativity. *J Am Chem Soc*, 105(26), 7512-7516.

Patzer, S. I., & Hantke, K. (1998). The ZnuABC high-affinity zinc uptake system and its regulator Zur in *Escherichia coli*. *Mol Microbiol*, 28(6), 1199-1210.

Patzer, S. I., & Hantke, K. (2000). The zinc-responsive regulator Zur and its control of the znu gene cluster encoding the ZnuABC zinc uptake system in *Escherichia coli*. *J Biol Chem*, 275(32), 24321-24332.

Paulsen, I. T., & Saier, M. H., Jr. (1997). A novel family of ubiquitous heavy metal ion transport proteins. *J Membr Biol*, 156(2), 99-103.

Pearson, R. G. (1963). Hard and soft acids and bases. *J Am Chem Soc*, 85(22), 3533-3539.

Qiao, W., Mooney, M., Bird, A. J., Winge, D. R., & Eide, D. J. (2006). Zinc binding to a regulatory zinc-sensing domain monitored *in vivo* by using FRET. *Proc Natl Acad Sci U S A*, 103(23), 8674-8679.

Rae, T. D., Schmidt, P. J., Pufahl, R. A., Culotta, V. C., & O'Halloran, T. V. (1999). Undetectable intracellular free copper: the requirement of a copper chaperone for superoxide dismutase. *Science*, 284(5415), 805-808.

Rebelo, J., Auerbach, G., Bader, G., Bracher, A., Nar, H., Hösl, C., Schramek, N., Kaiser, J., Bacher, A., Huber, R., Fischer, M. (2003). Biosynthesis of pteridines. Reaction mechanism of GTP cyclohydrolase I. *J Mol Biol*, 326(2), 503-516.

Reith, F., Rogers, S. L., McPhail, D. C., & Webb, D. (2006). Biomineralization of gold: biofilms on bacterioform gold. *Science*, 313(5784), 233-236.

Reith, F., Lengke, M. F., Falconer, D., Craw, D., & Southam, G. (2007). The geomicrobiology of gold. *ISME J*, 1(7), 567-584.

Rensing, C., McDevitt, S.F. (2013). The copper metallome in prokaryotic cells. *Met Ions Life Sci*, 12, 417-450.

Robinson, N. J., & Winge, D. R. (2010). Copper metallochaperones. *Annu Rev Biochem*, 79, 537-562.

Robinson**,** N. J., & Glasfeld, A. (2020). Metalation: nature's challenge in bioinorganic chemistry. *J Biol Inorg Chem*, 25(4), 543-545.

Rodionov, D. A., Vitreschak, A. G., Mironov, A. A., & Gelfand, M. S. (2003). Comparative genomics of the vitamin B12 metabolism and regulation in prokaryotes. *J Biol Chem*, 278(42), 41148-41159.

Roth, J. R., Lawrence, J. G., & Bobik, T. A. (1996). Cobalamin (coenzyme B12): synthesis and biological significance. *Annu Rev Microbiol*, 50(1), 137-181.

Rzeznicka, K., Schatzle, S., Bottcher, D., Klein, J., & Bornscheuer, U. T. (2010). Cloning and functional expression of a nitrile hydratase (NHase) from Rhodococcus equi TG328-2 in *Escherichia coli*, its purification and biochemical characterisation. *Appl Microbiol Biotechnol*, 85(5), 1417-1425.

Saier, M. H., Jr., Eng, B. H., Fard, S., Garg, J., Haggerty, D. A., Hutchinson, W. J., Jack, D. L., Lai, E. C., Liu, H. J., Nusinew, D. P., Omar, A. M., Pao, S. S., Paulsen, I. T., Quan, J. A., Sliwinski, M., Tseng, T. T., Wachi, S., & Young, G. B. (1999). Phylogenetic characterization of novel transport protein families revealed by genome analyses. *Biochim Biophys Acta*, 1422(1), 1-56.

Saito, M. A., Sigman, D. M., & Morel, F. M. M. (2003). The bioinorganic chemistry of the ancient ocean: the co-evolution of cyanobacterial metal requirements and biogeochemical cycles at the Archean–Proterozoic boundary? *Inorganica Chimica Acta*, 356, 308-318.

Scherer, J., & Nies, D. H. (2009). CzcP is a novel efflux system contributing to transition metal resistance in *Cupriavidus metallidurans* CH34. *Mol Microbiol*, 73(4), 601-621.

Schmidt, C., Schwarzenberger, C., Große, C., & Nies, D. H. (2014). FurC regulates expression of *zupT* for the central zinc importer ZupT of *Cupriavidus metallidurans*. *J Bacteriol*, 196(19), 3461-3471.

Schneider, E., & Hunke, S. (1998). ATP-binding-cassette (ABC) transport systems: functional and structural aspects of the ATP-hydrolyzing subunits/domains. *FEMS Microbiol Rev*, 22(1), 1-20.

Schulz, V., Schmidt-Vogler, C., Strohmeyer, P., Weber, S., Kleemann, D., Nies, D. H., & Herzberg, M. (2021). Behind the shield of Czc: ZntR controls expression of the gene for the zinc-exporting P-type ATPase ZntA in *Cupriavidus metallidurans*. *J Bacteriol*, 203(11), 10-1128.

Schulz, V., Galea, D., Herzberg, M., & Nies, D. H. (2024). Protecting the Achilles heel: three FolE_I-type GTP-cyclohydrolases needed for full growth of metal-resistant *Cupriavidus metallidurans* under a variety of conditions. *J Bacteriol*, 206(2), e00395-23.

Schulz, V., Galea, D., Schleuder, G., Strohmeyer, P., Große, C., Herzberg, M., & Nies, D. H. (2024). The efflux system CdfX exports zinc that cannot be transported by ZntA in *Cupriavidus metallidurans*. *J Bacteriol*, 206(11), e00299-24.

Seeger, M. A., Schiefner, A., Eicher, T., Verrey, F., Diederichs, K., & Pos, K. M. (2006). Structural asymmetry of AcrB trimer suggests a peristaltic pump mechanism. *Science*, 313(5791), 1295-1298.

Shang, Z. G., Windsor, W. T., Liao, Y. D., & Wu, C. W. (1988). Purification of *Xenopus* transcription factor IIIA and 5 S RNA from 7 S ribonucleoprotein particle by ammonium sulfate precipitation. *Anal Biochem*, 168(1), 156-163.

Shelton, A. N., Seth, E. C., Mok, K. C., Han, A. W., Jackson, S. N., Haft, D. R., & Taga, M. E. (2019). Uneven distribution of cobamide biosynthesis and dependence in bacteria predicted by comparative genomics. *ISME J*, 13(3), 789-804.

Shin, J. H., Jung, H. J., An, Y. J., Cho, Y. B., Cha, S. S., & Roe, J. H. (2011). Graded expression of zinc-responsive genes through two regulatory zinc-binding sites in Zur. *Proc Natl Acad Sci U S A*, 108(12), 5045-5050.

Sigdel, T. K., Easton, J. A., & Crowder, M. W. (2006). Transcriptional response of *Escherichia coli* to TPEN. *J Bacteriol*, 188(18), 6709-6713.

da Silva, J. F., & Williams, R. J. P. (1991). The inorganic chemistry of life. *The Biological Chemistry of the Elements (Oxford: Clarendon Press, 1991)*.

Silver, S. (2003). Bacterial silver resistance: molecular biology and uses and misuses of silver compounds. *FEMS Microbiol Rev*, 27(2-3), 341-353.

Silver, S., & Hobman, J. L. (2007). Mercury microbiology: resistance systems, environmental aspects, methylation, and human health. In *Molecular microbiology of heavy metals* (pp. 357-370). Berlin, Heidelberg: Springer Berlin Heidelberg.

Sousa, F. L., Alves, R. J., Ribeiro, M. A., Pereira-Leal, J. B., Teixeira, M., & Pereira, M. M. (2012). The superfamily of heme-copper oxygen reductases: types and evolutionary considerations. *Biochim Biophys Acta*, 1817(4), 629-637.

Su, C. C., Long, F., Zimmermann, M. T., Rajashankar, K. R., Jernigan, R. L., & Yu, E. W. (2011). Crystal structure of the CusBA heavy-metal efflux complex of *Escherichia coli*. *Nature*, 470(7335), 558-562.

Sydor, A. M., Jost, M., Ryan, K. S., Turo, K. E., Douglas, C. D., Drennan, C. L., & Zamble, D. B. (2013). Metal binding properties of *Escherichia coli* YjiA, a member of the metal homeostasis-associated COG0523 family of GTPases. *Biochemistry*, 52(10), 1788-1801.

Symmons, M. F., Bokma, E., Koronakis, E., Hughes, C., & Koronakis, V. (2009). The assembled structure of a complete tripartite bacterial multidrug efflux pump. *Proc Natl Acad Sci U S A*, 106(17), 7173-7178.

Thauer, R. K., Diekert G., Schönheit. P. (1980). Biological role of nickel. *Trends Biochem Sci*, 5(11), 304-306.

Thauer, R. K. (1998). Biochemistry of methanogenesis: a tribute to Marjory Stephenson: 1998 Marjory Stephenson prize lecture. *Microbiology*, 144(9), 2377-2406.

Tibazarwa, C., Wuertz, S., Mergeay, M., Wyns, L., & van Der Lelie, D. (2000). Regulation of the *cnr* cobalt and nickel resistance determinant of *Ralstonia eutropha* (*Alcaligenes eutrophus*) CH34. *J Bacteriol*, 182(5), 1399-1409.

Tseng, T. T., Gratwick, K. S., Kollman, J., Park, D., Nies, D. H., Goffeau, A., & Saier, M. H., Jr. (1999). The RND permease superfamily: an ancient, ubiquitous and diverse family that includes human disease and development proteins. *J Mol Microbiol Biotechnol*, 1(1), 107-125.

Ucisik, M. N., Chakravorty, D. K., & Merz, K. M., Jr. (2015). Models for the metal transfer complex of the N-terminal region of CusB and CusF. *Biochemistry*, 54(27), 4226-4235.

Ueta, M., Wada, C., & Wada, A. (2020). YkgM and YkgO maintain translation by replacing their paralogs, zinc-binding ribosomal proteins L31 and L36, with identical activities. *Genes Cells*, 25(8), 562-581.

Vallee, B. L., & Galdes, A. (1984). The metallobiochemistry of zinc enzymes. *Adv Enzymol Relat Areas Mol Biol*, 56, 283-430.

Vandamme, P., & Coenye, T. (2004). Taxonomy of the genus *Cupriavidus*: a tale of lost and found. *Int J Syst Evol Microbiol*, 54(6), 2285-2289.

van der Lelie, D., Schwuchow, T., Schwidetzky, U., Wuertz, S., Baeyens, W., Mergeay, M., & Nies, D. H. (1997). Two-component regulatory system involved in transcriptional control of heavy-metal homoeostasis in *Alcaligenes eutrophus*. *Mol Microbiol*, 23(3), 493-503.

Vaneechoutte, M., Kampfer, P., De Baere, T., Falsen, E., & Verschraegen, G. (2004). *Wautersia* gen. nov., a novel genus accommodating the phylogenetic lineage including *Ralstonia eutropha* and related species, and proposal of *Ralstonia* [*Pseudomonas*] *syzygii* (Roberts *et al*. 1990) comb. nov. *Int J Syst Evol Microbiol*, 54(2), 317-327.

Van Houdt, R., Monchy, S., Leys, N., & Mergeay, M. (2009). New mobile genetic elements in *Cupriavidus metallidurans* CH34, their possible roles and occurrence in other bacteria. *Antonie Van Leeuwenhoek*, 96(2), 205-226.

Van Houdt, R., Monsieurs, P., Mijnendonckx, K., Provoost, A., Janssen, A., Mergeay, M., & Leys, N. (2012). Variation in genomic islands contribute to genome plasticity in *Cupriavidus metallidurans*. *BMC Genomics*, 13, 1-11.

VanZile, M. L., Cosper, N. J., Scott, R. A., & Giedroc, D. P. (2000). The zinc metalloregulatory protein *Synechococcus* PCC7942 SmtB binds a single zinc ion per monomer with high affinity in a tetrahedral coordination geometry. *Biochemistry*, 39(38), 11818-11829.

von Rozycki, T., & Nies, D. H. (2009). *Cupriavidus metallidurans*: evolution of a metal-resistant bacterium. *Antonie Van Leeuwenhoek*, 96(2), 115-139.

Wang, B., Dai, P., Ding, D., Del Rosario, A., Grant, R. A., Pentelute, B. L., & Laub, M. T. (2019). Affinity-based capture and identification of protein effectors of the growth regulator ppGpp. *Nat Chem Biol*, 15(2), 141-150.

Warren, M. J., Raux, E., Schubert, H. L., & Escalante-Semerena, J. C. (2002). The biosynthesis of adenosylcobalamin (vitamin B12). *Natural Prod Rep*, *19*(4), 390-412.

Weast, R. C., 1984. CRC handbook of chemistry and physics, CRC Press, Inc., Boca Raton, Florida, USA, 64 edn, 1984.

Wiesemann, N., Mohr, J., Große, C., Herzberg, M., Hause, G., Reith, F., & Nies, D. H. (2013). Influence of copper resistance determinants on gold transformation by *Cupriavidus metallidurans* strain CH34. *J Bacteriol*, 195(10), 2298-2308.

Wilcox, D. E. (1996). Binuclear metallohydrolases. *Chem Rev*, 96(7), 2435-2458.

Williams, R. J. (2001). Chemical selection of elements by cells. *Coord Chem Rev*, 216-217, 583-595.

Wimmer, R., Herrmann, T., Solioz, M., & Wuthrich, K. (1999). NMR structure and metal interactions of the CopZ copper chaperone. *J Biol Chem*, 274(32), 22597-22603.

Young, T. R., Martini, M. A., Foster, A. W., Glasfeld, A., Osman, D., Morton, R. J., Deery, E., Warren, M. J., & Robinson, N. J. (2021). Calculating metalation in cells reveals CobW acquires Co(II) for vitamin B(12) biosynthesis while related proteins prefer Zn(II). *Nat Commun*, 12(1), 1195.

Young, T. R., Deery, E., Foster, A. W., Martini, M. A., Osman, D., Warren, M. J., & Robinson, N. J. (2023). Two distinct thermodynamic gradients for cellular metalation of Vitamin B(12). *JACS Au*, 3(5), 1472-1483.

Zhang, Y., Rodionov, D. A., Gelfand, M. S., & Gladyshev, V. N. (2009). Comparative genomic analyses of nickel, cobalt and vitamin B12 utilization. *BMC Genomics*, 10, 78.

Zerkle, A. L., House, C. H., & Brantley, S. L. (2005). Biogeochemical signatures through time as inferred from whole microbial genomes. Am J Sci, 305(6-8), 467-502.

Curriculum vitae

Education and additional experience

July 2020 – June 2025	Research Assistant/Doctoral Candidate Institute of Biology/Microbiology Group of Prof. Dr. Dietrich H. Nies Faculty of Natural Sciences I Martin-Luther University Halle-Wittenberg
Oct. 2017 – July 2019	Master of Science (MSc) Field of study: Molecular Biotechnology Faculty of Biology-Geology Babeș-Bolyai University, Romania
Oct. 2014 – July 2017	Bachelor of Science (BSc) Field of study: Biochemistry Faculty of Biology-Geology Babeș-Bolyai University, Romania
Sept. 2010 – June 2014	Highschool “Moise Nioară”, Arad, Romania *Curriculum*: Natural Sciences, Bilingual English

---

March 2019 – July 2019	Erasmus Internship at Institute of Biology/Microbiology In the group of Prof. Dr. Dietrich H. Nies Faculty of Natural Sciences I Martin-Luther University Halle-Wittenberg

List of publications

Galea, D., Herzberg, M., Dobritzsch, D., Fuszard, M., & Nies, D. H. (2024). Linking the transcriptome to physiology: response of the proteome of *Cupriavidus metallidurans* to changing metal availability. *Metallomics*, 16(12), mfae058.

Schulz, V., **Galea, D.**, Schleuder, G., Strohmeyer, P., Große, C., Herzberg, M., & Nies, D. H. (2024). The efflux system CdfX exports zinc that cannot be transported by ZntA in *Cupriavidus metallidurans*. *J Bacteriol*, 206(11), e00299-24.

Galea, D., Herzberg, M., & Nies, D. H. (2024). The metal-binding GTPases CobW2 and CobW3 are at the crossroads of zinc and cobalt homeostasis in *Cupriavidus metallidurans*. *J Bacteriol*, 206(8), e00226-24.

Nies, D. H., Schleuder, G., **Galea, D.**, & Herzberg, M. (2024). A flow equilibrium of zinc in cells of *Cupriavidus metallidurans*. *J Bacteriol*, 206(5) e00080-24.

Hirth, N., Wiesemann, N., Kruger, S., Gerlach, M. S., Preussner, K., **Galea, D.**, Herzberg, M., Große, C., & Nies, D. H. (2024). A gold speciation that adds a second layer to synergistic gold-copper toxicity in Cupriavidus metallidurans. *Appl Environ Microbiol*, 90(4), e0014624.

Schulz, V., **Galea, D.**, Herzberg, M., & Nies, D. H. (2024). Protecting the Achilles heel: three FolE_I-type GTP-cyclohydrolases needed for full growth of metal-resistant *Cupriavidus metallidurans* under a variety of conditions. *J Bacteriol*, 206(2), e00395-23.

Conferences

Presenting author

Galea, D., Nies, D. H., “COG0523-family proteins CobW2 and CobW3 and the interplay between zinc and cobalt homeostasis in *Cupriavidus metallidurans*”, Annual Meeting VAAM, 23-26 March 2025, Bochum, Germany (Poster)

Galea, D., Herzberg, M., Nies, D. H., “Members of the COG0523-family of metallochaperones at the cross-roads of zinc and cobalt homeostasis in *Cupriavidus metallidurans*”, Summer Webinar on Minerals and Trace Elements (GMS), 2nd July 2024 (Talk)

Galea, D., Herzberg, M., Nies, D. H., “Cobalt homeostasis in the metal-resistant bacterium *Cupriavidus metallidurans* CH34 is controlled by zinc availability”, ISM9, 17-21 June 2024, London, UK (Poster/Poster Flash Presentation)

Galea, D., Herzberg, M., Bütof, L., Nies, D. H., “Characterization of the three CobW proteins shed new light on the metal pools of *Cupriavidus metallidurans* CH34”, Annual Meeting VAAM 2023, 10-13 September 2023, Göttingen, Germany (Poster)

Galea, D., Herzberg, M., Bütof, L., Nies, D. H., “Characterization of the metal pools of the highly metal resistant betaproteobacterium *Cupriavidus metallidurans* CH34”, Annual Meeting GMS 2023, 31.8-2.9.2023, Berlin, Germany (Poster/Poster Flash Presentation)

Galea D., Herzberg, M., Fuszard, M., Dobritzsch, D., Nies, D. H, “The heavy metal resistome of *Cupriavidus metallidurans* CH34”, FEMS 2023, 9-13 July 2023, Hamburg, Germany (Poster)

Galea, D., Văcar, L., Fechete, L. I., Weindorf, D. C., Podar, D., “Assessment of rhizosphere associated bacteria from mercury-contaminated sites and the molecular determinants involved”, Young Researchers in BioSciences Symposium, 22-29 July 2018, Cluj-Napoca, Romania (Talk)

Galea, D., Podar, D., “Mercury resistant bacteria from the rhizosphere of facultative metallophytes: a potential for bioremediation of contaminated sites”, Young Researchers in BioSciences Symposium, 14-19 August 2017, Cluj-Napoca, Romania (Poster presentation)

Acknolwedgements

First and foremost, I would like to thank my supervisor, Prof. Dr. Dietrich H. Nies, for the mentorship throughout this PhD project. During this time, I've received unwavering support, steady guidance, and above all, a mentor who showed me the importance of being a grounded scientist. >> Dear Prof. Nies, I hope homeostasis between the PhD supervisor and the PhD Student has been reached. <<

I would like to thank Prof. Dr. Andrea Sinz and Prof. Dr. Kevin Waldron for providing further expertise.

I want to thank the Nies group, which despite considerably changing its composition throughout my PhD, made my time here memorable in unique ways. I want to thank Martin for his help and patience while I was learning how to operate the ICP-MS and for his critical discussions. I cannot write this part without remembering all the coffee breaks with Vlada and Martin. I want to thank Conny and Grit for the "Mittagessen" and for talking with me in German, even if that was sometimes in a very challenging "Brachwitzer dialect". Thank you all for every small and significant way that contributed to my reaching this point. I will always fondly remember the "Mittagessen", made special by Manu and Christin.

I would like to thank Gary Sawers for his scientific insights and for sharing some common sense of humour (not always easy to find that in a German institute). I am very grateful to Marco and Dörte for taking short breaks with me and keeping my spirits up, especially towards the end of my PhD when the 3rd floor became emptier. I want to thank the whole Sawers group (Doro, Michelle, Christopher, Anne, Stefan, and many more) for the enjoyable moments I spent on the 2nd floor.

I want to thank Dirk for his support when I had to perform ICP-MS measurements and I couldn't fight the argon bottles by myself. I am thankful to the whole team at the Proteomics Core Facility for their assistance with the mass spectrometry experiments.

I want to heartedly acknowledge and thank all my friends in Halle (Vlada, Chantal, Robert, Lorenz, "the Kids", and many more) for helping me build a life here. I also am thankful to my friends back home for their encouragement despite the distance.

Everything of the above has been held up by a foundation. This is my family and I want to thank them for their invaluable support in all my educational pursuits.

Eidesstattliche Erklärung

Hiermit erkläre ich an Eides statt, dass ich mich mit der vorliegenden Arbeit erstmals um die Erlangung des Doktorgrads bewerbe, die vorliegende Arbeit selbstständig und ohne fremde Hilfe verfasst habe, andere als die von mir angegebenen Quellen und Hilfsmittel nicht benutzt habe und die den benutzten Werken wörtlich oder inhaltlich entnommenen Stellen als solche kenntlich gemacht habe.

Halle (Saale), August 2025

Diana Galea